POLITECNICO DI TORINO

Master's Degree in Civil Engineering

MASTER'S DEGREE THESIS

Dynamic Identification of Confined Masonry for existing buildings via AI techniques

Supervisor:

Prof.
PhD. Eng. Marco Domaneschi

Candidate:

Santiago Londoño López

Co-supervisor:

PhD. Eng. Raffaele Cucuzza

OCTOBER 2023 - A.Y. 2022/2023

Dedicatoria

Al llegar al final de un camino es inevitable pensar en los momentos que se vivieron durante el recorrido... sin lugar a duda repetiría este sendero, sin pensarlo dos veces, y después de más de 5 años sin cambiar ni la más mínima cosa.

A Dios le agradezco la vida, le agradezco mi vida y le pongo mi corazón a su disposición, para así sea de la más mínima manera tocar la vida de los demás, tal y como ha tocado la mía al hacerme coincidir con otros y llenar de cosas bonitas mi camino.

A mis padres*, no hay palabras para agradecer todo lo que han hecho por mí, ni tiempo suficiente para manifestarles el amor tan inmenso que siento por ustedes. Les dedico esta producción y el logro académico que la acompaña, pues es gracias a ustedes que se obtuvo todo esto y que obtendré todo lo que se vendrá, uno de mis propósitos ha sido y será siempre honrarlos y enorgullecerlos.*

A mi hermanita*, la amo con la vida y me enorgullece verla crecer, espero ser el ejemplo de lo no tan bueno y lo bueno que se debe hacer, espero que todo lo que haga te sirva de aprendizaje para seguir adelante en tu camino.*

A mis amigos, y hermanos que conseguí y/o traje conmigo a Italia*, sin ustedes esta experiencia no hubiese sido la misma. Me llena de alegría contar con personas tan maravillosas y espero que cuenten conmigo para toda la vida. Sus acciones por mas insignificantes que crean que sean, marcaron algo en mi corazón. Cosas como un momento para escuchar mis pensamientos, brindar un consejo, ver una película, compartir un desayuno, empacar y/o guardar mis pertenencias cuando yo huía de un país por una pandemia global, prepararme un plato de comida, recibirme en su casa de manera desinteresada, bailar una canción o regalarme una sonrisa son cosas que me motivan a seguir adelante todos los días. No hay más que decir, saben quienes son. Infinitas gracias por todo.*

Finalmente quiero agradecer también al momento histórico que viví, pues me permitió regresar a mi país, compartir con muchas personas, inclusive algunas de ellas que ya no están conmigo y vivenciar experiencias que quisa nunca hubiese vivido.

Acknowledgements:

I would like to express my sincere gratitude to **Professor Marco Domaneschi,** I knew since the first moment I met him during my master's courses that a path working alongside him would be an amazing choice. The Doctor, as I call him, despite the time, distance and unfortunate situations never gave up on me so for this I´m truly grateful. His guidance, expertise, and unwavering support at any time (even during after-hours) were invaluable throughout this journey. Your insightful feedback and encouragement have played a crucial role in shaping this thesis.

I would also like to extend my heartfelt appreciation to my co-tutor, **Raffaele Cucuzza,** for his valuable contributions and constructive insights. Since I was put under his supervision, I felt the support and his potential as a professional. The collaborative effort and the time he invested in me have enriched my understanding and enhanced the overall quality of this work. Doctor Cucuzza is without a doubt a role model for me.

I am truly fortunate to have had the privilege of working under both of your mentorships, and I am grateful for the patience and encouragement you have provided. Your commitment to excellence has inspired me to strive for the highest standards in my academic pursuits and the path I´m about to begin is highly influenced by you two.

Thank you both for your invaluable guidance and support.

Abstract

This work explores recent developments in strategies and methods for the preservation and upgrading of existing structures. The primary focus is on evaluating the dynamic characteristics of confined masonry buildings situated in Southern Italy, with an emphasis on leveraging advanced Structural Health Monitoring (SHM) technologies, sensor data collection, and tailored survey techniques to gain in-depth insights into their structural condition. The study involves the deployment of various sensor configurations and employs an optimal placement procedure to monitor and identify modal parameters effectively.

Operational Modal Analysis (OMA) and unsupervised machine learning, such as clustering, are used to analyse experimental data and identify key modal parameters. To fine-tune the structural models, artificial intelligence techniques are applied, along with an optimisation process designed to minimise the disparity between numerical and experimental frequencies. Finite Element (F.E.) models are created using SAP2000, taking into account the buildings' mechanical and geometric properties obtained from the survey. Genetic Algorithms, implemented in MATLAB, are used to dynamically adjust structural parameters until predefined criteria are met.

The outcomes of this study present a standardised approach for handling the inspection, identification, and calibration phases of F.E. models, providing a practical procedure for the dynamic assessment of confined masonry buildings.

Contents

Chapter 1

Introduction

Regarding the conservation and retrofitting of existing structures, several methodologies have been studied and new techniques have been implemented over the last decade. Nowadays the improvement in Structural Health Monitoring (SHM) technologies, sensor data collection, and specific survey procedures lead to a deep knowledge of the status of existing structures and allows to provide accurate modelling. Specifically, the assessment of the dynamic behaviour of existing buildings can be considered as one of the main tasks for researchers.

Within this context, two confined masonry buildings located in the south of Italy were adopted as case studies with the aim of conducting the dynamic identification and assessing their dynamic behaviour.

Different configuration layouts of the sensors have been implemented to perform the monitoring phase using the optimal sensor placement procedure in order to detect the modal parameters.

The in situ experimental data has been analysed using Operational Modal Analysis (OMA). Additionally, clustering unsupervised machine learning has been performed for processing the experimental data and identifying main modal parameters.

To obtain a feasible calibration of the structural parameter of the models, AI techniques have been adopted and an optimisation procedure has been implemented with the aim to reduce the discrepancy between the numerical frequencies obtained from the models and the experimental ones. Thus, a F.E. model for each case study has been prepared by using the SAP2000 F.E code taking into account the mechanical and geometrical properties of the buildings derived from the survey. Then, Genetic Algorithm has been used for the implementation of the optimisation procedure in MATLAB. At each step of the process, the structural parameters of the numerical models have been dynamically changed until the fulfilment of the defined stopping criteria.

The result of this study points to a standard procedure to approach the inspection, identification, and calibration phases of FE models leading to obtaining a feasible procedure for the dynamic identification of confined masonry buildings.

The thesis presents the following organisation: in Chapter 2, a brief overview of the masonry history, construction techniques of masonry and the most promising techniques in the field of model updating and the most common calibration problem will be discussed. In Chapter 3 a generic description of both case studies as well as the results obtained by the survey campaign will be introduced, respectively. Chapter 4 provides the relevant information on the buildings retrieved from existing data prior to the beginning of the surveys performed for this work. Chapter 5 introduced in a concise way the survey campaign carried out, and the sensor layout configuration adopted during the acquisition phase and data retrieved.

Chapters 6 and 7 present the processing and interpretation of the dynamic test used, for the first traditional operational modal analysis and the last one integrating Machine Learning and Artificial Intelligence Chapter 8 introduces some details regarding the modelling of the Finite Element model and the preliminary consideration of their accuracy. In Chapter 9, the outcomes obtained by the Manual Calibration and updating procedures used to achieve such results are presented here. in a complementary way chapter 10 refers to the Artificial Intelligence Optimisation used in terms of modal calibration, the process will be discussed and details about the setting criteria of the F.E model initial calibration will be clearly defined. In Chapter 11 concludes the work, the main results of the overall thesis will be summarised, and new frontiers of this research will be suggested.

Chapter 2

State of the Art

2.1 Masonry

Considered a composite structure made of single units piled and bound together with a mortar material. Its popularity around the world resides among many that do not require skilled labour, meaning for most of the population the possibility to develop housing projects in an easy and expedited way. Masonry relies on the different materials used to create the blocks or bricks, natural stone, calcium silicate and concrete are some of the most popular ones. Regarding the binder material, several materials or composites are used as mortar, among the most important ones are bitumen, chalk, lime/cement based, glue or other less elaborated. Mainly the selection of materials to elaborate the Masonry relies on the evolution of society, the technology available and the materials at disposal in the region. [12]

Aside from housing and refugee development, Masonry has played a key role in the development of communities worldwide, being used for the construction of monuments, civil, medical, and religious Infrastructure. [12]

The widespread use of a technique amazed valuable knowledge of its behaviour, particular the masonry advantages to withstand vertical loads are well-known. But as the study of structures becomes a discipline, the direct influence of the traditional masonry (un-reinforced) in the seismic performance of the buildings arises as a main concern.

Massive and very often critical damages due to strong seismic events were more evident, proving that traditional unconfined masonry buildings were not well prepared to resist seismic inertial forces and the tensile and shear stress may lead to the failure of the masonry elements generating consequently local failures or global collapses. [12]

Therefore, some new construction techniques involving new materials, structural configuration, and mixed solutions gain participation in the construction field. The development of such will be discussed in the following chapter as well as the most prominent technique relevant for this study.

2.1.1 Historical use of Masonry

From the Pyramids in Egypt or Mesopotamia, the Colosseum in Rome, India´s Taj Mahal, the Great Wall of China and other massive historical constructions or landmarks have been built using masonry. The first known usage of masonry dates about 6.000 years ago when sun-baked bricks were used for the construction of residential structures, 2000 years after that uniform shapes as well as moving from sun-baking to firing the bricks were important changes in order to improve the durability of the clay element. Since then, the process of brick fabrication has evolved involving new materials and industrialised processes to gain mechanical properties and enhance durability, but the principle remains unaltered.

Unreinforced masonry buildings (URM) were the trend in several continents for most of the classical era until the beginning of the modern era such favouritism stopped due to the acknowledgement of unsatisfactory performance under even moderate seismic events, specifically for the construction with inadequate wall quantification, irregular wall arrangement and low strength materials. [24]

A clear solution example of such previously introduced problems is for instance the "New trends of innovative materials" such as ACC Autoclave Aerated Concrete which has been available in the market since the beginning of the twentieth century, they aim to reduce weight and therefore the acting mass, a keystone in seismic horizontal acting forces. [7]

The confidence in URM behaviour of the masonry construction is still conceived as poor or insufficient condition that has moved the industry to the implementation of mixed RC and masonry solutions as well as implement as much as possible innovative materials and technologies. [7]

The extended use of confined masonry to reconstruct the southern region of Italy after the 1908 Messina earthquake, could set an example of this transition to confined masonry structures, as this reconstruction can be seen as the final adoption of recommendations issued by the 1909 Italian Royal Decree to use CM. Construction workers overcame the existing reluctance to adopt confined masonry when it was proved that the adoption of Reinforced Concrete frames as anti-seismic structures will provide extra reinforcement to the URM.[24][20][3] Disregarding the previous milestone in the regulation of confined masonry, the Italian national Annex and European/international codes addressed in an insufficient way the seismic safety design criteria aimed at Confined masonry. Parallel to that the literature targeted to study CM is not deterministic to aboard the issue and the inconclusive result leads to no further development. [24]

With the previous statement and reviewing the history of mankind up to the 21st century, masonry is without hesitation the most used construction technique, even in seismic areas. However, as the construction techniques improved, and the structural mechanics pointed out the limitations of Masonry buildings under the effects of lateral loads the calling to implement Reinforced Concrete as construction material gained strength over the years. Nevertheless, Masonry construction URM or RCM is still dominant as a preferred technique for low-rise buildings, particularly as it retains an advantage over its competitors in terms of sound and heat insulation, durability, cost, and Eco-efficiency. Encouraging the industry and academia to pursue further and conclusive methodologies for the study and standardisation of Masonry construction.[3]

2.1.2 Confined Masonry

The development of Reinforced Concrete Frames as an alternative to URM allows to impulse the optimisation of Masonry as it was conceived moving from a structure very capable of managing gravitational load but deficient in withstanding horizontal loads to a new branch of masonry called Confined Masonry. This new technique combines the same fundamental components in frame construction added with masonry infills, the construction process was modified and now the reinforced masonry wall supports the seismic loads as the resized reinforced concrete elements confined the masonry. [20]

Significant improvement can be appreciated while using tie-members in reinforced concrete, particularly when a seismic event occurs enhancing the ductility of the overall structure.

Working as coupled elements the confined masonry technique is obtained due to the wall restriction during construction, this achievement was gained in the process of raising the masonry in the first stage and then casting the concrete frames around it, opposite to the behaviour of masonry acting as merely an infill, this occur when the order is changed, and the masonry is placed in secondary stage therefore adding only over-imposed weight to the structure. [10]

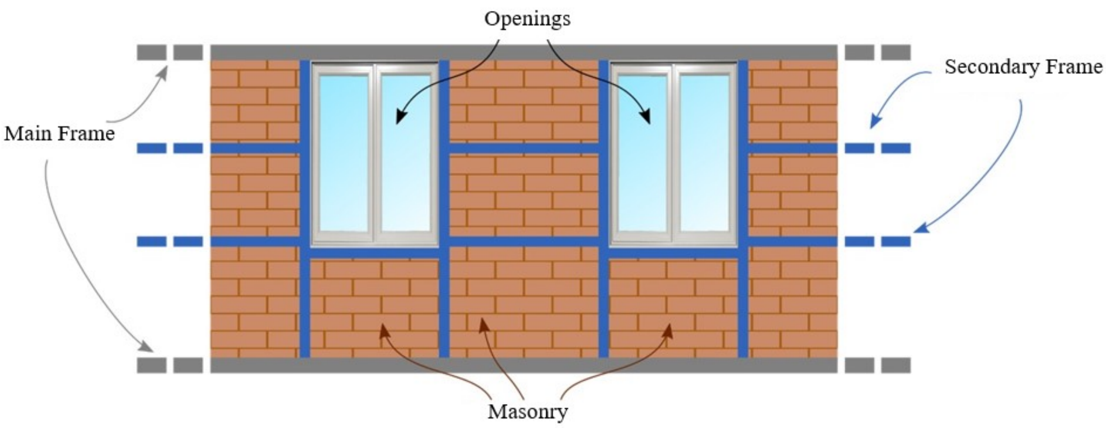

Figure 2.1: Confined Masonry Scheme

An important remark must be considered when discussing the behaviour of confined masonry. The confined elements do not perform as the reinforced concrete confining one, this criteria must be considered during the analysis of the structure. But the gain in the overall behaviour with respect to URM is proven as the stability, and integrity of the wall for in-plane and out-of-plane when seismic forces act. Leading to an increase in the strength of the walls and reducing the brittleness of the elements.

[21]

In terms of efficiency compared to the reinforced concrete frame construction method, confined masonry provides smaller sections due to the active participation of masonry panels to withstand the load, this effect leads to optimise the distribution of ground stress and smaller foundations are required. [3]

Once briefly introduced the rhetorical discussion that led to the development of CM as well as the parts that compose Confined Masonries such as Bricks Panel, Mortar, Tie-Columns and Tie-Beams. It's interesting to present the effect of adjusting parameters strictly related to CM. Some studies allow contextualising this behaviour as [21] did when CM is subjected to seismic actions.

Effect of Wall Width:

As the wall width increases initial stiffness, elastic limit, maximum and residual strength but the direct consequence is a fallback in the ductility of the wall. Now relating the width with the height of the wall can be stated that reducing the length-to-height ratio of a wall tends to enhance its initial ductility. This improvement arises from the increased flexural deflection or the contribution due to yielding in the vertical tensile reinforcement bars located in the Confined Masonry Walls. [21]

Effect of Opening Dimensions:

Openings in confined masonry tend to be restricted by secondary frames, this disposition plays a key role in the behaviour of the structure such by increasing the dimensions (length and height) of openings confined by tie-elements, a reduction in strength and initial stiffness is detected but an increase in initial ductility is achieved. [21]

Effect of Wall Thickness:

In the market, there are several brick typologies and disregarding the material used to cast them the dimension may influence the behaviour of the structure; such effect is associated with the thickness of the wall. For instance, considering increasing the thickness of the wall, the maximum and residual strength, the ductility, and the elastic limit increases. [21]

Effect of Tie-member:

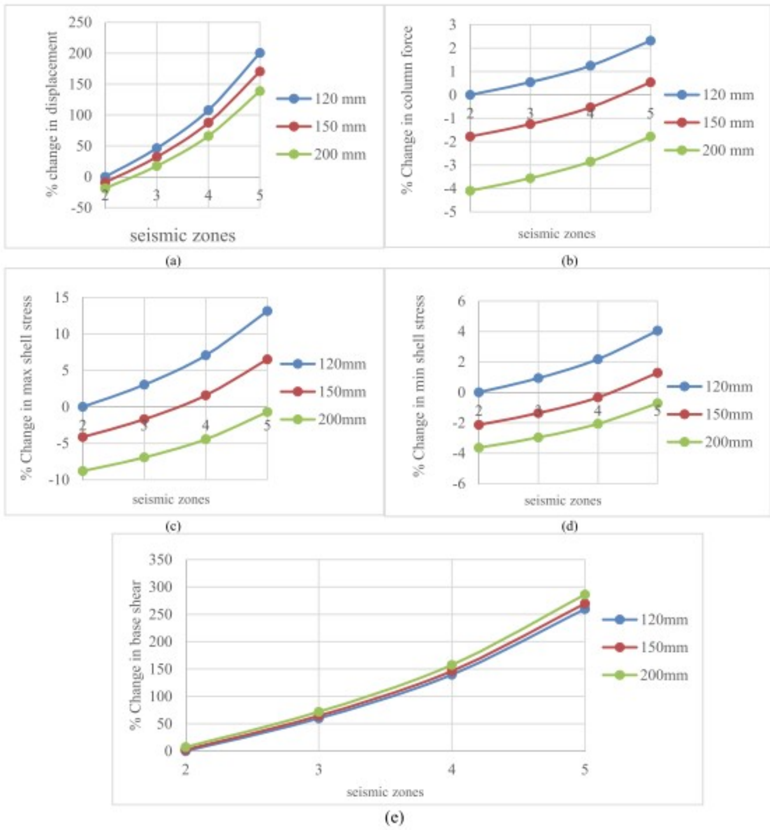

Figure 2.2: Simplified Formulation Modelling [10]

As a generalised conclusion from several studies, all agree that placing the confining elements in the wall contributes to the behaviour with respect to URM, however increasing the amount of such confining elements within the wall, and changing the position and size affects the behaviour, such as just by increasing the number of tie-columns the initial ductility, strength and stiffness of the confined masonry wall increases. [21]

Considering the graphs obtained by [10] In his investigation, 3 types of bricks with the same material but changing their thickness are analysed for the seismic load equivalent as if the walls were in zones 2,3,4 and 5. They report the percentage of change with respect to zone 1 while some parameters are modified.

2.1.3 Masonry Typologies

Regarding the existing typologies several classifications can be done, particularly in the interest of the structural behaviour of the wall panels and the entire structure, two philosophies of classification can be performed.

Classification 1: Structural Configuration Relying Seismic Response:

As the components interact in different ways the first categorisation is related to their behaviour such been the following:

A) Adherent Reinforced Concrete and Masonry Walls: In this case is evident the combined response and cooperation.

B) Independent Reinforced Concrete and Masonry: Contrary to the previous, in this category the elements work independently.

Identifying that the target and evolution of masonry consists of involving reinforced concrete confining frames with the masonry panels the focus of the further categorisation will be section A, now being:

A1) Existence of reinforcing concrete beam frames only at the level of the floors.

A2) Confined Masonry including vertical tie-member for masonry opening as well.

For both previous categorisations, a significant interaction of RC elements and masonry is detected, now on modifying the traditional failure damage modes for concrete and masonry being analysed independently.

Especially in subsection A1, the influence of RC ring beams primarily impacts the behaviour of masonry spandrels. Consequently, the interaction effects are localised, and addressing them involves adjusting the strength criteria of these elements while maintaining the other commonly assumed conditions for masonry unchanged.

In contrast, for Subsection A2, the interaction effects are more pronounced, leading to significant modifications in the behaviour of masonry panels. In this scenario, the assessment of internal forces typically involves conceptualising the combined RC-masonry system as a frame with diagonal bracing, this approach aims to simulate the masonry panel as an equivalent strut, also other approaches to analyse the system as a whole may be used. Properly designed, this latter subsection is intended to enhance the seismic response of the structure, resulting in a reduction in critical design parameters.[24]

Classification 2: Block Materials:

The cast technique originated 6000 years ago and is conceptually the same however some modifications have been made, particularly the process has become an industrialised procedure that has increased the quality by improving the techniques within the production cycle. Despite the previous affirmation a distinguish can be made regarding the base material used for the hardening of the bricks, the most relevant ones will be exposed:

1) Clay bricks: Most common brick typology worldwide, some definitions are strictly related to dimensions and mechanical properties achieved during the drying process, but ultimately a clay block is the result of mixed Clay with water. As it's one of the most antique methods the use of raw materials is typical so degradation and damage are more common in this typology but as its widespread covering and cladding additives were developed the damaging effects can be reduced.

2) Fly Ash bricks: Result of fabricating blocks with Portland Cement, Fly Ash, sand, and water. The usage of these components attempts to improve the compressive strength but compromises the weight due to the increase in the density with respect to a standard clay brick. The inclusion of Fly Ash potentially provides benefits like the removal of pollution agents and allows the incorporation of residues from industrial processes. Also, thermal properties are improved due to low heat absorption but that might be a drawback considering its application in countries during the winter season.

3) Low Weight Concrete Bricks (LWC): This panel incorporates the same components as the Fly Ash Bricks but adds a foaming agent during the fabrication process. Such inclusion reduces the density and improves elasticity, compressibility, water resistance, vibration absorption, and acoustic efficiency. A gain in construction speed and a simplification in the installation process is appreciated with this material. Regarding the disadvantages, complications arise during fabrication, mainly due water content sensibility of the mixture, also sensible to heavy abrasion and due to the

porosity of the material a reduction in the compressive strength is noted.

4) Autoclaved Aerated Concrete AAC= was originally popular in the mid-1900s due to its low mass weight, AAC infill walls have a big effect on how structures respond to earthquakes, making them more rigid and strong without reducing their ability to move. The utilisation of AAC infill walls significantly influences the seismic response of structures by enhancing their tensile/compressive strength ratio, all while preserving their capacity for movement, nevertheless, the previous affirmation is still valid as a ratio when ultimate mechanical properties are analysed the porosity arises some brittleness and the final compressive strength is lower than a tradition brick. [20] A way to effectively compare the previously presented material categories is the test performed by [20], in their study the base shear (direct effect computed using the mass of the structure) and compressive/tensile stresses in the masonry were computed for seismic zones equivalent accelerations. As seen in the graph the base shear values of a frame made of AAC blocks are the lowest, while those of a frame made of LWC panels and clay bricks are the highest and increase with the number of seismic zones. Compressive and tensile stresses at all zones were the highest/lowest for clay bricks across all seismic zones while that of AAC block is minimum.

This means that, as described in the material categories definition, the AAC block is the lightest and is capable of withstanding the lowest stresses, being the toughest one the traditional clay brick. With these valuable data, regarding the condition of any particular case, a proper selection can be performed.

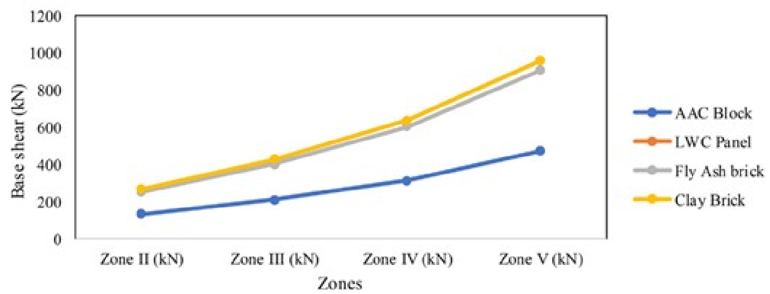

Figure 2.3: Material Infills Base Shear Test Conducted by [20]

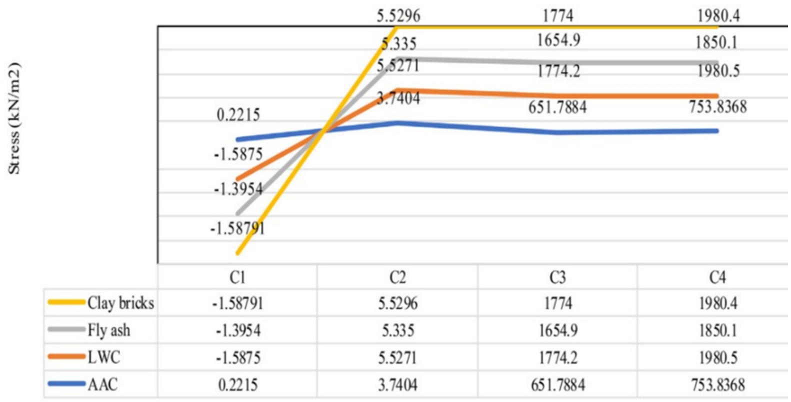

Figure 2.4: Material Infills Stresses Behaviour Conducted by [20]

2.1.4 Existing Computational Methods to Analyse Confined Masonry

For Masonry study, computational Methods to develop a feasible and definitive methodology have proven to be quite limited. The scientific investigation of the interaction effects in masonry structures faces a challenge due to the limited set of numerical tools available for such studies [24]

While there are numerous codes for building design and detailing, they often harbour loopholes, particularly in provisions for seismic effects, tie-member design, and detailing [20]. To address these challenges several techniques based on theoretical assumptions have been proposed, for instance, the Strut-and-Tie Model (STM) emerges as a comprehensive design and analysis technique, simulating truss-like arrangements within structural components. This model allows for the determination of internal forces, with compression resisted by struts and tension by ties, interconnected at nodes. Among the advantages of this strategy is the possibility to directly control the stiffness participation due to the masonry infill by modifying the section, the material of the Strus-Tie or the frame columns. studies [10] [3]

The Equivalent Strut Model (ESM) and Strut and Tie Model (STM) as seen are proposed for CM but also can be used for masonry-infilled RC structures, respectively, providing simplified approaches for practical design and analysis, catering to a trade-off between accuracy, computational demands, and available time[3]

Finite Element (FE) modelling has been a key concept for studying the behaviour of confined masonry (CM) walls. The advancement in computational resources allowed us to study the behaviour of the CM panel in various levels of detail and precision associated with it, each with its trade-offs. Three strategies, detailed micro-modelling, simplified micro-modelling, and macro-modelling, were proposed [3]

Detailed micro-modelling involves modelling with its distinctly mechanical and continuum properties the masonry units, the mortar, and the interfaces individually, demanding computational intensity and detailed joint property knowledge. An approach to computing all these variables is the use of the Discrete Element Method (DEM) and precise LiDAR-based modelling. Nonetheless, the accuracy it offers is mostly overwhelmed by the computationally intensive requirements and the calculation demand for major structures. [3]

A more practical but still accurate strategy is the Simplified micro-modelling where lumps mortar joints and mortar-unit interfaces into a single element, offering a less computationally taxing alternative with a trade-off in accuracy with respect to the analysis done with DEM, provides a sufficient level of refinement when focused in modelling an intermediate level. [3]

The introduction of macro-element modelling in 1970 marked a significant step for seismic assessment of masonry structures, offering a viable approach to address these challenges [9]. It treats masonry components as a homogeneous continuum with isotropic or an-isotropic mechanical properties, reducing accuracy but enhancing computational efficiency, making it suitable for studying global behaviour in larger panels. [3]

In seismic assessment, simplified methods are favoured over complex 2-D/3-D finite element approaches due to practical considerations, especially in parametric studies involving numerous structures where dynamic analysis becomes economically unfeasible [14]

2.2 Structural Health Monitoring

SHM is conceived as a process to predict vulnerability or near-real-time assessment of a structure particularising implementing a Damage Detection Strategy. It relies on the available information and is as precise as possible to guarantee a correct assessment of the risk and status of the structure. Scientists and engineers have proposed their own approaches to evaluate the elements, relying on alternatives as every independent case of study demands. Nevertheless, the process always requires the same global phases as described; geometric collection, sensor planning, sensor placement, data acquisition, data transferring and storage, data management, information interpretation, and finally some final assessment relying on the obtained results. [26][16]

The preservation of heritage and infrastructure poses an interesting concern for communities, pushing the concept of SHM into the territorial management authority's agenda with the task of applying these new processes to provide for several strategic structures such as fire stations, hospitals, town halls, offices open to the public the protection and monitoring they require. Therefore, the assessment of the vulnerability of historic and strategic buildings has become a crucial point for planning risk mitigation.[8]

A successful SHM procedure relies on collecting proper health metrics of the structure, therefore a key milestone in the process involves the adequate integration of several sensors, devices, and auxiliary tools, such as a measurement system, an acquisition system, a data processing system, a communication/warning system, an identification/modelling system, and a decision-making system. This full setup will feed the numerical model representative of the building's operational condition, providing the structure's status and calibrated information to analyse future events. Consider for instance exciting the model with collected data of a quake or other effects to derive the damages that it may have caused. [16][15]

2.2.1 Optimal Sensor Placement (OSP) and Optimal Sensor Number (OSN)

Prior to the in-situ inspection is recommended to always perform a survey plan, in this process is mandatory to evaluate, according to the typology of the structure, the procedure that will be performed in the field work. Considering this philosophy three main questions must be approached; first is the variables that I must measure, for instance, acceleration, in what direction? with which equipment? Second, where the variables should be measured? And third, how many measurements are enough for an accurate work? [26]

The previous inquiries began the research for answers, being the scope to locate the most informative locations to place the sensors, minimising the number and its management cost without losing in the process accuracy of the structure health diagnosis and the quality. So, in this way, the problem was split and targeted into two survey problems: localisation and determination of an effective number of sensors.[5] [6]

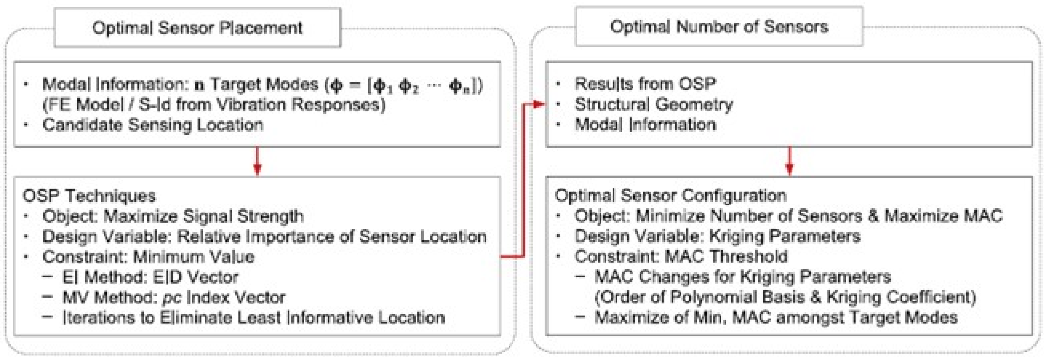

Figure 2.5: OSP OSN Flow Diagram conducted by [5]

Significant improvements have been made, particularly concerning optimal sensor placement (OSP) techniques. As depicted in the following graph, which illustrates the evolution of the number of journal papers within the realm of OSP, structural health monitoring, and damage detection using data sourced from the Scopus database, it is evident that the scientific community has been actively engaged in advancing knowledge in this critical area [26]

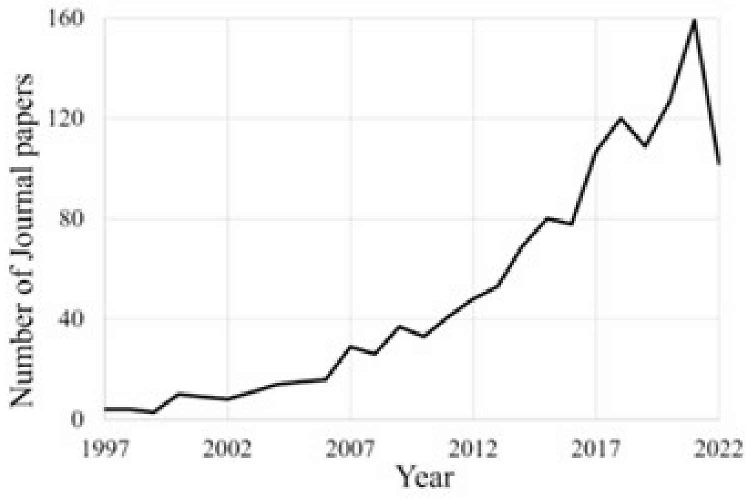

Figure 2.6: Number of Journal published in Scopus by [26]

Despite these advancements, a prevailing challenge persists—the restraining cost associated with sensors, which stands out as a primary impediment to the widespread implementation of structural health monitoring methodologies. Recognising this constraint, various OSP methodologies have been developed to address the financial constraints associated with sensor deployment. These innovative approaches seek to optimise the placement of a limited number of sensors strategically, pre-emptively identifying the most effective locations aimed at deriving dynamic characteristics, such as mode shapes. By doing so, these OSP methods contribute not only to cost mitigation but also enhance the overall efficiency and effectiveness of structural health monitoring initiatives [26]

The number, location, and measure direction of the sensors are particularly crucial when considering flexible structures, where a torsional mode and two transverse modes are integral to the analysis. Notably, the outermost locations, often accessible in typical measurement conditions, yield consistent results in the Optimal Sensor Placement (OSP) method, enhancing the interpretation of multiple dynamic modes [5]. While sensor placement metrics methods are computationally efficient, the importance of linear independence, crucial for distinguishing each mode, is underscored by the Sensor Elimination Methods. The MAC matrix, for instance, serves as a significant acceptance criterion, ensuring the observability and independence of modes

[26]

It is recommended to identify the optimised locations of limited accelerometers using OSP methods applied to Finite Element Models (FEMs) with initial material properties. The emphasis on installing sensors on the roof rather than the first floor is noteworthy, [26]. Furthermore, the suggestion to produce multiple sensor arrays with different formulations and compare them based on performance indicators highlights the need for a thorough approach to sensor configuration [11]

From a mathematical standpoint, the optimal sensor placement (OSP) is articulated as a constrained topological combinatorial optimisation problem. Defining an optimum criterion, or objective function, is essential for the goal of sensor positioning, aligning with the investigation of the mechanical system in matter [11]. In essence, to monitor the most significant information accurately, strategic sensor placement is a main scope, considering structural dynamics and mathematical optimisation principles as well. Another alternative for optimisation is the effective independence method (EIM) is a widely employed approach, notably presented by Kammer and Brillhart in 1996 and tailored for in-orbit modal identification of large space structures. The EIM leverages the determinant of the Fisher information matrix, providing a foundation for defining an optimal sensor array. Wang et al. (1998) have further advanced this concept with the kinetic energy method (KEM), a modified version of EIM. The KEM specifically aims to maximise the measured kinetic energy of the mechanical system by introducing a weighting mechanism involving the mass matrix, thereby yielding an energy matrix [11]

In practical terms, when deciding on the number of sensors and sampling frequency, designers face a delicate balance influenced by economic and technological constraints. The compromise between these factors is a crucial initial step. Subsequently, the implementation of MAC, EIM, or KEM becomes advisable to delineate optimum sensor placements and assess the expected covariance matrix of the coefficient response. It's worth noting that the economic evaluation should extend beyond merely considering the number of sensors, as the positions and other characteristics of the networks can significantly impact the total cost. This underscores the complexity of the decision-making process, where economic efforts must be carefully weighed against the desired precision and efficiency of the sensor array, aware of this situation some authors consider placing in the decision-making context a proper engineering judgement base among many in research and past experiences.[11] [25]

According to the information previously presented a wider and brief picture of the OSP methods will be presented and the most relevant characteristics of the 2 branches shall be discussed in the following lines.

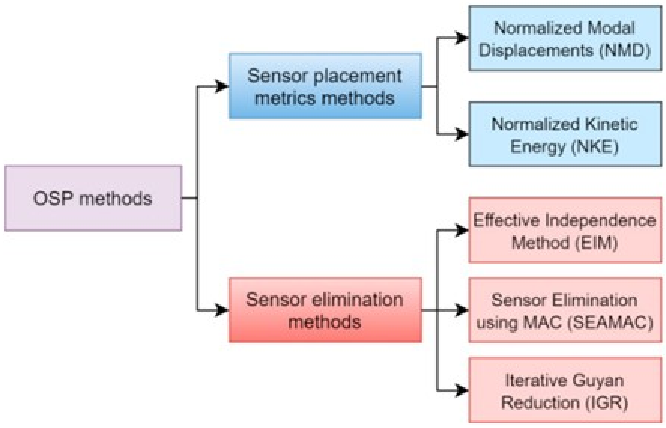

Figure 2.7: OSP Methods performed by [26]

Sensor Placement Metrics Methods:

Sensor placement metric methods serve as fundamental tools for optimising the selection and deployment of sensors. These methods rely on sophisticated sensor placement matrices to discern candidate sensors strategically. Among the myriad techniques, the Normalized Modal Displacement (NMD) method stands out, intricately tied to the observability of target modes through the lens of weighted modal displacement. While various modal displacement approaches exist, the preference for weighted modal displacement in the NMD method is not arbitrary; it aligns with the recommendations outlined by FEM tools (2021). This deliberate choice emphasises the significance of incorporating weighted modal displacement as a pivotal metric for effective sensor placement. In a parallel vein, the innovative Normalized Kinetic Energy (NKE) method, focuses on the distribution of kinetic energy considering that it assumes a central role as the metric for identifying locations characterised by substantial modal participation. This dual exploration of NMD and NKE methods illuminates the nuanced strategies employed in sensor placement, paving the way for a deeper understanding of how these methodologies contribute to advancing modal analysis and structural dynamics research. [26]

Sensor Elimination Methods:

The intricacies of sensor elimination methods come to the forefront with the overarching goal of refining the initial pool of sensors and examining the impact of elimination criteria. A prominent approach in this domain is the Effective Independence Method (EIM), as outlined by Demirlioglu et al. (2023). EIM strategically employs the linear independence of mode shapes as a pivotal elimination criterion, ensuring the avoidance of singularity in the Fisher information matrix. When Kammer introduced this methodology, adopted a distinct approach by seeking the optimal set of degrees of freedom for sensor placement among man-provided candidate locations. This method relies on the fundamental principle of ensuring linear independence among the mode shapes considered in the analysis, thus contributing to the intricate landscape of sensor elimination strategies [26][6]

The Modal Assurance Criterion (MAC) serves as well as a widely adopted tool for comparing mode shapes, calculating the squared cosine of the angle between two such shapes and like this eliminating redundant elements. A further application of MAC would be Sensor Elimination using MAC (SEMAC) method, the sensor elimination process aims to minimise the off-diagonal terms of the MAC matrix. Complementing these strategies is the Iterative Guyan Reduction (IGR) method, presented by Ostachowicz et al. (2019), which ingeniously eliminates degrees of freedom characterised by small mass-to-stiffness ratios. As the IGR method computes reduced mass and stiffness matrices, it effectively refines the sensor configuration by systematically eliminating less influential components from the structural model.[26]

Closing the ideas provided for sensor elimination methods, the Euclidean norm in EIM is employed to reflect signal strength indices at candidate nodes, providing a comprehensive evaluation. Modal Assurance Criterion (MAC) thresholds play a crucial role in determining the number of sensors, emphasising the importance of accurately estimating target mode shapes.

To infer modal estimates for unobserved locations. The Kriging model, expressed as a sum of linear regression and random error, utilises a weighted sum of known neighbours. The random error is assumed as the realisation of a stochastic process This comprehensive exploration of OSP techniques, signal strength evaluation, and the utilisation of statistical tools like Kriging contributes to the ongoing discourse on optimising sensor configurations, providing valuable insights into the process of structural health monitoring and damage detection [6][5]

2.3 Modal Identification

The importance of understanding the modal characteristics of structures becomes highly relevant in the context of ensuring safety and practicability. In the event of unforeseen dynamic events, such as earthquakes, the knowledge derived from modal analysis becomes instrumental in guaranteeing the structural integrity of buildings. Recent research has not only dealt with the immediate effects of earthquakes but has also focused on investigating the long-term impacts, including damage induced by past seismic events and particularly the role of non-structural elements such as masonry infills in influencing structural behaviour [8]. This emphasises the evolving nature of structural dynamics research, seeking to comprehensively address the complexities associated with real-world structural responses.

Two primary methods for experimentally identifying the dynamic parameters of structures are widely employed in contemporary research: Experimental Modal Analysis (EMA) and Operational Modal Analysis (OMA) [13] . EMA involves exciting the structure with known inputs, such as impulse hammers, drop weights or electrodynamics shakers, and subsequently measuring the structural response. These methods provide valuable insights into modal characteristics, including natural frequencies, damping ratios, and mode shapes, which are essential for model analysis, validation, and overall structural safety [13]. OMA will be further addressed as an independent section, considering the relevance of this methodology for the study of existing structures.

Modal testing, with its roots in advanced mechanics and aerospace engineering, has expanded its applicability to civil engineering, especially concerning historical masonry structures [13] Originally designed for both input and output measurements, modal parameters have become integral in refining finite element models. This evolution is particularly notable in the context of vibration tests applied to historical masonry structures, showcasing the adaptability of modal testing methodologies to diverse structural scenarios [13]. According to the Brincker criterion, a key concept vital in the process of ensuring the accuracy of modal properties requires time series data collected be at least 1000 times longer than the fundamental period estimated period. Some literature advocates for an even more extensive period of 2000 times longer, highlighting the precision required in capturing the intricate dynamics of structures through modal analysis [16]. This criterion serves as a guiding principle for experimental modal analysis, ensuring robust and reliable outcomes in the study of structural dynamics.

2.3.1 Operational Modal Analysis

In Operational Modal Analysis (OMA), a distinctive approach is considered, in this case the structure is excited by an unknown input force, primarily ambient vibrations induced by factors like traffic loads, wind, and waves [13]. Unlike Experimental Modal Analysis (EMA), OMA does not require external excitation sources, making it an attractive methodology for dynamic parameter identification. The structure's response to ambient conditions is measured, providing valuable insights into modal characteristics. This method proves particularly advantageous in scenarios where traditional external excitation may be impractical or undesirable, allowing for the dynamic assessment of structures under natural operating conditions [13].

The integration of OMA results into Finite Element Models (FEMs) offers a powerful means to define material and unknown section properties accurately [26]. This calibration, based on operational modal analysis results from ambient vibration testing (AVT) using accelerometers, enhances the fidelity of FEMs, providing a more realistic representation of the structural behaviour. The use of environmental vibrations as a means of dynamic identification is emphasised as a valid method for strategic structures. OMA, through its ability to capture responses under high-energy dynamic and environmental excitation, contributes significantly to the development of numerical models that estimate structural responses under natural excitation such as wind or adjacent traffic [8].

Environmental vibration tests, categorised under OMA, have become a prominent experimental method for evaluating the dynamic behaviour of structures on a large scale, eliminating the need for specific excitation equipment. This approach minimises interference with the ordinary use of the structure, enabling in situ monitoring and dynamic identification of strategic structures [8]. The advantages of this approach include speed of execution, low meddling, ease of algorithm implementation, precision of results based on experimental OMA data, and the ability to model complex structures in a straightforward manner [8].

One of the key objectives of the OMA dynamic identification process is to establish a reliable numerical model, typically based on Finite Element modelling. This model serves as a foundation for further assessments, potentially reducing the need for extensive on-site or laboratory tests. It becomes a valuable tool for evaluating the effectiveness of interventions related to rehabilitation or strengthening, supporting continuous monitoring for damage assessment[16]. The inherent capability of OMA to excite global vibration modes under normal surrounding conditions further underscores its utility in comprehensive structural dynamic assessments [23]

2.4 Deriving Modal Parameter Identified using OMA

The integration of in-situ dynamic tests into the structural safety assessment approach is almost mandatory for validating numerical models. Operational Modal Analysis (OMA) emerges as a valuable tool in this regard, offering experimental data that facilitates the updating process of Finite Element (FE) models. This updating process is crucial to estimating accurate structural properties, and its primary goal is to minimise disparities between numerical and experimental modal parameters—such as frequencies and modal forms—bringing the numerical model closer to the experimental one [8]. Validated FE models are useful for evaluating the structural operativity of strategic buildings, a fundamental aspect in emergency management scenarios. Ensuring that these critical structures do not suffer damage compromising their operation within the urban system's Emergency Limit Condition (ELC). [8].

The Seismic Model from Ambient Vibration (SMAV) methodology, founded on the extraction of experimental modal parameters, such as modal frequencies and mode shapes, forms the basis for calculating the seismic response of structures through dynamic linear analysis [8].

As AVT provides only out-put data it's clear that frequency response function (FRF) or impulse response functions (IRF) are not an outcome of the calculation therefore exploring modal parameter identification methods is required, the theoretical review recognises the broad of techniques available. Researchers often employ multiple methods within the same survey to compare results. The analysis of data can be conducted in the time-domain or frequency-domain, leading to the two most commonly used techniques for modal parameter identification in Operational Modal Analysis: Frequency Domain Decomposition (FDD) and Stochastic Subspace Identification (SSI) [16]. Output-only modal identification methods, widely used in Structural Health Monitoring (SHM), span the time domain, frequency domain, and time–frequency domain, offering a comprehensive approach to understanding structural behaviour [29]. These methodologies collectively contribute to a nuanced exploration of modal parameters, enriching the understanding and applicability of modal analysis in diverse engineering contexts.

2.4.1 Time Domain Methods

Time-domain methods encompass a range of techniques, and SSI stands out among them. The Ibrahim Time Domain (ITD) method, auto-regressive-moving-average (ARMA) model-based time-series method, the eigensystem realisation algorithm (ERA), and natural excitation technique (NExT) are among the diverse set of approaches in the time-domain domain. Each method has its unique strengths, and the SSI method, with its solid mathematical foundations and proven accuracy, plays a crucial role in advancing modal parameter identification techniques in civil engineering [29].

Considering the Stochastic Subspace Identification (SSI) technique stands out as a prominent time-domain method in the field of modal parameter identification. This technique involves the identification of statistical state space matrices from time data, leading to the extraction of modal parameters through the eigenvalue decomposition of these matrices, thereby obtaining the natural frequencies of the system. The modes are subsequently identified through stabilisation diagrams that visually represent modal parameters. In the literature, SSI is presented in two distinct variants, each operating on different data sets [16].

SSI has gained widespread adoption due to its unique merits, including solid mathematical foundations, high accuracy, and robustness. Proof of this is the verified similar result when compared to the peaks of the PSD Matrix for natural frequencies. This method is particularly favoured in civil engineering for modal parameter identification. Notably, the SSI technique is often preferred when closely spaced frequencies are expected, especially in scenarios involving symmetry, where frequency domain methods face challenges in estimating such modes [13]. Moreover, in applications involving continuous monitoring, SSI offers advantages. Automated modal identification algorithms, coupled with multivariate statistical analysis or Principal Component Analysis (PCA), can effectively mitigate environmental effects, and detect structural damage, highlighting the versatility of SSI in addressing real-world challenges [16].

The fundamental approach of the SSI method for modal identification involves establishing a state-space model based on the dynamic responses of the target structure. Subsequently, modal parameters are estimated by analysing the output and state matrices derived from the established state-space model. This approach underscores the systematic and mathematical meticulously employed in the SSI method for extracting meaningful modal information from structural responses [29].

2.4.2 Frequency Domain Methods

In the category of frequency domain methods, representative techniques include the Peak-Picking method, Frequency Domain Decomposition (FDD), and Enhanced FDD (EFDD). These methods share a common principle, focusing on the peak values of power spectral density functions that are proximate to the natural frequency. The Peak-Picking method, as a fundamental approach, involves selecting peaks from the power spectral density function to identify modal frequencies. Similarly, the Frequency Domain Decomposition (FDD) method operates by decomposing the system into single-degree-of-freedom systems and extracting modal frequencies from the peaks of the power spectral density function. The Enhanced FDD (EFDD) further refines this process, emphasising the enhancement of frequency domain decomposition for more accurate modal parameter estimation. These frequency domain methods collectively contribute to the rich landscape of modal analysis, providing versatile tools for researchers and practitioners in understanding and characterising structural behaviour [29].

Furthermore, the Frequency Domain Decomposition (FDD) technique stands as it relies on the diagonalization of the Power Spectral Density matrix (PSD), computed from registered accelerations through Singular Value Decomposition (SVD). Singular values and vectors obtained through peak picking in this matrix correspond to the amplification factors in resonance and mode shapes, respectively. FDD is a non-parametric technique, wherein modes are estimated through signal processing, demonstrating its efficacy in extracting modal information from dynamic responses. The estimation of modal damping ratios, along with natural frequencies, is often achieved through the Enhanced Frequency Domain Decomposition (EFDD), indicating the adaptability and refinement of FDD in addressing complex structural dynamics [16].

2.5 Modal Calibration

After structure Modal Parameters are derived a Finite Element Model (FEM) modal response calibration must be performed, such technique will be a key focus when deriving accurate models, and holds significance across various applications, like damage detection, health monitoring, structural control, and assessment. The meticulous consideration of details becomes paramount. While simplifications may be introduced during modelling, it is essential to acknowledge the complexity of actual structures, as evident in construction blueprints. Structural geometry and material homogeneity present uncertainties that necessitate model calibration by modifying such parameters with a certain unknown grade. Calibration tuning processes can be undertaken manually or through automatic model calibration using algorithms or specialised software. The former involves trial and error, guided by engineering judgement [13]. The global panorama of such techniques will be discussed below.

Higher accuracy in finite element (FE) models is reached along macro and micro updating methodologies. This traditionally involves a two-stage approach. Initially, parameters identified as highly influential, particularly stiffness and uncertainties in materials, are manually adjusted to align the model with experimental results. This hands-on adjustment provides an immediate improvement in the agreement between the model and real-world observations. Subsequently, a sensitivity analysis is executed to delve into the effects of uncertainties on modal parameters. This in-depth examination guides further manual updates to the model, ensuring a more precise representation of the structural behaviour [23].

Considering that the multi-phase approach required to achieve an accurate FE model emphasises the necessity of extensive experimental campaigns and high-fidelity FE modelling approaches. Classical geometrical modelling approaches, relying on idealised geometries and ignoring deformations or irregularities, are discouraged. A critical aspect highlighted is the reliance on a model updating process that considers dynamic or static behaviour. This recommended process serves to reduce input uncertainties and guarantee the accurate representation of the structural behaviour within the FE model [4].

The literature delineates the methodologies of model updating into deterministic and probabilistic approaches. Deterministic approaches, widely adopted for their simplicity and lower computational costs, remain the mainstream choice. However, probabilistic approaches offer a distinct advantage by allowing the quantification of model input parameters, thereby enhancing the accuracy and reliability of the results. Considering the deterministic approaches, the so-called multi-objective techniques stand out. These techniques seek optimum values for model inputs, aligning model outputs with multiple objectives simultaneously. Despite the increase in computational cost, the algorithm benefit lies in the quantification of uncertainty while at least one of the targets is satisfied without being tight by the rest of the solution [4].

The Deterministic approach may use the NSGA-II algorithm in processing the results therefore a Pareto front with a n number of dominant solutions depending on each case study will be obtained. The analysis of discrepancies in frequency and modal displacement terms yields optimal possible solutions. The robustness of these solutions is highlighted by the genetic algorithm avoiding the process of local solutions. Furthermore, the automation of the workflow in this process facilitates its implementation in other case studies. This automation, coupled with the global analysis capabilities, positions multi-objective calibration as an ideal framework for applications ranging from digital twins to the development of damage prediction algorithms based on modal parameters, or even the analysis of extreme events [4].

Several recommendations focused on exploring the significance of various material and geometric parameters. The references from [23] and [15] provide insights into the sensitivity of key elements and proposes modelling approaches for enhanced accuracy.

Reference [23] delves into the sensitivity of elastic modulus, particularly in reinforced concrete (RC) shell elements and masonry (CM) wall elements. The elastic modulus of these elements exhibited higher sensitivity to torsion and front-to-back modes, however, torsion and second sway modes are also triggered depending on the floor plan of the structure, either way with the highest sensitivity in torsional mode provides a control parameter for iterative manual calibration.

The mass density of different elements emerged as a crucial parameter [23]. The mass was identified as the most influential, equally affecting torsion, front-to-back, and second sway modes.

The thickness of shell elements played a pivotal role, displaying the highest sensitivity coefficients across all target modes [23]. Conversely, other shell elements exhibited relatively small sensitivity, emphasising the specific importance of the upper-level element's thickness.

The density of nonstructural masonry walls, a composite material, demonstrated a wide range of possible density properties [23]. An initial assumption of mass density was studied based on physical meaningfulness, underlining the variability and importance of this parameter for the mass density parameter previously discussed.

The success of the FE model updating based on Ambient Vibration Test (AVT) [23] emphasises the high-quality test data, efficient modal identification, and reliability of the updating procedure. After reviewing the technical data it's clear that in the correlation between FE and AVT incorporating nonstructural components represents a significant contribution to both stiffness and mass. Notably, longitudinal masonry walls and transversal cavity walls influenced specific modes, illustrating the nuanced contributions of different structural elements.

Foundation conditions were found to be insignificant in terms of global modes of structure [23]. The elimination of localised modes associated with nonstructural cladding elements was successfully achieved using shell elements without bending capability, such. This rational approach is particularly applicable to slender elements.

In the context of infilled reinforced concrete (RC.) frame structures, reference[15] advocates for conventional modelling approaches based on beam and shell elements, dismissing the need for sophisticated numerical models for infills. The procedure, when applied to real structures, proved effective, leading to the development of a numerical model with significant predictive accuracy for both translational and torsional modes.

This section has explored the sensitivity of key parameters in civil structures particularising Masonry-related bodies and proposed innovative modelling approaches. The in-depth analysis of elastic modulus, mass parameters, and thickness, coupled with successful FE model updating and the elimination of localised modes, underscores the importance of considering various elements in structural analysis. Additionally, the proposed methodology for masonry panel characterisation and the endorsement of conventional modelling approaches for infills contribute to advancing the state-of-the-art in structural engineering. It´s applicability will be studied and further pushed in the upcoming chapters relating the methodology with 2 cases of study.

Chapter 3

Introduction to Messina Buildings

The University of Messina is an academic institution located in the northeast region of Messina Island, the university was founded in 1548 by Pope Paul III. Just over a century later, in 1678, the institution was closed following an anti-Spanish revolt. The University was later re-established in 1838 by King Ferdinand II and, apart from a brief closure due to the anti-Bourbon uprising of 1847, the university remained open and flourishing until the earthquake that devastated Messina in 1908 destroyed much of the University's facilities and equipment, as well as claiming the lives of many professors and students. However, as early as 1909, the Faculty of Law Salvatore Pugliatti reopened its doors, and in the subsequent years, the Faculties of Arts, Sciences, Pharmacy, and Medicine followed. Year after year, the University regained vitality, successfully overcoming even the period of reconstruction after the Second World War. Due to the uprising of the university and the crescent expansion of the faculties, the physical facilities are split among several buildings along the city, consequently, some characteristics of the analysed ones will be presented.[2].

Figure 3.1: Aerial View Messina University zone [2]

3.1 University Messina: Building Piazza XX Settembre

The building located in Piazza XX Settembre, Messina, is an academic building characterised by hosting within his rooms lectures, staff offices, libraries, auditoriums, and exhibition rooms. Is located near the historic centre of Messina (ME) between the streets: Anastasio Coco (North), Felice Bisazza (South), Piazza XX Settembre (West) and Giacomo Alfonso Borelli (East). It is also located near other strategic buildings such as the "Empedocle" Scientific High School to the south of the current position and the Main City Pharmacy to the west. The structure constitutes the central complex of the Science Department of Political and Legal Studies (SCIPOG) of the University of Messina. It stands in an area of relatively flat land that surrounds the perimeter of the institute with public roads. An important remark is the internal underground corridor (figure 3.2) between the basement of the structure and the surrounding ground.

Figure 3.2: Ground Beams connected to Structure´s Ground Level

This particular situation also considers connection beams at the level of the ground floor, acting as support and restraining the in-plane. The building is divided into three levels, one of which is a basement and two above grounds. The basement is accessible via two distinct staircases; a fourth level consists of the partial covering of the stair tower. The building borders are partly paved except for a perimeter that faces green areas. The entire building is spread over one covered area of approximately 1000 m2 for the basement and the ground floor, regarding the first floor the area becomes approximately 800 m2. The construction type of the building is mainly masonry mixed with a reinforced concrete structure with a prominent curb on the head.

Mechanical and geometrical properties will be derived in further chapters. However, as a contextualisation, the test plan proposed during a survey contract included both on-site and laboratory investigations destructive, semi-destructive or non-destructive. The investigations will characterise the structures from a material, geometric and detail point of constructive perspective.

Figure 3.3: Antique Photo University of Messina Piazza XX Settembre [2]

3.2 University of Messina: Building Via Concezione

The building houses the Faculty of Cognitive, Psychological, Pedagogical, and Cultural Studies. This complex is located at number 6 Concezione Street in Messina. On its surroundings can be found the tourist port of Messina (ME) between the streets: Gran Priorato (North), San John of Malta (South), Concezione (West) and Placida (East). It is located near other strategic units such as the prefecture to the east, the Carabinieri command to the south and the "Pascoli – Crispi" School to the west. The Juvara gym, located to the north of the building, appears to be an independent body, during surveys it was detected an empty cavity was detected which backs the starting hypothesis of independence from the building being analysed.

The structure is constituted of three levels, one of which is underground and two above ground level. The basement is accessible through two separate staircases. The semi-elevated floor can also be reached via a small ramp located in front of the main entrance on the public road. It is situated on a flat terrain, bordered to the north by other structures, and to the east, south, and west by public roads. Along the main facade of the building (Via Concezione), there are two small courtyards equipped with an external staircase providing access to the raised floor. The entire building covers an approximate indoor area of about 1,370 m2.

Figure 3.4: Aerial View University of Messina Building Via Concezione [2]

Chapter 4

Technical survey results from the University of Messina

In the months of July and August 2022, comprehensive structural assessments were conducted for both buildings in charge of L & R Laboratori e Ricerche s.r.l. The purpose of these investigations was a research project addressed to investigate the properties and characteristics of the structure. The research was conducted as part of the HCH LOW-COST GEOENGINEERING CHECK Research Project, focused on two concise buildings part of the University of Messina: the first one situated via Concezione 6, housing the Department of Cognitive, Psychological, Pedagogical Sciences and Cultural Studies, and the second one located in Piazza XX Settembre, hosting the Department of Political Science. The investigative process was carried out employing a low-cost multi-sensory system designed for the diagnosis, protection, and conservation of historical and cultural heritage, the methodology used involved both on-site and laboratory examinations, ranging from destructive to semi-destructive or non-destructive types. Reports detailing the findings were officially received on May 22, 2023, and subsequently reviewed on June 5. This documentation serves as a comprehensive account of the structural evaluations, describing the material, geometric, and construction aspects of the examined structures.

4.1 Technical survey results: Building located in Piazza XX Settembre,

In this section will be presented a brief description and photographic evidence of the methodology and test typology used in the characterisation of the University of Messina located in Piazza XX Settembre. Also, the quantity of inspections performed will be displayed in the following list:

A. Two (2) Endoscopic tests were performed for the characterisation of the masonry, one in the Stair A of the First Floor and the other one in the Stair A but at the ground level.

B. Fifteen (15) Visual identification essays were conducted on masonry and concrete elements, validating materials and dimensions of the elements. As seen in the next figure 4.1

Figure 4.1: Visual Identification Survey 6 Piazza XX Settembre L & R Laboratori e Ricerche s.r.l. July 2022

C. Twelve (12) Magneto metric investigations with Pacometer test equipment.

D. Two (2) core samples were taken from concrete with a relative compressive strength test. As seen in the next figure 4.2

Figure 4.2: Concrete Core Sampling Survey 7 Piazza XX Settembre L & R Laboratori e Ricerche s.r.l. July 2022

E. Six (6) Reinforcement sampling and related tensile test.

F. Two (2) Simple flat jacks for estimating the in-situ stresses present in the investigated wall section.

G. Two (2) double flat jacks for the mechanical characterisation (compressive resistance) of the load-bearing walls in question.

For all the previous tests the precise locations are reported in the figures below:

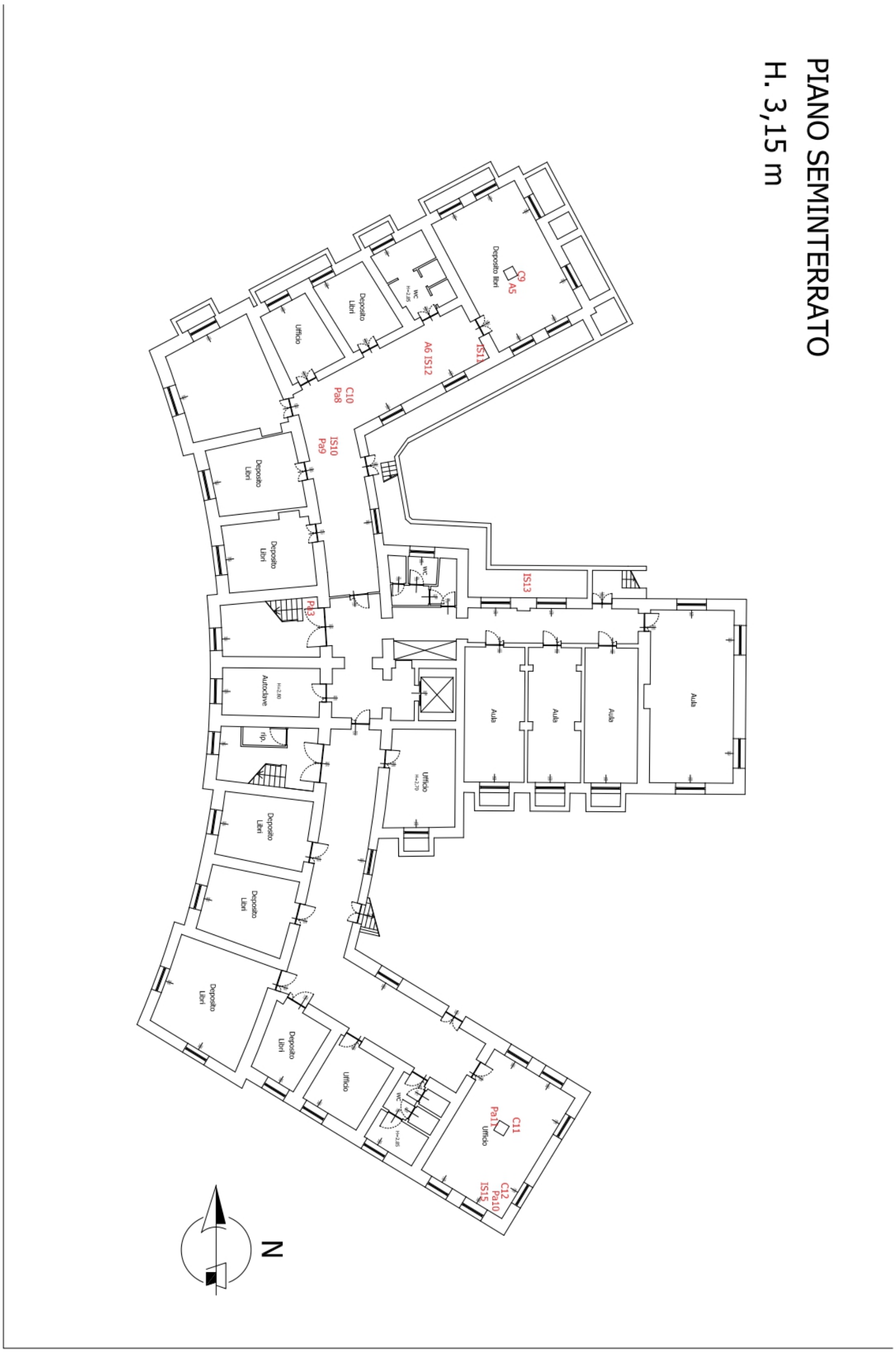

Figure 4.3: Floor Plan: Basement Piazza XX Settembre Survey Marks

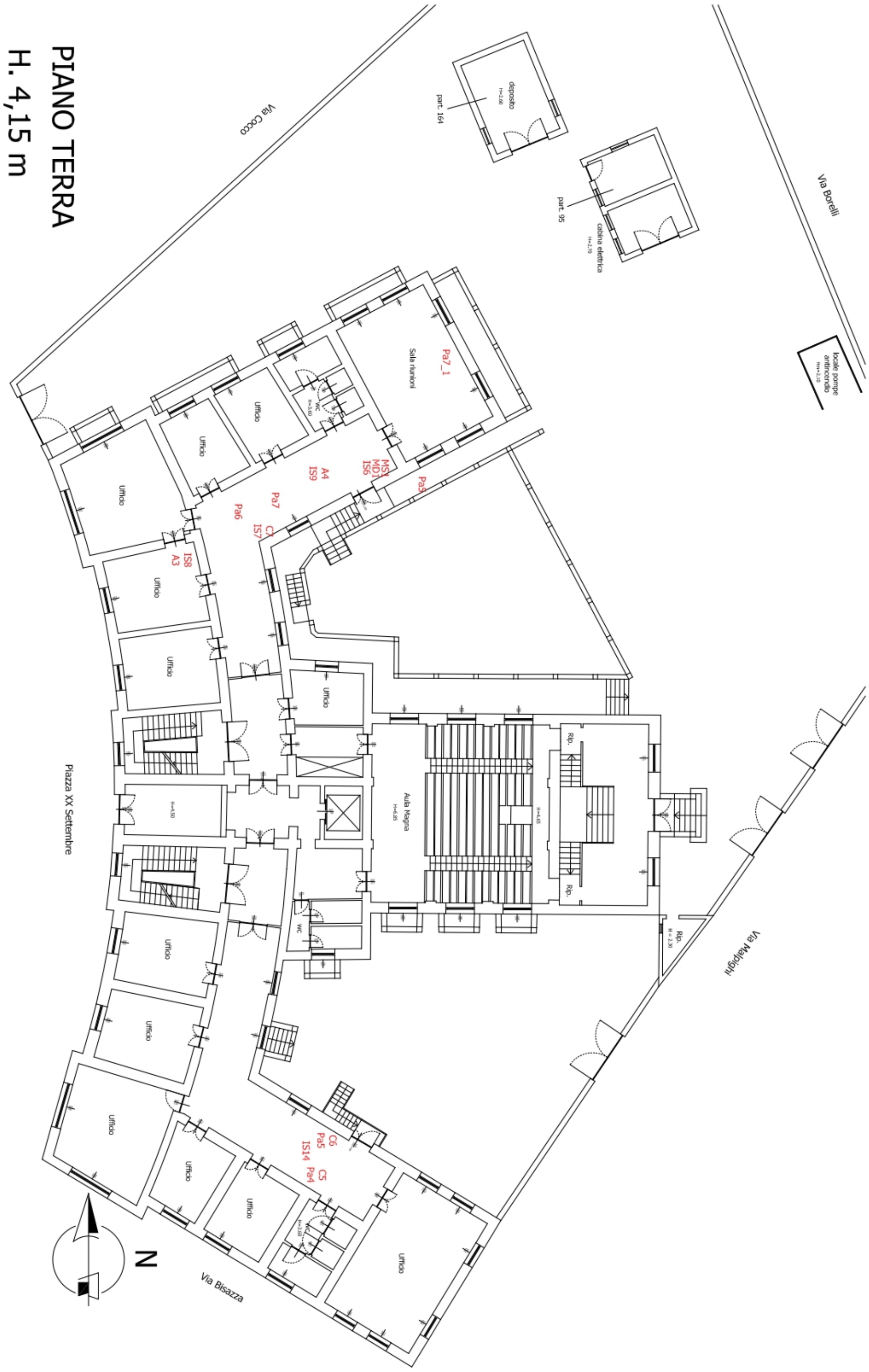

Figure 4.4: Floor Plan: Ground Floor Piazza XX Settembre Survey Marks

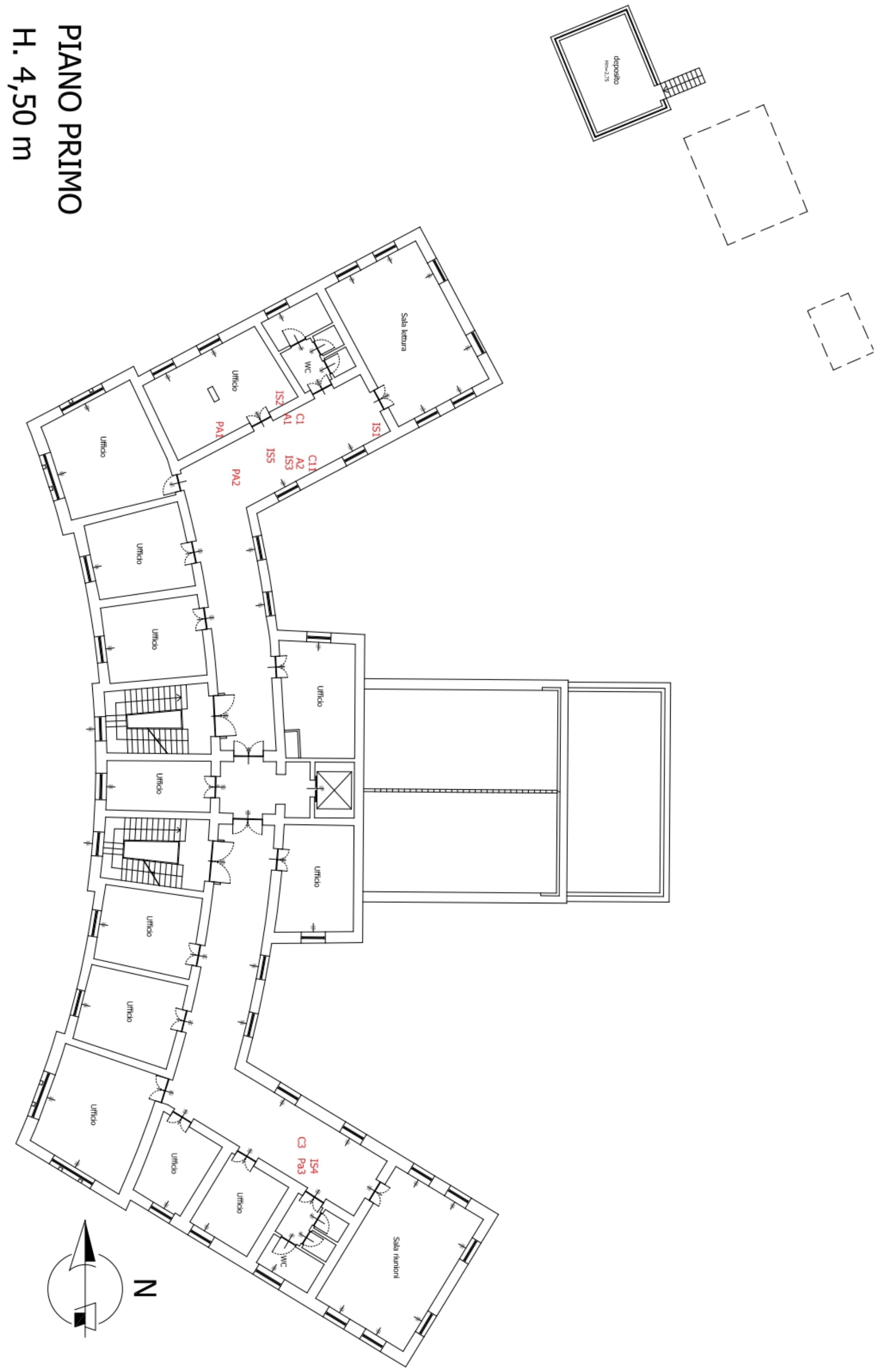

Figure 4.5: Floor Plan: First Floor XX Settembre Survey Marks

Observations regarding the results derived from the test performed in the laboratory from the samples obtained in-situ by L (&) R Laboratori e Ricerche s.r.l. will be summarised and presented below:

A. The structural diagrams and explanatory images obtained from the endoscopic examinations conducted on the walls reveal the presence of masonry made using solid bricks with the presence of mortar joints between elements. Also, the presence of perimetral concrete elements was noticed. Those contribute to the definition of a confinement frame for the masonry itself.
B. The tests carried out on the walls reveal a good degree of bonding as well as an optimal state of conservation of the masonry. Furthermore, the masonry from the surveys appears quite regular.
The tests conducted on the main concrete elements allow us to ascertain good maintenance of the cement mortar and the relative reinforcement, which is not corroded or with ongoing corrosion processes. The analysed reinforced concrete masonry confinement elements are characterised by longitudinal and transverse reinforcements for several typologies of cross sections, such elements will be called secondary frame elements. The principal and therefore major elements had bigger dimensions of the cross sections and the beam and columns elements conserved a consistent homogeneity.
Specifically at the slabs, the presence wood of and plaster from work leftovers cast a solid non-reinforced concrete floor slab.
C-D-E. The cores extracted and the concrete specimens despite the location of sampling, tested in the laboratory showed relatively uniform characteristic values. For the building in Piazza XX Settembre results are presented below:

Density mass:

- Average 2218 kg/m3.
- Maximum 2291 kg/m3.
- Minimum 2166 kg/m3.

Compressive resistance:

- Average 12.3 MPa.

- Maximum 16.1 MPa.
- Minimum 10.2 MPa.

Regarding the reinforcement bars: The depth of carbonation is not at a very precise value but varies between 2-5 cm and 10-20 cm. The reinforcing bars extracted and tested in the laboratory showed representatively homogeneous characteristic values. For the building via Piazza XX Settembre:

Yield stress

- Average 287 MPa
- Maximum 349 MPa.
- Minimum 260 MPa.

Breakdown voltage

- Average 409 MPa.
- Maximum 505 MPa.
- Minimum 352 MPa.

F. The in-situ stresses of the single flat jack tests were carried out on the ground floor:

- σ c=0.096MPa – Ground floor
- σ c=0.000 MPa – First floor

The significantly low-stress value detected, performing an analysis is evident that for an unloaded section in correspondence with the first floor-scale, A adopting the specific weight values equal to 18 kN/m3 (table C8.5.I of the NTC2018) calculated stress for position acting on the masonry is an order of magnitude higher than that obtained from the one detected on the tests on the ground floor, therefore this value will be considered as neglect-able.

G. Two tests were conducted with a double flat jack test which showed:

Ground floor

- Breakdown stress equal to 1.74 MPa.
- Elastic modulus at the 1st and 2nd cycles equal to 891 and 874 MPa respectively.

First floor – Staircase A

- Breakdown stress equal to 1.96 MPa.
- Elastic modulus at the 1st and 2nd cycles equal to 2815 and 2536 MPa respectively.

From the tests conducted, a clear lack of homogeneity in the results appears evident. Is easily spotted that there is a difference of an order of magnitude between the values of the elastic modulus obtained from the tests carried out on the two levels. The estimates obtained by adopting the values suggested by the standard are reported in Table C8.5.I of the NTC2018, the value of the average compressive strength in solid brick and lime mortar masonry varies between 2.6-4.3 N/mm2 therefore the value considered for those blocks will be subject to reference values found in the National Anex for Elastic modulus and compressive strength.

4.2 Technical survey results: Building located in Via Concezione.

A procedure like the one applied in Piazza XX Settembre will be adopted, providing a concise description and photographic evidence of the methodology and testing methods used for the characterisation of the University of Messina this time the building located in Via Concezione. The subsequent list will also outline the number of inspections conducted.

A. Two (2) Endoscopic tests for the characterisation of the masonry.
B. Fourteen (14) Visual essays on masonry and concrete elements.
C. Ten (10) Magneto metric investigations with Pacometer test.
D. Six (6) core samples were taken from concrete with a relative compressive strength test.

Figure 4.6: Core Sample Survey 3 Building Via Concezione L & R Laboratori e Ricerche s.r.l. August 2022

E. Six (6) Reinforcement sampling and related tensile test.

F. Two (2) Simple flat jacks for estimating the in-situ stresses present in the investigated wall section.

G. One (1) Double flat jack for the mechanical characterisation (compressive resistance) of the load bearing.

Figure 4.7: Double flat jacks for the mechanical characterisation Building Via Concezione L & R Laboratori e Ricerche s.r.l. August 2022

For all the previous tests the precise locations are reported in the figures below:

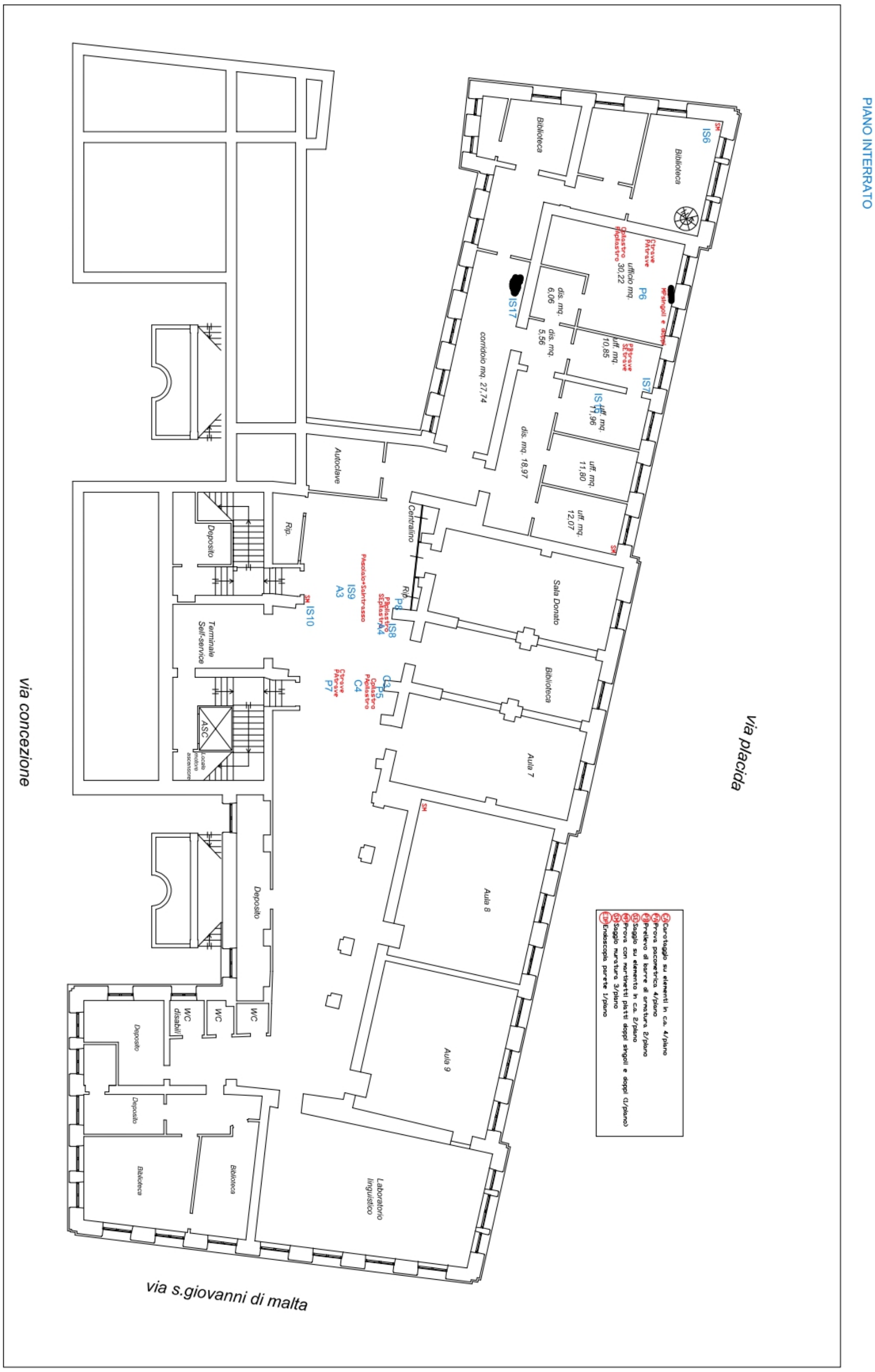

Figure 4.8: Floor Plan: Basement Via Concezione Survey Marks

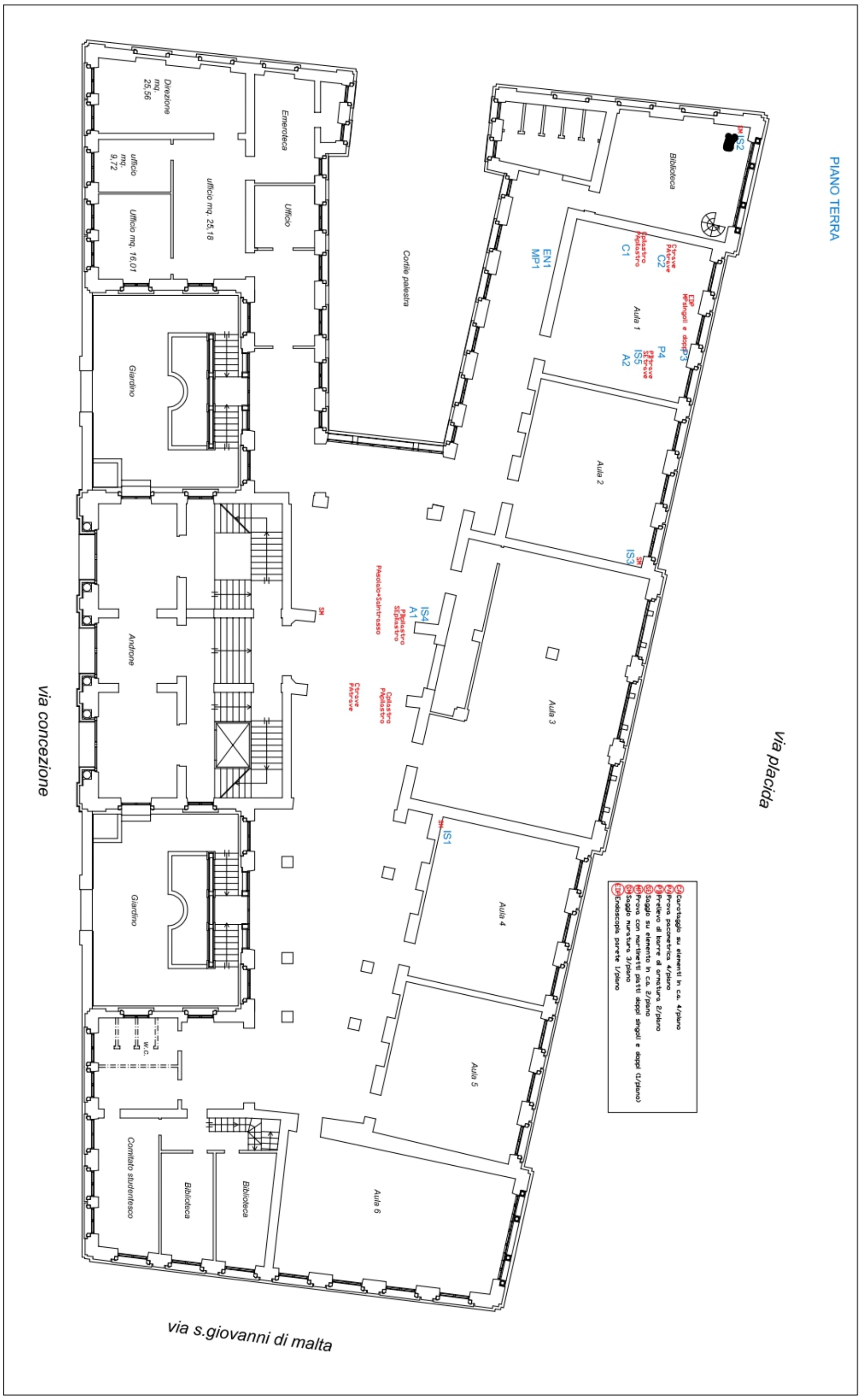

Figure 4.9: Floor Plan: Ground Level Via Concezione Survey Marks

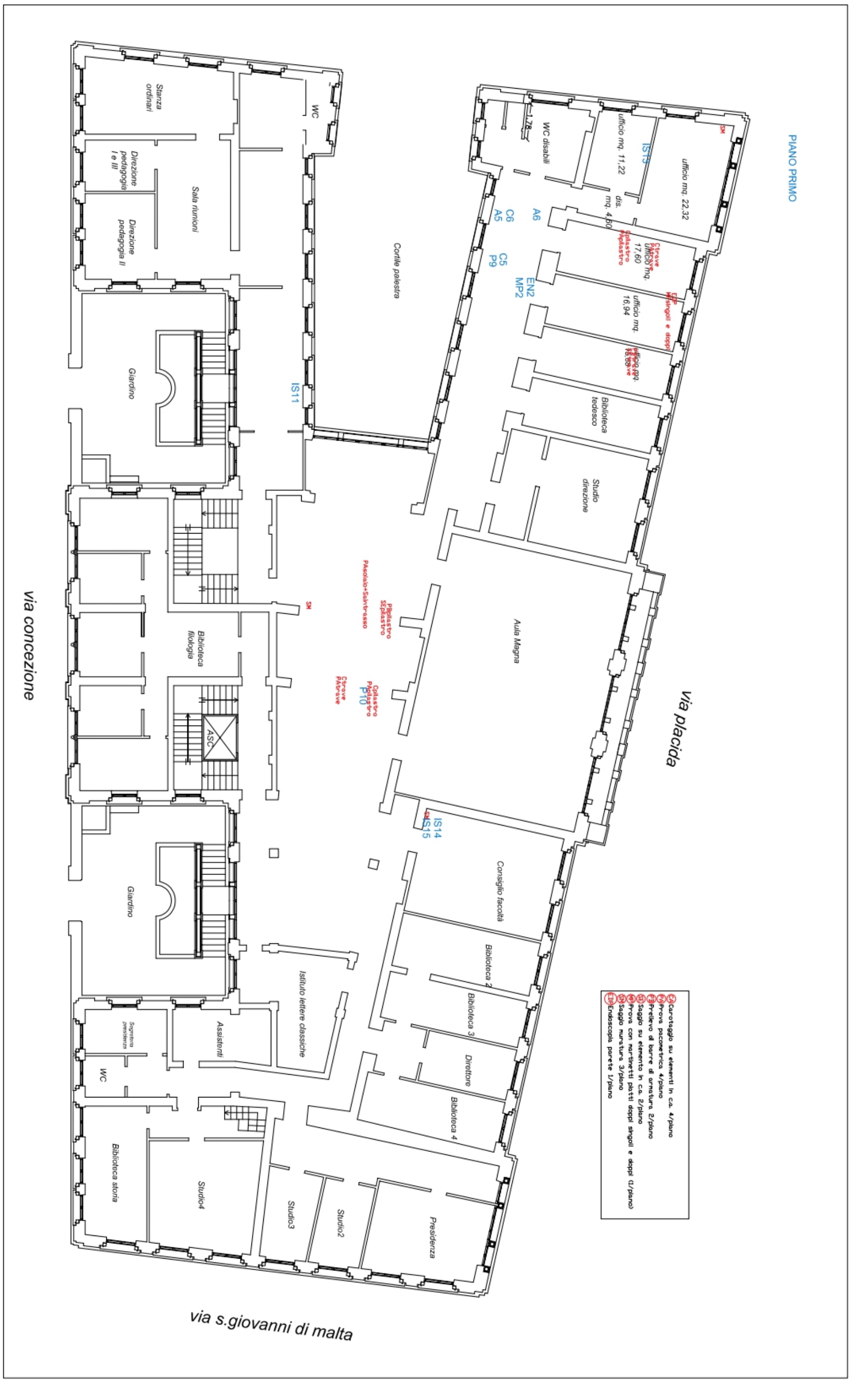

Figure 4.10: Floor Plan: First Level Via Concezione Survey Marks

Observations regarding the results derived from the test performed in the laboratory from the samples obtained in the inspection for the building located in Via Concezione by L& R Laboratori e Ricerche s.r.l. will be summarised and presented below:

A. The structural diagrams and detailed images obtained from the endoscopic examinations conducted on the walls reveal the presence of masonry made using solid bricks with clear indications of mortar stiffeners which contribute to the definition of a confinement frame for the masonry.

B. The tests carried out on the walls reveal a good degree of bonding as well as an optimal state of conservation of the masonry. Furthermore, the masonry appears quite regular from the surveys although the presence of rough-hewn stone elements of various sizes is also noted. The analysed reinforced concrete masonry confinement elements are characterised by longitudinal and transverse reinforcements for several typologies of cross sections, such elements will be called secondary frame elements. The principal and therefore major elements had bigger dimensions of the cross sections and the beam and columns elements conserved a consistent homogeneity.

C-D-E. The cores extracted and the concrete specimens tested in the laboratory showed representatively homogeneous characteristic values. For the building in via Concezione:

Density mass:

- Average 2274 kg/m3.
- Maximum 2355 kg/m3.
- Minimum 2131 kg/m3.

Compressive resistance:

- Average 11.9 MPa.
- Maximum 16.6 MPa.
- Minimum 7.5 MPa.

The depth of carbonation settles at around 5 cm with a peak at 10 cm for the 6 samples examined for the building via Concezione. The reinforcing bars extracted and tested in the laboratory showed homogeneous characteristic values. For the building in via Concezione:

Yield stress:

- Average 263 MPa.
- Maximum 314 MPa.
- Minimum 225 MPa.

Breakdown Stresses:

- Average 378 MPa.
- Maximum 436 MPa.
- minimum 312 MPa.

F. The in-situ stresses of the single flat jack tests were carried out on the ground floor:

- σ c=0.056 MPa – Ground floor
- σ c=0.04 MPa – First floor

The relevance of this test is the significantly low-stress value detected, performing an analysis is evident that for an unloaded section in correspondence with the first-floor scale, A adopting the specific weight values equal to 18 kN/m3 (table C8.5.I of the NTC2018) calculated stress for position acting on the masonry is an order of magnitude higher than that obtained from the one detected on the tests on the ground floor, therefore this value will be considered as neglect-able.

G. A single test was conducted with a double flat jack which showed:

- Breakdown stress equal to 0.87 MPa.
- Elastic modulus at the 1st and 2nd cycles equal to 753 and 619 MPa respectively.

The estimates obtained by adopting the values suggested by the standard are reported in Table C8.5.I of the NTC2018, the value of the average compressive strength in solid brick and lime mortar masonry varies between 2.6-4.3 N/mm2 therefore the value considered for those blocks will be subject to reference values found in the National Anex for Elastic modulus and compressive strength.

4.3 Thermographic data concerning the structural configuration of unexamined elements:

In this section, some relevant thermography images for the two buildings of interest are presented. Some substantial construction homogeneities are presented using mainly block masonry walls confined by mainframes (Columns and beams) and a secondary frame that surrounds the openings and is connected to the main frame by secondary RC elements (Figure 2.1). Figure 4.11 also shows the secondary beams on the upper floor of the main hall.

]

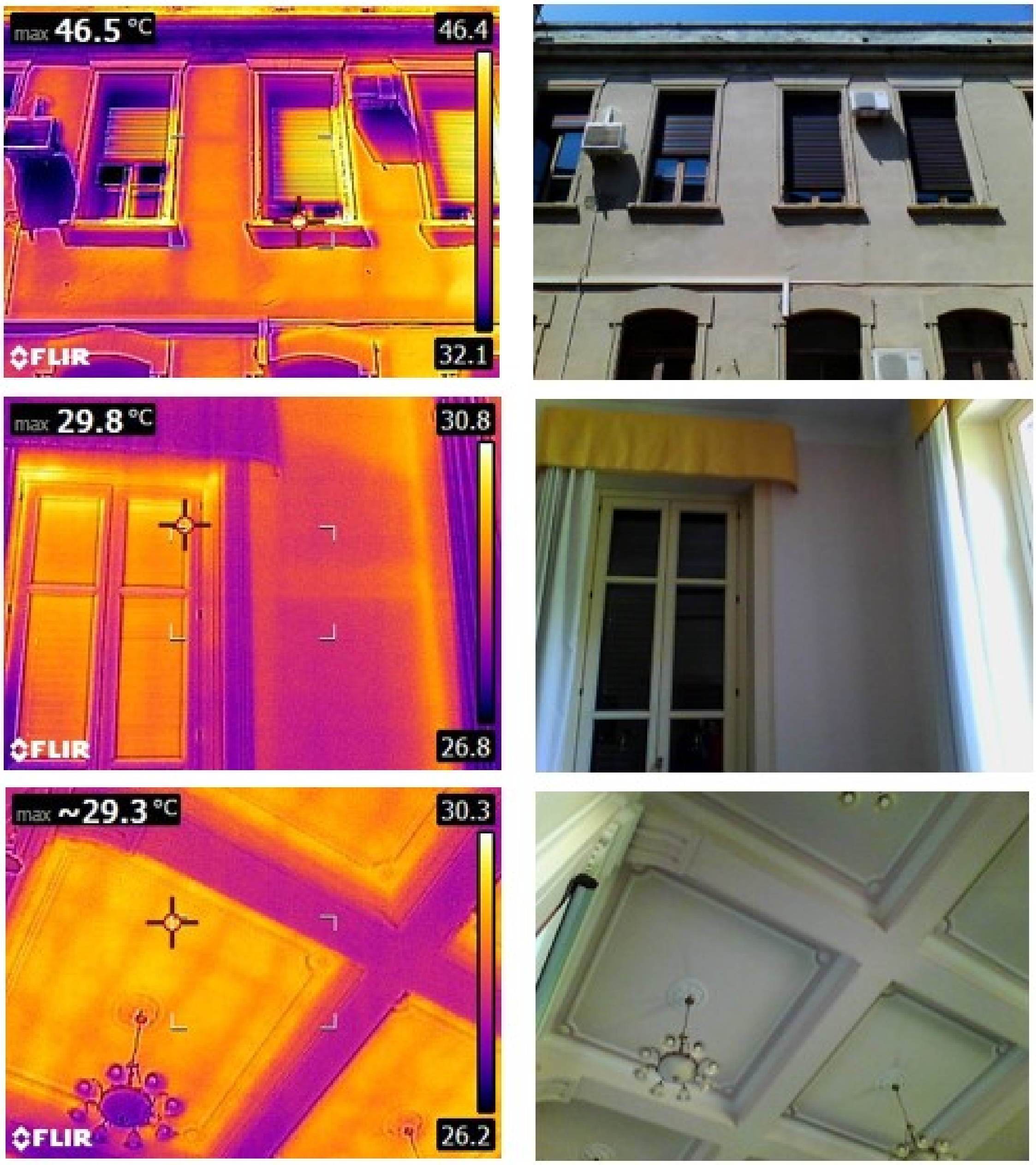

Figure 4.11: Thermographies of both buildings Facade University of Messina

Is evident that (Figure 4.11) represents in a very accurate way the construction method exposed in previous chapters as confined masonry (Figure 2.1). This is also consistent with the bibliographical research where was clearly established that after the Messina earthquake that occurred in 1908 much of the collapse infrastructure was rebuilt using a confined masonry technique and the one that remained stand was retrofitted using a consistent approach.

Now it´s reasonable to acknowledge the consistency of the structural characteristics for the two buildings of interest, in accordance with the similar typology and construction period that characterises both. In materials there is a rather minor difference, however, during the modelling chapter and subsequent model calibration, this aspect will be further targeted.

Also, regarding the number of investigations, particularly the measurements conducted with jacks, has been restricted to the “pertinent” structures. Notably, it is observed that the mandatory minimum number of investigations outlined in the 2019 Circular of the prevailing NTC2018 Regulation has not been performed.

These circular mandates a minimum quantity of investigations and tests to meet the stipulated standards, constituting a threshold of a minimum number of examinations and tests as presented next:

• The quantity and arrangement of the reinforcement verified for at least 15 % of the "primary" elements such as beams and pillars.
• 1 concrete specimen, per 300 m2 of building floor, 1 reinforcement sample per building level of the structure:

For the lack of representative information, the geometric and mechanical properties of the materials obtained from the tests will be assumed to be consistent also for all the structural elements of the same type or also for the ones that perform similar functions to the one of which the report has specific information.

In addition to what has already been reported above, for the purpose of this academic work, the level of knowledge of the structure is considered to be sufficient by virtue of the scope of the analysis that will be conducted in the following chapter. The dynamic identification of the structures under study will be achieved by solving an eigenvalue and eigenvector problem (modal analysis). In this work, NO structural verification will be conducted. In conclusion, after the analysis of the reported information is clear that compliance with the minimum number of investigations and tests must be mandatory in compliance with the legislation in force on the matter to conduct further analysis and even Deeper as a result of such labours.

Chapter 5

Survey Campaign Case of Study: Sensor Placement and Data Collection

Considering the methodologies available for the OSP and OSN, the procedure followed during the survey plan and subsequent survey campaign will be presented. This procedure has some consideration regarding technical and engineering expertise, in the closing remarks such thoughts will be further discussed.

The cases under study require to formulation of independent survey strategies, even if the buildings have some important resemblance. The beginning of the procedure conceives important consideration, applying such universally valid statements along with the inventory of available equipment and its limitations the survey plan was developed:

General consideration.

Sensors Typology:

In the dynamic identification field particularly for civil structures and infrastructures, the use of sensors (velocimeters or accelerometers) specifically designed for the purpose, whether tri-axial or uni-axial, is generally recommended. For these specific scenarios, 6 tri-axial velocimeters were available. As the survey required to preserve the normal use of the building and avoid further damage during the investigation OMA methodology was chosen, particularly the trend considered as AVT, for the sensor provides satisfactory sensitivity characteristics such as being able to capture environmental micro-tremors, particularly effective for rather rigid structures like the buildings in question, with main frequencies above 4Hz.

Vibration measurement examinations were conducted to delineate the modal properties of both structures. In relation to the monitoring system, the acquisition chain was constituted by seismic velocimeter SM-6, being a digital grade geophone based on the popular SM-4 design, it has a coil excursion (4mm) which makes it suitable in a vertical mode for lower frequencies and for the force of one G is exceeded. In horizontal mode, the large coil excursion of 10Hz makes it suitable for shear wave detection with planting faults of up to 20° without resorting to cumbersome levelling devices. The following table obtained by the manufacturer provides further information regarding the main technical aspects of the geophone.[1]

Model	**SM-6**
Natural Frequencies	***4.5 Hz***
Frequency Tolerance	.+/- 0.5Hz
Standard Coil Resistances +/- 5%	71 ohms, 375ohms
Transduction for 375 ohms coil	0.73
V/cm/seg	*0.29*
O.C.Damping +/- 5%	56%
Distortion with driving velocity of 1.8cm per second P-P at 12Hz	<0.2%
Maximun coil excursion	4mm P-P
Weight of moving mass	11.1 grams

Table 5.1: Technical Specifications Sensor SM-6 provided by [1]

Elevation location of the triaxial sensors:

OSP methodologies have derived several preliminary concepts, the idea was to implement such recommendations in the identification of desirable locations. In the output-only identification of the buildings, the first concept used was to target the sensor position on the last two floors (which should vibrate relatively more), second, the stiffest edges of the floors were proposed for positioning. Although the floors of the buildings were made of 20cm thick reinforced concrete (RC) supported by a lattice of beams also in RC, placing the sensors on the floors was avoided, as these would inevitably also be stressed by the vibrations of the floor itself. Finally, to corroborate the previous two concepts a visual inspection was performed with the idea of validating the continuity, stiffness, and integrity of the floors, as it was accepted now the possible elevation set-up was chosen and with such configuration proposed the identification of higher order bending modes should be achievable.

In-Plane location of the triaxial sensors:

For the in-plane sensor configuration, placement was meticulously considered as far as possible outside the total shape of the building. This strategic positioning aligns with the previously underpinning hypothesis of a rigid plane behaviour, enabling the identification of floor rotations at two designated points—preferably situated at diagonally opposite ends. This hypothesis underwent scrutiny in accordance with the NTC2018 regulations prior to implementation. To account for the unique layouts of the structures, specific sensor placements, called "local setups," were devised. These setups focused exclusively on delimited areas, such as pavilions which are characterised as isolated protrusions from a structural standpoint. In these instances, sensors were also situated at diagonally opposite corners of the shape to facilitate the identification of localised torsional modes as well.

On the orientation of the channels (Reference System.):

If for instance the reference system is considered to align with existing structural elements like beams it would have to involve additional post-processing calculations to effectuate the transformation of local coordinates into the global framework, a procedure that inherently introduces computational inaccuracies. To mitigate those local orientation effects the sensors were positioned using a compass, therefore all of them were oriented with respect to a global reference, and not to the local orientations. In this way, all local reference systems will be directly coherent with the global RS. Furthermore, for the same reason, they were all positioned with a positive increment direction in agreement.

On cable length and use of multiple setups, to be combined in post-processing:

The paramount determinant in formulating an effective sensor placement strategy is the length of the interconnecting cables. Given the cable length constraint of operating under a single setup, the survey campaign necessitated the implementation of multiple setups, both local and global, to be assembled during post-processing. The configurations were meticulously devised by sitting the control station at locations where the cables converge, at approximating "equidistant" points. This strategic placement easily guaranteed accessibility to points of interest, either via stairwells or through windows. To facilitate the integration of the diverse setups in use, fixed reference channels comprising at least one sensor were judiciously selected, avoiding signal overlapping or cross-referenced impulse.

Note on using multiple setups per building.

Preliminary qualitative insights can be drawn from specialised expertise and theoretical knowledge, particularly considering the structures under this study characterised by irregular plan geometry, as exemplified by the buildings under investigation. For instance, in the case of the structure situated in Piazza XX Settembre, it is anticipated that the three pavilions are expected to have local twisting and bending modes on the short side, which is more flexible, therefore, in relatively lower natural frequencies will be recorded, while their participation in global translational modes particularly in the direction of their long side will be expected stiffer and therefore at a relatively higher natural frequency.

As already mentioned, it was immediately verified that the rigid floor hypothesis was verified for all the floors (including the roof with a walkable possibility). In fact, the NTC2018 regulation requires at least 5 cm thickness in reinforced concrete floors; this condition was verified by more than required for both buildings under study. Furthermore, additional stiffening beams were declared and verified on site, again on both buildings. Improving more the assumption on rigid floor.

5.1 Sensor Set-Up Building located in Piazza XX Settembre

This case study originates from a research agreement established between Politecnico di Torino and the University of Messina. Subsequently, existing data was provided for examination and served as an initial reference. Building upon prior insights and partial results from previous investigations, the designated layout for Piazza XX Settembre was determined based on the four layouts outlined in the available information. The Politecnico di Torino team conducted its own dynamic identification tests under environmental excitation (AVT) on August 8, 2023. Considering cable length constraints, a predominant utilisation of local layouts was planned, while preserving global sections—both in terms of opposite points on the plan and, critically, to ensure the presence of sensors on various floors for each data acquisition. Following a preliminary analysis of the existing data, it was deduced that sensors on the lower floors did not provide data of satisfactory quality, particularly concerning minor vibration amplitudes. Consequently, the configurations detailed in the pre-existing data for the Piazza XX Settembre building were deemed valid for Operational Modal Analysis (OMA) purposes and were retained in the new dynamic tests, but the emphasis was placed on highlighting the sensor arrangement focused on the higher floors, specifically the first floor and the roof.

It is essential to note that all positions indicated on the plans were occupied by sensors located directly on the ground:

For each layout, the sensors are indicated in the four plan views corresponding to:

1. Basement floor.
2. Ground floor.
3. First floor.
4. Rooftop

Piazza XX Settembre - Sensor Placement Layout 1 (Politecnico di Torino Survey)

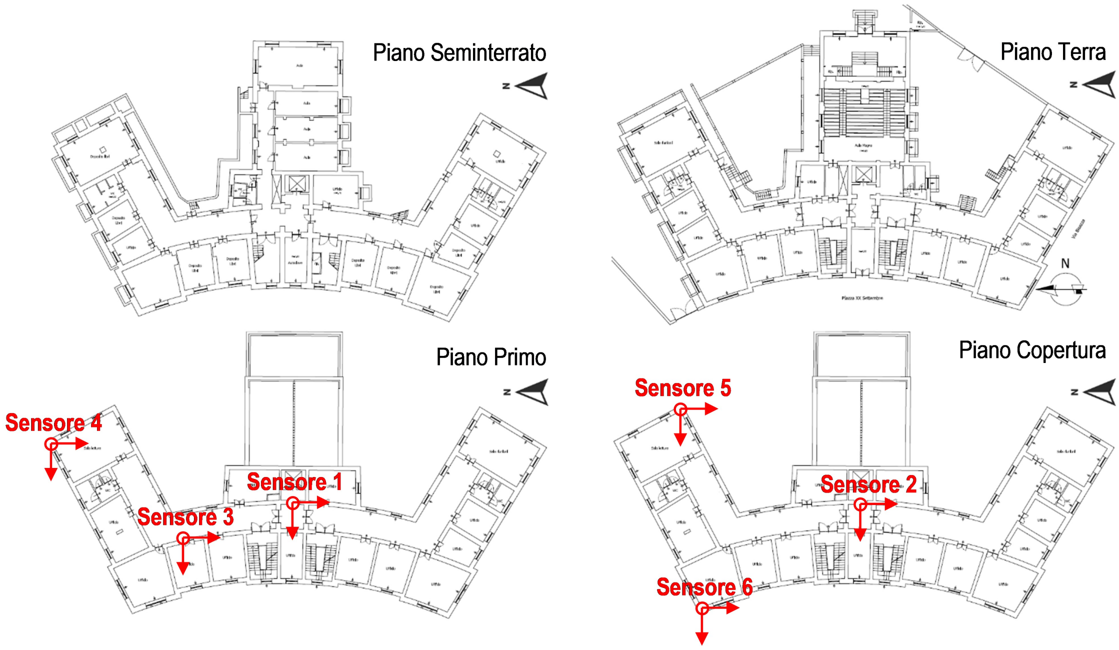

Figure 5.1: Coordinates of the sensor arrangement for layout 1, Politecnico Survey on Piazza XX Settembre

The precise coordinates for the sensors 1 to 6 displayed in Figure 5.1 will be displayed in Table 5.2

Sensor Location Layout 1	**X [m]**	**Y [m]**	**Z [m]**
Sensor 1	31.50	15.20	7.65
Sensor 2	31.50	15.20	12.65
Sensor 3	16.00	9.00	7.65
Sensor 4	0.00	20.00	7.65
Sensor 5	8.00	25.40	12.65
Sensor 6	8.00	0.00	12.65

Table 5.2: Coordinates of the sensor arrangement for layout 1, Politecnico Survey on Piazza XX Settembre

Piazza XX Settembre - Sensor Placement Layout 2 (Politecnico di Torino Survey)

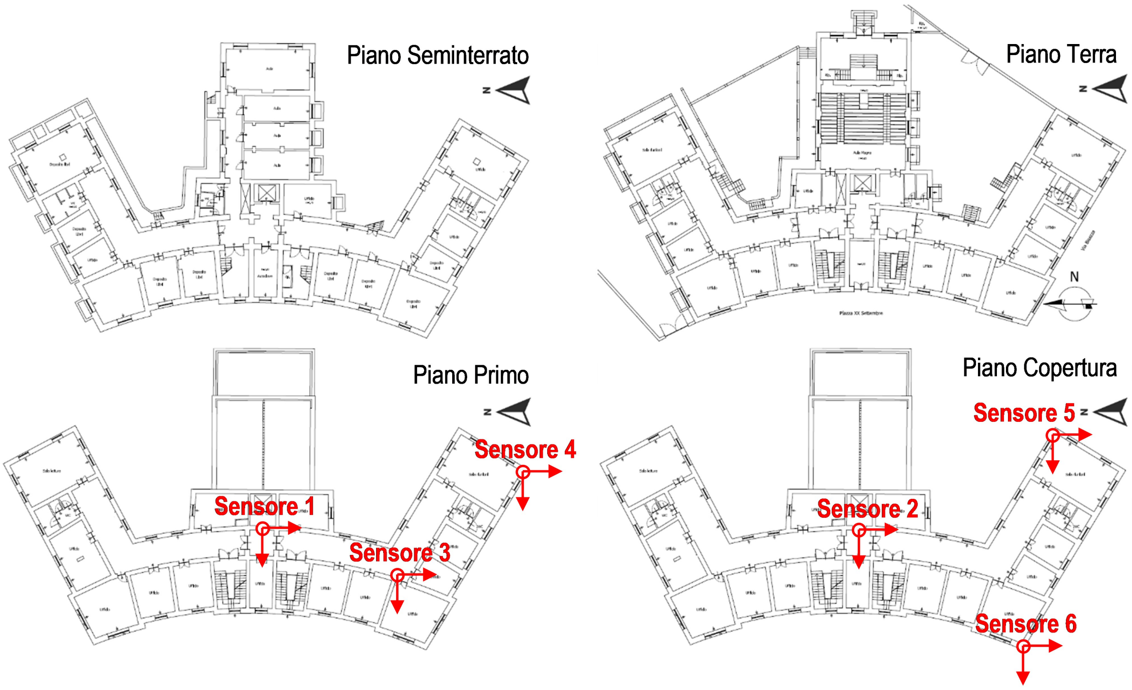

Figure 5.2: Coordinates of the sensor arrangement for layout 2, Politecnico Survey on Piazza XX Settembre

The precise coordinates for the sensors 1 to 6 displayed in Figure 5.2 will be displayed in the Table 5.3

Sensor Location Layout 2	**X [m]**	**Y [m]**	**Z [m]**
Sensor 1	31.50	15.20	7.65
Sensor 2	47.00	9.00	7.65
Sensor 3	63.00	20.00	7.65
Sensor 4	55.00	25.40	12.65
Sensor 5	55.00	0.00	12.65
Sensor 6	31.50	15.20	12.65

Table 5.3: Coordinates of the sensor arrangement for layout 2, Politecnico Survey on Piazza XX Settembre

Piazza XX Settembre - Sensor Placement Layout 3 (Politecnico di Torino

Survey)

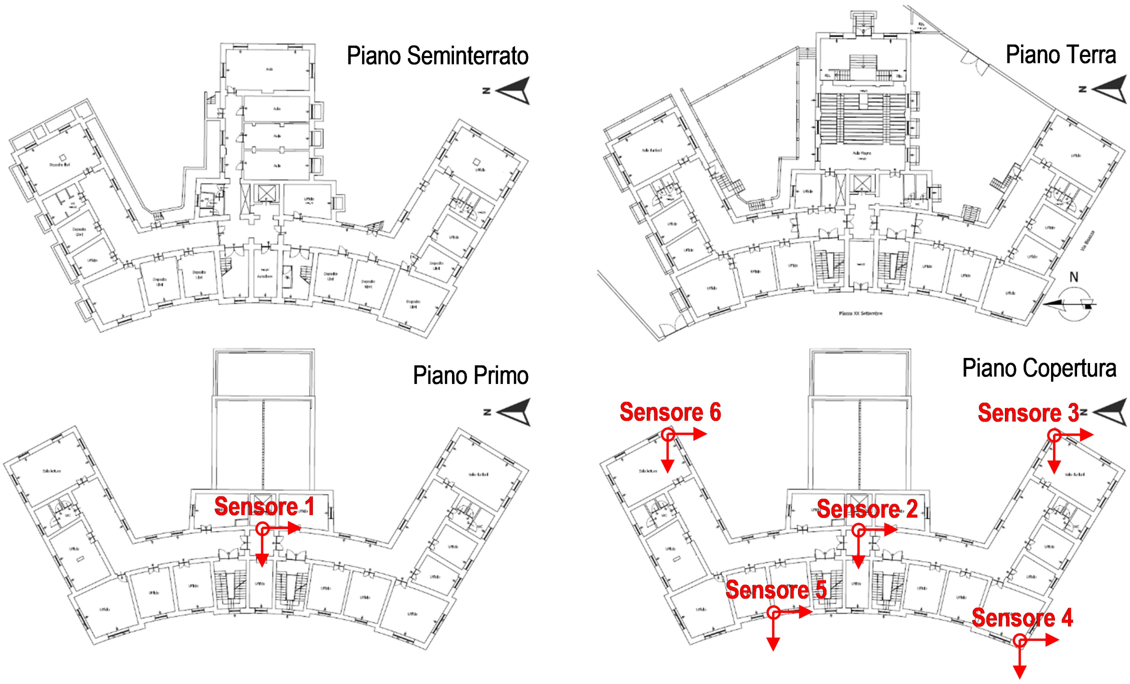

Figure 5.3: Coordinates of the sensor arrangement for layout 3, Politecnico Survey on Piazza XX Settembre

The precise coordinates for the sensors 1 to 6 displayed in Figure 5.3 will be displayed in Table 5.4

Sensor Location Layout 3	**X [m]**	**Y [m]**	**Z [m]**
Sensor 1	31.50	15.20	7.65
Sensor 2	31.50	15.20	12.65
Sensor 3	55.00	25.40	12.65
Sensor 4	55.00	0.00	12.65
Sensor 5	22.00	2.80	12.65
Sensor 6	8.00	25.40	12.65

Table 5.4: Coordinates of the sensor arrangement for layout 3, Politecnico Survey on Piazza XX Settembre

Piazza XX Settembre - Sensor Placement Layout 4 (Politecnico di Torino Survey)

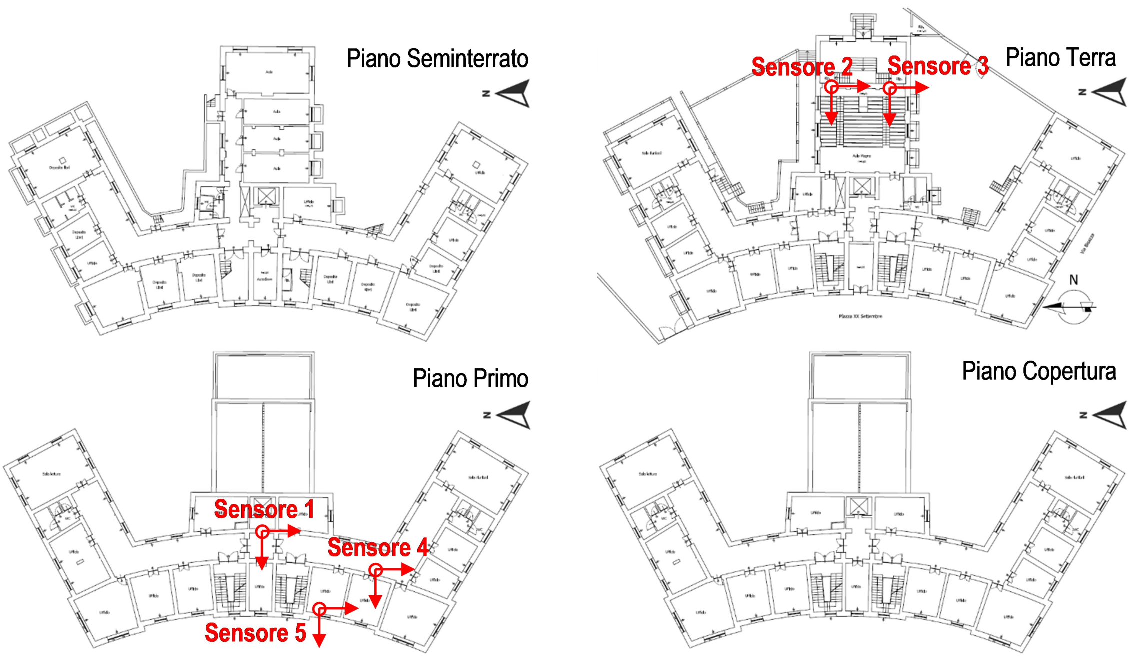

Figure 5.4: Coordinates of the sensor arrangement for layout 4, Politecnico Survey on Piazza XX Settembre

The precise coordinates for the sensors 1 to 5 displayed in Figure 5.4 will be displayed in Table 5.5

Sensor Location Layout 4	**X [m]**	**Y [m]**	**Z [m]**
Sensor 1	31.50	15.20	7.65
Sensor 2	28.00	30.80	3.15
Sensor 3	35.00	30.80	3.15
Sensor 4	47.00	9.00	7.65
Sensor 5	41.00	2.80	7.65

Table 5.5: Coordinates of the sensor arrangement for layout 4, Politecnico Survey on Piazza XX Settembre

5.2 Sensor Set-Up Building located in Via Concezione

The analysis of the Via Concezione Building, utilising the information retrieved from the University of Messina revealed that the first 5 inspections measured did not suffice the useful parameters for extracting modal information about the structure. Consequently, a new configuration was employed to survey the same structure on August 9, 2023. In both configurations, the focal point is to concentrate on distinct sections of the building being the analysed area as big as possible considering the equipment connection limitation but nevertheless, the survey was still a localised setup, while concurrently preserving global. This is achieved by orienting the geophones in opposing directions on the plan and ensuring sensors are positioned at different elevations for each acquisition. Notably, emphasis is placed on the upper levels during sensor placement. It is pertinent to note that the available sensors, specifically velocimeters, also referred to as geophones, were constrained to placement on the ground and in contact with the attic. Consequently, all positions indicated on the plans are on the walking surface, with sensors simply placed on the ground.

For each layout, the sensors are indicated in the four plan views corresponding to:

1. Basement floor.
2. Ground floor and mezzanine floor.
3. First floor.
4. Rooftop.

Via Concezione - Sensor Placement Layout 1 (Politecnico di Torino Survey)

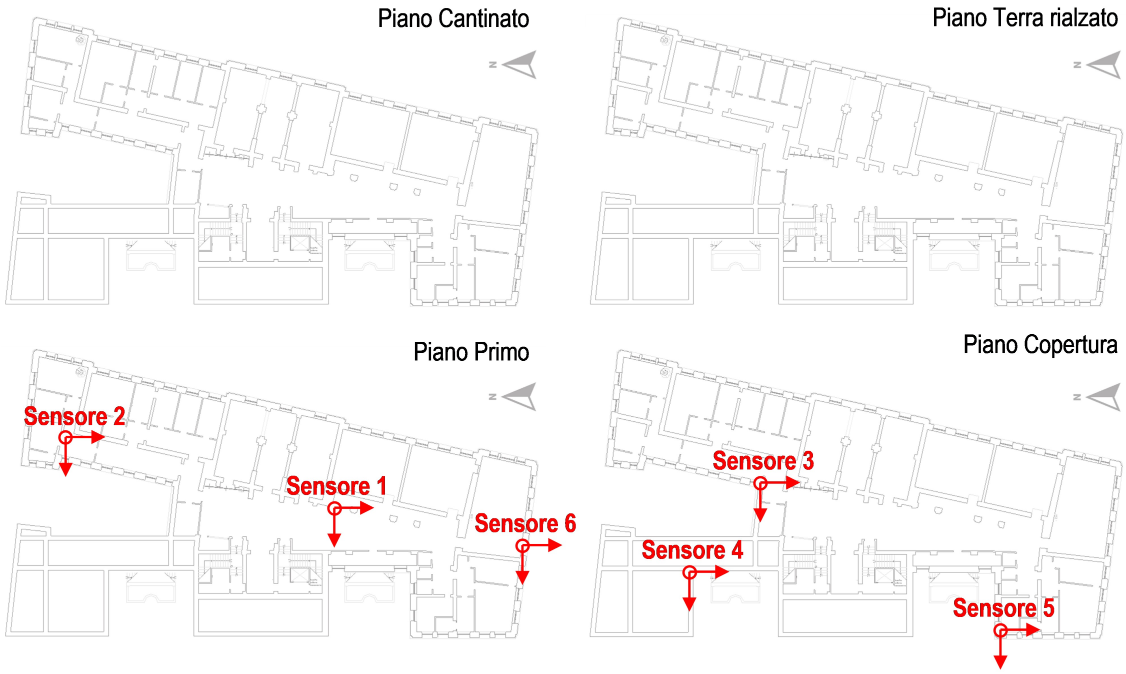

Figure 5.5: Coordinates of the sensor arrangement for layout 1, Politecnico Survey on Via Concezione

The precise coordinates for the sensors 1 to 6 displayed in Figure 5.5 will be displayed in Table 5.6

Sensor Location Layout 1	**X [m]**	**Y [m]**	**Z [m]**
Sensor 1	38.00	17.60	9.00
Sensor 2	12.00	21.00	9.00
Sensor 3	19.00	17.60	14.00
Sensor 4	12.00	7.60	14.00
Sensor 5	48.00	0.00	14.00
Sensor 6	61.00	10.50	9.00

Table 5.6: Coordinates of the sensor arrangement for layout 1, Politecnico Survey on Via Concezione

Via Concezione - Sensor Placement Layout 2 (Politecnico di Torino Sur-

vey)

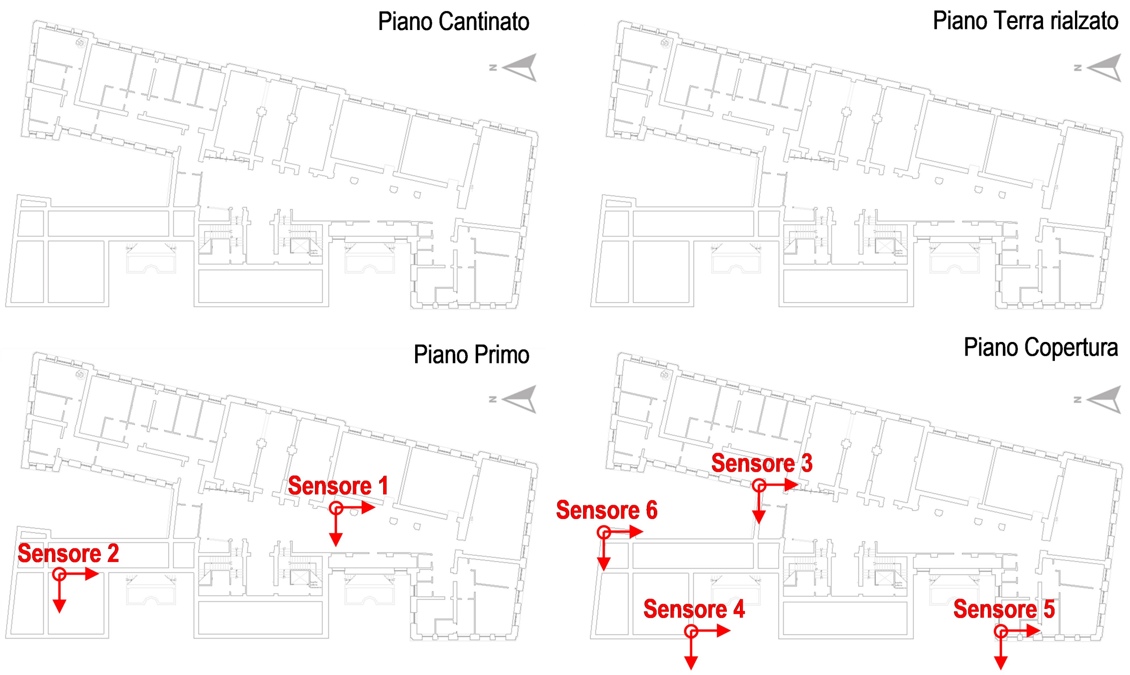

Figure 5.6: Coordinates of the sensor arrangement for layout 2, Politecnico Survey on Via Concezione

The precise coordinates for the sensors 1 to 6 displayed in Figure 5.6 will be displayed in the Table 5.7

Sensor Location Layout 2	**X [m]**	**Y [m]**	**Z [m]**
Sensor 1	38.00	17.60	9.00
Sensor 2	6.00	7.60	9.00
Sensor 3	19.00	17.60	14.00
Sensor 4	12.00	0.00	14.00
Sensor 5	48.00	0.00	14.00
Sensor 6	1.40	13.20	14.00

Table 5.7: Coordinates of the sensor arrangement for layout 2, Politecnico Survey on Via Concezione

Chapter 6

Processing and interpretation of Dynamic test results: Traditional Operational Modal Analysis (OMA)

In the context of Structural Health Monitoring (SHM), there are several possible techniques for signal analysis. In particular, output-only techniques under stationary inputs, such as environmental noise, are identified under the acronym operational modal analysis (OMA) [1]. The main OMA techniques are divided into parametric techniques, based on analytical regression models in the time domain, and non-parametric techniques; instead, based purely on statistical data processing [18]

The analysis techniques widely used in practice today for recording dynamic identifications under environmental excitation are mainly of two types: Enhanced Frequency Domain Decomposition (EFDD) and Covariance-Based Stochastic Subspace Identification (SSI-cov) [19]. EFDD is a non-parametric technique that operates in the frequency domain, while SSI-cov is a parametric technique that operates in the time domain. These two techniques were therefore also adopted in the present analysis of the dynamic identifications carried out under environmental excitation of the two buildings under study. The code used for the analysis is written in Python language, exploiting the open-source PyOMA library [17].

In the case of environmental vibration tests, the lack of control of the input translates into a lack of knowledge of the spectral distribution of its energy: the hypotheses on the input are not always completely satisfied nor is it possible to verify their validity and consequently the estimates of damping are inevitably affected by errors caused not only by noise but also by such erroneous assumptions on the input.

6.1 Processing results for building Piazza in XX Settembre:

The dynamic identification tests were conducted on 8 August 2023 on the building in Piazza XX Settembre and were carried out with sensors previously described, setting a higher sampling frequency of 250Hz. The sensors were arranged according to the 4 setups illustrated previously.

For setup 1 the acquisition duration is equal to 1200s, while for the other three setups 2-3-4 it is equal to 2400s.

For simplicity and practical analysis reasons, a simplified wire-frame geometric model of the monitored building was prepared as in Figure 6.1, also providing a new numbering of the nodes. In fact, even the monitored nodes have been effectively integrated into this new numbering, so as to unequivocally trace the position of the sensors in the various layouts to the same position in the building plan.

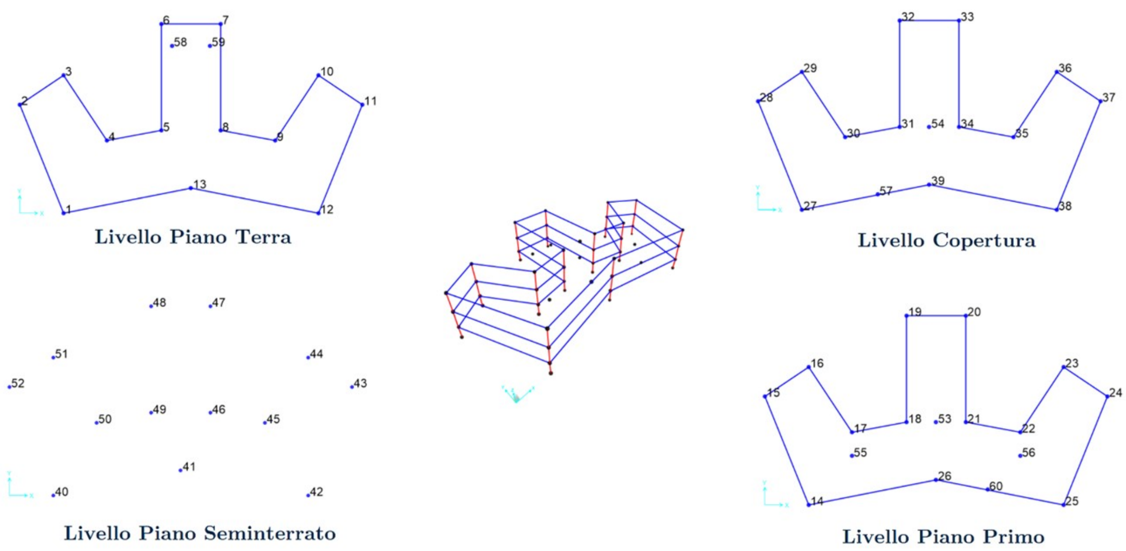

Figure 6.1: Simplified geometric wire frame FE model for building in Piazza XX Settembre

Using the new numbering of the simplified wire-frame FE model, the sensors of the 4 setups are therefore arranged according to the following numbering:

Setup	**Sensor 1**	**Sensor 2**	**Sensor 3**	**Sensor 4**	**Sensor 5**	**Sensor 6**
1	*53*	54	55	15	29	27
2	53	56	24	36	38	54
3	53	54	36	38	57	29
4	53	58	59	56	60	Not Used

As noted only node 53, introduced as sensor 1, is the only common reference left fixed between the various setups. This information is useful for a possible merging of the mode shapes with the PoSER technique [19], even with all the limitations and operational difficulties already discussed previously.

The recording graphs were divided into the vertical Z component and the in-plane components, respectively the X direction (North-South direction) and the Y direction (East-West direction). Obviously, the signals have undergone a de-trending process to be brought back to the origin and remove a possible constant shift of the signals. The unit of measurement for recordings is mV. To obtain a signal amplitude in units suitable for a speed, specific transduction factors were used for the instruments adopted. In particular, the transduction factor of sensor 1 is equal to 4.23 V/inch/s, which then requires a further conversion to obtain the speed in cm/s, while the transduction factor of the other sensors is equal to 0.29 V/ cm/s, already directly providing a speed measurement in cm/s.

The results of the numerical analyses with traditional OMA techniques are presented below for the various setups.

6.1.1 Layout 1 Analysis for building in Piazza XX Settembre:

For the experimental Campaign, the registered signals for Layout 1 are reported in the following figures :

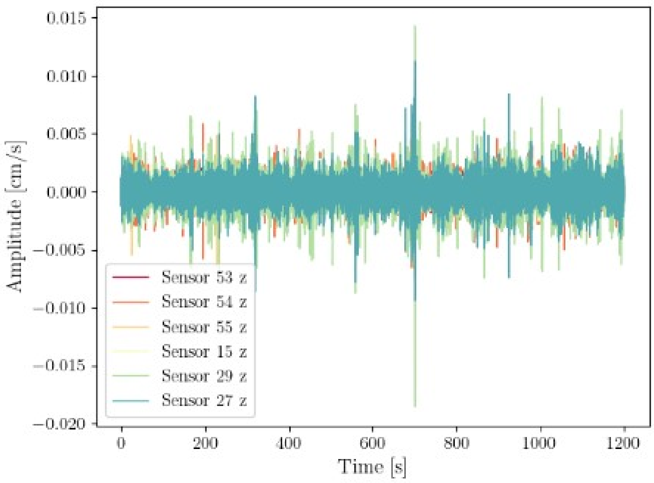

Figure 6.2: Signals recorded continuously in Layout 1 of Piazza XX Settembre for Z direction

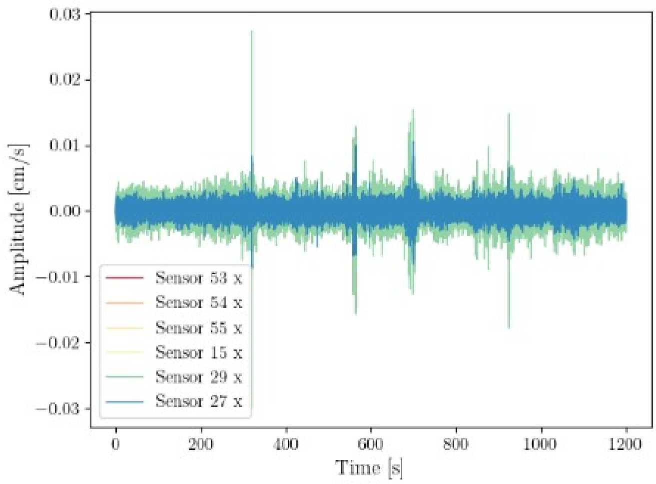

Figure 6.3: Signals recorded continuously in Layout 1 of Piazza XX Settembre for X direction

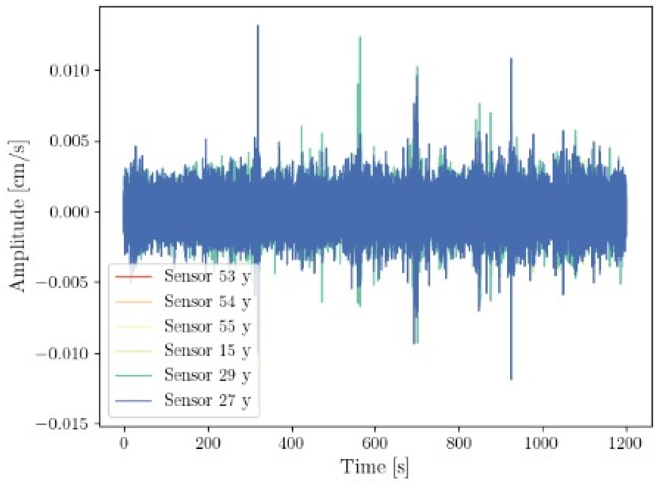

Figure 6.4: Signals recorded continuously in Layout 1 of Piazza XX Settembre for Y direction

To further refine the analyses, the signals were decimated with a decimation factor of 5, to increase the resolution of the information and attempt to identify the most probable first natural frequencies of the monitored system. The stabilisation diagram superimposed on the SVD (Singular Value Decomposition) of the PSD (Power Spectral Density) is shown in Figure 6.5. From this, it was possible to identify four possible natural frequencies of the system. The results in terms of frequencies, damping and mode shapes are reported in the following Tables6.1 6.2:

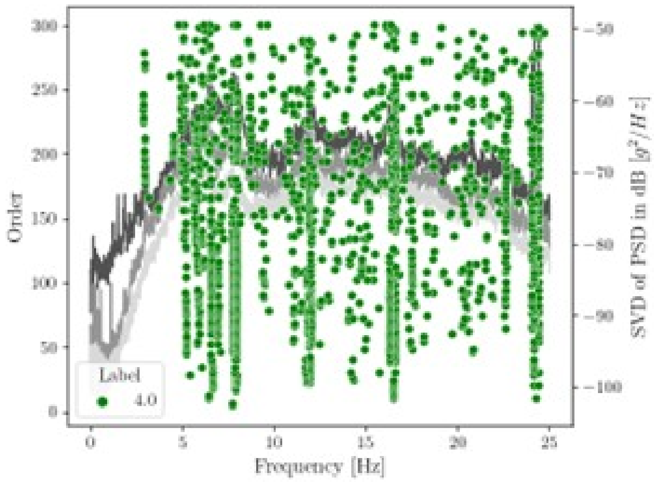

Figure 6.5: Stabilisation diagram presenting only the stable poles superimposed on the SVD of the PSD considering only the first 3 SVs, Layout 1, Piazza XX Settembre

EFDD		**SSI-cov**	
f [Hz]	**Damping [%]**	**f [Hz]**	**Damping [%]**
5.23	0.01%	5.19	2.24%
6.67	0.03%	6.69	2.60%
7.83	1.63%	7.96	3.75%
11.97	0.01%	11.93	2.63%

Table 6.1: Frequency and damping obtained with EFDD and SSI-cov for Setup 1 Piazza XX Settembre

	EFDD				**SSI-cov**			
f [Hz]	**5.23**	**6.67**	**7.83**	**11.97**	**5.19**	**6.69**	**7.96**	**11.93**
ϕ_{ij}	-0.2085	-0.0361	0.0623	0.1707	0.2468	-0.0451	0.0655	0.1885
	-0.1262	-0.0184	0.053	0.1359	0.1612	-0.0071	0.0573	0.1371
	-0.1325	-0.0245	0.0406	0.1417	0.1716	-0.0328	0.062	0.1426
	0.0857	0.0123	-0.0266	-0.074	-0.0758	0.0137	-0.0537	-0.1492
	-0.6017	-0.027	0.0706	0.2485	0.7826	-0.1883	0.2439	0.139
	-0.7699	-0.0857	0.1304	0.4151	1	-0.1463	0.1307	0.3851
	0.117	-0.0471	0.0307	-0.0071	-0.1888	-0.0348	0.0465	0.1563
	0.1226	0.0783	-0.0009	-0.3039	-0.1304	0.0691	0.0818	-0.3101
	0.5525	-0.1149	0.1452	-0.0656	-0.4709	-0.0325	0.1151	-0.0737
	0.0951	0.0617	0.0708	0.2013	-0.1118	0.0578	0.1047	0.1733
	-0.4133	-0.032	-0.279	-0.0797	0.3138	-0.0584	-0.3444	-0.0805
	-0.3142	0.5673	0.3886	0.3648	0.0913	0.5529	0.3521	0.4058
	0.1762	-0.1691	-0.0715	0.2157	-0.068	-0.1503	-0.002	0.272
	-0.0307	1	1	1	-0.2727	1	1	1
	1	-0.3306	0.4403	0.6913	-0.7477	-0.14	0.4715	0.8037
	-0.1481	0.0565	-0.0199	-0.0773	0.0706	0.0456	-0.0019	-0.0945
	0.9586	-0.5735	0.1496	0.2739	-0.6376	-0.3838	0.1561	0.3819
	-0.275	0.1784	0.054	0.2601	0.1639	0.2237	-0.1531	0.0205

Table 6.2: Mode shapes obtained with EFDD and SSI-cov Layout 1

6.1.2 Layout 2 Analysis for building in Piazza XX Settembre:

For the experimental Campaign, the registered signals for Layout 2 are reported in the following figures:

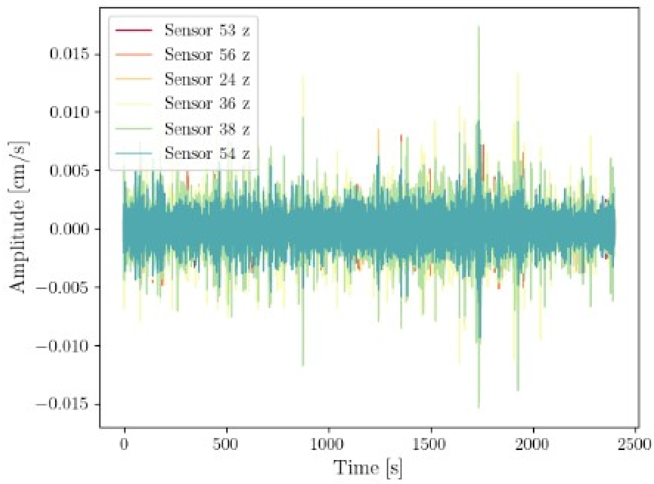

Figure 6.6: Signals recorded continuously in Layout 2 of Piazza XX Settembre for Z direction

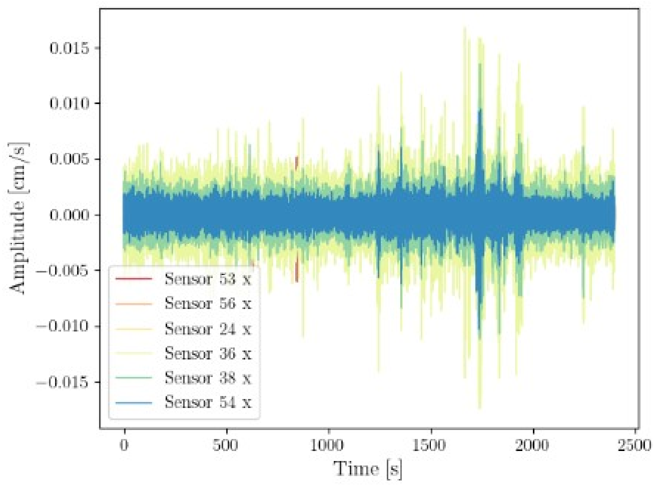

Figure 6.7: Signals recorded continuously in Layout 2 of Piazza XX Settembre for X direction

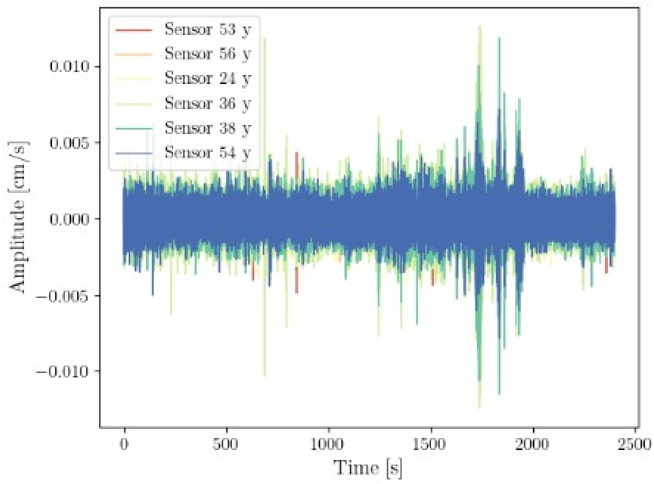

Figure 6.8: Signals recorded continuously in Layout 2 of Piazza XX Settembre for Y direction

To further refine the analyses, the signals were decimated with a decimation factor of 5, to increase the resolution of the information and attempt to identify the most probable first natural frequencies of the monitored system. The stabilisation diagram superimposed on the SVD (Singular Value Decomposition) of the PSD (Power Spectral Density) is shown in Figure 6.9. From this, it was possible to identify four possible natural frequencies of the system. The results in terms of frequencies, damping and mode shapes are reported in the following tables 6.3 6.4

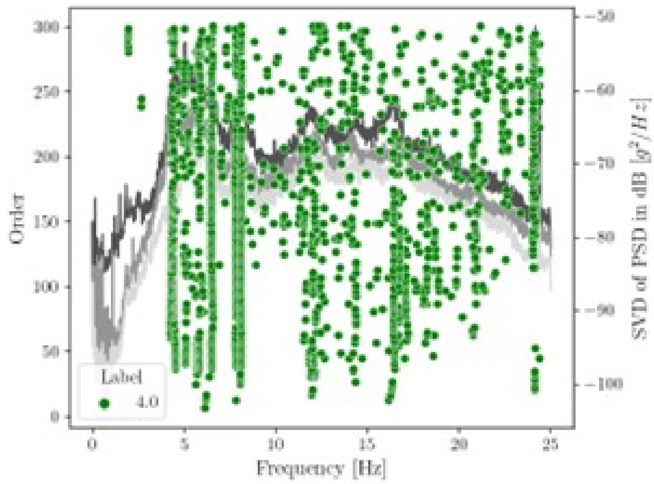

Figure 6.9: Stabilisation diagram presenting only the stable poles superimposed on the SVD of the PSD considering only the first 3 SVs, Layout 2, Piazza XX Settembre

EFDD		**SSI-cov**	
f [Hz]	**Damping [%]**	**f [Hz]**	**Damping [%]**
4.5	0.13%	4.48	4.30%
6.41	1.73%	6.51	3.65%
8.21	0.46%	8.11	3.09%
12.15	0.00%	12.14	3.25%

Table 6.3: Frequency and damping obtained with EFDD and SSI-cov for Layout 2 Piazza XX Settembre

	EFDD				**SSI-cov**			
f [Hz]	**4.5**	**6.41**	**8.21**	**12.15**	**4.48**	**6.51**	**8.11**	**12.14**
ϕ **ij**	-0.1162	0.0585	-0.0352	0.064	0.2553	0.0664	0.1132	0.2109
	-0.0832	0.0366	0.0224	0.037	0.2162	0.0404	0.0688	0.1822
	-0.0809	0.0468	-0.0569	0.0237	0.2051	0.0566	0.1193	0.1587
	0.0681	-0.0012	-0.0033	-0.1847	-0.0025	-0.0078	-0.1241	0.2963
	0.2008	-0.0022	0.1211	-0.1357	-0.2384	-0.0057	-0.2875	-0.1902
	0.5615	-0.1378	-0.2351	-0.0326	-0.5861	-0.1698	0.1994	0.0924
	0.0215	-0.0481	-0.0311	0.0762	0.0261	-0.0721	0.1637	-0.1852
	0.7832	0.2516	-0.1036	0.0126	-0.7028	0.2216	0.3086	-0.144
	-0.3584	-0.3123	-0.4157	-0.0824	0.3309	-0.3271	0.5309	-0.1628
	0.3005	0.0992	0.1006	0.121	-0.2536	0.0688	0.078	-0.4993
	1	1	1	1	-0.8766	1	-0.7197	1
	0.9184	-0.0967	-0.714	-0.614	-0.881	-0.1863	0.7936	-0.653
	-0.196	0.0568	-0.0127	-0.1779	0.2823	0.0526	-0.0128	0.2434
	0.5757	0.2325	-0.5923	-0.2699	-0.4258	0.1581	1	-0.1537
	-0.949	0.0787	0.1733	0.3176	1	0.1319	0.0187	0.3309
	0.0911	-0.0484	-0.0003	0.0491	-0.0848	-0.0328	-0.0668	-0.1233
	-0.3161	0.173	-0.5029	-0.3293	0.5176	0.0844	0.6414	-0.6444
	-0.4074	0.1216	-0.0938	0.2732	0.5201	0.1149	0.2283	0.1428

Table 6.4: Mode shapes obtained with EFDD and SSI-cov Layout 2

6.1.3 Layout 3 Analysis for building in Piazza XX Settembre:

For the experimental Campaign, the registered signals for Layout 3 are reported in the following figures:

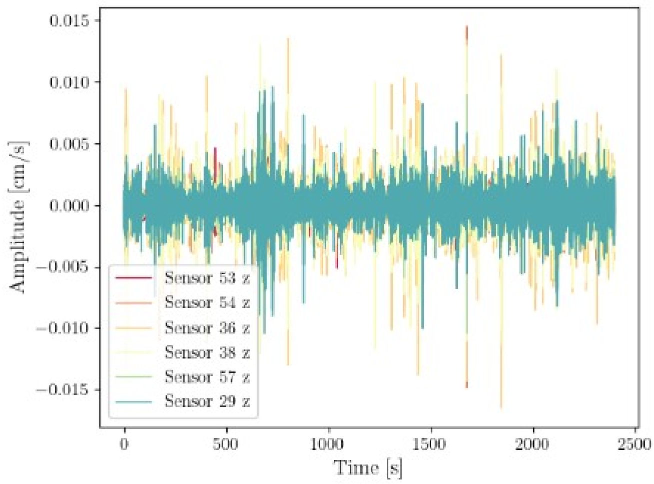

Figure 6.10: Signals recorded continuously in Layout 3 of Piazza XX Settembre for Z direction

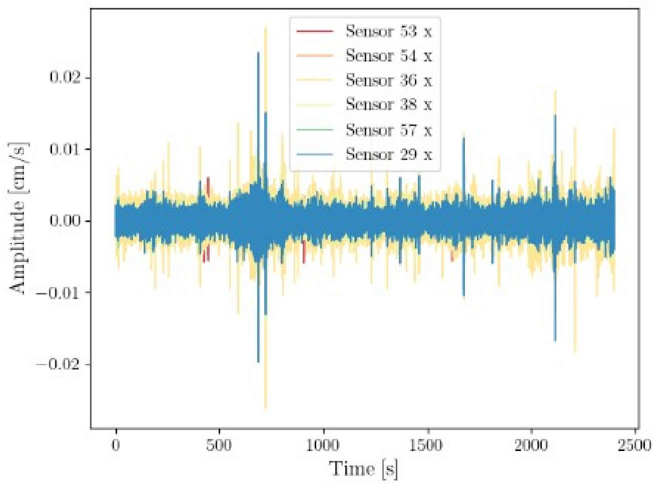

Figure 6.11: Signals recorded continuously in Layout 3 of Piazza XX Settembre for X direction

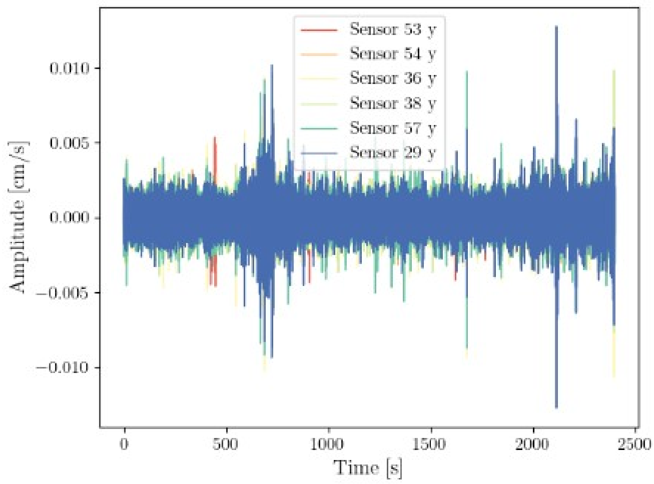

Figure 6.12: Signals recorded continuously in Layout 3 of Piazza XX Settembre for Y direction

To further refine the analyses, the signals were decimated with a decimation factor of 5, to increase the resolution of the information and attempt to identify the most probable first natural frequencies of the monitored system. The stabilisation diagram superimposed on the SVD (Singular Value Decomposition) of the PSD (Power Spectral Density) is shown in Figure 6.13. From this, it was possible to identify four possible natural frequencies of the system. The results in terms of frequencies, damping and mode shapes are reported in the following tables 6.5 6.6

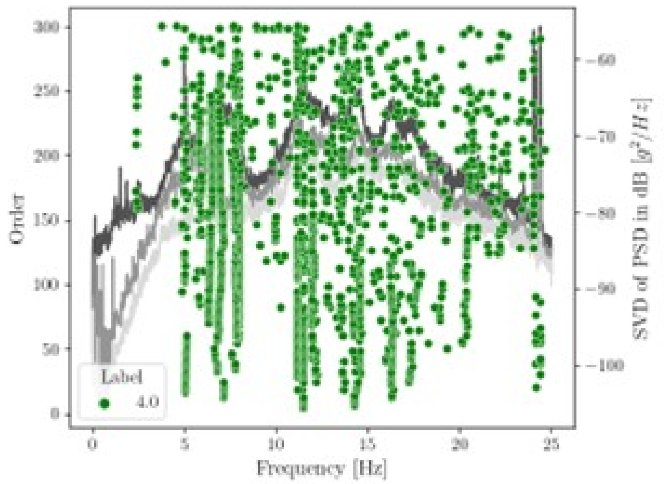

Figure 6.13: Stabilisation diagram presenting only the stable poles superimposed on the SVD of the PSD considering only the first 3 SVs, Layout 3, Piazza XX Settembre

EFDD		**SSI-cov**	
f [Hz]	**Damping [%]**	**f [Hz]**	**Damping [%]**
5.08	0.38%	5.03	1.37%
6.63	0.60%	6.52	3.64%
7.85	0.07%	7.91	3.66%
11.97	0.00%	12	2.49%

Table 6.5: Frequency and damping obtained with EFDD and SSI-cov for Layout 3 Piazza XX Settembre

	EFDD				SSI-cov			
f [Hz]	**5.08**	**6.63**	**7.85**	**11.97**	**5.03**	**6.52**	**7.91**	**12**
ϕ **ij**	-0.205	0.063	-0.08	0.011	0.217	0.072	0.05	-0.035
	-0.142	0.044	-0.075	-0.021	0.143	0.051	0.075	-0.111
	-0.165	0.044	-0.045	-0.033	0.15	0.044	0.002	-0.124
	0.053	-0.039	0.031	0.215	-0.063	-0.006	-0.03	0.638
	-0.069	0.14	0.026	-0.289	0.468	0.029	-0.33	-0.27
	-0.096	0.172	-0.175	0.191	0.66	0.124	0.119	0.236
	0.204	0.086	-0.053	0.06	-0.206	0.057	0.047	0.236
	1	1	-0.449	1	-0.62	1	1	1
	0.669	-0.056	0.058	-0.553	-0.814	-0.181	-0.419	-0.463
	-0.117	0.045	-0.066	-0.067	0.237	0.043	0.085	-0.41
	0.575	0.282	-0.31	-0.145	-0.233	0.149	-0.01	-0.206
	-0.596	0.093	-0.235	0.343	1	0.145	0.301	0.253
	-0.012	0.001	0.021	-0.01	0.075	-0.016	-0.053	-0.019
	0.047	0.037	0.076	0.31	-0.158	0.066	-0.344	0.31
	0.132	0.001	-0.291	-0.618	-0.472	0.267	0.44	-0.398
	0.05	0.128	0.076	0.035	-0.018	0.181	-0.093	0.077
	-0.1	0.427	1	-0.152	0.328	0.345	-0.581	-0.065
	-0.139	-0.483	-0.001	-0.062	0.16	-0.808	0.122	-0.036

Table 6.6: Mode shapes obtained with EFDD and SSI-cov Layout 3

6.1.4 Layout 4 Analysis for building in Piazza XX Settembre:

For the experimental Campaign, the registered signals for Layout 4 are reported in the following figures:

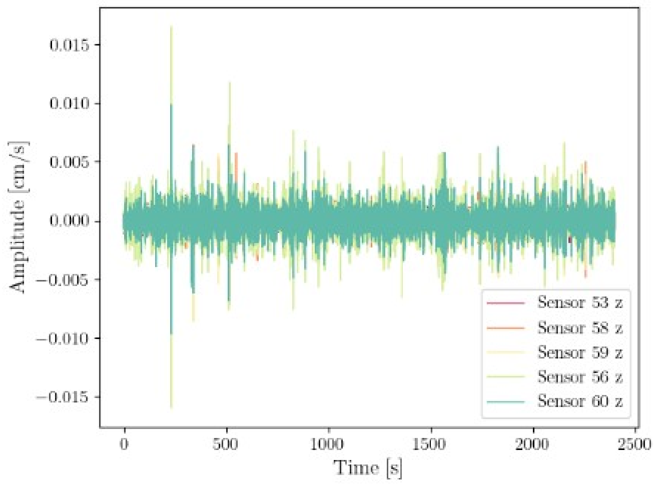

Figure 6.14: Signals recorded continuously in Layout 4 of Piazza XX Settembre for Z direction

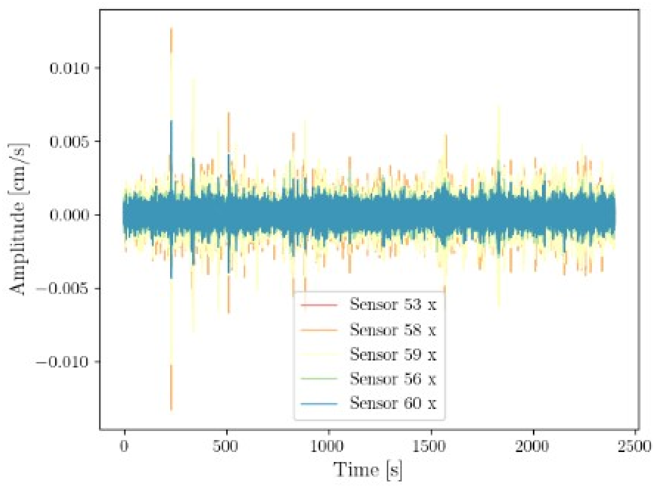

Figure 6.15: Signals recorded continuously in Layout 4 of Piazza XX Settembre for X direction

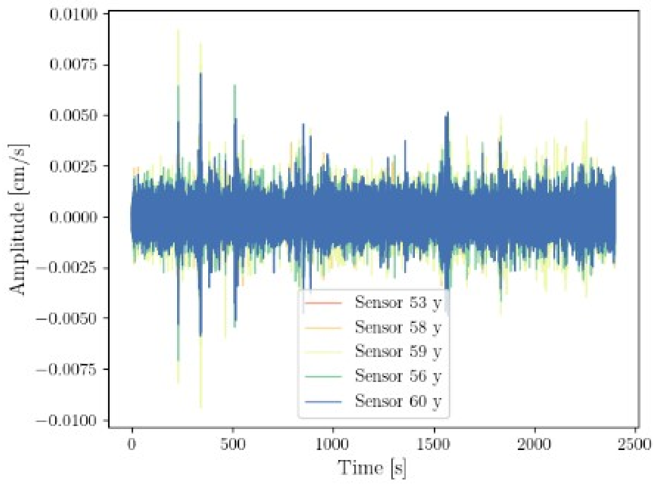

Figure 6.16: Signals recorded continuously in Layout 4 of Piazza XX Settembre for Y direction

To further refine the analyses, the signals were decimated with a decimation factor of 5, to increase the resolution of the information and attempt to identify the most probable first natural frequencies of the monitored system. The stabilisation diagram superimposed on the SVD (Singular Value Decomposition) of the PSD (Power Spectral Density) is shown in Figure 6.17. From this, it was possible to identify four possible natural frequencies of the system. The results in terms of frequencies, damping and mode shapes are reported in the following tables 6.7 6.8

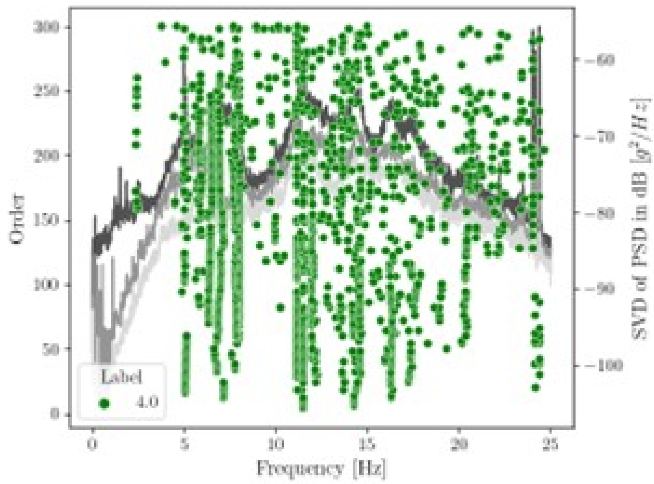

Figure 6.17: Stabilisation diagram presenting only the stable poles superimposed on the SVD of the PSD considering only the first 3 SVs, Layout 4, Piazza XX Settembre

EFDD		**SSI-cov**	
f [Hz]	**Damping [%]**	**f [Hz]**	**Damping [%]**
5.09	0.58%	5.06	2.56%
6.76	4.25%	6.9	5.66%
7.85	0.17%	7.81	4.03%
11.53	0.35%	11.47	2.22%

Table 6.7: Frequency and damping obtained with EFDD and SSI-cov for Layout 4 Piazza XX Settembre

	EFDD				**SSI-cov**			
f [Hz]	**5.09**	**6.76**	**7.85**	**11.53**	**5.06**	**6.9**	**7.81**	**11.47**
ϕ **ij**	-0.24367	0.047155	-0.09724	0.011722	0.266713	0.108511	0.048573	-0.04303
	-0.13881	0.080332	-0.04994	0.007619	0.147154	0.076959	0.099462	-0.13952
	-0.18841	0.010334	-0.03549	-0.01078	0.16702	0.074847	0.002596	-0.12074
	0.087037	-0.05415	0.071288	0.264174	-0.09848	-0.01322	-0.03285	0.638697
	-0.0783	0.105515	0.065474	-0.26692	0.487502	-0.00646	-0.28963	-0.30138
	-0.06624	0.212702	-0.12501	0.199385	0.693251	0.079869	0.09446	0.255574
	0.192869	0.053569	-0.0389	0.095369	-0.24328	0.037175	0.050629	0.231431
	1.043436	0.959979	-0.41899	0.970185	-0.63634	1.021258	0.9606	0.983712
	0.638038	-0.07479	0.020302	-0.5376	-0.82981	-0.15279	-0.45626	-0.48172
	-0.08783	0.061636	-0.02945	-0.06959	0.194065	0.057152	0.103912	-0.41772
	0.527092	0.248235	-0.35341	-0.16981	-0.20714	0.115343	-0.02193	-0.17653
	-0.63642	0.094124	-0.23788	0.354389	1.028487	0.149055	0.31272	0.299784
	0.024037	-0.04143	0.014397	0.038691	0.115417	-0.00806	-0.05762	-0.04015
	0.003399	0.057963	0.082164	0.346256	-0.15039	0.016937	-0.34376	0.306624
	0.155222	0.047283	-0.33424	-0.65132	-0.49769	0.279298	0.402802	-0.36694
	0.059544	0.086314	0.030517	0.003668	-0.04678	0.198552	-0.06939	0.125539
	-0.12467	0.399501	0.985737	-0.1392	0.28255	0.391558	-0.53684	-0.08689
	-0.16011	-0.52521	0.03431	-0.0302	0.168751	-0.84649	0.079754	-0.05819

Table 6.8: Mode shapes obtained with EFDD and SSI-cov Layout 4

6.2 Processing results for building Via Concezione:

These tests were carried out by the Politecnico on 9 August 2023, preparing two setups (layout 1 and 2) for the building in Via Concezione with measurements with longer time duration (at least approximately 30 continuous minutes) compared to the acquisitions relating to the data already provided by University of Messina, and setting a sampling frequency of 250Hz. Specifically, for setup 1, the acquisition duration is equal to 3610s while for setup 2 it is equal to 2400s. For simplicity and practical analysis reasons a simplified wire-frame geometric FE model of the monitored building was prepared as in Figure 6.18, also providing a new numbering of the nodes. In fact, even the monitored nodes have been effectively integrated into this new numbering, to unequivocally trace the position of the sensors in the various layouts to the same position in the building plan.

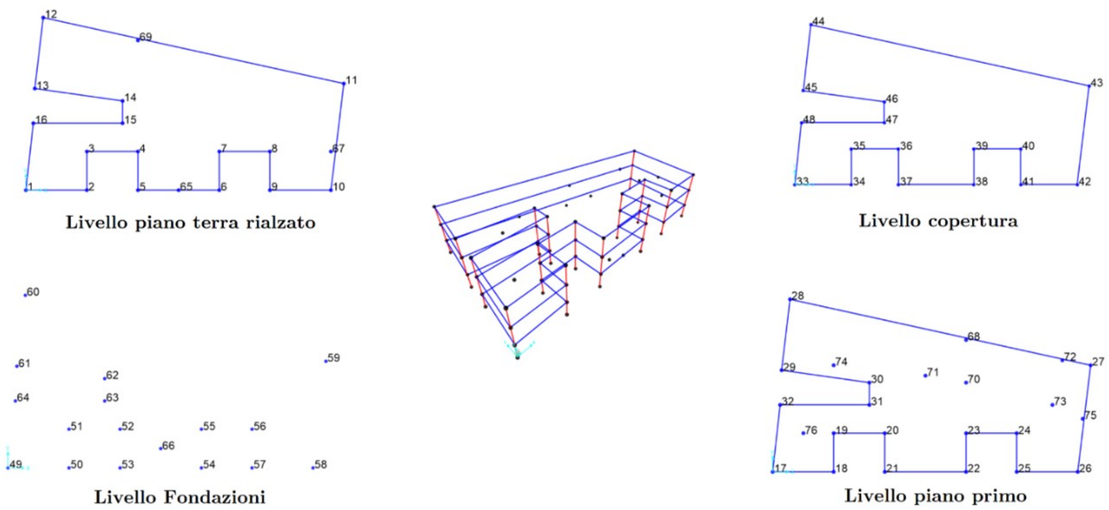

Figure 6.18: Simplified geometric wire frame FE model for building in Via Concezione

Using the new numbering of the simplified wire-frame model, the sensors of the 2 setups are therefore arranged according to the following numbering:

Setup	Sensor 1	Sensor 2	Sensor 3	Sensor 4	Sensor 5	Sensor 6
1	70	74	46	35	41	75
2	70	76	46	34	41	48

It can be seen how nodes 70, 46 and 41 are respectively sensors 1, 3 and 5, truthfully coincide with the common references established during the writing of this document. This information will prove to be useful for the future merging of the mode shapes considering the PoSER technique [19]. The recording graphs are divided into the vertical Z component and the components in the plane, respectively X direction (North-South direction) and Y direction (East-West direction). Is evident that the signals have undergone a de-trending process to be brought back to the origin and remove a possible constant shift of the signals. The unit of measurement for recordings is mV. To accomplish the signal amplitude in units suitable for a speed, specific transduction factors were used for the instruments adopted. In particular, the transduction factor of sensor 1 is equal to 4.23 V/inch/s, which then requires a further conversion to obtain the speed in cm/s, while the transduction factor of the other sensors is equal to 0.29 V/ cm/s, as those were already directly providing a speed measurement in cm/s. The results of the numerical analysis with traditional OMA techniques are presented below for the two setups 1 and 2.

6.2.1 Layout 1 Analysis for building in Via Concezione:

For the experimental Campaign, the registered signals for Layout 1 are reported in the following figures:

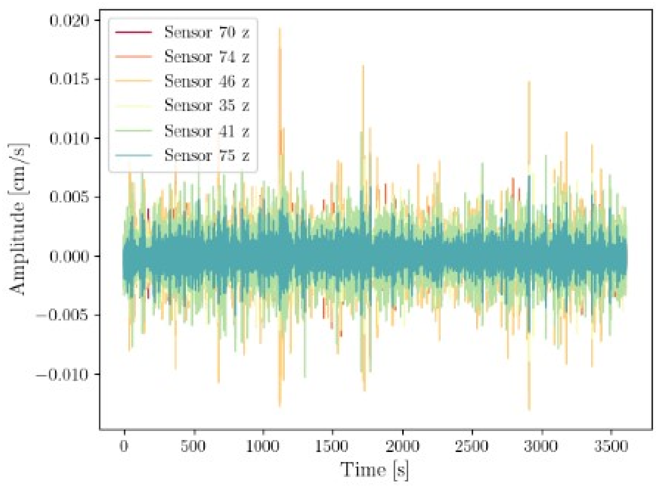

Figure 6.19: Signals recorded continuously in Layout 1 of Via Concezione for Z direction

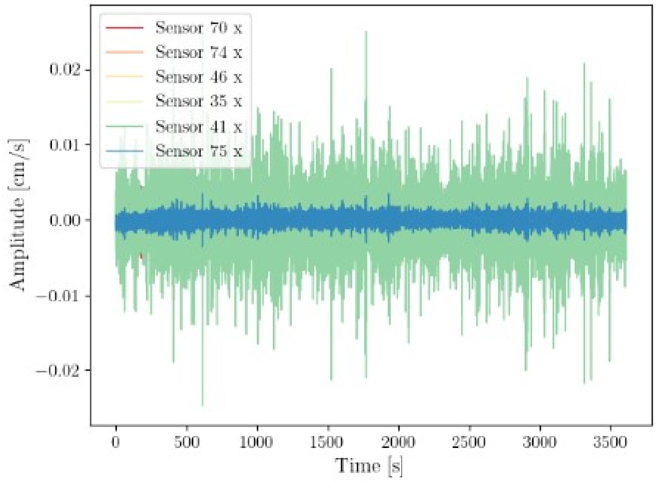

Figure 6.20: Signals recorded continuously in Layout 1 of Via Concezione for X direction

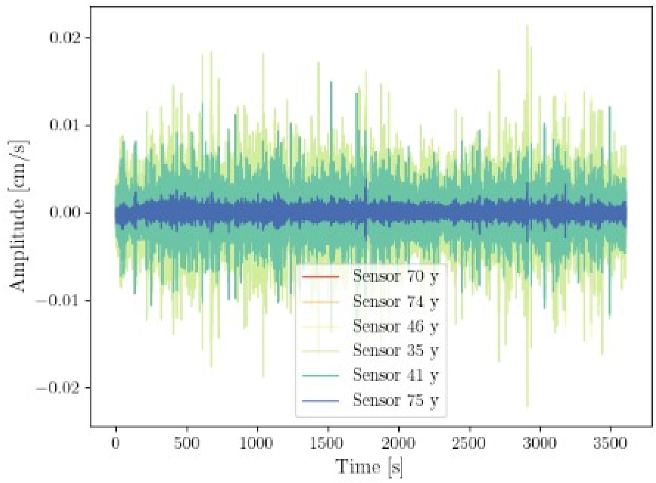

Figure 6.21: Signals recorded continuously in Layout 1 of Via Concezione for Y direction

To further refine the analyses, the signals were decimated with a decimation factor of 5, to increase the resolution of the information and attempt to identify the most probable first natural frequencies of the monitored system. The stabilisation diagram superimposed on the SVD (Singular Value Decomposition) of the PSD (Power Spectral Density) is shown in Figure 6.22. From this, it was possible to identify four possible natural frequencies of the system. The results in terms of frequencies, damping and mode shapes are reported in the following tables 6.9 6.10.

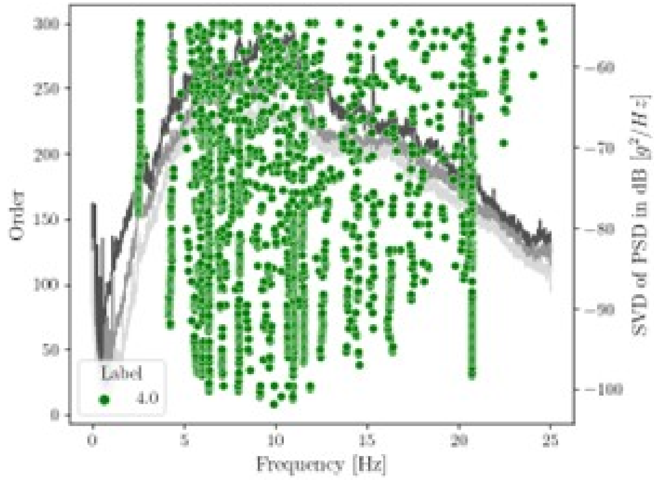

Figure 6.22: Stabilisation diagram presenting only the stable poles superimposed on the SVD of the PSD considering only the first 3 SVs, Layout 1, Via Concezione

EFDD		**SSI-cov**	
f [Hz]	**Damping [%]**	**f [Hz]**	**Damping [%]**
4.29	0.01%	4.29	8.71%
6.39	0.94%	6.37	4.21%
8	0.34%	8	2.86%
11.05	0.29%	10.97	2.70%

Table 6.9: Frequency and damping obtained with EFDD and SSI-cov for Layout 1 Via Concezione

	EFDD				**SSI-cov**			
f [Hz]	**4.29**	**6.39**	**8**	**11.05**	**4.29**	**6.37**	**8**	**10.97**
Φ ij	-0.4628	0.0502	0.0255	0.0028	-0.5372	0.0475	0.0273	0.0555
	-0.302	0.046	-0.0105	0.0309	-0.3485	0.0478	-0.0091	0.095
	-0.3666	0.0307	0.0194	0.0179	-0.4107	0.0439	0.026	0.0885
	0.0779	-0.0385	-0.0297	0.0435	0.0843	-0.02	-0.0606	0.0133
	0.3913	-0.0404	-0.023	-0.0611	0.4537	-0.0836	0.0226	-0.0553
	-0.2935	0.1723	-0.0091	-0.0924	-0.3166	0.1672	-0.0361	-0.0905
	0.2081	0.0232	-0.0465	0.0596	0.2265	0.0447	-0.1085	0.1913
	-0.8796	0.0276	-0.0623	-0.0334	-0.9126	-0.0143	-0.0251	0.0253
	-0.7621	-0.3202	-0.0735	0.3173	-0.782	-0.3149	-0.0361	0.2779
	0.1622	0.1376	0.1553	-0.0164	0.1767	0.1782	0.2003	-0.1121
	-0.2132	0.1272	0.1784	0.7458	-0.2887	0.1202	0.1583	0.6299
	1	1	1	1	1	1	1	1
	-0.0759	-0.0119	0.0017	-0.0733	-0.0645	0.0188	0.0026	0.0331
	0.2475	-0.2597	-0.6415	-0.2634	0.0901	-0.253	-0.7604	-0.436
	0.6613	-0.0196	-0.1923	0.094	0.7903	-0.0273	-0.1423	-0.0225
	-0.0339	0.0311	0.0196	0.002	0.0532	0.0701	0.0104	0.0043
	-0.0833	-0.0526	-0.1371	-0.006	-0.1415	-0.0462	-0.1777	-0.0123
	-0.0866	0.048	-0.0712	0.0987	-0.1097	0.0466	-0.0875	0.0845

Table 6.10: Mode shapes obtained with EFDD and SSI-cov Layout 1VC

6.2.2 Layout 2 Analysis for building in Via Concezione:

For the experimental Campaign, the registered signals for Layout 2 are reported in the following figures:

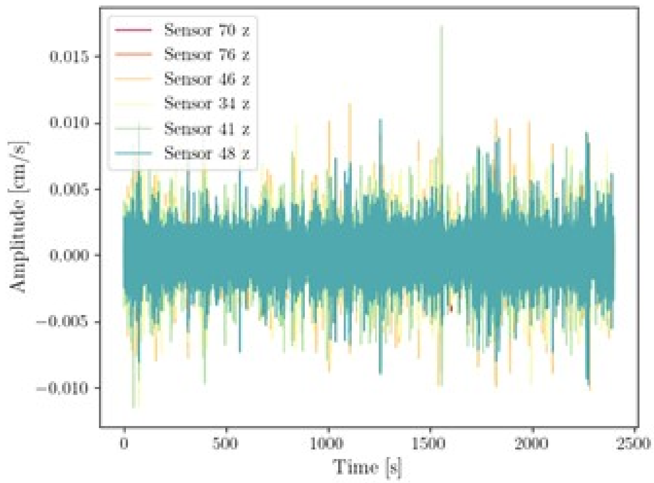

Figure 6.23: Signals recorded continuously in Layout 2 of Via Concezione for Z direction

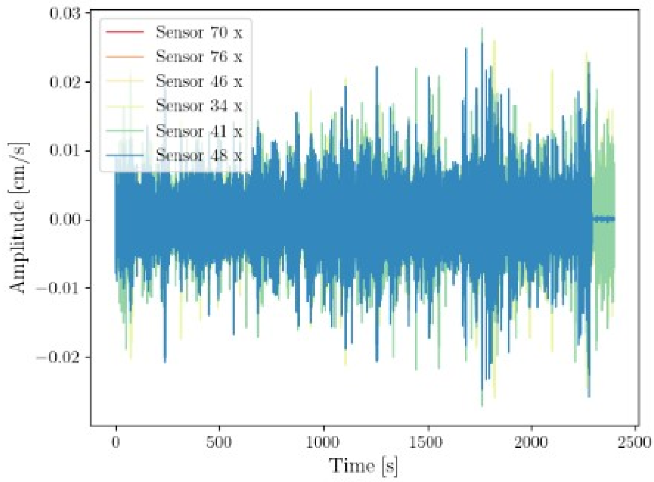

Figure 6.24: Signals recorded continuously in Layout 2 of Via Concezione for X direction

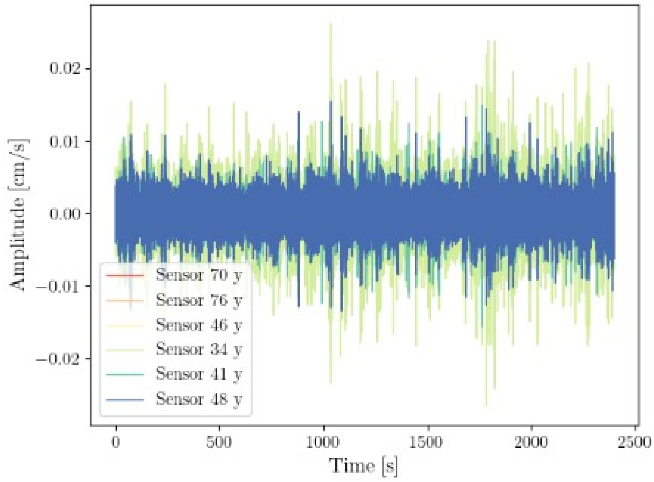

Figure 6.25: Signals recorded continuously in Layout 2 of Via Concezione for Y direction

To further refine the analyses, the signals were decimated with a decimation factor of 5, to increase the resolution of the information and attempt to identify the most probable first natural frequencies of the monitored system. The stabilisation diagram superimposed on the SVD (Singular Value Decomposition) of the PSD (Power Spectral Density) is shown in Figure 6.26. From this, it was possible to identify five possible natural frequencies of the system. The results in terms of frequencies, damping and mode shapes are reported in the following tables.6.11 6.12

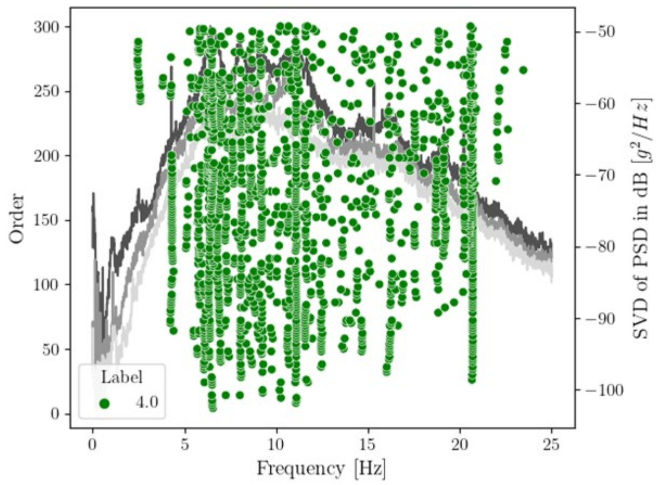

Figure 6.26: Stabilisation diagram presenting only the stable poles superimposed on the SVD of the PSD considering only the first 3 SVs, Layout 2, Via Concezione

EFDD		**SSI-cov**	
f [Hz]	**Damping [%]**	**f [Hz]**	**Damping [%]**
4.28	0.11%	4.32	4.93%
6.77	4.23%	6.39	3.88%
8.04	0.87%	8.06	2.46%
9.24	0.71%	9.18	2.72%
11.18	0.48%	11.08	2.46%

Table 6.11: Frequency and damping obtained with EFDD and SSI-cov for Layout 2 Via Concezione

	EFDD					SSI-cov				
f [Hz]	**4.28**	**6.77**	**8.04**	**9.24**	**11.18**	**4.32**	**6.39**	**8.06**	**9.18**	**11.08**
Φ ij	-0.3222	-0.055	-0.028	-0.0442	-0.018	-0.177	-0.0594	-0.0394	-0.0594	-0.0097
	-0.2018	-0.0485	-0.0052	-0.0528	-0.0033	-0.1508	-0.0641	-0.0164	-0.0625	0.0247
	-0.2523	-0.0393	-0.0289	-0.0427	-0.0144	-0.0635	-0.0479	-0.0433	-0.0517	0.0089
	0.0351	-0.2019	0.0255	0.0869	-0.0221	0.1013	-0.2043	-0.0804	0.1159	-0.071
	0.3679	-0.4552	-0.1512	0.2213	-0.2196	-0.0611	-0.4092	-0.1284	0.1865	-0.2088
	-0.1493	0.413	-0.0766	-0.0059	-0.1854	-0.1239	0.3653	-0.0448	0.0285	-0.1871
	0.1334	-0.0734	-0.0251	-0.1293	0.0192	0.1507	-0.0017	0.0864	-0.1982	0.0716
	-0.7686	0.1029	0.0319	0.2149	-0.0242	-0.6522	-0.0119	0.0106	0.1777	-0.0067
	-0.7103	0.3042	0.0079	0.3089	0.1594	-0.036	0.2762	0.0552	0.2586	0.2313
	-0.0818	0.1844	-0.0407	0.0114	-0.104	-0.029	0.1413	-0.1	0.0698	-0.1494
	-0.2436	-0.7092	1	-0.893	0.0699	-0.004	-0.7495	1	-0.8426	0.0899
	1	-0.9744	-0.8454	0.9508	0.5929	0.3358	-0.7888	-0.9395	0.6851	0.5662
	-0.0565	-0.065	0.0414	-0.1252	-0.0527	-0.2391	-0.0065	-0.013	-0.0385	0.0043
	0.192	0.0944	0.3462	1	-0.1161	0.0587	0.2727	0.6426	1	-0.1549
	0.4995	0.1283	0.144	0.3366	0.0996	1	-0.0364	0.0992	0.2902	0.0751
	0.1134	-0.4798	0.0839	0.121	-0.0734	0.1581	-0.4543	-0.0207	0.1162	-0.117
	-0.3508	1	-0.0786	-0.1001	1	0.2284	1	-0.0844	-0.0735	1
	-0.3711	0.9598	-0.0424	-0.1404	-0.2509	-0.1522	0.8641	0.0035	-0.0035	-0.2534

Table 6.12: Mode shapes obtained with EFDD and SSI-cov Layout 2VC

6.3 Closing remarks from the results with traditional OMA techniques

The processing and consequent analysis of the data acquired from AVT under the philosophy of traditional OMA techniques required a rather laborious process of analysis, peak-picking, and interpretation. Nonetheless, as illustrated in the previous subsection, the results obtained made it possible to grasp the most probable modal parameters of the structure guaranteed by having a sufficient data acquisition range of the senseable signals. Given that the Enhanced Frequency Domain Decomposition (EFDD) is based on the calculation of the response spectra starting from the recorded data, long-term recordings were also intended and performed to contain the error in the estimation of the spectra and, therefore, to extract the modal parameters in a more reliable way. However, although in principle this technique is capable of identifying even nearby modes, in the case of modes that are not sufficiently distant from one to another the damping and therefore the whole estimation is unreliable due to decay phenomena.

A relatively more accurate estimate of the damping, even in the presence of close-by modes, is obtained through the SSI (Stochastic Subspace Identification), in this case, long acquisition duration guarantees a more stable and reliable identification of the modal parameters and, in particular, of the damping ratios. In conclusion, the most probable modal parameters associated with the first modes of the analysed structures were identified through the cumulative appearance of similarities in the results between the various setups analysed. Furthermore, two different techniques (EFDD and SSI-cov) were used to cross-reference the results and guarantee independence giving mutual validation among both procedures.

Ahead a cutting-edge analysis technique in the field of SHM will be displayed, based on an evolution of traditional techniques combined in an effective way with the automatic recognition of the most probable modal parameters through the use of Machine Learning and Artificial Intelligence, thus avoiding the prone-to-error manual process of the traditional peak-picking method. In this way, could be compare the natural frequencies identified with traditional OMA techniques with advanced techniques, giving the process a further validation of the modal parameters.

Chapter 7

Processing and interpretation of the Dynamic test results – integrating OMA techniques, Machine Learning and Artificial Intelligence (AI).

As introduced in section [cite State of The Art OMA Techniques], SSI-cov is nowadays one of the most widespread OMA techniques regarding the latest developments in SHM. However, this technique still requires careful man-made decision making compromising his intervention with detailed engineering criteria and knowledge. Such direction given by the engineer in charge of analysing the data and defining the threshold parameters will govern the analysis algorithm, for instance by deciding over the number of block rows of the Hankel matrix and the maximum order of the system.

Reviewing the concepts identified by [28][27], for different sub-thresholds of the same output-only signal recorded on the same structure should always identify the same recurring modal parameters, given that, even when the environmental input varies, the structural system is always the same and it is hypothesised in a linear field under current type excitation. Furthermore, in the traditional SSI-cov technique, once the stabilisation diagram has been obtained, the user is required to have a certain degree of experience and sensitivity in grasping the most probable alignments of the stable poles considering all the information available. Given the recurrent difficulties for objectively interpreting the stabilisation diagram, in traditional OMA it is commonly seen to use at least two techniques such as EFDD and SSI-cov for mutual validation, such can be performed by applying a superposition of the stabilisation diagram over the diagram of the SVD (Singular Value Decomposition) of the PSD (Power Spectral Density).

As evidenced in the previous chapters, it is strongly motivated the investigate cutting-edge techniques attempting to reduce the user intervention and further automatic control of the dynamic identification process. There are numerous new techniques that have been developed in the last period, often oriented towards automatic OMA (A-OMA) and/or approaches based on artificial intelligence, such as automatic clustering techniques of stable poles in the stabilisation diagram. Considering such new developments and the improvement in the procedure it could provide, the use of a recent technique called Intelligent Automatic Operational Modal Analysis (i-AOMA) [22], in these cases using only phase 1 of the method.

In summary, the technique allows to perform a series of quasi-Monte Carlo sampling of the parameters that govern the SSI-cov algorithm and, consequently, automatically analyse a certain number of stabilisation diagrams obtained from different input parameters and different portions of the same signal. The essence of the method then lies in superimposing all the stable poles of the different analyses on a global stabilisation diagram, and in analysing the alignments of the most recurrent stable poles through a ***Machine Learning technique*** based on a ***non-parametric statistical method called kernel estimation of density***, or ***kernel density estimation (KDE)***. The KDE graph will represent the probability density along the axis of natural frequencies, identifying with its peaks the most probable and recurring modal parameters of the analysed structural system. The extraction of peaks is also managed automatically, through a statistical selection criterion, which also allows to provide a degree of reliability in the identified natural frequency. By default, this threshold is set at a type 1 error probability of 1%, i.e. that a particular mode, even when selected, is still a false mode and without any correspondence with the physics of the problem under consideration.

7.1 i-AOMA Processing: Building located in Piazza XX Settembre.

7.1.1 Layout 1 AI - Analysis for building in Piazza XX Settembre:

The Layout 1 collected data, will undergo a process of detrending and decimation using a scaling factor of 5, afterwards, it was analysed with the i-AOMA technique phase 1. Specifically, a number equal to 40 steps for the SSI-cov analysis was set. The algorithm automatically identified the admissible range of input parameters, thus defining how to perform the quasi-Monte Carlo sampling of the block-rows parameters, maximum order of the system, length of the signal sub-threshold and position in which to centre the threshold to extract. After the 40 fixed analyses, the algorithm outputs a global stabilisation diagram, overlaying the results of all the analyses performed, as shown in Figure 7.1.

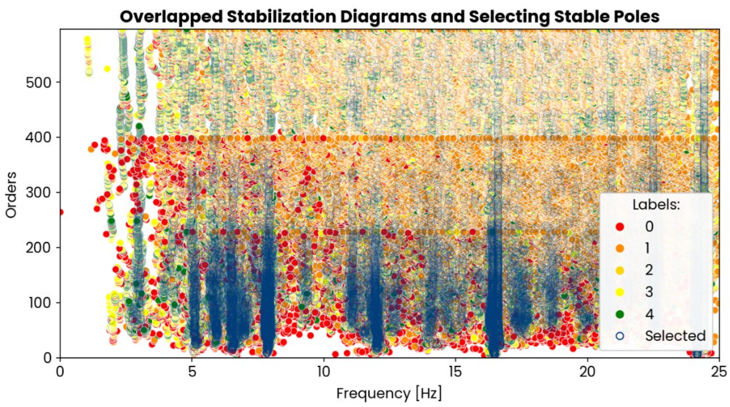

Figure 7.1: Global Stabilisation Diagram Layout 1

The algorithm then automatically removed the false poles and kept only the stable poles, as shown in Figure 7.2 7.3. Finally, the same figure shows the KDE graph which was estimated starting from the global stabilisation diagram cleaned of the false modes. KDE is still retaining a bit of noise, perhaps requiring a greater number of analyses. However, with a number of iterations equal to 40, considered as a good compromise between computational burden and analysis time, the algorithm still identified 5 possible most promising natural frequencies in the analysis range within the Nyquist frequency (25Hz).

Layout 1	Frequency i-AOMA [Hz]	7.96	16.61	24.06	24.17	24.42

Table 7.1: Automatically obtained Natural Frequencies Layout1

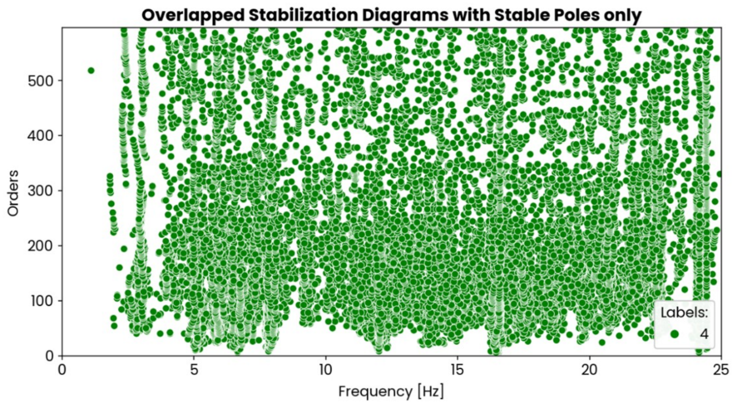

Figure 7.2: Global stabilisation diagram keeping only the stable poles Layout 1

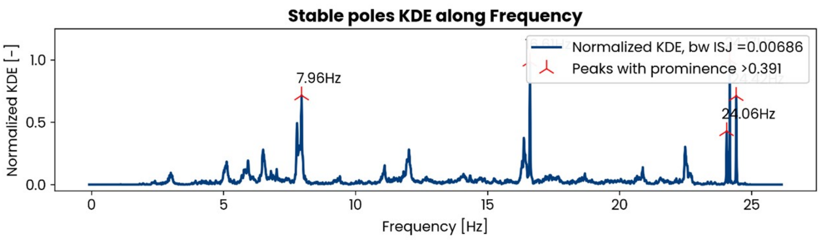

Figure 7.3: Estimated KDE with identification of the most probable peaks automatically extracted by the algorithm for Layout 1

Regarding Layout 1 transformed under i-AOMA based on Machine Learning seemed to preliminary confirm only the mode at around 7.8Hz also identified with traditional OMA techniques.

7.1.2 Layout 2 AI - Analysis for building in Piazza XX Settembre:

The Layout 2 collected data, will undergo a process of detrending and decimation using a scaling factor of 5, afterwards, it was analysed with the i-AOMA technique phase 1. Specifically, a number equal to 40 steps for the SSI-cov analysis was set. The algorithm automatically identified the admissible range of input parameters, thus defining how to perform the quasi-Monte Carlo sampling of the block-rows parameters, maximum order of the system, length of the signal sub-threshold and position in which to centre the threshold to extract. After the 40 fixed analyses, the algorithm outputs a global stabilisation diagram, overlaying the results of all the analyses performed, as shown in Figure 7.4.

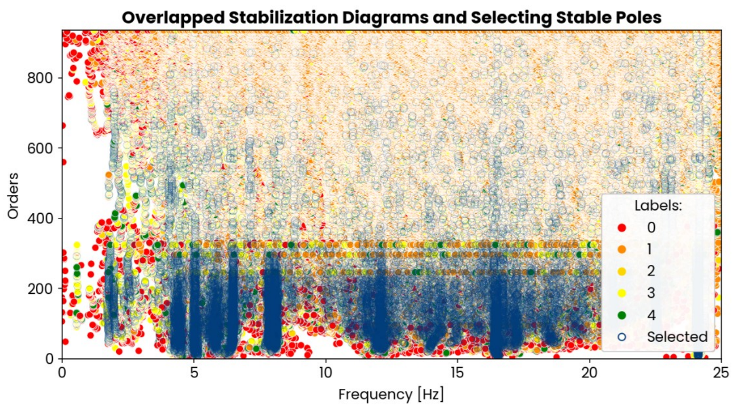

Figure 7.4: Global Stabilisation Diagram Layout 2

The algorithm then automatically removed the false poles and kept only the stable poles, as shown in Figure 7.5 7.6. Finally, the same figure shows the KDE graph which was estimated starting from the global stabilisation diagram cleaned of the false modes. KDE is still retaining a bit of noise, perhaps requiring a greater number of analyses. However, with a number of iterations equal to 40, considered as a good compromise between computational burden and analysis time, the algorithm still identified 8 possible most promising natural frequencies in the analysis range within the Nyquist frequency (25Hz).

Layout 2	Frequenze i-AOMA [Hz]	5.05	6.46	7.87	8.1	16.45	22.52	24.05	24.17

Table 7.2: Automatically obtained Natural Frequencies Layout2

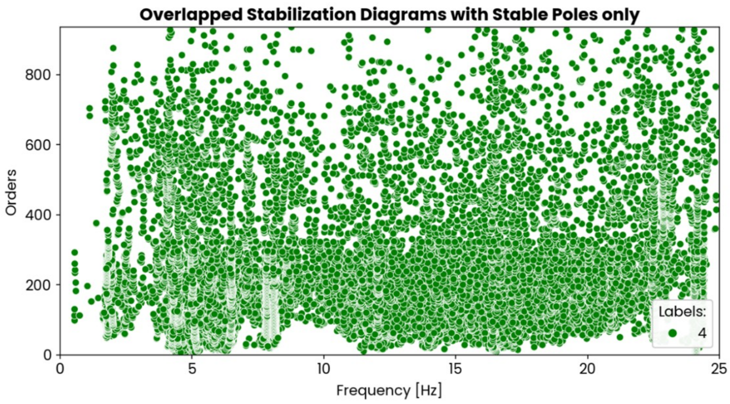

Figure 7.5: Global stabilisation diagram keeping only the stable poles Layout 2

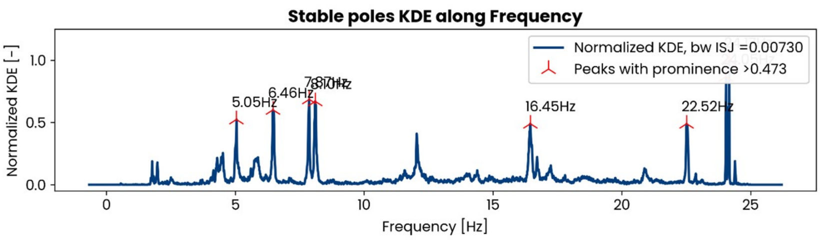

Figure 7.6: Estimated KDE with identification of the most probable peaks automatically extracted by the algorithm for Layout 2

Regarding the Layout 2 transformed under i-AOMA based on Machine Learning seemed to confirm only the mode at around 4.5Hz, 6.4Hz and 8.2Hz, also identified with traditional OMA techniques.

7.1.3 Layout 3 AI - Analysis for building in Piazza XX Settembre:

The Layout 3 collected data, will undergo a process of detrending and decimation using a scaling factor of 5, afterwards, it was analysed with the i-AOMA technique phase 1. Specifically, a number equal to 40 steps for the SSI-cov analysis was set. The algorithm automatically identified the admissible range of input parameters, thus defining how to perform the quasi-Monte Carlo sampling of the block-rows parameters, maximum order of the system, length of the signal sub-threshold and position in which to centre the threshold to extract. After the 40 fixed analyses, the algorithm outputs a global stabilisation diagram, overlaying the results of all the analyses performed, as shown in Figure 7.7.

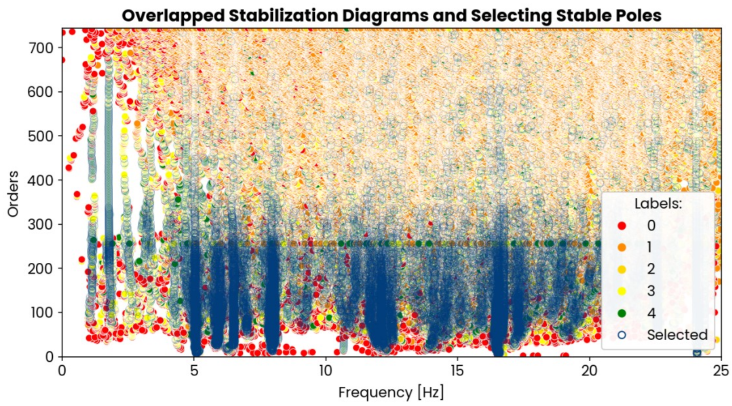

Figure 7.7: Global Stabilisation Diagram Layout 3

The algorithm then automatically removed the false poles and kept only the stable poles, as shown in Figure 7.8 7.9. Finally, the same figure shows the KDE graph which was estimated starting from the global stabilisation diagram cleaned of the false modes. KDE is still retaining a bit of noise, perhaps requiring a greater number of analyses. However, with a number of iterations equal to 40, considered as a good compromise between computational burden and analysis time, the algorithm still identified 7 possible most promising natural frequencies in the analysis range within the Nyquist frequency (25Hz).

Layout 3	Frequenze i-AOMA [Hz]	5.06	6.51	8.04	12.11	16.75	24.04	24.17

Table 7.3: Automatically obtained Natural Frequencies Layout3

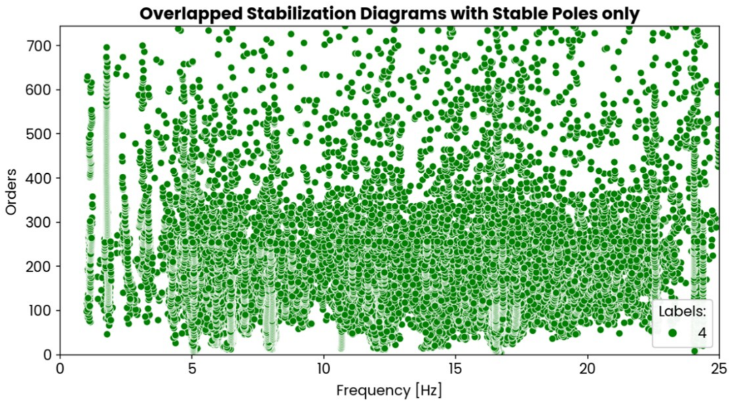

Figure 7.8: Global stabilisation diagram keeping only the stable poles Layout 3

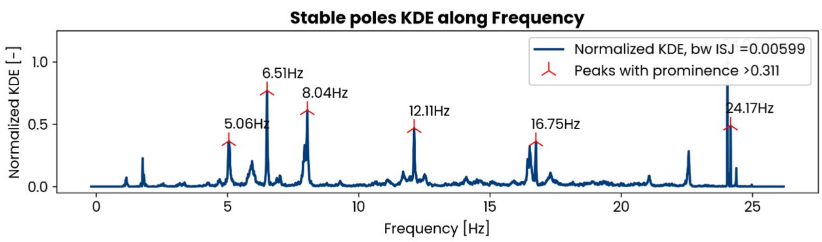

Figure 7.9: Estimated KDE with identification of the most probable peaks automatically extracted by the algorithm for Layout 3

Regarding Layout 3 transformed under i-AOMA based on Machine Learning seemed to preliminary confirm only the mode at around 4.5Hz, 6.4Hz, 8.2Hz and 11.0Hz, also identified with traditional OMA techniques.

7.1.4 Layout 4 AI - Analysis for building in Piazza XX Settembre:

The Layout 4 collected data, will undergo a process of detrending and decimation using a scaling factor of 5, afterwards, it was analysed with the i-AOMA technique phase 1. Specifically, a number equal to 40 steps for the SSI-cov analysis was set. The algorithm automatically identified the admissible range of input parameters, thus defining how to perform the quasi-Monte Carlo sampling of the block-rows parameters, maximum order of the system, length of the signal sub-threshold and position in which to centre the threshold to extract. After the 40 fixed analyses, the algorithm outputs a global stabilisation diagram, overlaying the results of all the analyses performed, as shown in Figure 7.10.

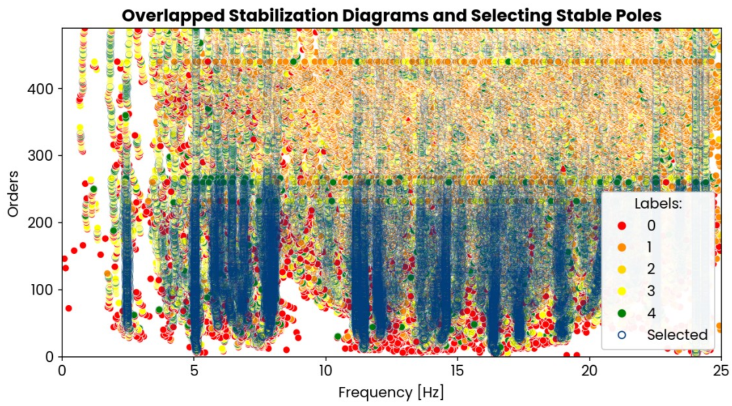

Figure 7.10: Global Stabilisation Diagram Layout 4

The algorithm then automatically removed the false poles and kept only the stable poles, as shown in Figure 7.11 7.12. Finally, the same figure shows the KDE graph which was estimated starting from the global stabilisation diagram cleaned of the false modes. KDE is still retaining a bit of noise, perhaps requiring a greater number of analyses. However, with a number of iterations equal to 40, considered as a good compromise between computational burden and analysis time, the algorithm still identified 7 possible most promising natural frequencies in the analysis range within the Nyquist frequency (25Hz).

Layout 4	Frequenze i-AOMA [Hz]	5.05	11.16	11.47	14.56	22.54	24.03	24.39

Table 7.4: Automatically obtained Natural Frequencies Layout4

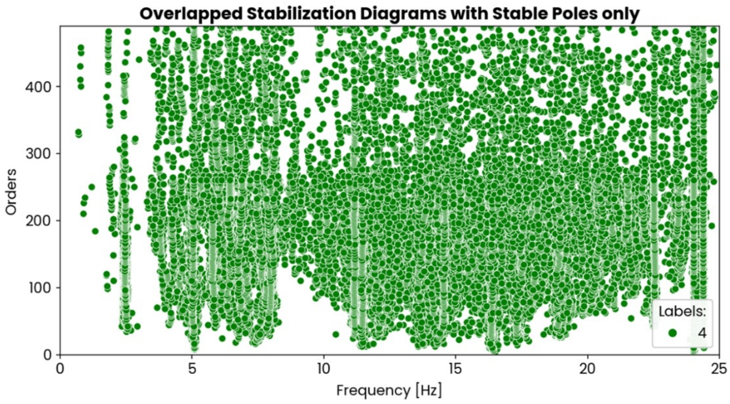

Figure 7.11: Global stabilisation diagram keeping only the stable poles Layout 4

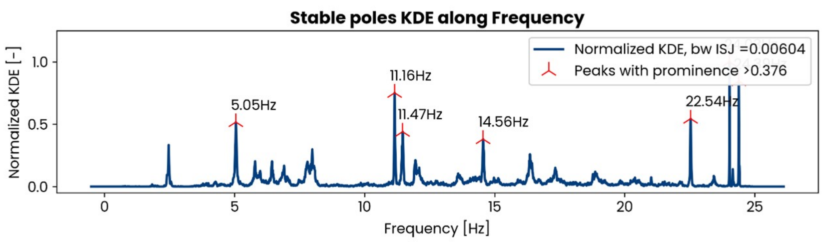

Figure 7.12: Estimated KDE with identification of the most probable peaks automatically extracted by the algorithm for Layout 4

Regarding the Layout 4 transformed under i-AOMA based on Machine Learning seemed to confirm only the mode at around 4.5Hz and 11.0Hz, also identified with traditional OMA techniques.

7.2 i-AOMA Processing: Building located in Via Concezione

7.2.1 Layout 1 AI - Analysis for building in Via Concezione:

The Layout 1 collected data, will undergo a process of detrending and decimation using a scaling factor of 5, afterwards, it was analysed with the i-AOMA technique phase 1. Specifically, a number equal to 40 steps for the SSI-cov analysis was set. The algorithm automatically identified the admissible range of input parameters, thus defining how to perform the quasi-Monte Carlo sampling of the block-rows parameters, maximum order of the system, length of the signal sub-threshold and position in which to centre the threshold to extract. After the 40 fixed analyses, the algorithm outputs a global stabilisation diagram, overlaying the results of all the analyses performed, as shown in Figure 7.13.

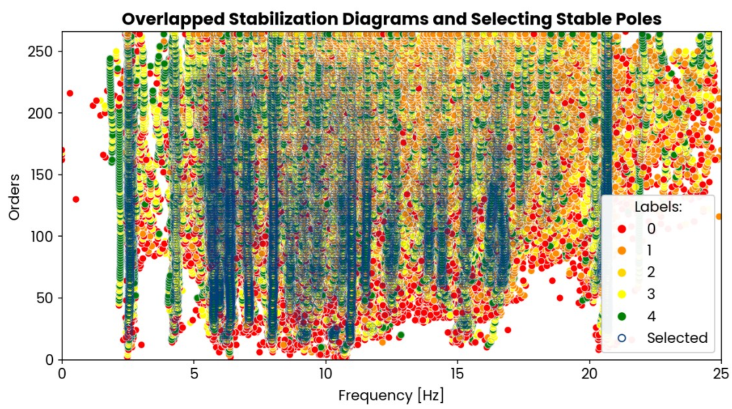

Figure 7.13: Global Stabilisation Diagram Layout 1 Via Concezione

The algorithm then automatically removed the false poles and kept only the stable poles, as shown in Figure 7.14 7.15. Finally, the same figure shows the KDE graph which was estimated starting from the global stabilisation diagram cleaned of the false modes. KDE is still retaining a bit of noise, perhaps requiring a greater number of analyses. However, with a number of iterations equal to 40, considered as a good compromise between computational burden and analysis time, the algorithm still identified 5 possible most promising natural frequencies in the analysis range within the Nyquist frequency (25Hz).

Layout 1	Frequenze i-AOMA [Hz]	6.36	8	11	20.58	20.69

Table 7.5: Automatically obtained Natural Frequencies Layout 1 Via Concezione

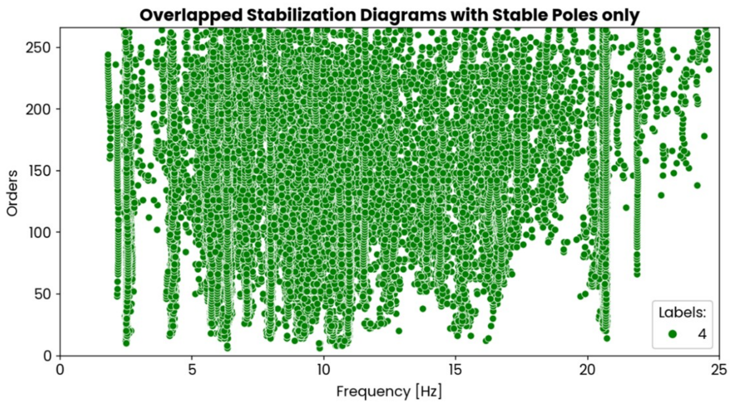

Figure 7.14: Global stabilisation diagram keeping only the stable poles Layout 1 Via Concezione

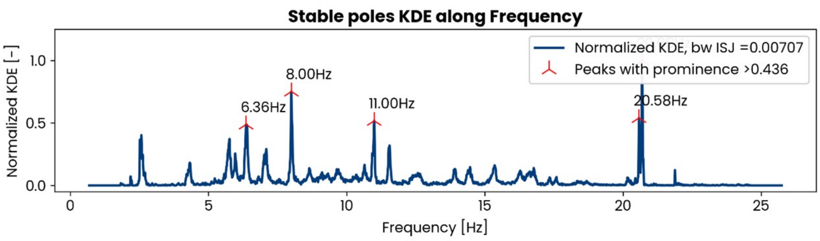

Figure 7.15: Estimated KDE with identification of the most probable peaks automatically extracted by the algorithm for Layout 1 Via Concezione

Regarding Layout 1 transformed under i-AOMA based on Machine Learning seemed to preliminary confirm the modes around 6.3 Hz, 8.0 Hz and 11.0 Hz also identified with traditional OMA techniques.

7.2.2 Layout 2 AI - Analysis for building in Via Concezione:

The Layout 2 collected data, will undergo a process of detrending and decimation using a scaling factor of 5, afterwards, it was analysed with the i-AOMA technique phase 1. Specifically, a number equal to 40 steps for the SSI-cov analysis was set. The algorithm automatically identified the admissible range of input parameters, thus defining how to perform the quasi-Monte Carlo sampling of the block-rows parameters, maximum order of the system, length of the signal sub-threshold and position in which to centre the threshold to extract. After the 40 fixed analyses, the algorithm outputs a global stabilisation diagram, overlaying the results of all the analyses performed, as shown in Figure 7.16.

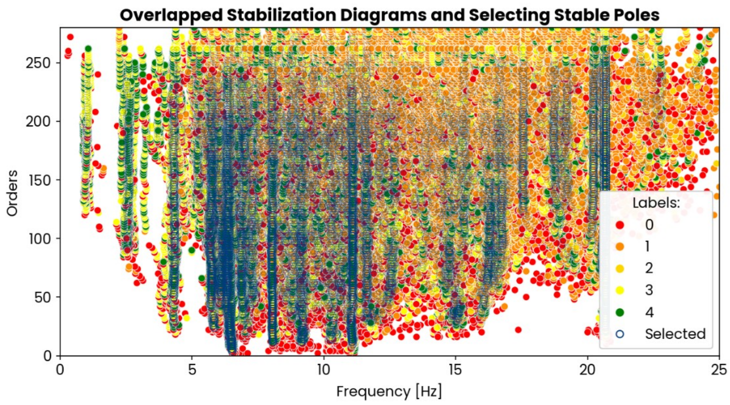

Figure 7.16: Global Stabilisation Diagram Layout 2 Via Concezione

The algorithm then automatically removed the false poles and kept only the stable poles, as shown in Figure 7.17 7.18. Finally, the same figure shows the KDE graph which was estimated starting from the global stabilisation diagram cleaned of the false modes. KDE is still retaining a bit of noise, perhaps requiring a greater number of analyses. However, with a number of iterations equal to 40, considered as a good compromise between computational burden and analysis time, the algorithm still identified 4 possible most promising natural frequencies in the analysis range within the Nyquist frequency (25Hz).

Layout 2	Frequenze i-AOMA [Hz]	8	11.09	20.61	20.7

Table 7.6: Automatically obtained Natural Frequencies Layout 2 Via Concezione

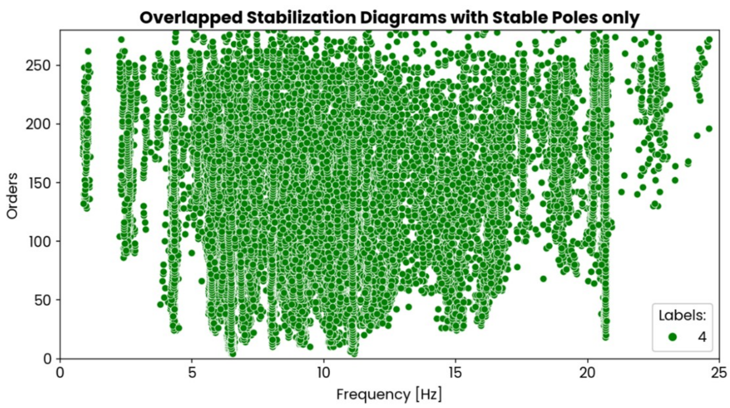

Figure 7.17: Global stabilisation diagram keeping only the stable poles Layout 2 Via Concezione

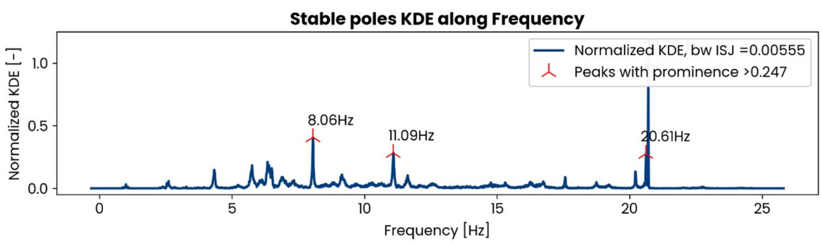

Figure 7.18: Estimated KDE with identification of the most probable peaks automatically extracted by the algorithm for Layout 2 Via Concezione

Regarding Layout 2 transformed under i-AOMA based on Machine Learning seemed to preliminary confirm the modes at around 8.0 Hz and 11.0 Hz also identified with traditional OMA techniques.

7.3 Closing Remarks from the results obtained with i-AOMA techniques.

AOMA techniques (based on Machine Learning). The i-AOMA technique was used to compare the modal parameters obtained with the traditional OMA approach and validate their values. The main advantage of automatic techniques is that minimal effort is required from the user since most of the process is managed completely autonomously by the algorithm. However, it is evident to underline how, in this context, an arbitrary number of analyses equal to 40 was set which represented a good compromise between the computational burden required and the analysis time spent. However, the modes identified with the i-AOMA technique have not always found their coupling partner derived from the usage of traditional OMA techniques (EFDD and SSI-cov). The main causes are in fact to be traced back to the complexity of the buildings analysed, which would therefore also require a substantial number of analyses in order to obtain less noise into the estimation of the KDE and allow a simpler selection of the actually recurring modal parameters. Furthermore, it is worth noting that with a manual approach very close modes were associated with a single mode characterised therefore by a single natural frequency. Instead, it is essential to underline how the i-AOMA method was able to capture, with so little analysis, very similar and recurring modes, probably due to decay phenomena or other.

In any case, it is possible to state that the use of the two joint traditional OMA techniques (EFDD and SSI-cov), together with the use of techniques based on artificial intelligence and automatic procedures such as i-AOMA, has allowed to have a global vision of the results, found with a certain guarantee between the different techniques adopted and between the different setups used.

Chapter 8

Finite Element Modelling and Modal Analysis: Case of Study Piazza XX Settembre and Via Concezione

8.1 Opening considerations:

The first case study structure under which the investigation will be developed is used by the Department of Political and Legal Sciences for the University of Messina. The building under study is characterised by being composed of a single structural body. During the inspection, 1 main entrance was detected in Piazza XX Settembre while secondary entrances were in correspondence with the 2 internal courtyards. Specifically, the internal part of the building borders an external space that is partly green and partly paved. The entire building is spread over a covered area of approximately 1000 m2 in the basement and on the ground floor, and approximately 800 m2 on the first floor. The previous data can be appreciated in the following satellite images and Street View Add-in in Google Earth Platform: Figures 8.1 8.2 8.3

Figure 8.1: Satellite Image 1 Piazza XX Settembre - Google Earth

Figure 8.2: Satellite Image 2 Piazza XX Settembre - Google Earth

Figure 8.3: Street View Reference Image 3 Piazza XX Settembre - Google Earth

Consistent with the construction technique of the time, the structure was built using masonry confined by reinforced concrete elements which appears to be one of the most widespread construction types in the area of interest. In correspondence with the cellar floor only, the perimeter wall is made up of concrete partitions placed adjacent to a masonry wall made of rough-hewn ashlars of various sizes and terracotta bricks. For these reasons, it is reasonable to think that the building appears as a mixed structure with a masonry load-bearing structure and reinforced concrete stiffening elements for both the external walls and the internal load-bearing vertical elements. Check the Figure 2.1.

The building is constituted of a basement and two floors above ground. It is noticed that the overall structure roof slab is coincident with the first-floor inner roof. All floor slabs were constructed using a solid reinforced concrete slab, thus exhibiting bidirectional plate behaviour. The roof is accessible via a retractable ladder located near the north side of the first floor. Furthermore, the entire roof is accessible, except for the roof of the main hall.

The vertical reference levels of the structure are specified as follows:

- Base level for FEM modelling will be in the bottom level of the basement "Piano Semiterrato"
- Inter story height of the Basement will be 3.15m [Global=3.15m]
- The height of the Ground Floor "Piano Terra" will be 4.5m [Global=7.65m].

• For the first Floor "Primo Piano" the height will be set at 5.0 m [Global=12.65m]
• The service room located on the roof will have a height of 3.0m [Global=15.65m]
• Particularly, in the area of the auditorium "Aula Magna" the clearance will be 7.5m measured from the ground floor [Global=10.65m]

Where the road edge was set as the reference height. During the inspection, despite the entire area being almost flat, the presence of a slope of the road edge along the perimeter of the building being more accentuated along two particular transversal directions of the same was observed.

Below are reported the architectural plans for the existing levels:

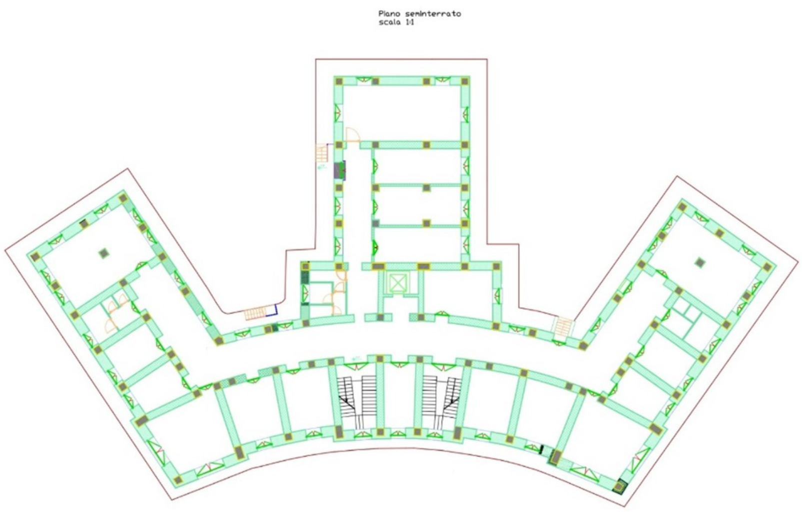

Figure 8.4: Basement Plan -4.1m Piazza XX Settembre

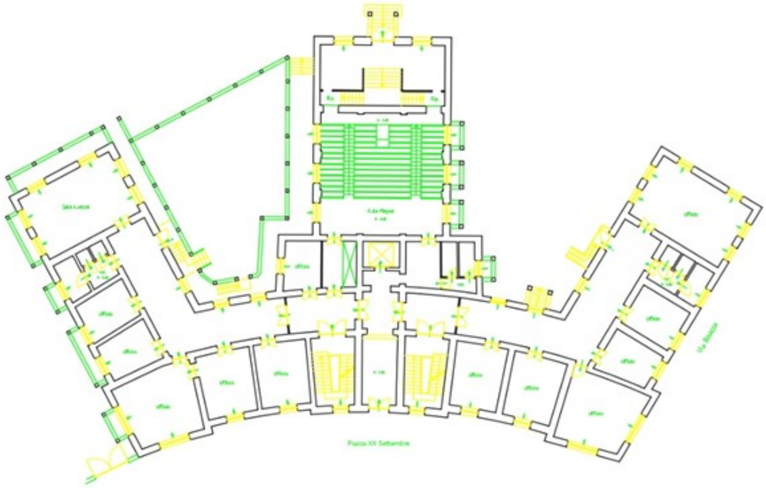

Figure 8.5: Ground Floor Plan 0m Piazza XX Settembre

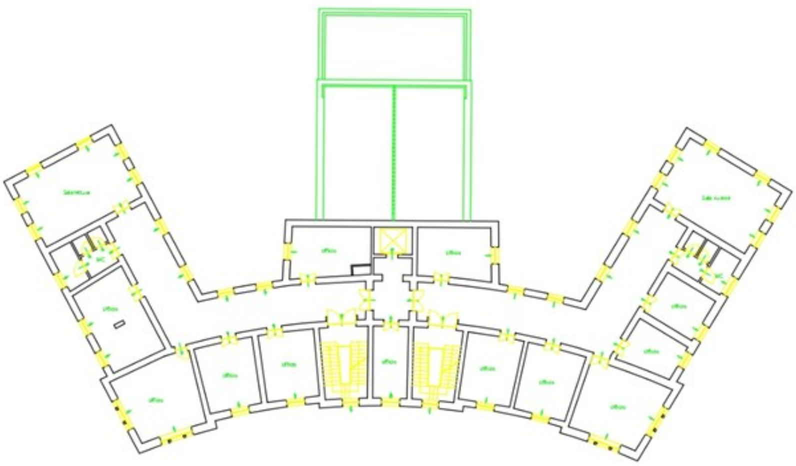

Figure 8.6: First Floor Plan +5.0m Piazza XX Settembre

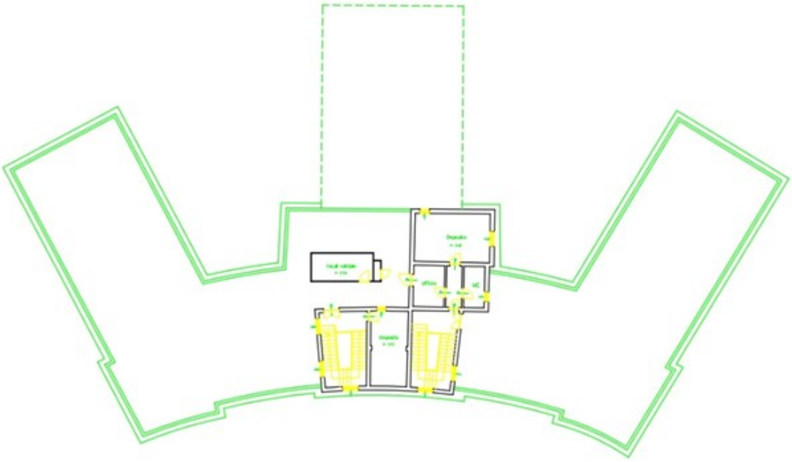

Figure 8.7: Roof Plan +10.0m Piazza XX Settembre

The Second case study structure under which the investigation will be developed is used by the Department of Cognitive, Psychological, Pedagogical and Cultural Studies Sciences. The building is characterised by being composed of a single structural body. During the inspection, 3 main entrances were detected in via Concezione while secondary entrances were located in correspondence with the 2 internal courtyards equipped with an external staircase leading to the mezzanine floor.

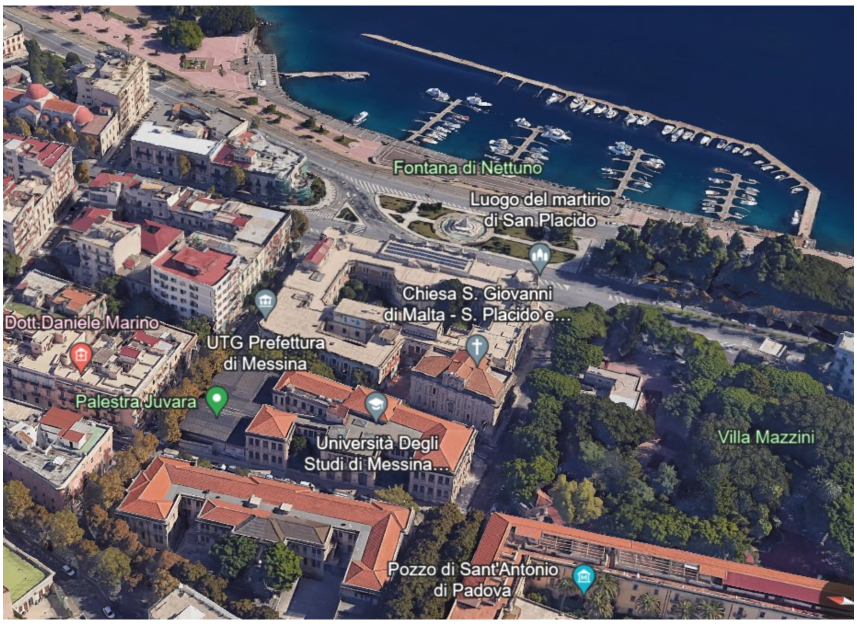

Figure 8.8: Satellite Image 1 Via Concezione - Google Earth

Figure 8.9: Satellite Image 2 Via Concezione - Google Earth

Consistent with the construction technique of the time, the structure in Via Concezione was also built using masonry confined by reinforced concrete elements. In correspondence with the cellar floor only, the perimeter wall is made up of concrete partitions placed adjacent to a masonry wall made of rough-hewn ashlars of various sizes and terracotta bricks. For these reasons, it is reasonable to think that the building appears as a mixed structure with a masonry load-bearing structure and reinforced concrete stiffening elements for both the external walls and the internal load-bearing vertical elements.

The building in Via Concezione is constituted of a basement and two floors above ground. It is noticed that the overall structure roof slab is coincident with the first-floor inner roof. All floors were created using a solid reinforced concrete slab, thus exhibiting bidirectional plate behaviour. The roof is accessible via a retractable ladder located near the north side of the first floor. Furthermore, only 30% of the roof can be walked on since the presence of floor plan obstructions such as skylights and tilted roofs is observed along the remaining part.

The vertical reference levels are:

- Foundations-based level is approximately -4.10 m from the reference plane.
- Average level assumed for the ground floor is equal to 0 m.

- Ground floor level at approximately 1.50 m.
- First-floor level at approximately 5.00 m.
- Roof level at approximately 10.00 m.

Here as well the road edge was set as the reference height but the presence of a slope of the road edge along the perimeter of the building being more accentuated along two particular transversal direction was observed.

Below are reported the architectural plans for the existing levels:

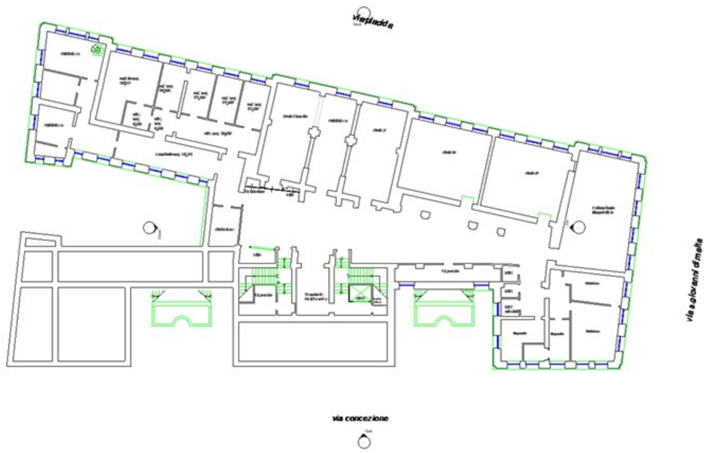

Figure 8.10: Basement Plan -4.1m Via Concezione

Figure 8.11: Ground Floor Plan 0m Via Concezione

Figure 8.12: First Floor Plan +5.0m Via Concezione

8.2 Legal Reference Framework.

All the activities carried out and the subjects of this report refer to the following regulatory framework:

• OPCM 3274 (2003). Ordinanza del Presidente del Consiglio dei Ministri del 20 Marzo 2003 Considerations regarding general criteria for the seismic classification of the national territory and technical regulations for constructions in seismic areas. Official Gazette dated 8/05/2003.
• Ministerial Decree of 01/17/2018 – "New technical standards for construction" (Complementary to NTC-18).
• CSLLPP Circular dated 01/21/2019 n.7 – "Instructions for the application of the Update of the new technical standards for construction" (Complementary Circular).

8.3 Data retrieved during the Survey Phase to Creation of a BIM model of the building.

To proceed with the numerical modelling of the building it was necessary to collect and interpret all the information obtained during the survey phase. Specifically, it was decided to create a BIM model using the Autodesk Revit software entirely based on the information received by the University of Messina. Starting from the Updated CAD files and verifying the data in Point Clouds format created based on the 3D laser scanner survey. The Process followed to develop the BIM is presented in section 8.3.1 until section 8.3.6

8.3.1 Point cloud inspection, data collection for technical drawings validation

The first step to guarantee the modelling accuracy was to perform a between-the-ground-floor construction blueprint with photo metrics retrieved during the LiDAR Scanner inspection of the building.

During the data collection, cloud points were raw acquired, and such information was filtered and processed within Autodesk ReCap software.

Figure 8.13: Point Cloud Autodesk Revit Import Piazza XX Settembre

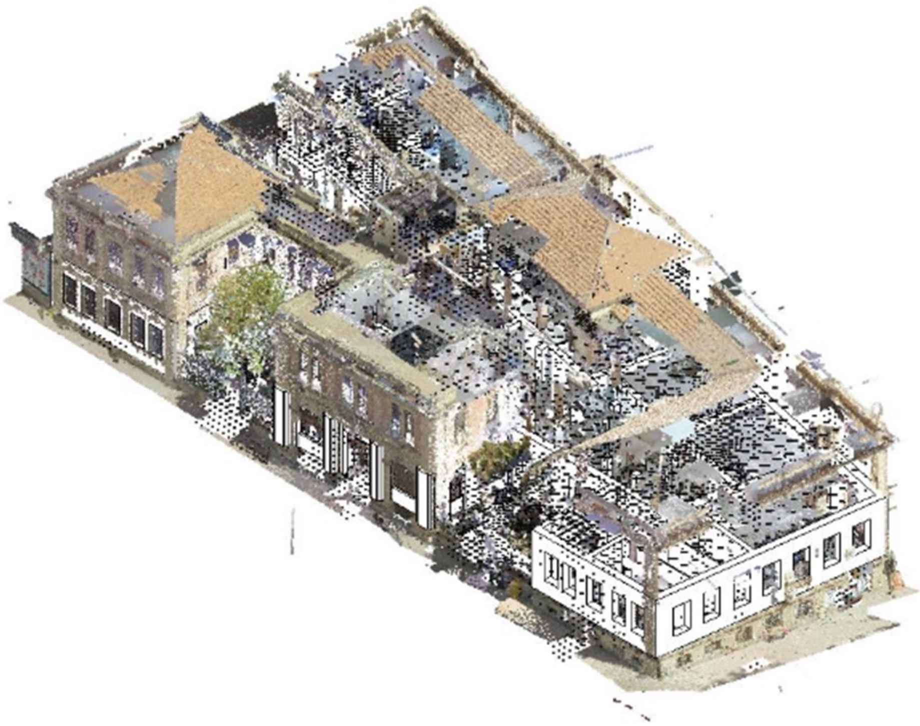

Figure 8.14: Point Cloud Autodesk Revit Import Via Concezione

Once in Autodesk Revit, the filtered point clouds generated in the previous steps as well as the supplied technical drawings were imported and referenced in order to validate the dimensions of the building and the gross geometric information regarding the floor plans and the height of the inter stories (reference levels) In the figures below the result of the superposition of geometrical information can be appreciated.

Figure 8.15: Elevation Superposition of Point Cloud with DWG Files for Piazza XX Settembre

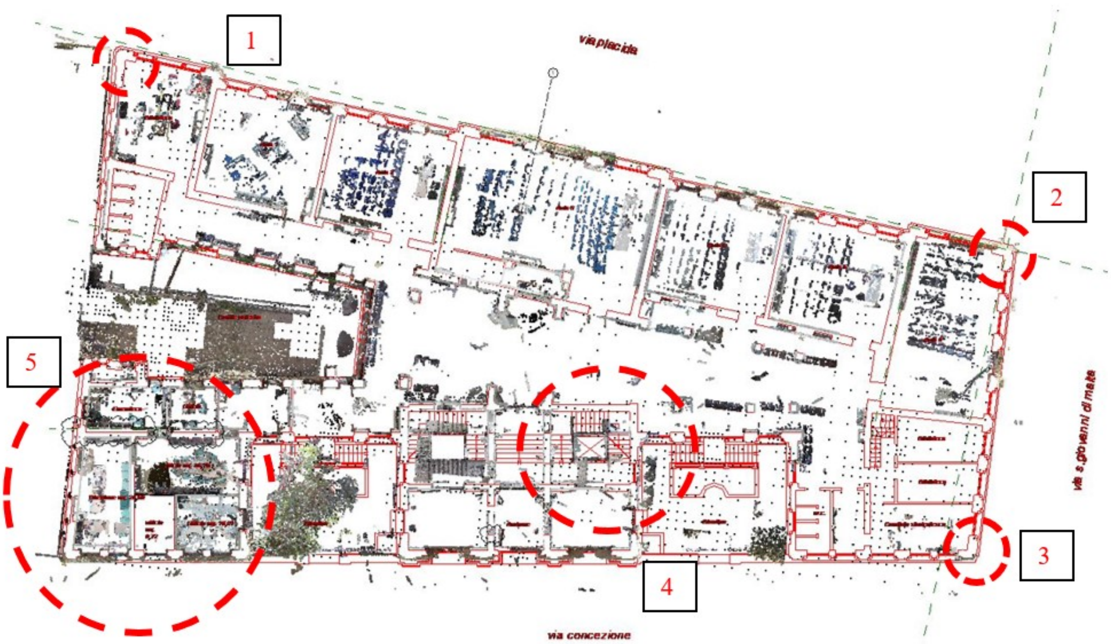

Figure 8.16: Superposition of Point Cloud with DWG Files for Via Concezione

According to the dashed reference points 1,2,3,4 and 5 the corners of the building provide the certainty of the outer dimensions of the building, as well as the angles and orientation of the wall in the floor plan. Also, elevation lines set in the point clouds can be established with a high level of confidence in the alignment of fixed structural points that replicate along the levels of the buildings.

8.3.2 Story by Story, the identification of important remarks within the technical drawings.

Once the Auto CAD files were validated using the point clouds obtained directly from a field data collection, the following step required to analyse the correlation of each level with the following to identify the continuity of vertical structural elements, as well as to present a valuable assumption of where are located the mainframe of the structure (considering this building to be constructed as a confined masonry structure).

To begin the process previously mentioned is mandatory to eliminate in the technical drawing all the information that avoids a clear appreciation of the relevant data, therefore only the walls, partitions, windows, facade elements and stairs were conserved during the filtering process the results can be highlighted in the following figures:

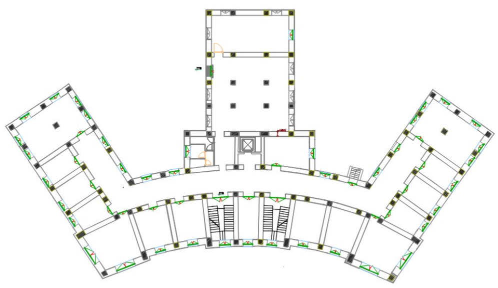

Figure 8.17: Filter DWG Plan Basement Piazza XX Settembre

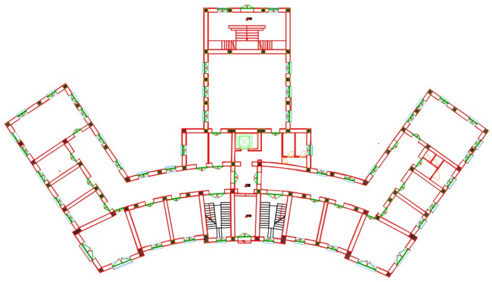

Figure 8.18: Filter DWG Plan Ground Floor Piazza XX Settembre

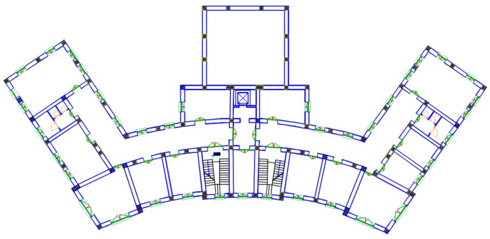

Figure 8.19: Filter DWG Plan First Floor Piazza XX Settembre

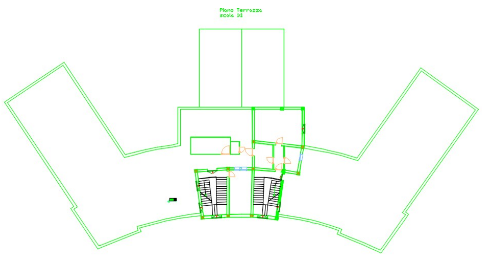

Figure 8.20: Filter DWG Roof Piazza XX Settembre

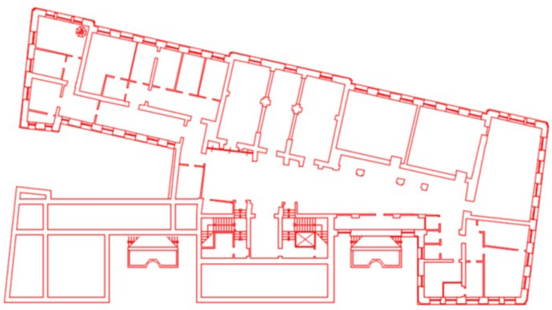

Figure 8.21: Filter DWG Plan Basement Via Concezione

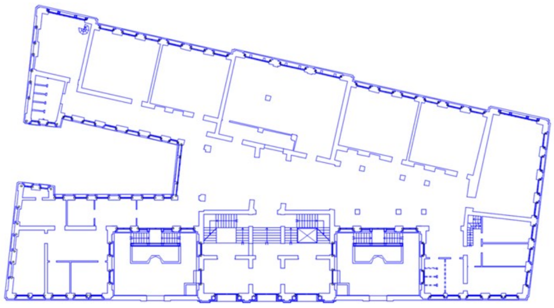

Figure 8.22: Filter DWG Plan Ground Floor Via Concezione

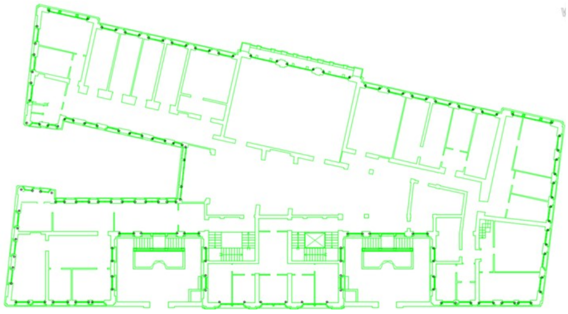

Figure 8.23: Filter DWG Plan First Floor Via Concezione

The independent floor plants were assigned a Datum according to the information presented in the supplied technical drawings and validated using the point clouds.

With certainty of the information presented on each floor is time to analyse all the levels of the building together therefore a superposition is once again performed but this time within All the Auto-CAD files already presented. The result will allow us to identify (with acceptable engineering criteria) the mainframe considering such as an equivalent structure that will allow us to model the behaviour of the confined masonry using frames and shells.

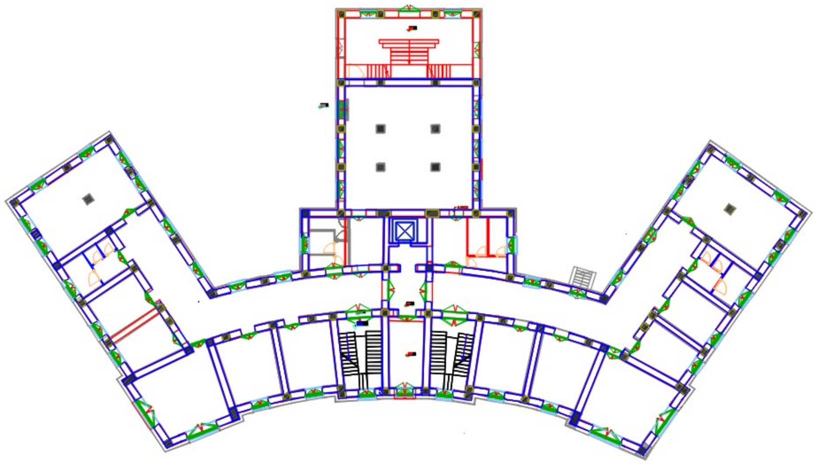

Figure 8.24: DWG Super position Piazza XX Settembre

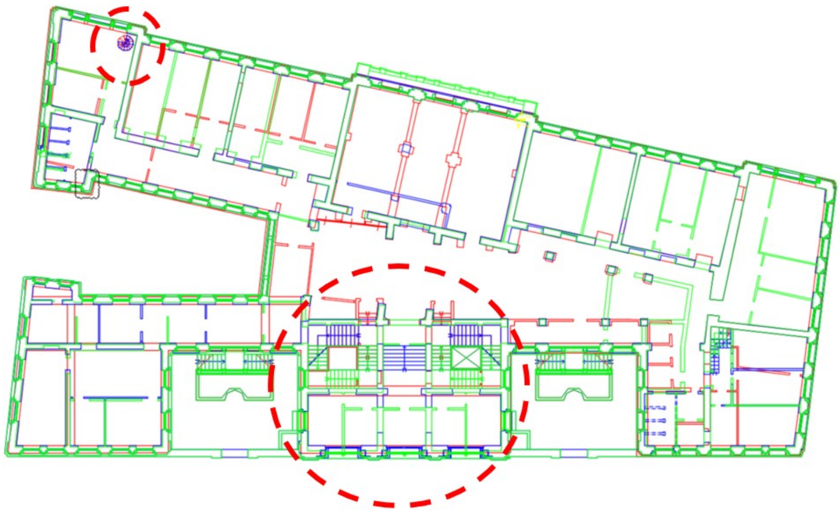

Figure 8.25: DWG Super position Via Concezione

Can be noticed that the superposition was well performed as the criteria were not based on matching the facade or the corners of the building but focusing the efforts on having a *perfect alignment in the stairs shaft.* **The results were optimal to proceed with the following steps.**

8.3.3 Definition of the main frame.

As the floor plans were already aligned the choosing of a main frame was only required to set criteria based on the literature available for this process. The proposal for the first iteration in the FE calculations is presented ahead. It's important to establish that for these early/mid stages, the dimensions of the structural elements are an approximation based on the experience and literature.

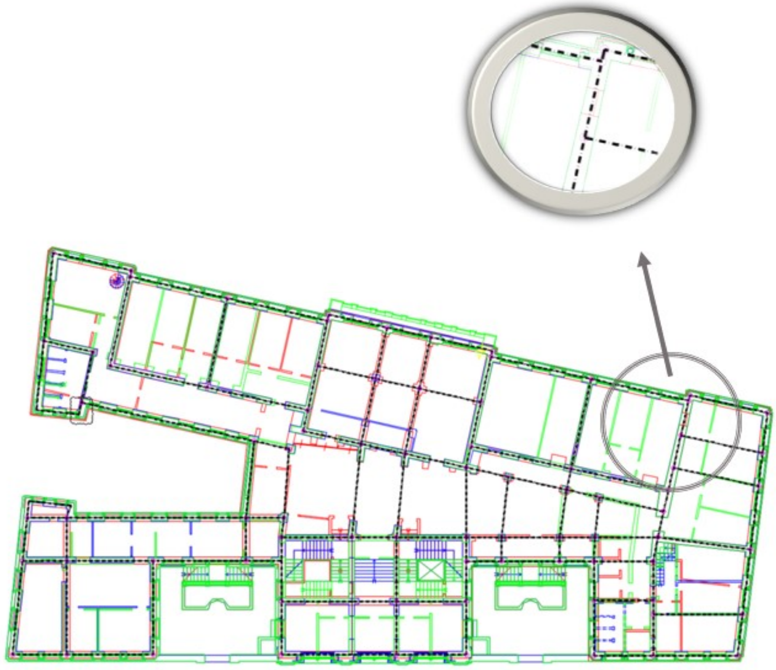

Figure 8.26: Mainframe Axis location

As the mainframe the following assumptions were made for the first iteration, pending the behaviour and experimental results collected the information will change or remain unaltered:

- Columns dimensions: 350mm x 350mm
- Beams dimensions: 300mm x 500mm
- Slabs will be studied as Thin Shells or Thin Plates approximate thickness 100 mm.
- Walls and partitions with the same criteria as the slabs considering a thickness of 100mm.

8.3.4 Definition of the secondary frame

Recalling the general scheme for confined masonry introduced in section 1 of this report can be noticed by the introduction of a secondary frame. The literature and state of the art regarding the analysis of masonry structures recommend the use of such secondary structures to properly model the behaviour near the opening and also to mimic the reality of the construction illustrated in the tomography data presented as well. Therefore only rest to define where to place the secondary beams and columns. The criteria in this case were to locate the secondary columns parallel to the window openings, place a secondary beam below the window to frame it and finally an extra intermediate secondary to support and connect the openings between them and with the main frame. Ahead are some figures to illustrate the placing of the secondary columns near the openings.

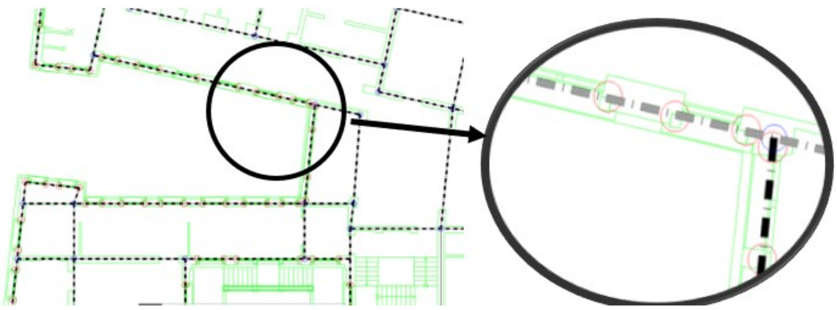

Figure 8.27: Secondary frame Axis location

As presented the red circle intends to highlight the position of the secondary column framing and connecting the opening as described before. Here some assumptions were made for the first iteration, pending on the behaviour and experimental results collected the information will change or remain unaltered:

- Secondary Columns dimensions: 200mm x 200mm
- Secondary Beam dimensions: 200mm x 200mm

8.3.5 From 2D Auto-CAD to Revit 3D Modelling.

Once the Auto-CAD files are prepared with all the information listed before the following step was importing the data to Revit, using the import tool for DWG/DXF allowed to have an adequate template for each floor and proceed with an ease modelling phase of the structures respecting the criteria presented before.

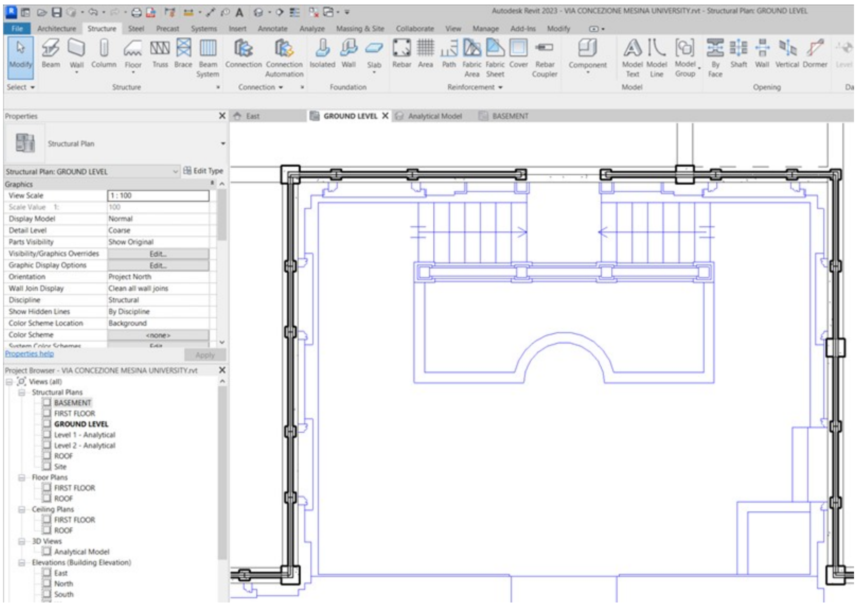

Figure 8.28: Usage of DWG template for Modelling Structural Elements in Revit

The following figures 8.29 8.30 8.31 8.32 represent isometric views (North-East, North-West, South-East and South-West respectively) of the model for Piazza XX Settembre in which it is possible to appreciate the spatial arrangement of the vertical and horizontal elements that constitute the structure.

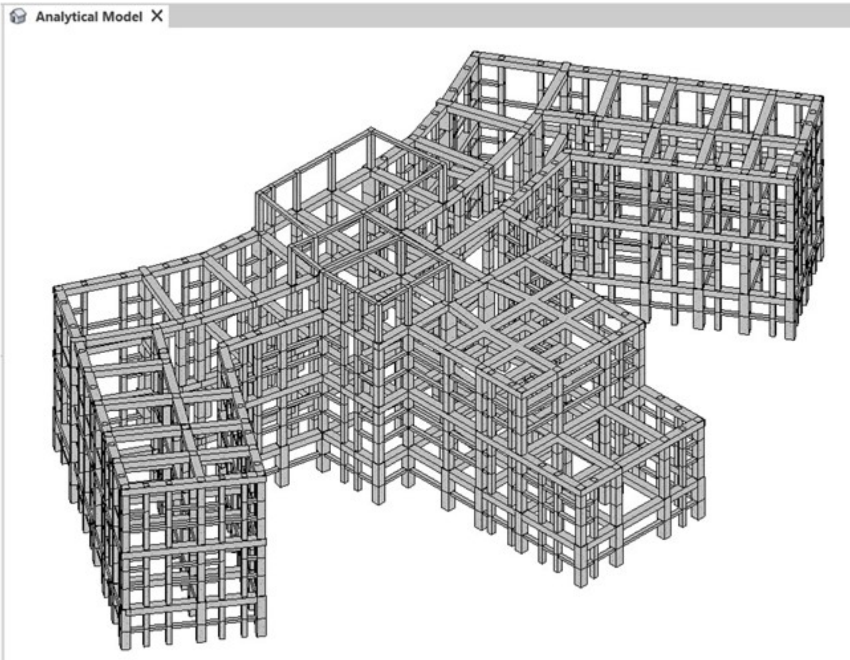

Figure 8.29: North-East Isometric View for Piazza XX Settembre

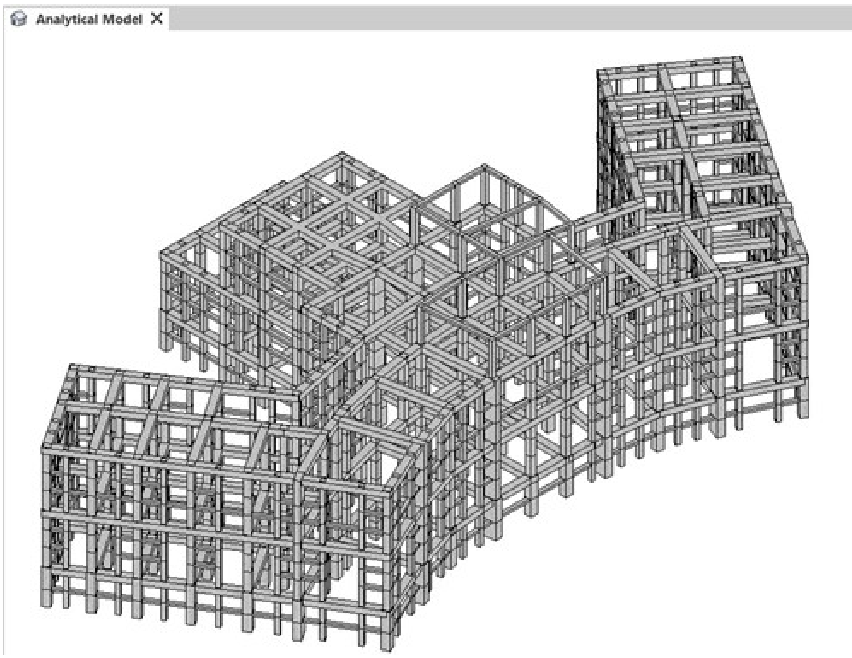

Figure 8.30: North-West Isometric View for Piazza XX Settembre

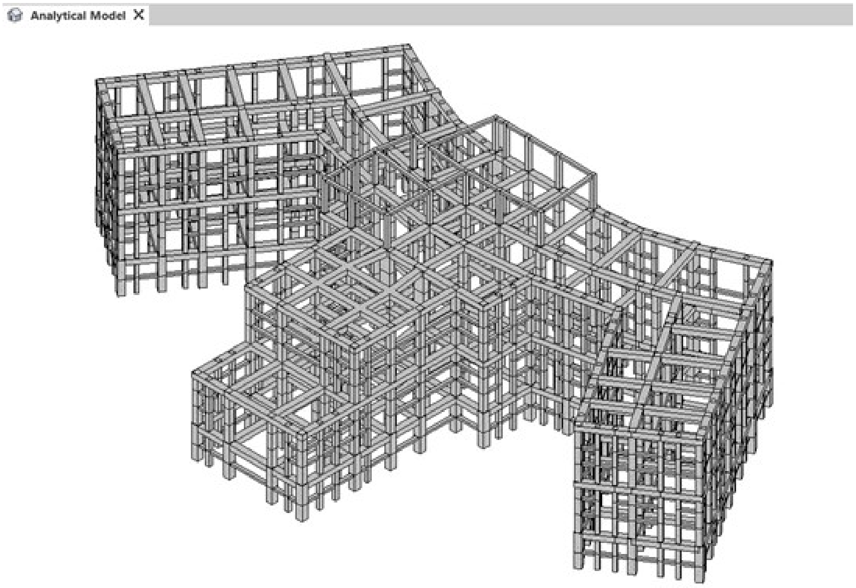

Figure 8.31: South-East Isometric View for Piazza XX Settembre

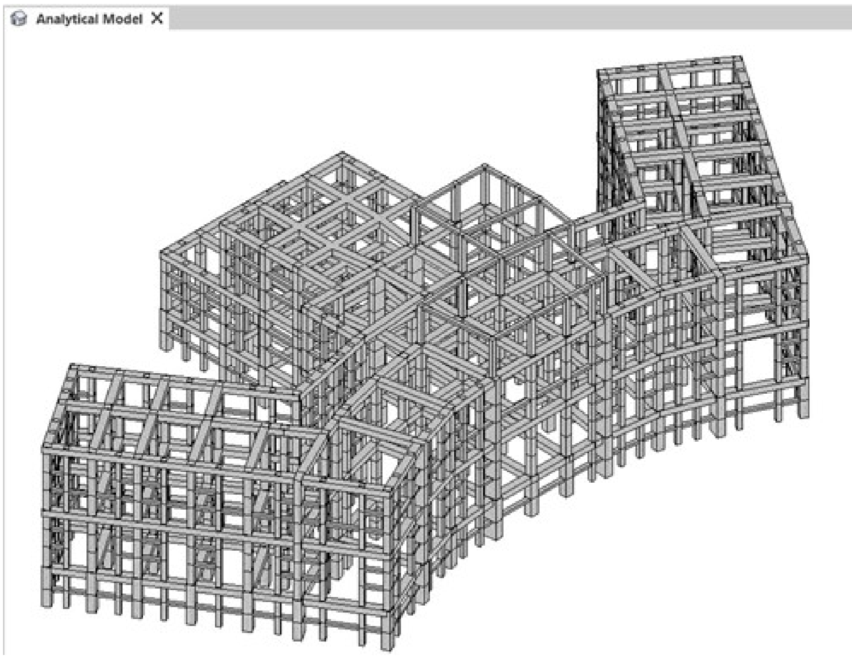

Figure 8.32: South-West Isometric View for Piazza XX Settembre

The same criteria used for Piazza XX Settembre are applied to the model of Via Concezione which could be validated by the spatial arrangement of the vertical and horizontal elements that constitute the structure. The following figures 8.33

8.34 8.35 8.36 represent isometric views (North-East, North-West, South-East and South-West respectively)

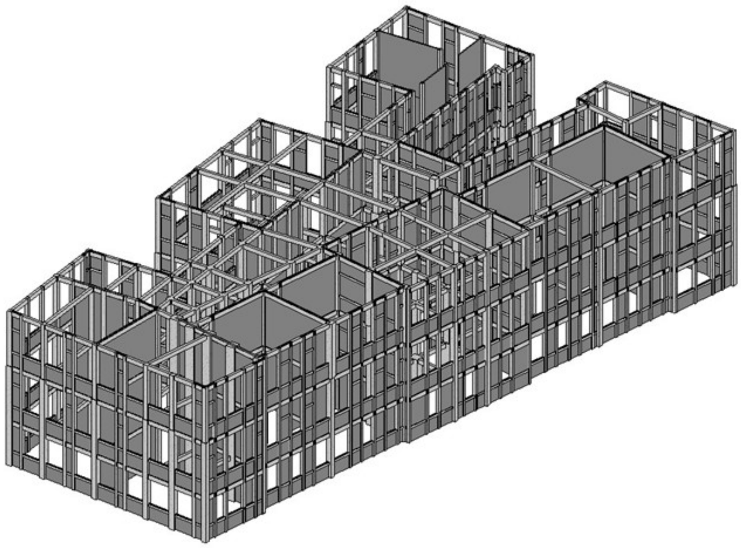

Figure 8.33: North-East Isometric View for Via Concezione

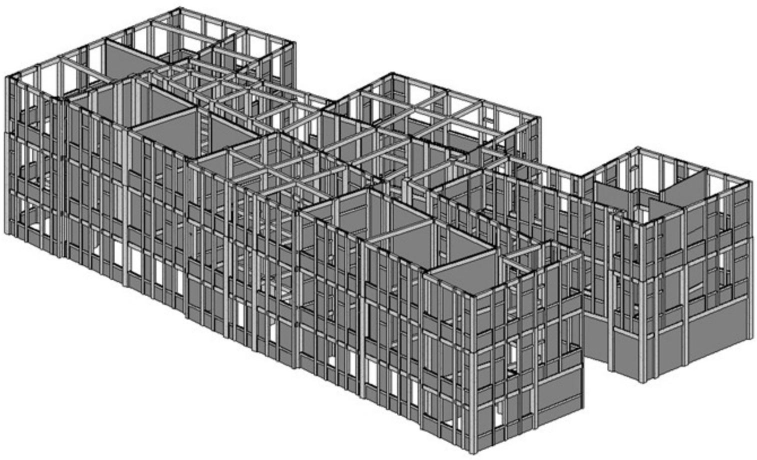

Figure 8.34: North-West Isometric View for Via Concezione

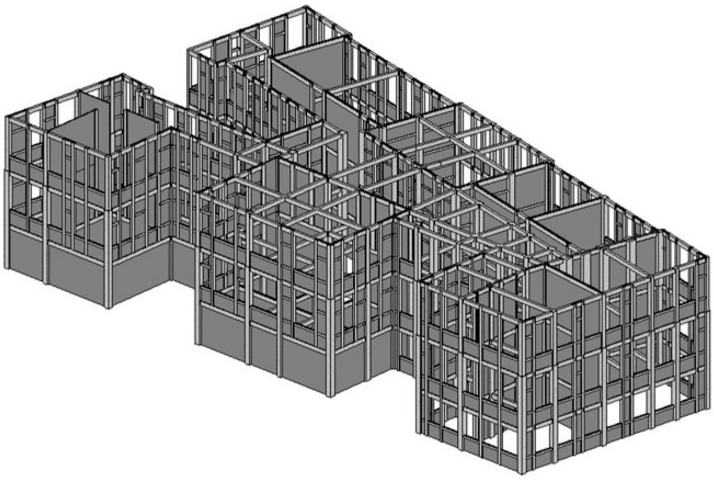

Figure 8.35: South-East Isometric View for Via Concezione

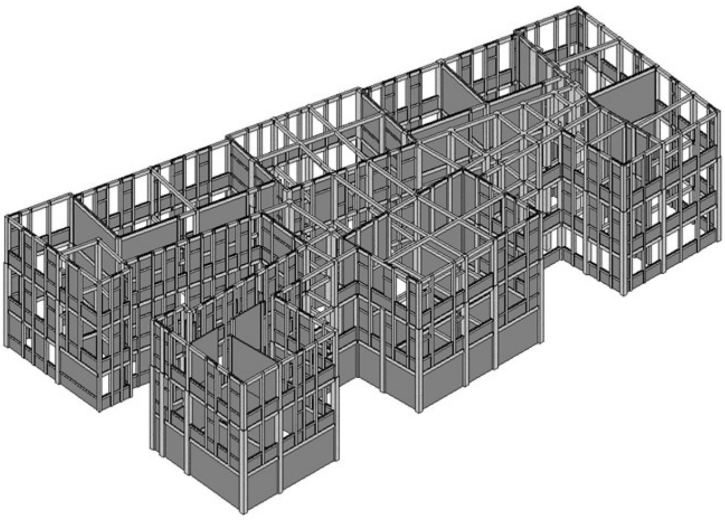

Figure 8.36: South-West Isometric View for Via Concezione

Besides what was already mentioned, in Figures 8.37 8.38 it is possible to observe a detail of the modelling of the perimeter wall in which the openings have been considered as indicated by the graphic drawings. We proceeded to model the masonry within each frame so that it was confined within the stiffening elements.

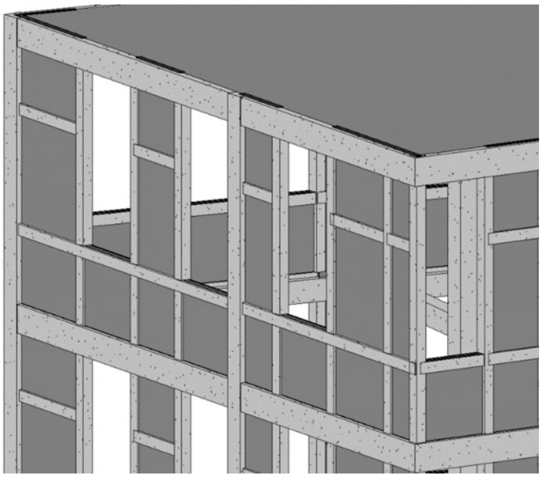

Figure 8.37: Detail of Modelled Infills using Structural Wall properties in Revit

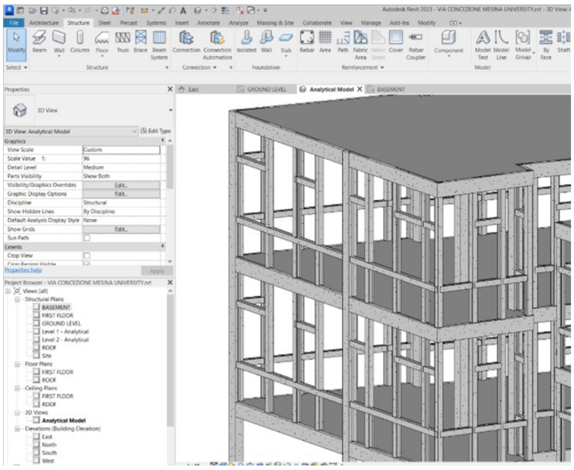

Figure 8.38: Detail of Modelled Mainframe and Secondary frame using Revit Structural Elements

Finally, as already observed in the previous sections, to take into account the slope of the road edge, only the part of the perimeter wall of the cellar floor which appeared to be in free elevation with respect to the ground was modelled. By adopting this approach, modelling the pressures of the ground on the structure was neglected. It was considered reasonable to assume that the perimeter wall of the cellar level was constrained by rigid joints precisely at the height of the road edge. This condition was not widely accepted as valid because as seen in Figure 8.39 for building in Piazza XX Settembre few in the basement were separated from the surrounding floor by an underground corridor for which the elastic constrain was adopted directly in the FEA software. This assumption is reasonable since, although cavities or vents separating the building from the ground were detected during the inspection, these are rigidly connected by concrete beams.

Figure 8.39: Underground Corridor Building Piazza XX Settembre

In the next Figures 8.40 8.41, would be possible to observe a detail of the modelling of the cellar wall in which the slope of the roadside was considered, neglecting the contribution of the masonry below this level.

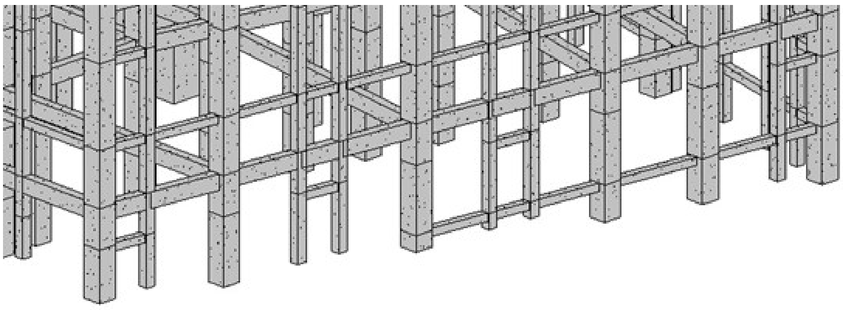

Figure 8.40: Interrupted perimeter model due Slope in the surrounding Ground

Figure 8.41: Actual in-site Condition for Terrain Slope

8.3.6 Generating and Exporting the Analytical Model:

As the 3D model satisfies all the criteria, thresholds, goals and requirements set for the preliminary stage of analysis the model can be exported to SAP 2000 using the export format IFC or the direct link developed by CSI Inc. called CSiXRevit available on the CSI website to transfer the analytical model to SAP 2000. Such a Plugin requires generating an Analytical Model in Revit, such work will be performed using the algorithm available within the Revit software related to the Dynamo interface. It´s important to consider before analysing the model in SAP to perform a severe verification. This step is vital to achieve a proper and valid analysis. This step requires a close review of the node's connections,

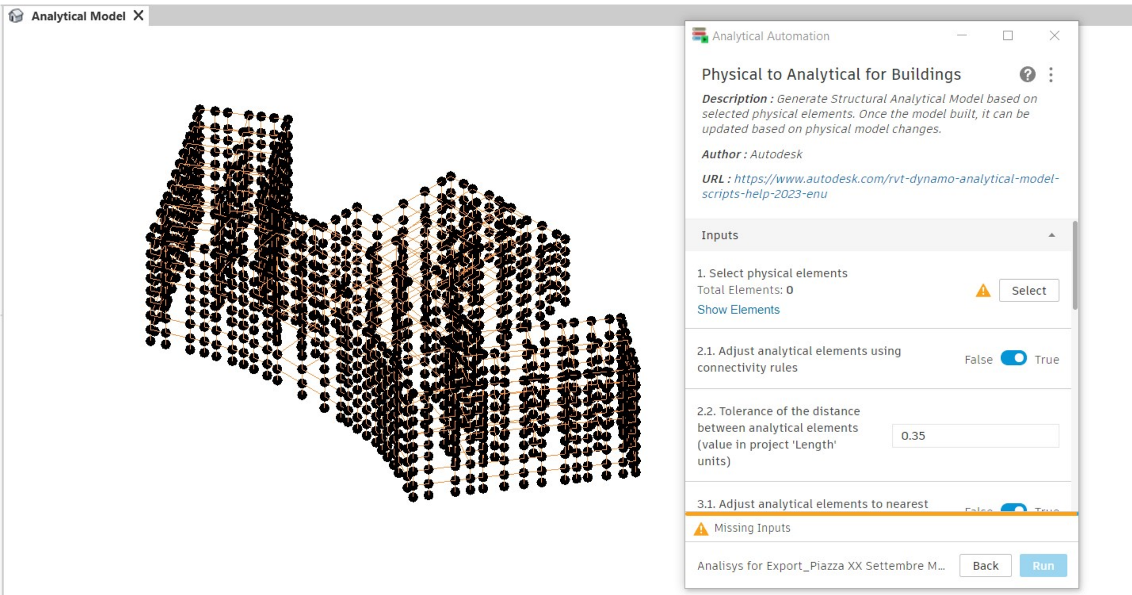

Figure 8.42: Revit Dynamo interface for Analytical Model Creation Piazza XX Settembre

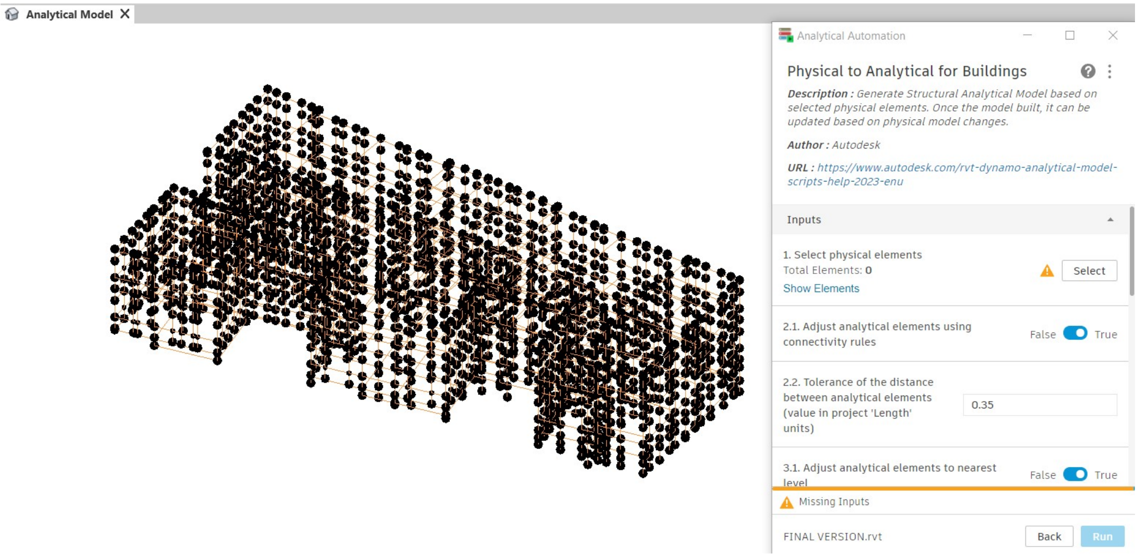

Figure 8.43: Revit Dynamo interface for Analytical Model Creation Via Concezione

8.4 Finite element numerical modelling

Once both export files were created using the Analytical Model export tool from Revit, the transfer and import were performed, such a process was smoothly done thanks to the direct compatibility using the direct link, and all the nodes and elements of the structure were recognised by the FEM software. Subsequently will be described the amount of nodes and elements transferred for each structure, but an important consideration must be made regarding the connection mentioned for the Thin Shell elements (used to modelled the slabs and walls).

For Piazza XX Settembre the entire analytical model consisted of 2057 nodes, 113 beam elements and 73 shell elements*.

For Via Concezione the entire analytical model consisted of 2000 nodes, 126 beam elements and 87 shell elements*.

**The process of mesh generation for structural elements derived from transferred geometries, as pertinent to the structures analysed in these cases of study, occasionally generated compatibility issues. This conflict manifests particularly when the meshing of shell elements is misaligned with the finite partitions of primary and secondary frame elements, resulting in the creation of unrestrained elements. These free elements, reduced the real influence on the mass participation as were not activated and if so manifested abnormal deformations during modal analysis.*

Therefore the final solution for such issues was to compromise the automatised data transferring of the whole model, just to particularly focus on the skeleton (main and secondary frames), leaving the modelling of shell walls and slabs to be performed manually on the FE software SAP 2000.

Specifically, each single structure appeared modelled as follows:

- All the walls, perimeter and internal, were modelled using shell elements, adopting for each element the dimensions found on site or obtained from the graphic documents received from the University of Messina.
- All the vertical elements, whether they are isolated Pillars or whether they are located inside the masonry, effectively contributing to the definition of the confinement frame, have been modelled with Columns elements.

• All the beams placed at the top of the internal and external walls were modelled using beam elements with the exception of the lattice beams placed to support the attic.

In fact, such beams were considered as additional mass inside the floors following the scheme shown in figure 8.44. During the inspection, the beams emerged from the floor for a common length of approximately 40 cm. Having considered a typical centre distance of approximately 1.5 m, recorded for the majority of the beams on each floor, it was possible to homogenise the beams by adopting a single section that took into account the slab and the relevant beams supporting it.

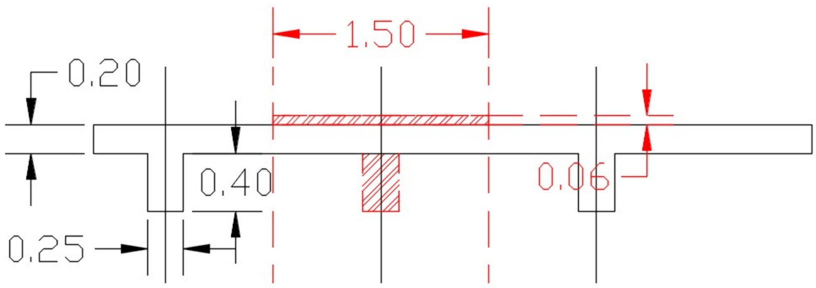

Figure 8.44: Equivalent Superimposed load due Slab Beams

Specifically, by adopting the approach described above, an additional layer representing the beams was placed as a superimposed load to back the concept of the elements neglected during the modelling. This extra weight on the floor equals approximately 6 cm in equation 8.4 the number is derived. This assumption is consistent with the aims of the study, as the interest was to represent as faithfully as possible to reality the distribution of mass and stiffness within the structure without having to investigate the resisting capacity of each element through structural checks.

$$A_{eq} = b \text{ h} \tag{8.1}$$

$$h = \frac{A_{eq}}{b} \tag{8.2}$$

$$h = \frac{(0,25)(0,4)}{1,5} \tag{8.3}$$

$$h = 0,06 \text{ m} \tag{8.4}$$

• The Floor Slabs were modelled as Membranes infinitely rigid in their plane by constraining all the nodes lying on each plane through the diaphragm command already implemented within the software. The hypothesis of a rigid deck, which causes the cancellation of the normal stresses (N) and bending moments (My) on the members, is congruent with the real static scheme, as these stresses are effectively absent on the floor beams due to the presence of a solid concrete slab (20cm). As already fully described in the previous paragraph, this value was increased by considering an additional thickness of 6 cm, obtained from the beam-slab homogenisation process, reaching a total thickness of 26 cm.
• All the nodes of the elevated reinforced concrete structures were considered fully fixed joints, consistently with what is usually assumed for concrete framed structures.
• As regards the connection of the beams with the columns, a rigid constraint was created that was guaranteed by the presence of the walls placed to support the beams, thus preventing their flexural rotations. It was feasible to think that reinforced connections were provided between the main support beam and the column, so the approach used is consistent with the structural behaviour of the building.
• Rigid interlocking constraints were also adopted for the foundations both for the walls of the cellar floor and for the vertical reinforced concrete elements. As described in the previous paragraphs, for the perimeter wall of the cellar floor only, a rigid joint was modelled near the road edge in line with the slopes recorded during the survey.

Right below perspective views of the solid FEM models will be reported for the building of Piazza XX Settembre and consecutively for Via Concezione, in which it will be possible to distinguish each structural element by type and material used through the use of different colours.

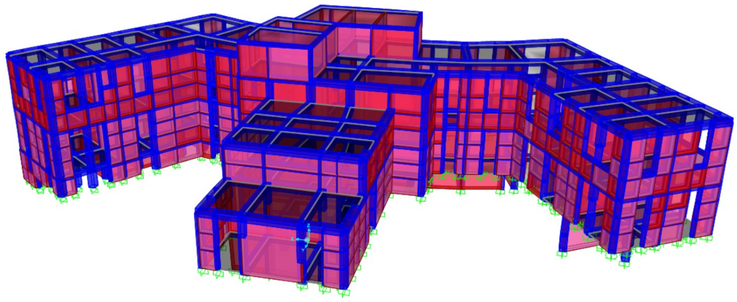

Figure 8.45: Isometric South-East View Finite Element Model SAP2000 for Piazza XX Settembre

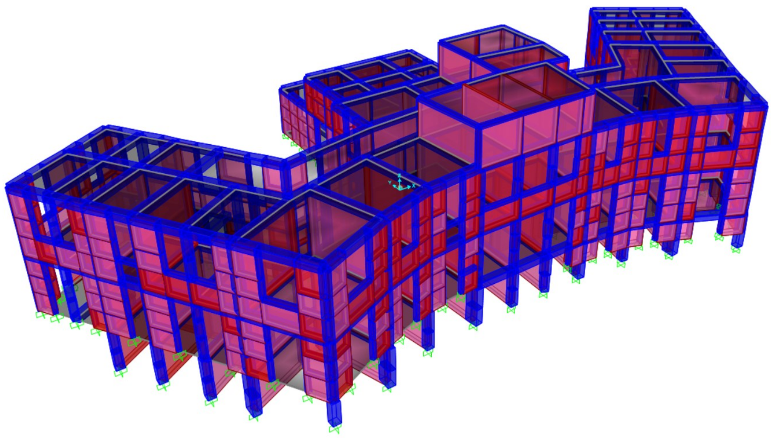

Figure 8.46: Isometric North-West View Finite Element Model SAP2000 for Piazza XX Settembre

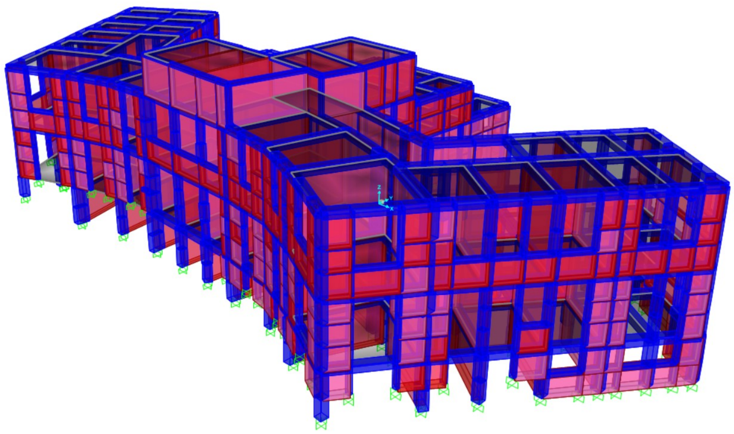

Figure 8.47: Isometric North-East View Finite Element Model SAP2000 for Piazza XX Settembre

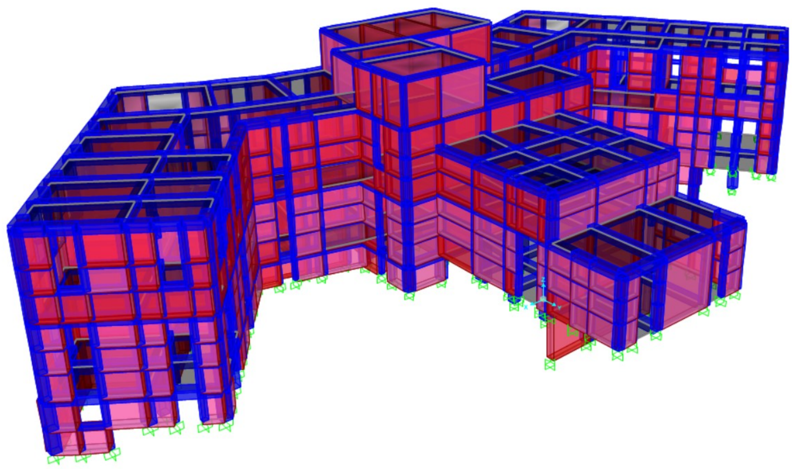

Figure 8.48: Isometric South-East View Finite Element Model SAP2000 for Piazza XX Settembre

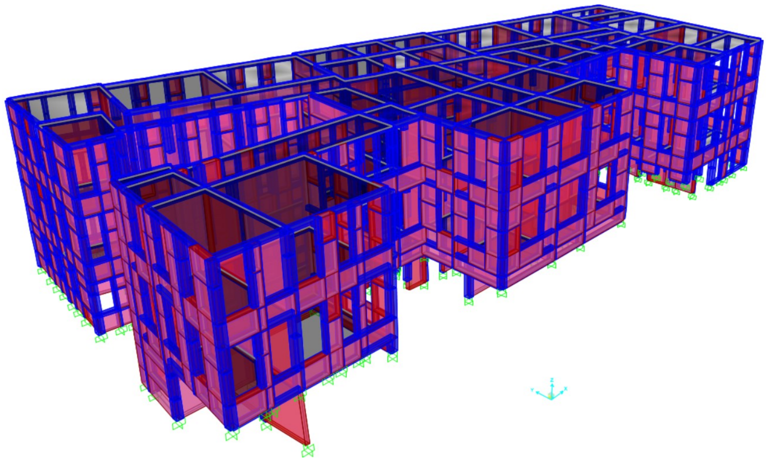

Figure 8.49: Isometric South-East View Finite Element Model SAP2000 for Via Concezione

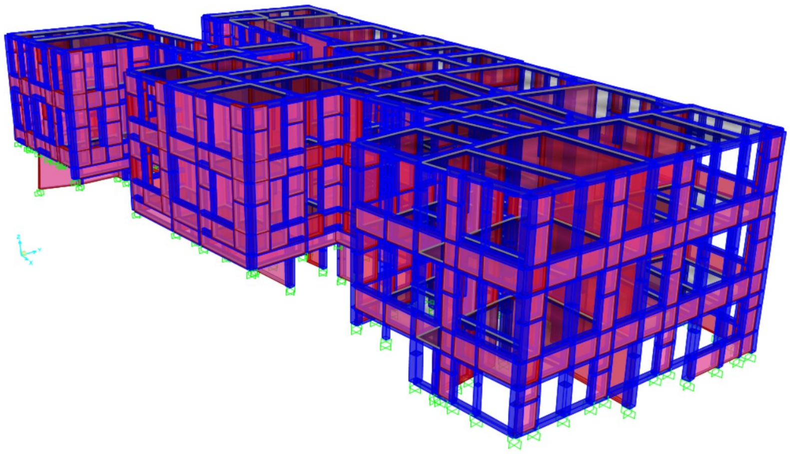

Figure 8.50: Isometric North-West View Finite Element Model SAP2000 for Via Concezione

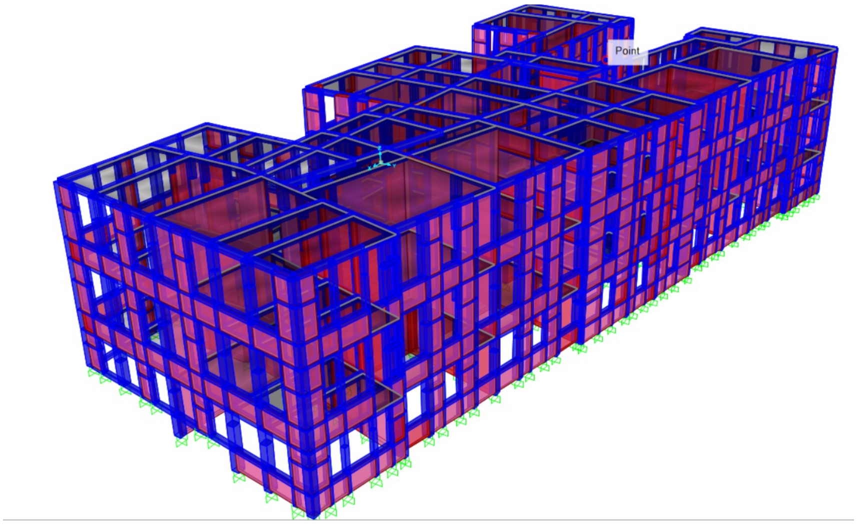

Figure 8.51: Isometric North-East View Finite Element Model SAP2000 for Via Concezione

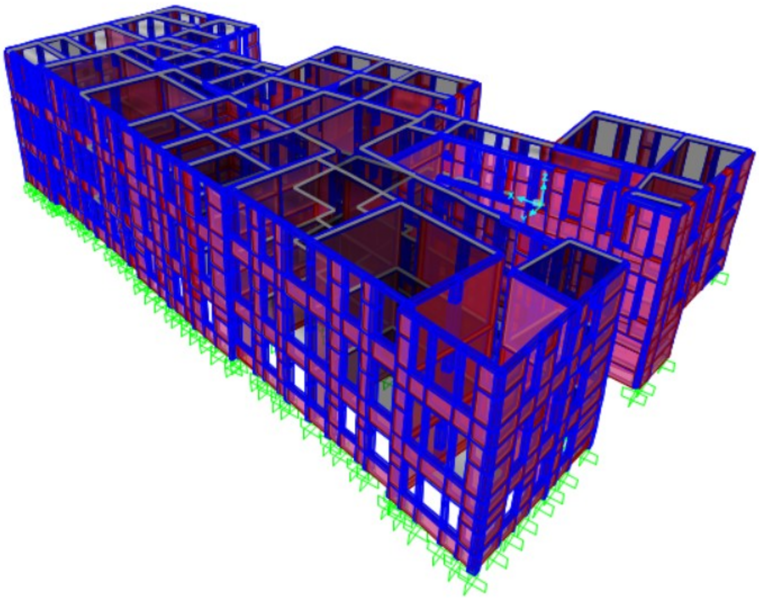

Figure 8.52: Isometric South-East View Finite Element Model SAP2000 for Via Concezione

Details are also reported on the modelling of the internal walls on a typical floor (first floor) and of the floors which guarantee a rigid behaviour of the floor horizontals present at the various levels inside the building.

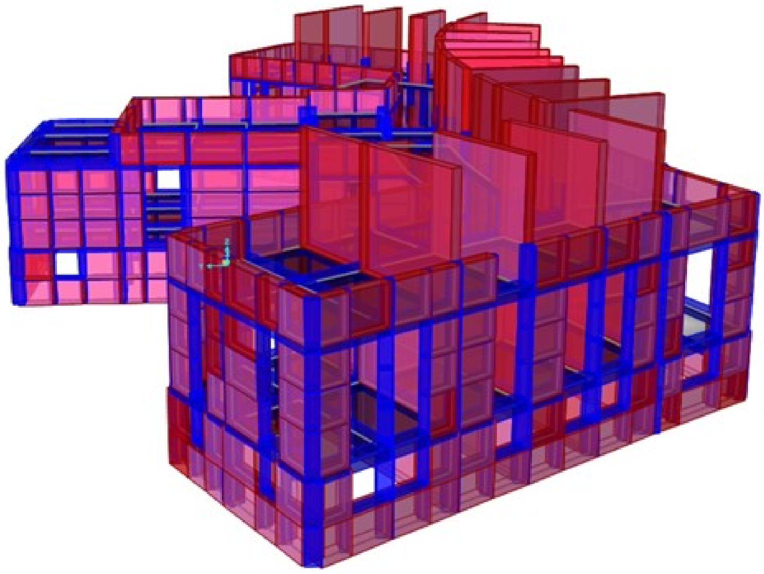

Figure 8.53: Detail of Wall modelling using Thin Shell Elements and Thickness as reported in the surveys and technical reports Piazza XX Settembre

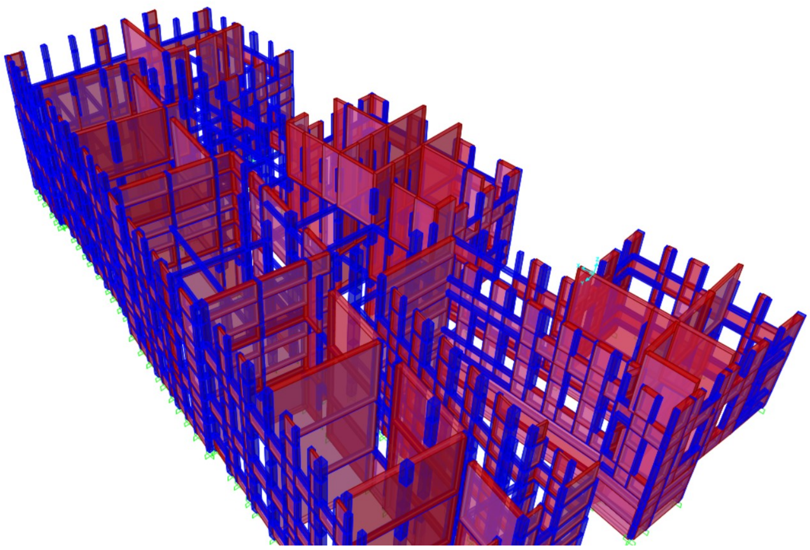

Figure 8.54: Detail of Wall modelling using Thin Shell Elements and Thickness as reported in the surveys and technical reports Via Concezione

8.5 Mechanical characteristics of the materials and Load Definition.

This chapter will individualise the information feed the materials properties and loads definition for both cases of Study, respectively Piazza XX Settembre and Via Concezione, it´s worth mentioning that in both cases the main source of information was the technical report supplied by the University of Messina analysed and surveyed by L& R Laboratori e Ricerche s.r.l. However, the engineering knowledge and technical expertise of my advisor committee are considered during the process of adequately modelling the reality in the behaviour of both buildings.

8.5.1 Masonry:

In the process of assigning mechanical characteristics of the masonry for both cases of study, Was decided to proceed by adopting the values obtained from the investigation campaign carried out on the building.

For the values of stiffness and tensile strength the result reported in the summary file for the existing tests with double jacks was the only reference, here is reported the information:

Via Concezione:

• Breakdown stress equal to 0.87 MPa.
• Elastic modulus at the 1st and 2nd cycle respectively equal to E1=753MPa and E2=619 MPa. • It adopted an Elastic modulus average value equal to Efin= 686 MPa.

Piazza XX Settembre:

Ground floor

• Breakdown stress equal to 1.74 MPa.
• Elastic modulus at the 1st and 2nd cycle respectively equal to E1=891MPa and E2=874 MPa. We proceeded by adopting an average value equal to Efin= 882 MPa.

First floor – Staircase A

• Breakdown stress equal to 1.96 MPa.

• Elastic modulus at the 1st and 2nd cycle respectively equal to E1=2815MPa and E2=2536 MPa. We proceeded by adopting an average value equal to Efin= 2675 MPa.

General conditions for both buildings:

From the laboratory tests for Piazza XX Settembre and Via Concezione, it was not possible to identify a value relating to the density of the masonry so it was decided to adopt the value suggested by the national Italian Annex for the type of masonry detected:

Tipologia di muratura	f (N/mm^2)	τ_0 (N/mm^2)	f_{v0} (N/mm^2)	E (N/mm^2)	G (N/mm^2)	w (kN/m^3)
	min-max	min-max		min-max	min-max	
Muratura in pietrame disordinata (ciottoli, pietre erratiche e irregolari)	1,0-2,0	0,018-0,032	- -	690-1050	230-350	19
Muratura a conci sbozzati, con paramenti di spessore disomogeneo (*)	2,0	0,035-0,051	- -	1020-1440	340-480	20
Muratura in pietre a spacco con buona tessitura	2,6-3,8	0,056-0,074	- -	1500-1980	500-660	21
Muratura irregolare di pietra tenera (tufo, calcarenite, ecc,)	1,4-2,2	0,028-0,042	- -	900-1260	300-420	13 ÷ 16(**)
Muratura a conci regolari di pietra tenera (tufo, calcarenite, ecc,) (**)	2,0-3,2	- -	0,10-0,19	1200-1620	400-500	
Muratura a blocchi lapidei squadrati	5,8-8,2	- -	0,18-0,28	2400-3300	800-1100	22
Muratura in mattoni pieni e malta di calce (***)	2,6-4,3	0,05-0,13	0,13-0,27	1200-1800	400-600	18
Muratura in mattoni semipieni con malta cementizia (es,: doppio UNI foratura ≤40%)	5,0-8,0	- -	0,20-0,36	3500-5600	875-1400	15

Figure 8.55: Table C8.5.1-Circular 2019

As already highlighted in the paragraph dedicated to the interpretation of the laboratory tests presented in the Technical Reported by L& R Laboratori e Ricerche s.r.l., it suggested a tensile strength and stiffness value recorded on site that is significantly lower than those suggested by the National Annex for the type of masonry being studied. For the preliminary modelling phase, it was decided to adopt the values obtained from the experimental tests although, in the future, will be evaluated whether to modify those values due to the fact that there are not a sufficient number of tests for a good level of certainty in the characterisation of the masonry.

Given the purposes of this analysis, these values will be adopted without considering any reductive safety coefficient relating to the material or confidence level.

8.5.2 Concrete:

To incorporate the mechanical attributes of reinforced concrete elements into the model, a decision was made to utilise values derived from an investigative campaign conducted on the structure. Emphasis on referencing the resistance values associated with each structural type (i.e. Columns, Beams), which were acquired through compression tests performed on retrieved specimens.

Piazza XX Settembre:

Sample ID	Test Date	Location	H Sample [mm]	Diameter Sample [mm]	Density Mass [kg/m3]	Compressive Strength [Mpa]
C9	05/08/2022	Basement Stair A Column	94	94	2216	11.3
C10	05/08/2022	Basement Stair A Beam	94	94	2291	16.1
C11	05/08/2022	Basement Stair B Column	74	74	2166	10.2
C12	05/08/2022	Basement Stair B Beam	74	74	2170	10.8
					Design Value	
					2210.75	12.1

Table 8.1: Characteristic values adopted in the model – Basement plan

Sample ID	Test Date	Location	H Sample [mm]	Diameter Sample [mm]	Density Mass [kg/m3]	Compressive Strength [Mpa]
C1-1	05/08/2022	GroundFloor Stair B Beam	94	94	2218	15.8
C1-2	05/08/2022	GroundFloor Stair A Beam	94	94	2213	10.7
					Design Value	
					2215.5	13.3

Table 8.2: Characteristic values adopted in the model – Ground floor.

Sample ID	Test Date	Location	H Sample [mm]	Diameter Sample [mm]	Density Mass [kg/m3]	Compressive Strength [Mpa]
C5-1	05/08/2022	First Floor Stair A Column	94	94	2196	12.9
C5-2	05/08/2022	First FloorStair A Beam	94	94	2239	12.3
C6-1	05/08/2022	First Floor Stair B Column	94	94	**2202**	11
C6-2	05/08/2022	First Floor Stair B Beam	94	94	2238	11.8
					Design Value	
					2212.3	12.1

Table 8.3: Characteristic values adopted in the model – First floor.

Via Concezione

Sample ID	Test Date	Location	H Sample [mm]	Diameter Sample [mm]	Density Mass [kg/m3]	Compressive Strength [Mpa]
C3-1	05/08/2022	Basement Central Corridor Column	94	94	2311	11.3
C3-2	05/08/2022	Basement Central Corridor Column	94	94	2308	11.6
C4-1	05/08/2022	Basement Central Corridor Column	74	74	2281	16.5
C4-2	05/08/2022	Basement Central Corridor Column	74	74	2279	16.6
					Design Value	
					2294.75	14

Table 8.4: Characteristic values adopted in the model – Basement plan.

Sample ID	Test Date	Location	H Sample [mm]	Diameter Sample [mm]	Density Mass [kg/m3]	Compressive Strength [Mpa]
C1-1	05/08/2022	GroundFloor Column	74	74	2276	10.1
C1-2	05/08/2022	GroundFloor Column	74	74	2301	9.4
					Design Value	
					2288.5	9.8

Table 8.5: Characteristic values adopted in the model – Ground floor.

Sample ID	Test Date	Location	H Sample [mm]	Diameter Sample [mm]	Density Mass [kg/m3]	Compressive Strength [Mpa]
C5-1	05/08/2022	First Floor Column Via Placida	74	74	2274	13.2
C5-2	05/08/2022	First Floor Column Via Placida	74	74	2273	13.8
C6-1	05/08/2022	First Floor Column Via Placida	74	74	2355	12.5
					Design Value	
					2300.7	13.2

Table 8.6: Characteristic values adopted in the model – First floor.

8.5.3 Reinforcing bars:

The incorporation of reinforcements was omitted as their impact was deemed negligible for achieving proper distribution of mass and stiffness in the examined cases of study.

8.5.4 Loads definition implemented in the virtual model

For the Piazza XX Settembre and Via Concezione buildings, analysed as cases of study, the determination of permanent static loads acting upon the structural framework was an important target due to its significance to the modal analysis conducted. So, it was chosen to depict the load configuration that most faithfully replicates the operational state during the acquisition of experimental signals, ensuring congruence in the subsequent comparison between experimentally detected frequencies and those derived from the model. Consequently, the implemented loads in the model corresponded to the intrinsic weight of all structural components (walls, vertical elements) plus an imposed dead weight required for the National Annex which is related to the dead mass permanently acting on the reinforced concrete floors, the weight was computed for each specific sector according to its usage and subsequently applied to the corresponding members.

• Given the absence of a survey on the floor to take into account the weight of internal dividing elements and the equipment necessary to carry out the activities of the structure, it was decided to assume a value equal to G2= 0.8 kN/m2 as the non-structural permanent load. For the roofing, a value equal to G2= 0.5 kN/m2 was assumed.

Load Tipology	**Area**	**Value [kN/m2]**
G1 Equivalent Weight Slab	Inter Story	6.5
G2	Inter Story	0.8
G1 Equivalent Weight Slab	Roof	6.5
G2	Roof	0.5

Table 8.7: Load Assignment

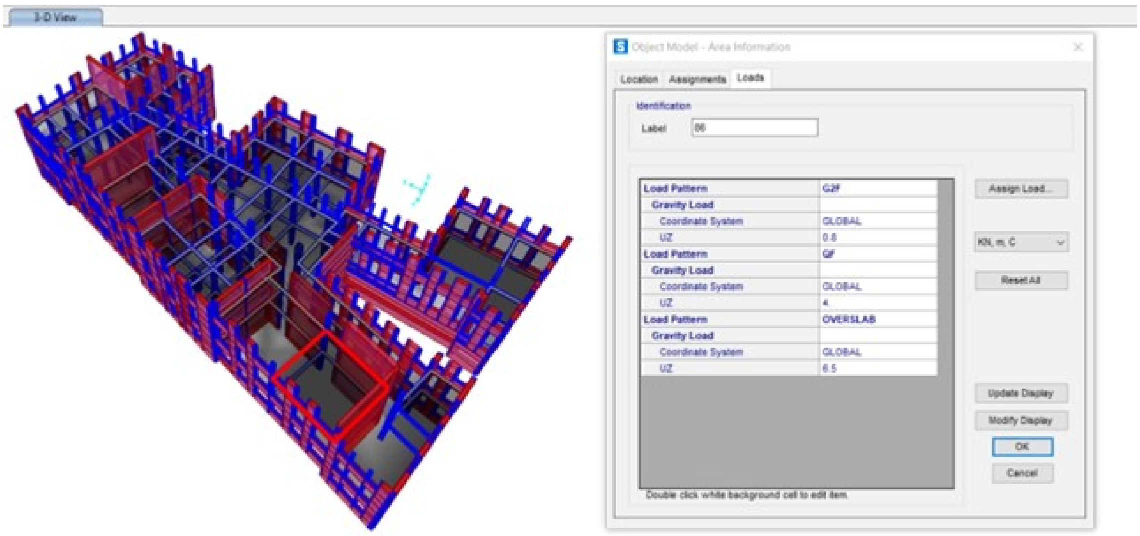

Figure 8.56: Load Pattern for InFloor Slab Via Concezione

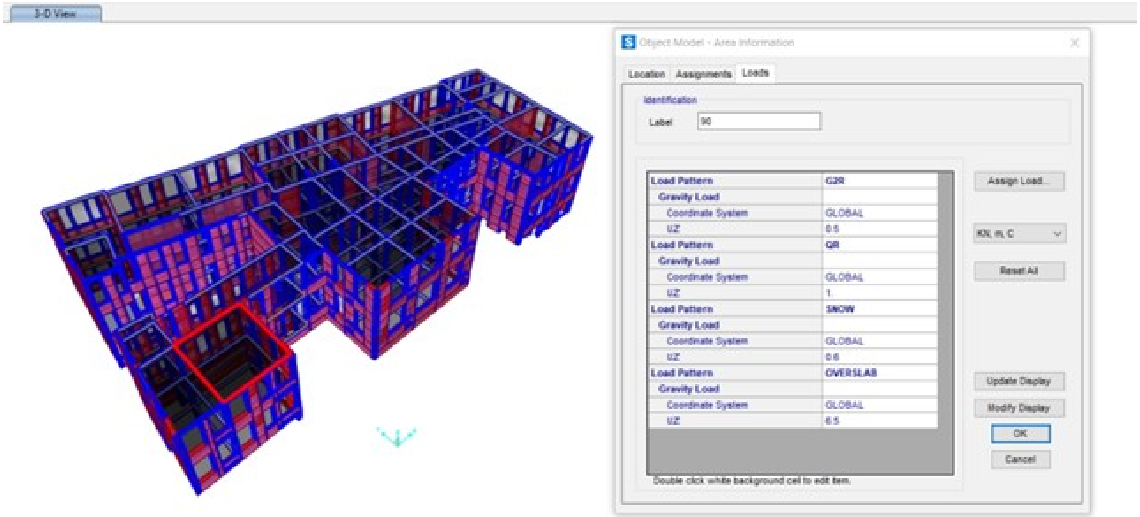

Figure 8.57: Load Pattern for Roof Slab Via Concezione

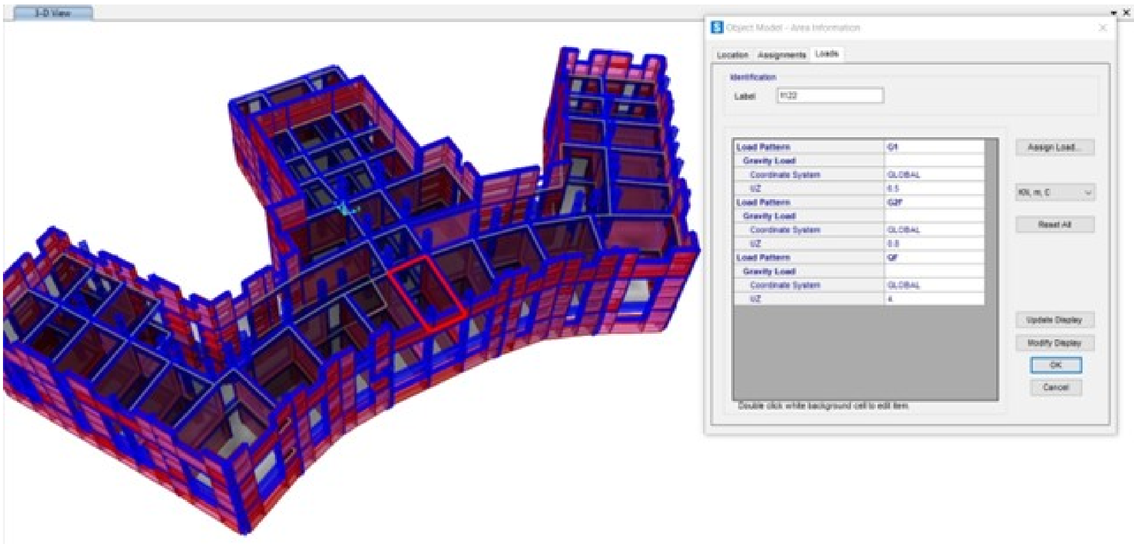

Figure 8.58: Load Pattern for In Floor Slab Piazza XX Settembre

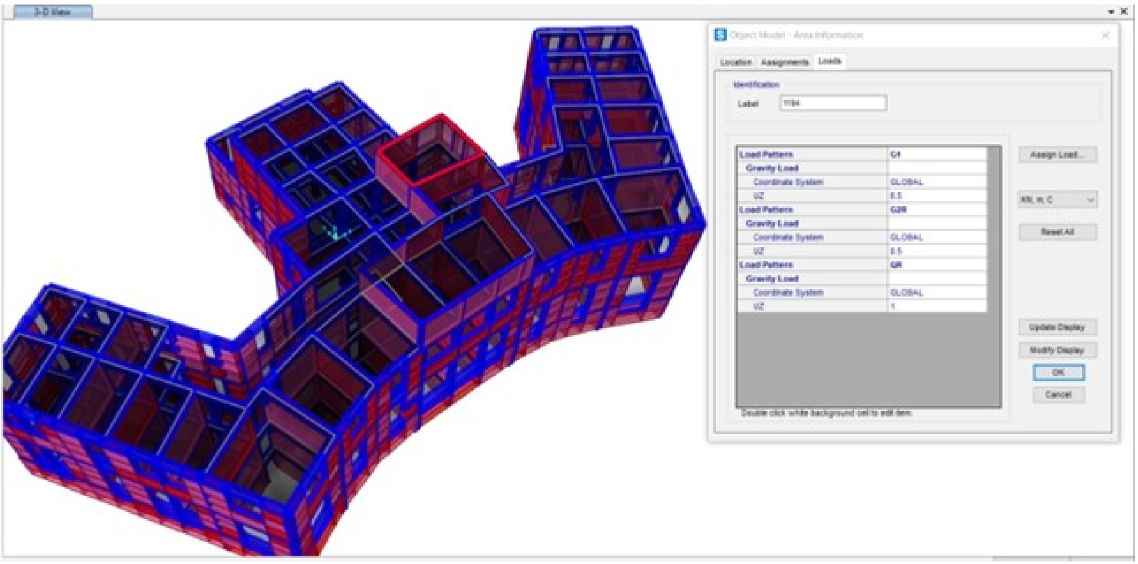

Figure 8.59: Load Pattern for Roof Slab Piazza XX Settembre

8.6 Modal analysis: fundamental modes and modal shapes of the building.

Having previously formulated models for the initial two structures based on the specified assumptions, the current objective is to obtain the fundamental modes of vibration and their associated mode shapes. This outcome was derived through the solution of an eigenvalue and eigenvector problem. The results obtained account for the initial geometries and material properties, such will be systematically presented for each distinct case under investigation.

As stated, the target of the modelling calibration is to correctly fix a number of periods/frequencies of the existing structure to the FE model, in the current cases of study the 3 principal modes of vibration were identified considering the percentage of mass activated in the respective directions. Although a larger number of calculated modes will be reported in the tables ahead, the modal analysis reveals the presence of numerous local modes considered negligible for the purposes of the analysis, so it will be interesting to plot only the first 8 modes even though 15 were considered for the analysis.

8.6.1 Piazza XX Settembre

Table 8.8 will introduce the data for the modelled conditions in V.0, afterwards The figures depicting the Modal deformation for the first 8 modes will be displayed:

<table>
<tr><th colspan="2">Piazza XX Settembre</th><th>Model:</th><th colspan="2">Version V.0</th></tr>
<tr><th>Material</th><th>Location</th><th>Compressive Strength [Mpa]</th><th>Elastic Modulus [MPa]</th><th>Density Mass [Kg/m3]</th></tr>
<tr><td rowspan="3">Concrete</td><td>Basement</td><td>12.1</td><td>30000</td><td>2210.75</td></tr>
<tr><td>Ground Floor</td><td>13.3</td><td>30000</td><td>2215.5</td></tr>
<tr><td>First Floor</td><td>12.1</td><td>30000</td><td>2212.3</td></tr>
<tr><td rowspan="2">Masonry</td><td>Ground Floor</td><td>1.74</td><td>1200*</td><td>1500</td></tr>
<tr><td>First Floor</td><td>1.96</td><td>1200*</td><td>1500</td></tr>
</table>

Table 8.8: Mechanical Properties Model V.0 Piazza XX Settembre

Now a summary table will introduce the results obtained for Model V.0, in bold will be highlighted the principal directions and rotation.

Mode	**Frequency [Hz]**	**Period [s]**	**UX**	**UY**	**SumUX**	**SumUY**	**RZ**	**SumRZ**
1	4.083	0.245	0.027	0.000	0.027	0.000	**0.789**	0.789
2	5.032	0.199	**0.793**	0.000	0.820	0.001	0.030	0.818
3	5.818	0.172	0.000	**0.750**	0.820	0.751	0.004	0.822
4	6.335	0.158	0.000	0.003	0.820	0.753	0.000	0.822
5	6.792	0.147	0.000	0.002	0.820	0.755	0.000	0.822
6	9.739	0.103	0.000	0.001	0.820	0.756	0.001	0.823
7	10.085	0.099	0.000	0.000	0.820	0.756	0.000	0.823
8	10.108	0.099	0.000	0.000	0.820	0.756	0.000	0.823
9	10.452	0.096	0.000	0.000	0.820	0.756	0.008	0.830
10	10.548	0.095	0.001	0.000	0.821	0.756	0.002	0.832
11	10.601	0.094	0.001	0.000	0.821	0.756	0.023	0.855
12	10.71	0.093	0.000	0.000	0.822	0.756	0.029	0.884
13	10.853	0.092	0.000	0.000	0.822	0.756	0.001	0.885
14	10.883	0.092	0.000	0.001	0.822	0.757	0.000	0.885
15	10.945	0.091	0.000	0.001	0.822	0.759	0.016	0.902

Table 8.9: Results Modal Piazza XX Settembre Mode V.0 Analysis: Frequency, Periods and Modal Mass Participation Ratios

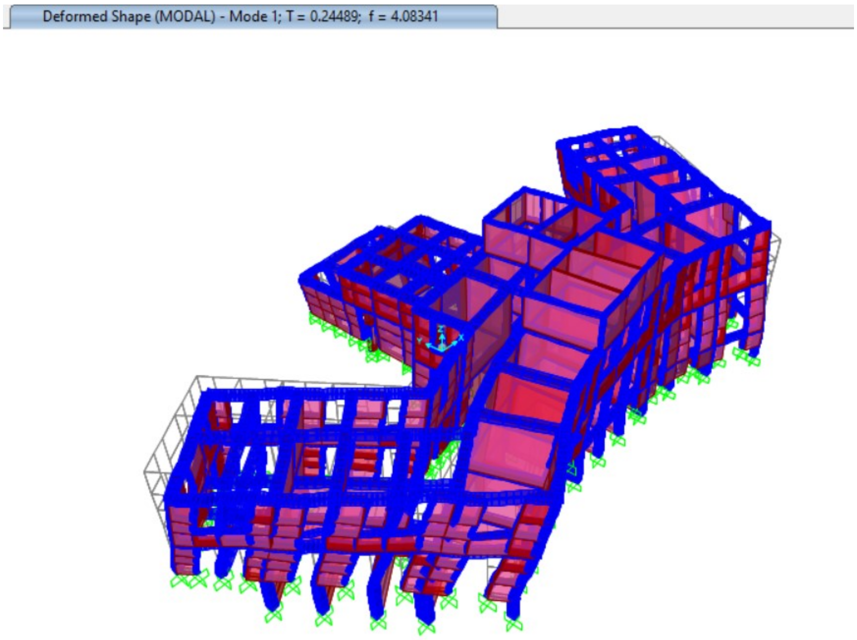

Figure 8.60: Modal Deformation Mode 1 Model V.0 Piazza XX Settembre

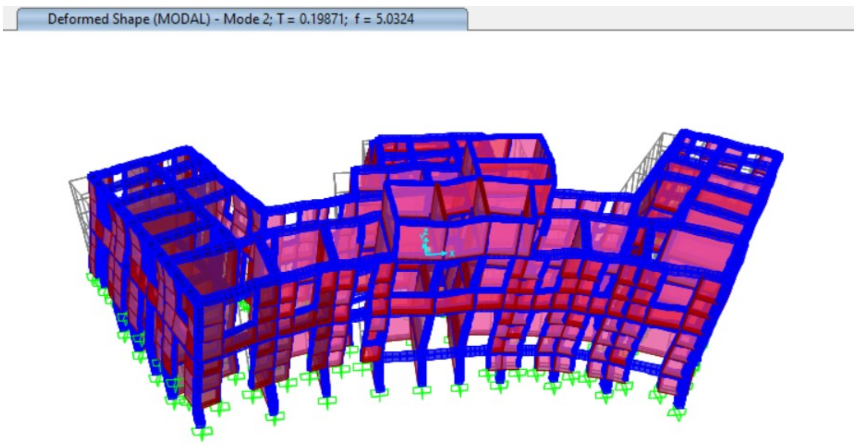

Figure 8.61: Modal Deformation Mode 2 Model V.0 Piazza XX Settembre

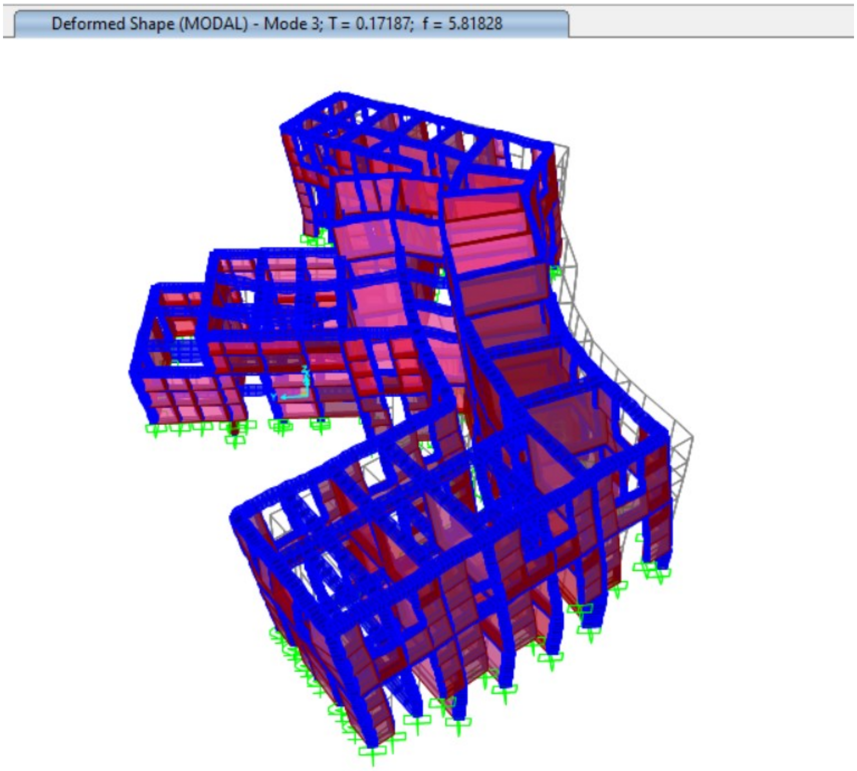

Figure 8.62: Modal Deformation Mode 3 Model V.0 Piazza XX Settembre

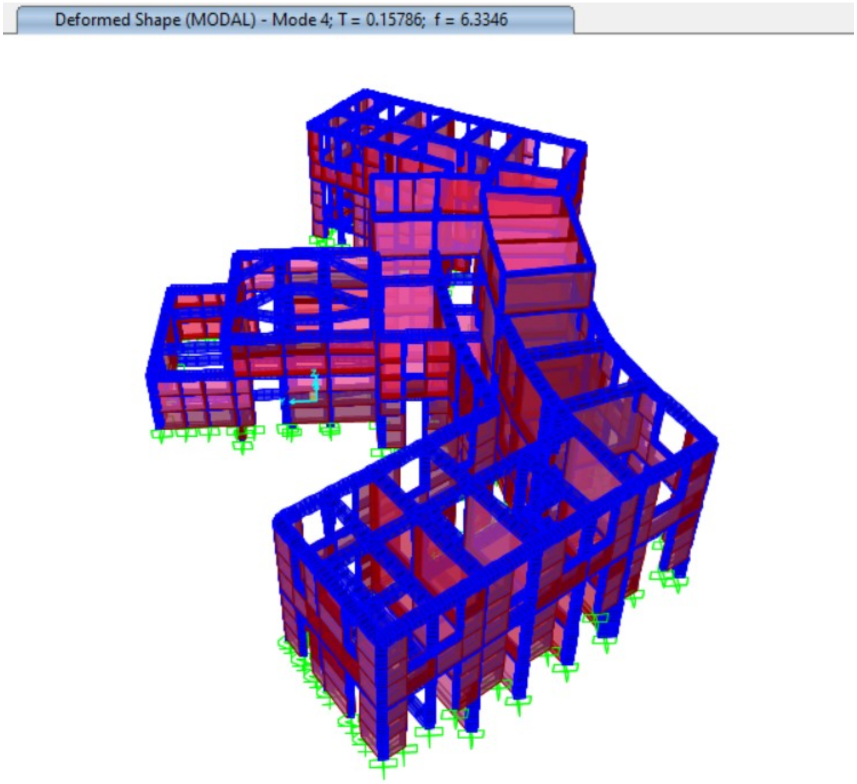

Figure 8.63: Modal Deformation Mode 4 Model V.0 Piazza XX Settembre

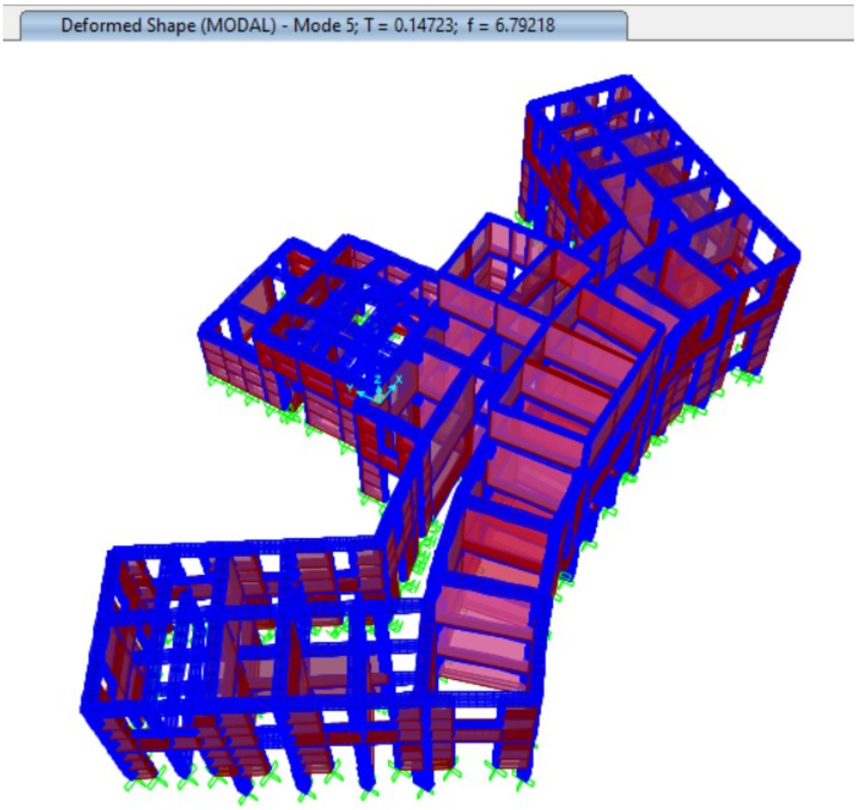

Figure 8.64: Modal Deformation Mode 5 Model V.0 Piazza XX Settembre

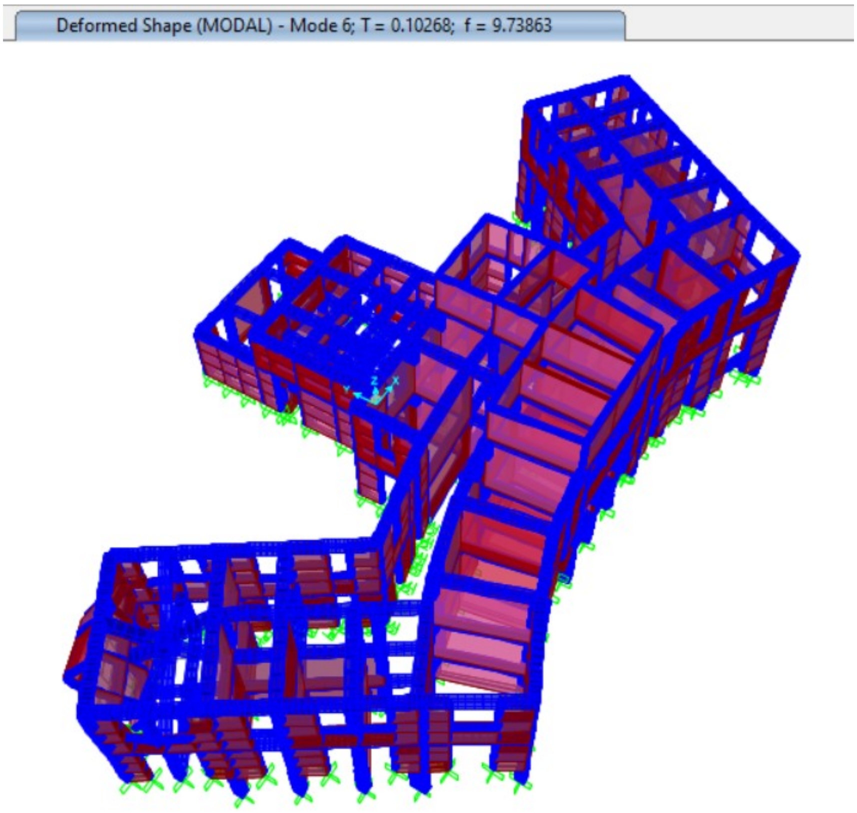

Figure 8.65: Modal Deformation Mode 6 Model V.0 Piazza XX Settembre

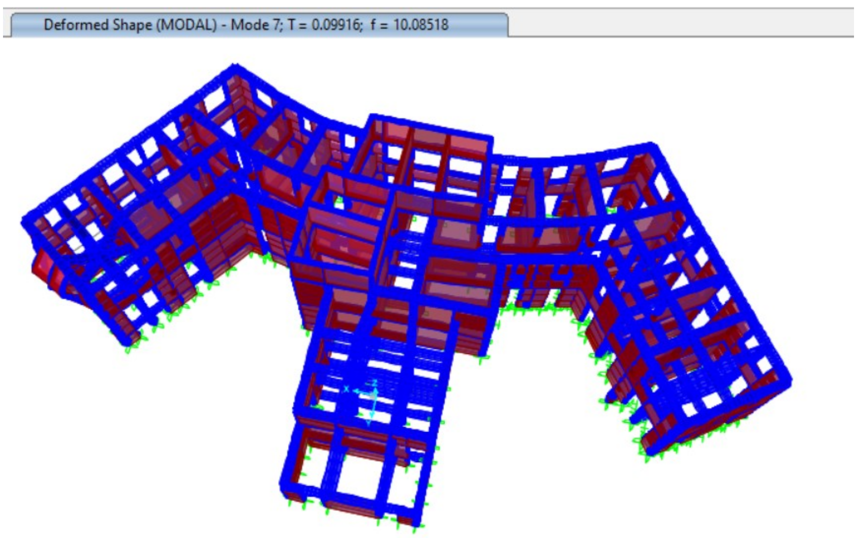

Figure 8.66: Modal Deformation Mode 7 Model V.0 Piazza XX Settembre

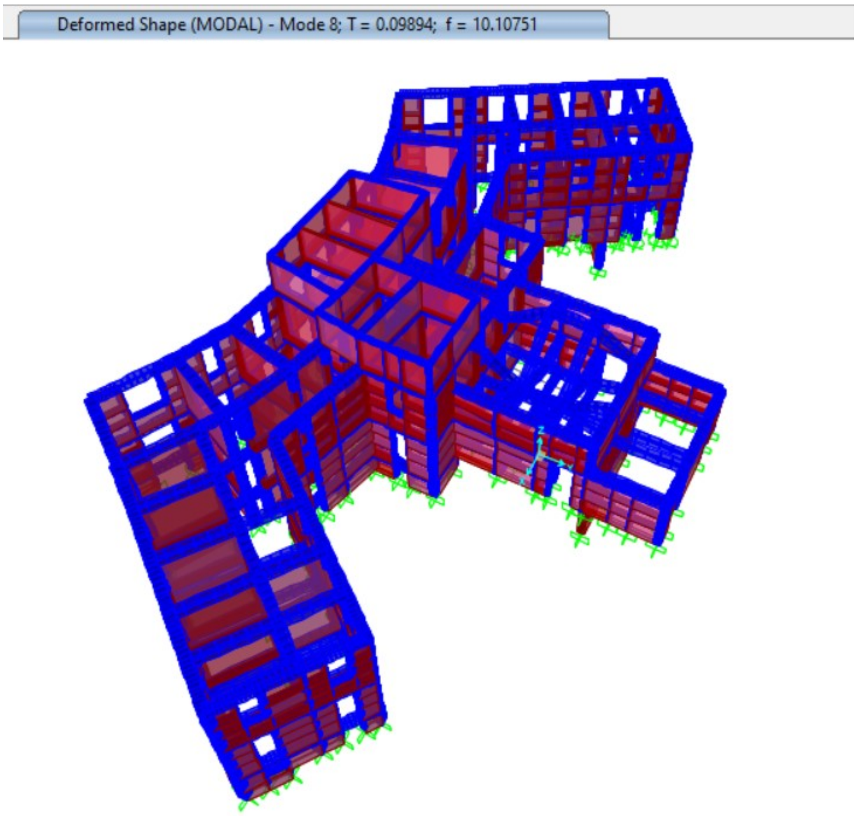

Figure 8.67: Modal Deformation Mode 8 Model V.0 Piazza XX Settembre

8.6.2 Via Concezione:

Table 8.10 will introduce the data for the modelled conditions in V.0, afterwards The figures depicting the Modal deformation for the first 8 modes will be displayed:

Via Concezione		**Model:**	**Version V.0**	
Material	**Location**	**Compressive Strength [Mpa]**	**Elastic Modulus [MPa]**	**Density Mass [Kg/m3]**
Concrete	Basement	14	30000	2294.75
	Ground Floor	9.8	30000	2288.5
	First Floor	13.2	30000	2300.7
Masonry	Ground Floor	0.86	1200*	1500
	First Floor	0.86	1200*	1500

Table 8.10: Mechanical Properties Model V.0 Via Concezione

Now a summary table will introduce the results obtained for Model V.0, in bold will be highlighted the principal directions and rotation.

Mode	**Frequency [Hz]**	**Period [s]**	**UX**	**UY**	**SumUX**	**SumUY**	**RZ**	**SumRZ**
1	3.671	0.272	0.103	0.004	0.103	0.004	**0.618**	0.618
2	4.278	0.234	0.000	0.000	0.103	0.004	0.000	0.618
3	5.535	0.181	0.000	0.000	0.103	0.004	0.000	0.618
4	5.887	0.170	0.036	**0.674**	0.138	0.678	0.000	0.618
5	5.936	0.168	0.000	0.003	0.139	0.681	0.000	0.618
6	6.264	0.160	**0.570**	0.034	0.708	0.715	0.102	0.720
7	6.487	0.154	0.026	0.000	0.734	0.715	0.003	0.723
8	8.921	0.112	0.000	0.005	0.734	0.720	0.005	0.728
9	8.957	0.112	0.001	0.000	0.735	0.720	0.000	0.728
10	9.275	0.108	0.000	0.002	0.735	0.722	0.001	0.729
11	9.600	0.104	0.000	0.000	0.735	0.722	0.000	0.729
12	9.646	0.104	0.000	0.000	0.735	0.723	0.000	0.730
13	9.976	0.100	0.001	0.000	0.736	0.723	0.000	0.730
14	10.005	0.100	0.001	0.000	0.737	0.723	0.001	0.731
15	10.034	0.100	0.001	0.001	0.738	0.723	0.001	0.732

Table 8.11: Results Modal Via Concezione Mode V.0 Analysis: Frequency, Periods and Modal Mass Participation Ratios

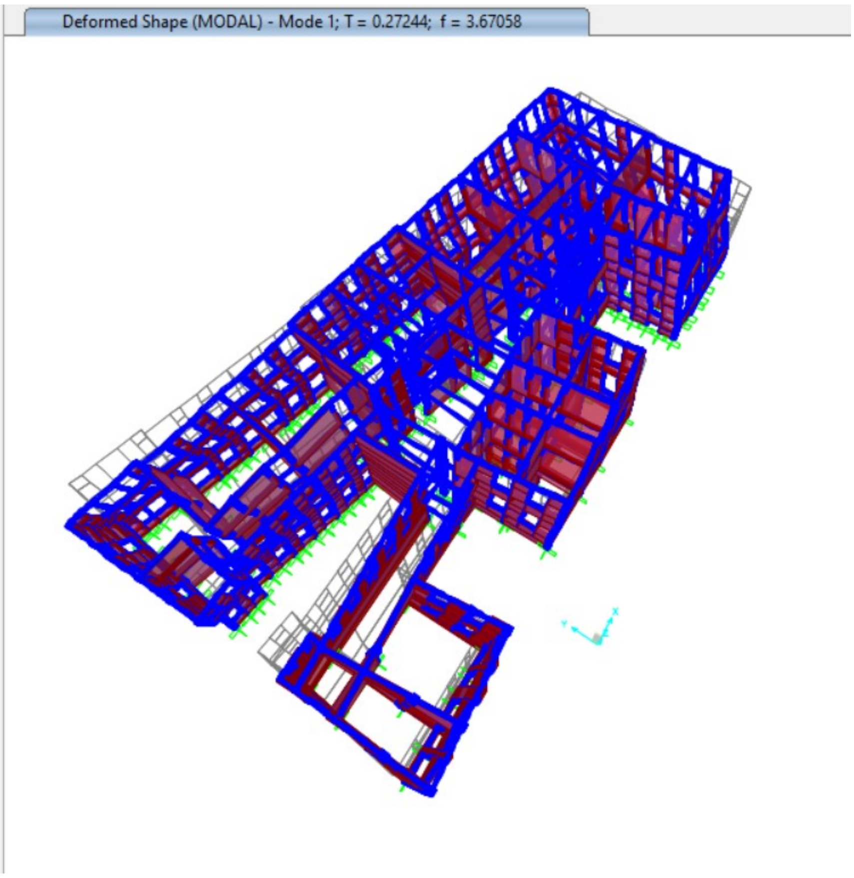

Figure 8.68: Modal Deformation Mode 1 Model V.0 Via Concezione

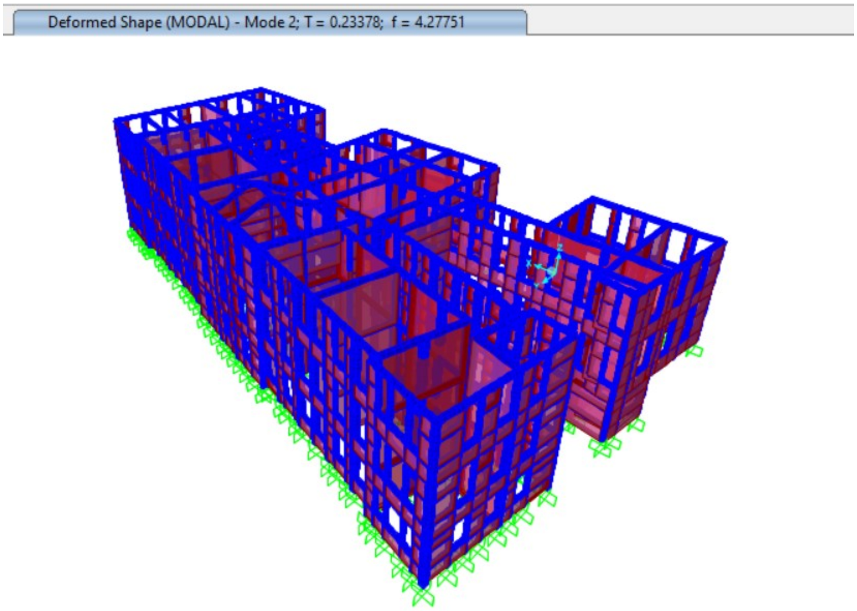

Figure 8.69: Modal Deformation Mode 2 Model V.0 Via Concezione

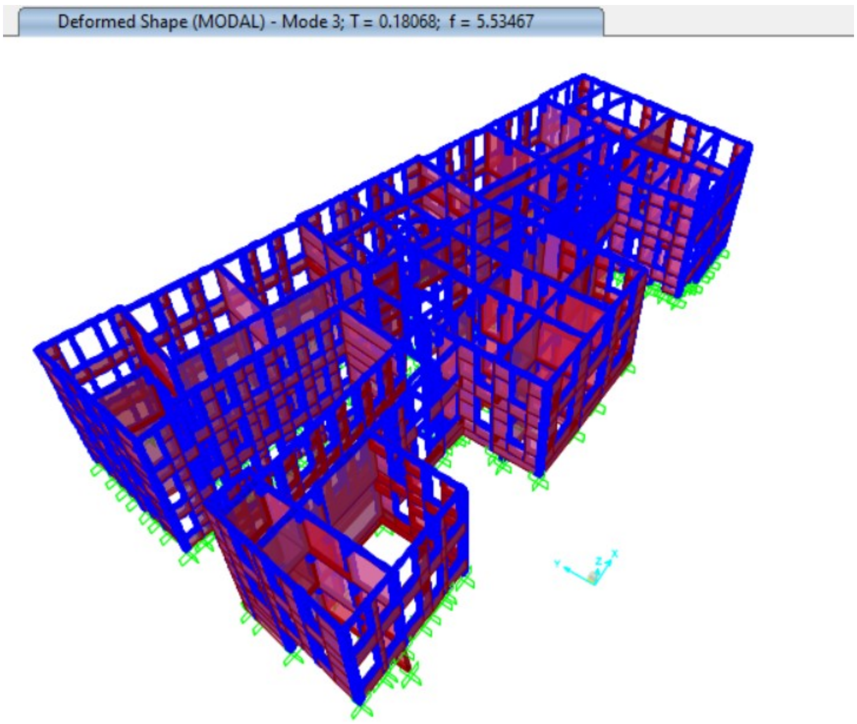

Figure 8.70: Modal Deformation Mode 3 Model V.0 Via Concezione

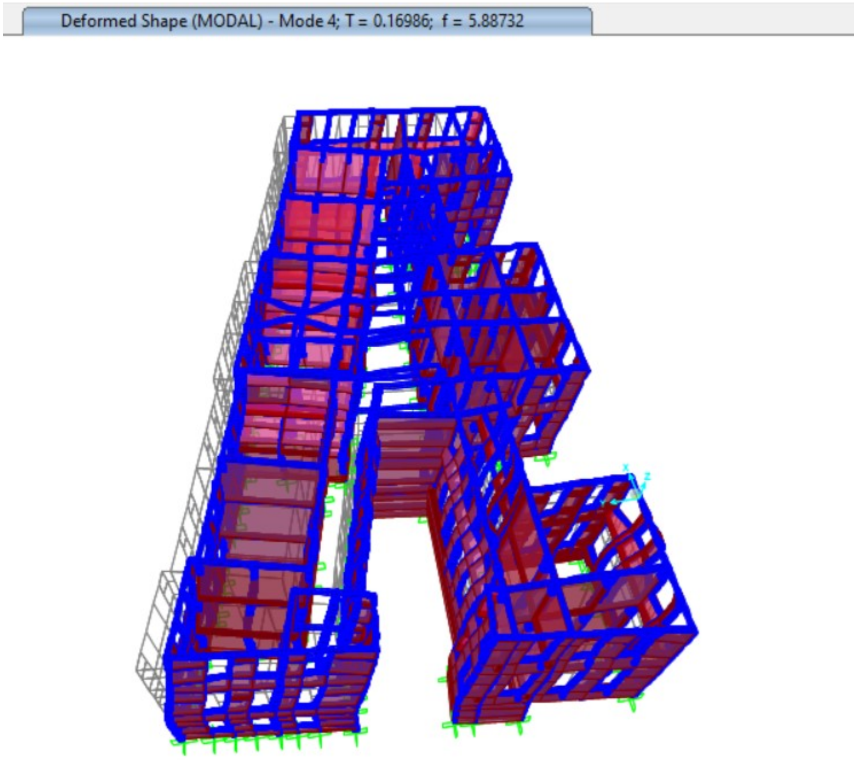

Figure 8.71: Modal Deformation Mode 4 Model V.0 Via Concezione

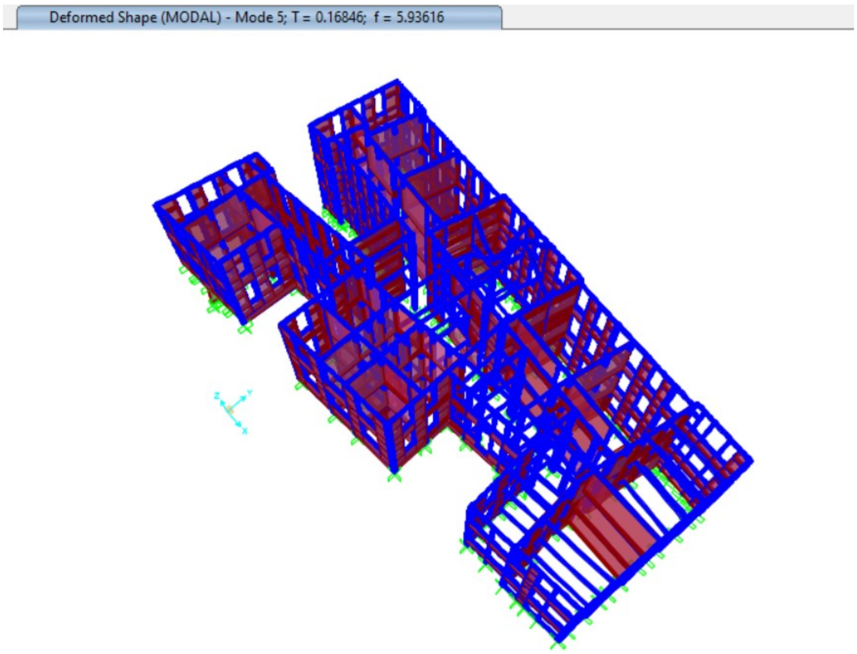

Figure 8.72: Modal Deformation Mode 5 Model V.0 Via Concezione

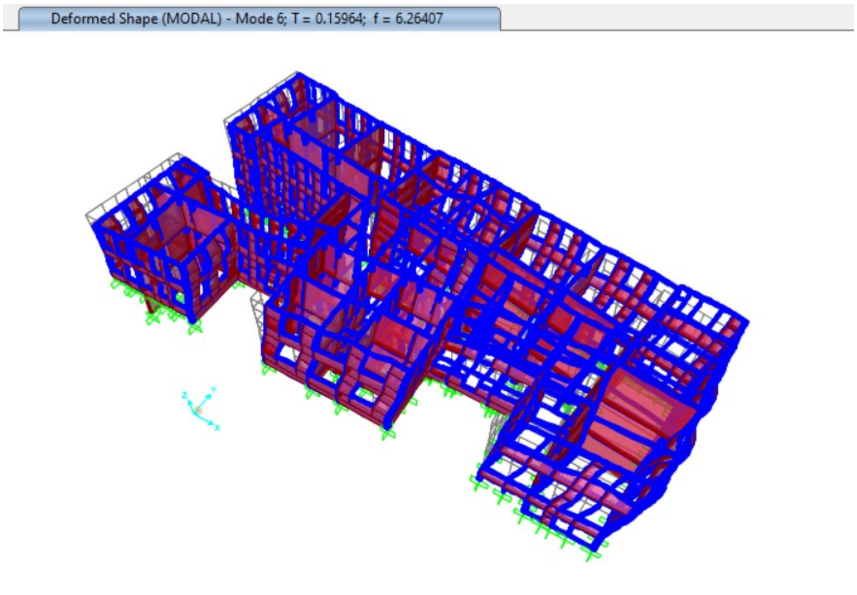

Figure 8.73: Modal Deformation Mode 6 Model V.0 Via Concezione

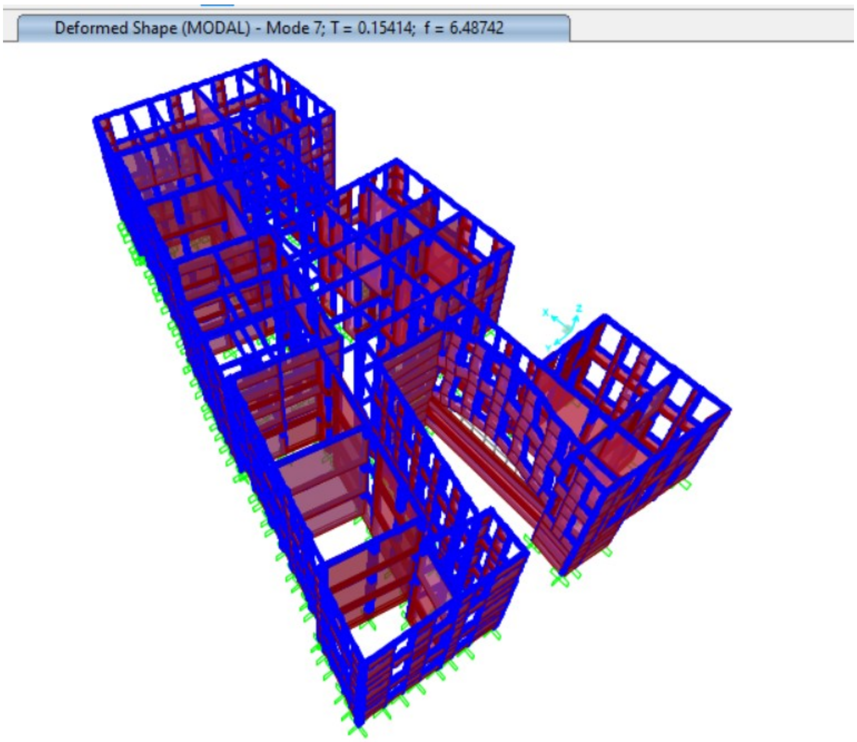

Figure 8.74: Modal Deformation Mode 7 Model V.0 Via Concezione

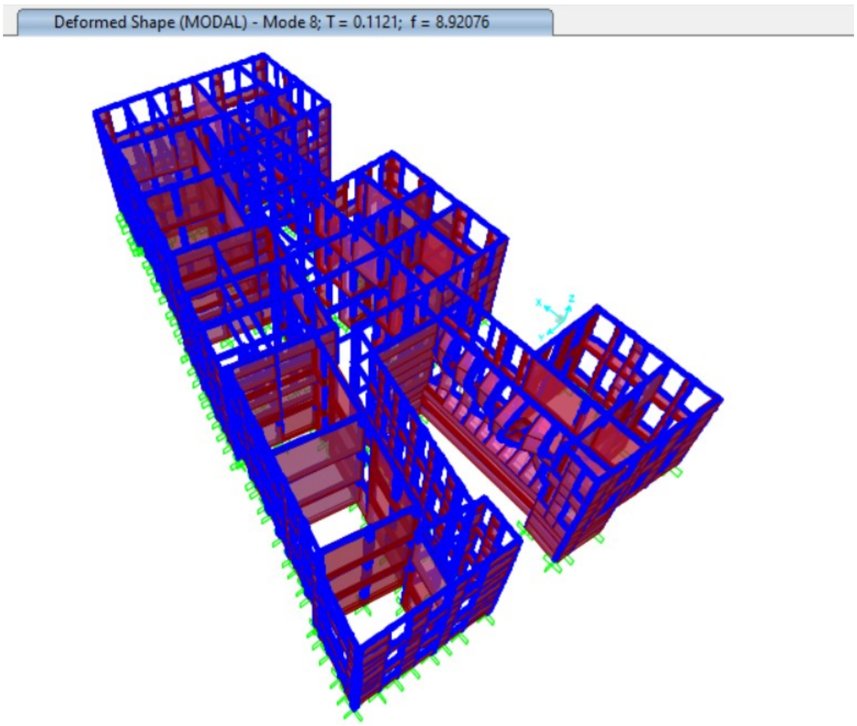

Figure 8.75: Modal Deformation Mode 8 Model V.0 Via Concezione

Chapter 9

Manual Calibration for the Finite Element Models:

This chapter delves into the manual calibration process for both cases under study, the concepts and premises established in preceding chapters will be further expanded upon the foundational concepts. The primary objective is to delineate the intricacies of the manual calibration procedure, with a specific emphasis on articulating the structural parameters carefully selected throughout sensibility analysis. The crux of this calibration endeavour lies in minimising the gap between the frequencies observed on-site through experimentation AVT and the corresponding numerical frequencies obtained from the Finite Element (F.E) models. This meticulous calibration process assumes a key role in validating the dynamic behaviour inherent in the F.E models.

In contrast to the automatic calibration approach hinging on Artificial Intelligence, the exploration of the manual calibration process is an alternative course. Rather than entrusting the calibration to automated algorithms, here is adopted a methodical and hands-on approach. In the quest to identify and understand the structures under scrutiny. This manual approach, notably, seeks to refine the models through manual iterative adjustments. The following narrative unfolds the distinctive nuances of this manual calibration process, shedding light on the sensitivity of the parameters understudy and preparing useful concepts for creating strategies for the upcoming automatic model updating.

9.1 Piazza XX Settembre

For this case of study the beginning of the analysis will be based on the results for Analysis V.0 recalling table 8.8 8.9 using those values as starting point several new models will be created trying to achieve better solutions each time until reaching a desirable difference percentage with respect to the values obtained in the AVT. (Goal- Difference less than 15% in all 3 principal modes)

9.1.1 Piazza XX Settembre Model V.1

For modal calibration Model V.1 a variable parameter change is used to update the F.E model and close the gap between the experimental values and the results obtained from the solution of the eigenvalue and eigenvector problem will be reported in table 9.1:

it´s important to highlight that considering the variability related to the additional unaccounted load due to the presence of internal partitions in the floor slab of which there is no direct knowledge derived from core sampling on the floors or endoscopic test for the definition of the composition of the finishing works it was decided to affect the superimposed load calculated in equation 8.44 **reducing the load from** $6.5\frac{kN}{m^2}$ **to** $5.8\frac{kN}{m^2}$

Piazza XX Settembre		**Model:**	**Version V.1**	
Material	**Location**	**Compressive Strength [Mpa]**	**Elastic Modulus [MPa]**	**Density Mass [Kg/m3]**
Concrete	Basement	12.1	32000	2210.75
	Ground Floor	13.3	32000	2215.5
	First Floor	12.1	32000	2212.3
Masonry	Ground Floor	1.74	1500*	1400
	First Floor	1.96	1500*	1400

Table 9.1: Mechanical Properties Piazza XX Settembre Model V.1

Ahead will be presented the result for the solution of the Eigenvalue and Eigenvector problem, the overall behaviour will be discussed in the closing remarks of the thesis.

Mode	**Frequency [Hz]**	**Period [s]**	**UX**	**UY**	**SumUX**	**SumUY**	**RZ**	**SumRZ**
1	4.4973	0.2224	0.0373	0.0004	0.0373	0.0004	0.7744	**0.7744**
2	5.4952	0.1820	**0.7821**	0.0001	0.8194	0.0005	0.0404	0.8148
3	6.2502	0.1600	0.0000	**0.7459**	0.8195	0.7464	0.0037	0.8185
4	6.676	0.1498	0.0000	0.0047	0.8195	0.7510	0.0000	0.8185
5	7.1492	0.1399	0.0000	0.0023	0.8195	0.7533	0.0000	0.8185
6	10.3586	0.0965	0.0001	0.0004	0.8196	0.7538	0.0005	0.8190
7	10.6409	0.0940	0.0000	0.0000	0.8196	0.7538	0.0000	0.8191
8	10.7163	0.0933	0.0000	0.0002	0.8196	0.7540	0.0001	0.8192
9	11.0414	0.0906	0.0002	0.0000	0.8198	0.7540	0.0001	0.8193
10	11.4663	0.0872	0.0001	0.0003	0.8199	0.7543	0.0144	0.8336
11	11.4936	0.0870	0.0000	0.0000	0.8199	0.7543	0.0004	0.8340
12	11.5174	0.0868	0.0012	0.0000	0.8211	0.7543	0.0003	0.8343
13	11.6318	0.0860	0.0002	0.0008	0.8214	0.7551	0.0157	0.8500
14	11.799	0.0848	0.0002	0.0011	0.8216	0.7562	0.0030	0.8530
15	11.8718	0.0842	0.0001	0.0002	0.8217	0.7564	0.0399	0.8929

Table 9.2: Results Modal Piazza XX Settembre Mode V.1 Analysis: Frequency, Periods and Modal Mass Participation Ratios

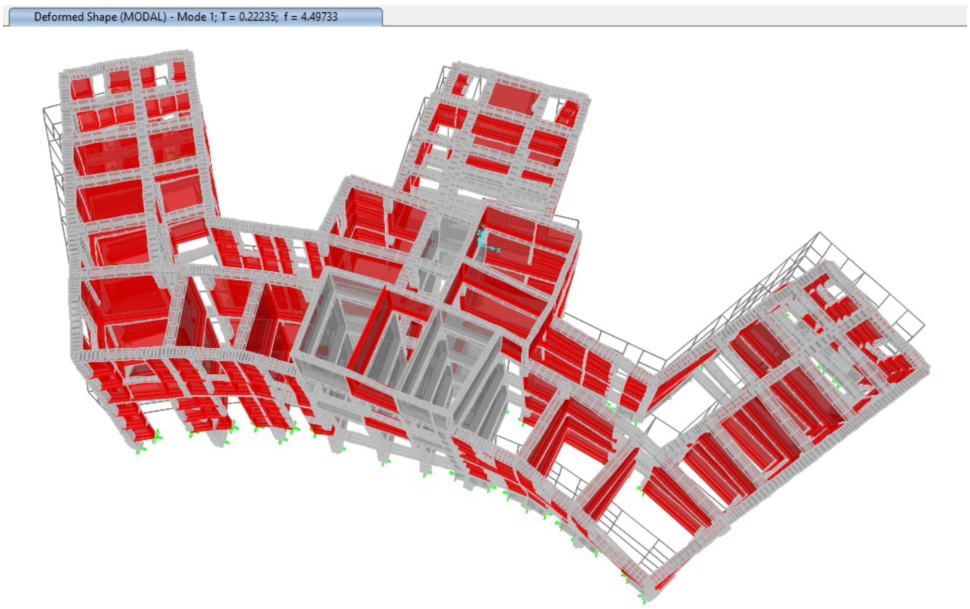

Figure 9.1: Modal Deformation Mode 1 Model V.1 Piazza XX Settembre

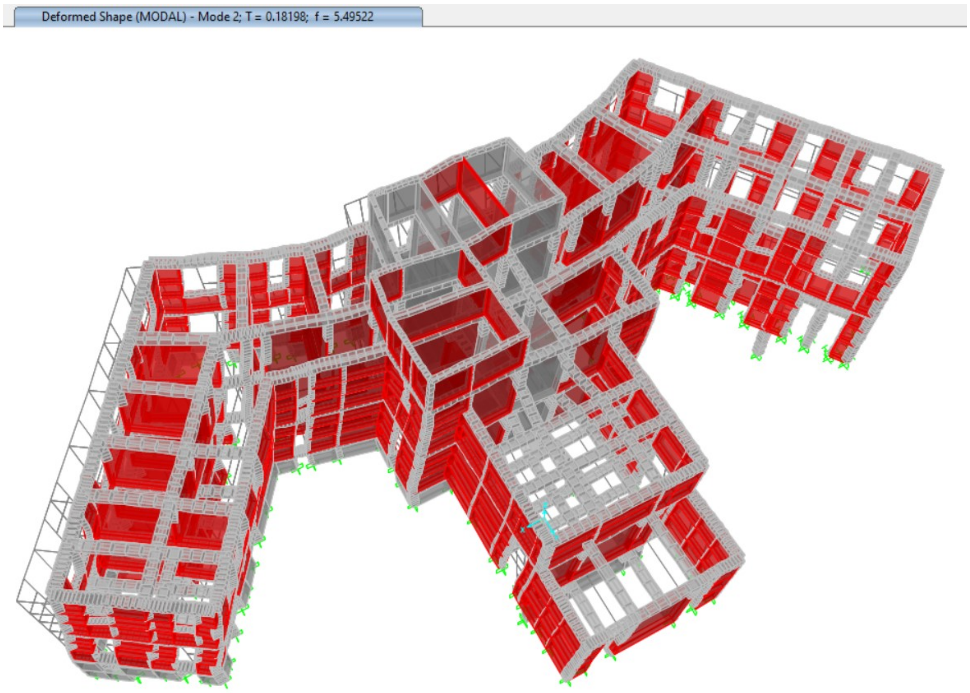

Figure 9.2: Modal Deformation Mode 2 Model V.1 Piazza XX Settembre

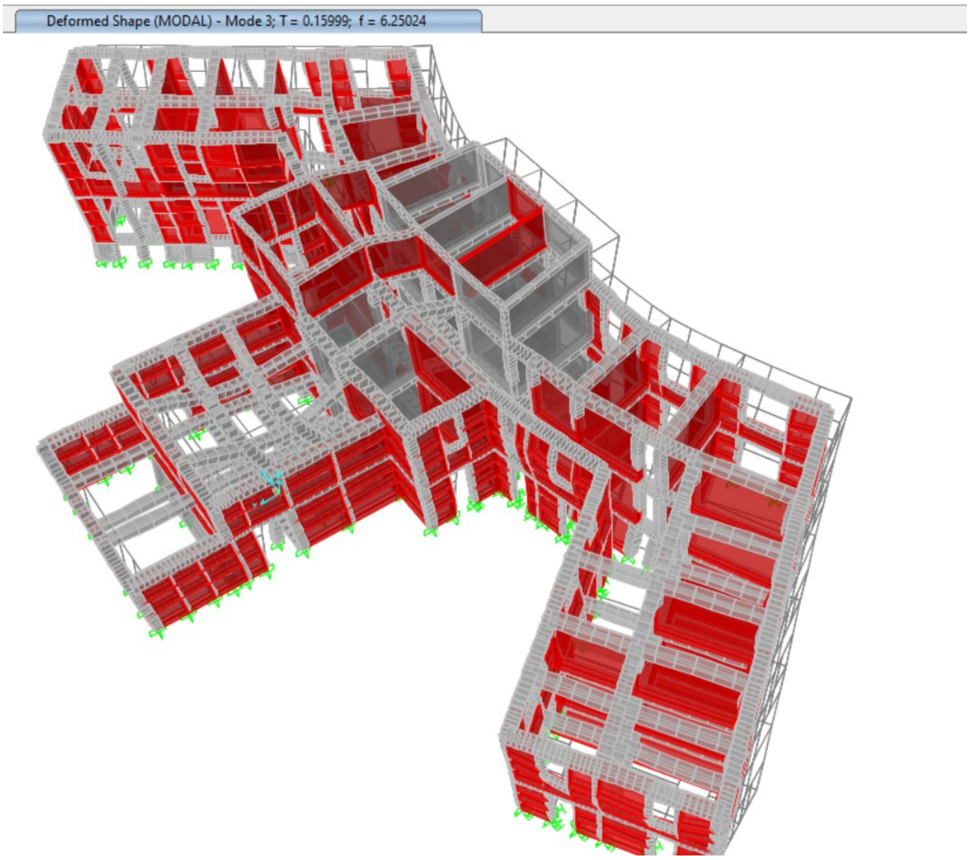

Figure 9.3: Modal Deformation Mode 3 Model V.1 Piazza XX Settembre

Building Piazza XX Settembre Step by Step Analysis						
Description	**Model Rz**		**Model Ty**		**Model Tx**	
AVT retrieved Frequencies [Hz]	5.08		6.63		7.85	
Mode V.0	4.083	-19.63%	5.032	-24.10%	5.818	-25.89%
Mode V.1	4.497	-11.47%	5.495	-17.12%	6.250	-20.38%

Table 9.3: Manual Calibration Step Model V1 - Evolution of Frequencies for Gap reduction Piazza XX Settembre

As appreciated in table 9.3 the objective was to increase the frequency of the structure with respect to Model V.0, for such purpose, the Stiffness must be increased and the mass reduced. Calibrating the model in this case required reducing the loads that will be converted into masses for the modal analysis and altering the stiffness, which as known is directly proportional to the young modulus of the materials therefore the chosen modifications to be done for Model V.1 were reducing the superimposed load and increased the Young Modulus of the materials. Note that the Density Mass of the masonry was also reduced due to the great uncertainty this material represented during the on-site tests.

9.1.2 Piazza XX Settembre Model V.2

For modal calibration Model V.2 a variable parameter change is used to update the F.E model and close the gap between the experimental values and the results obtained from the solution of the eigenvalue and eigenvector problem will be reported in table 9.4:

it´s important to highlight that the consideration made regarding the variability related to the additional unaccounted load is still unaltered being $5.8\frac{kN}{m^2}$

Piazza XX Settembre		**Model:**	**Version V.2**	
Material	**Location**	**Compressive Strength [Mpa]**	**Elastic Modulus [MPa]**	**Density Mass [Kg/m3]**
Concrete	Basement	12.1	32000	2210.75
	Ground Floor	13.3	32000	2215.5
	First Floor	12.1	32000	2212.3
Masonry	Ground Floor	1.74	1800*	1400
	First Floor	1.96	1800*	1400

Table 9.4: Mechanical Properties Piazza XX Settembre Model V.2

Ahead will be presented the result for the solution of the Eigenvalue and Eigenvector problem, the overall behaviour will be discussed in the closing remarks of the thesis.

Mode	Frequency [Hz]	Period [s]	UX	UY	SumUX	SumUY	RZ	SumRZ
1	4.7332	0.2113	0.0510	0.0004	0.0510	0.0004	**0.7589**	0.7589
2	5.7451	0.1741	**0.7692**	0.0001	0.8201	0.0005	0.0540	0.8129
3	6.412	0.1560	0.0000	**0.7386**	0.8201	0.7391	0.0037	0.8166
4	6.7096	0.1490	0.0000	0.0103	0.8201	0.7495	0.0001	0.8167
5	7.1744	0.1394	0.0000	0.0033	0.8201	0.7527	0.0000	0.8167
6	10.481	0.0954	0.0001	0.0004	0.8202	0.7531	0.0004	0.8171
7	10.6773	0.0937	0.0000	0.0000	0.8202	0.7531	0.0000	0.8171
8	10.84	0.0923	0.0000	0.0002	0.8203	0.7534	0.0002	0.8172
9	11.0908	0.0902	0.0003	0.0000	0.8205	0.7534	0.0000	0.8173
10	11.6114	0.0861	0.0000	0.0002	0.8206	0.7536	0.0023	0.8196
11	11.8018	0.0847	0.0004	0.0003	0.8209	0.7539	0.0001	0.8196
12	11.8658	0.0843	0.0002	0.0001	0.8212	0.7539	0.0002	0.8198
13	11.971	0.0835	0.0007	0.0010	0.8219	0.7549	0.0107	0.8305
14	12.0624	0.0829	0.0000	0.0001	0.8219	0.7550	0.0004	0.8308
15	12.2023	0.0820	0.0004	0.0007	0.8223	0.7557	0.0026	0.8334

Table 9.5: Results Modal Piazza XX Settembre Mode V.2 Analysis: Frequency, Periods and Modal Mass Participation Ratios

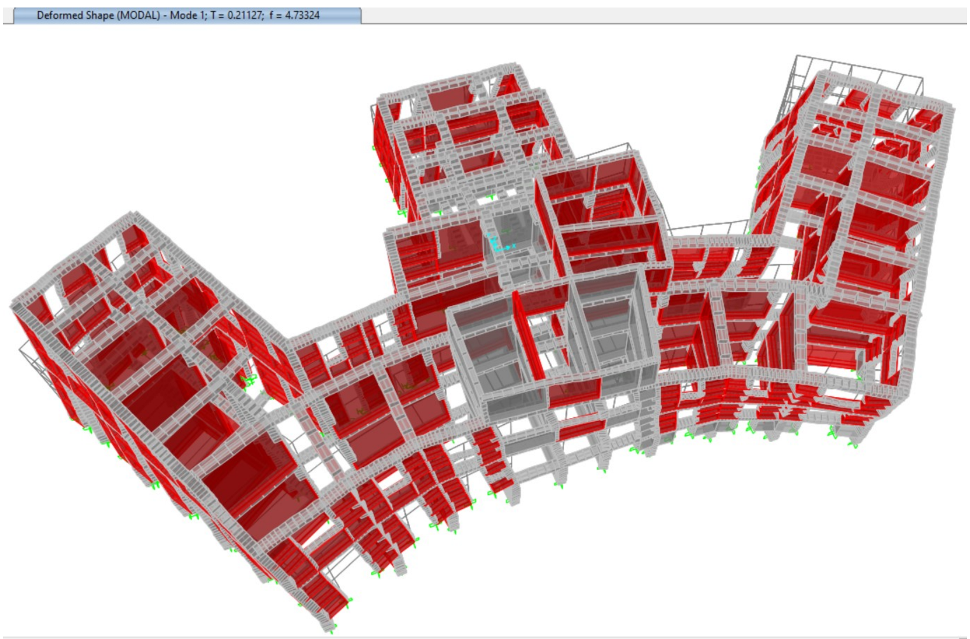

Figure 9.4: Modal Deformation Mode 1 Model V.2 Piazza XX Settembre

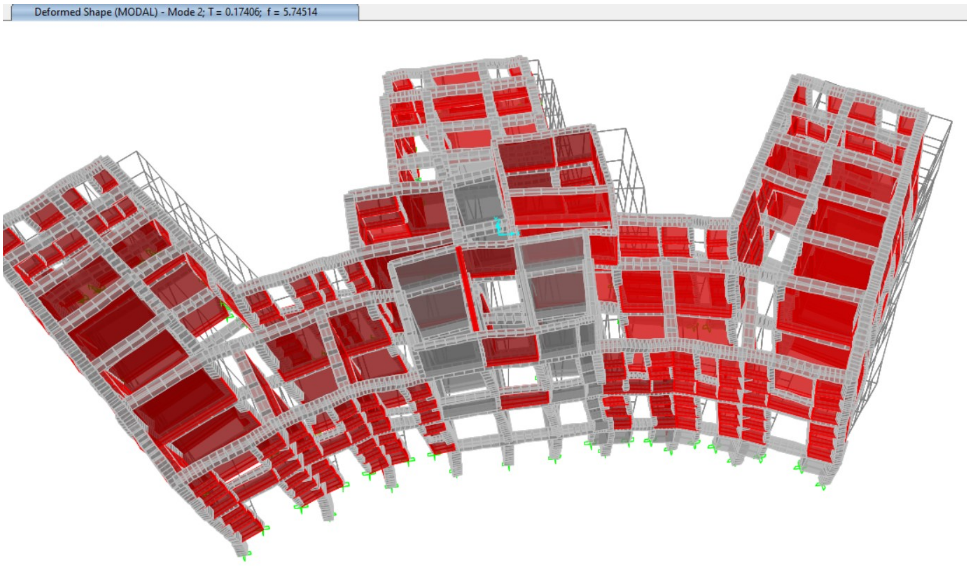

Figure 9.5: Modal Deformation Mode 2 Model V.2 Piazza XX Settembre

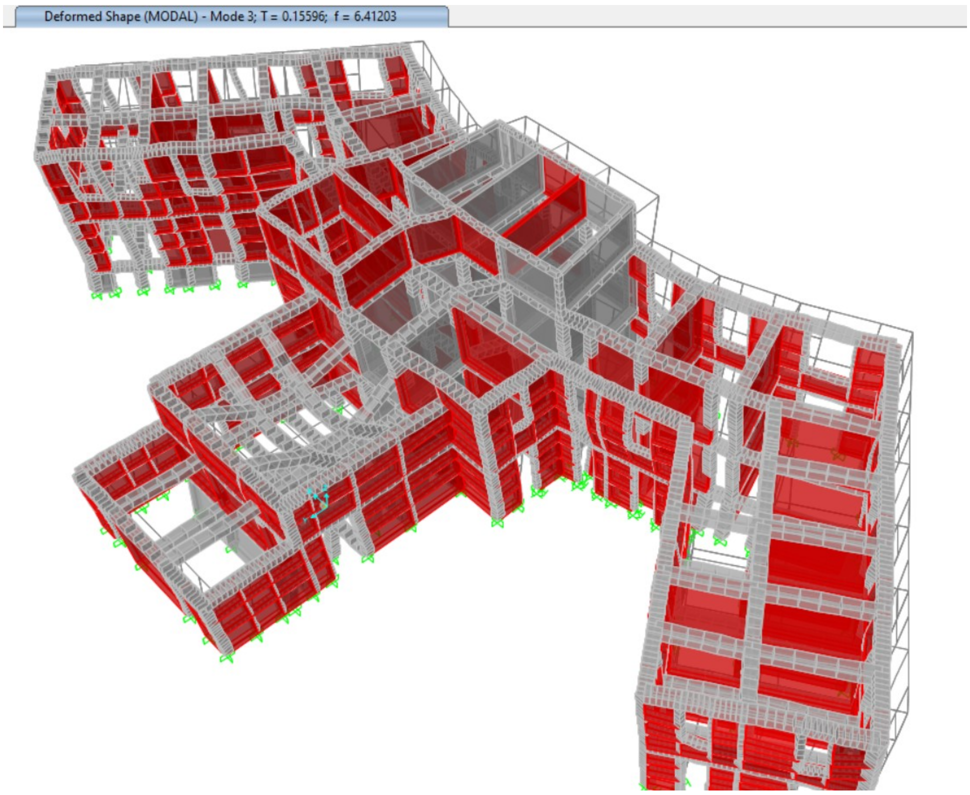

Figure 9.6: Modal Deformation Mode 3 Model V.2 Piazza XX Settembre

Building Piazza XX Settembre Step by Step Analysis						
Description	**Mode Rz**		**Mode Ty**		**Mode Tx**	
AVT retrieved Frequencies [Hz]	5.08		6.63		7.85	
Model V.0	4.083	-19.63%	5.032	-24.10%	5.818	-25.89%
Model V.1	4.497	-11.47%	5.495	-17.12%	6.250	-20.38%
Model V.2	4.733	-6.83%	5.745	-13.35%	6.412	-18.32%

Table 9.6: Manual Calibration Step Model V2 - Evolution of Frequencies for Gap reduction Piazza XX Settembre

As appreciated in table 9.6 the objective was to increase the frequency of the structure with respect to Model V.1, for such purpose, the Stiffness must be increased and the mass reduced. Calibrating the model in this case required reducing the loads that will be converted into masses for the modal analysis and altering the stiffness, which as known is directly proportional to the young modulus of the materials therefore the chosen modifications to be done for Model V.2 were increased the Young Modulus of the materials. Note that the Density Mass of the masonry was also reduced due to the great uncertainty this material represented during the on-site tests.

9.1.3 Piazza XX Settembre Model V.3

For modal calibration Model V.3 a variable parameter change is used to update the F.E model and close the gap between the experimental values and the results obtained from the solution of the eigenvalue and eigenvector problem will be reported in table 9.7:

it´s important to highlight that the consideration made regarding the variability related to the additional unaccounted load was reduced even more achieving a value equal to $5.5\frac{kN}{m^2}$

Piazza XX Settembre		**Model:**	**Version V.3**	
Material	**Location**	**Compressive Strength [Mpa]**	**Elastic Modulus [MPa]**	**Density Mass [Kg/m3]**
Concrete	Basement	12.1	32000	2210.75
	Ground Floor	13.3	32000	2215.5
	First Floor	12.1	32000	2212.3
Masonry	Ground Floor	1.74	1900*	1400
	First Floor	1.96	1900*	1400

Table 9.7: Mechanical Properties Piazza XX Settembre Model V.3

Ahead will be presented the result for the solution of the Eigenvalue and Eigenvector problem, the overall behaviour will be discussed in the closing remarks of the thesis.

Mode	**Frequency [Hz]**	**Period [s]**	**UX**	**UY**	**SumUX**	**SumUY**	**RZ**	**SumRZ**
1	4.9223	0.2032	0.0926	0.0004	0.0926	0.0004	**0.7153**	0.7153
2	6.7614	0.1479	0.0000	0.0353	0.0927	0.0358	0.0002	0.7155
3	6.8932	0.1451	0.0006	**0.7099**	0.0933	0.7457	0.0047	0.7201
4	7.2371	0.1382	0.0000	0.0078	0.0933	0.7535	0.0000	0.7202
5	7.8222	0.1278	**0.7247**	0.0013	0.8179	0.7548	0.1030	0.8232
6	10.5685	0.0946	0.0001	0.0006	0.8181	0.7554	0.0004	0.8236
7	10.7703	0.0928	0.0001	0.0000	0.8182	0.7554	0.0000	0.8236
8	10.9337	0.0915	0.0001	0.0003	0.8182	0.7557	0.0002	0.8238
9	11.2208	0.0891	0.0005	0.0000	0.8188	0.7557	0.0002	0.8240
10	11.7214	0.0853	0.0002	0.0002	0.8190	0.7559	0.0008	0.8248
11	11.9517	0.0837	0.0007	0.0002	0.8197	0.7561	0.0000	0.8248
12	12.0555	0.0830	0.0007	0.0000	0.8204	0.7561	0.0001	0.8249
13	12.1355	0.0824	0.0008	0.0014	0.8211	0.7575	0.0037	0.8286
14	12.1752	0.0821	0.0001	0.0000	0.8212	0.7575	0.0000	0.8286
15	12.3989	0.0807	0.0011	0.0009	0.8223	0.7584	0.0015	0.8301

Table 9.8: Results Modal Piazza XX Settembre Mode V.3 Analysis: Frequency, Periods and Modal Mass Participation Ratios

As observed in Table 9.8 due the modification performed over the structural properties (i.e Young Modulus, Density Mass, Superimposed load) selected as variables, the modes with the major mass participation have shifted, now being mode 1,3 and 5 the principal ones in rotation around Z, translation in Y and translation in X respectively. Modes 2 and 4 were local modes, not relevant to this analysis.

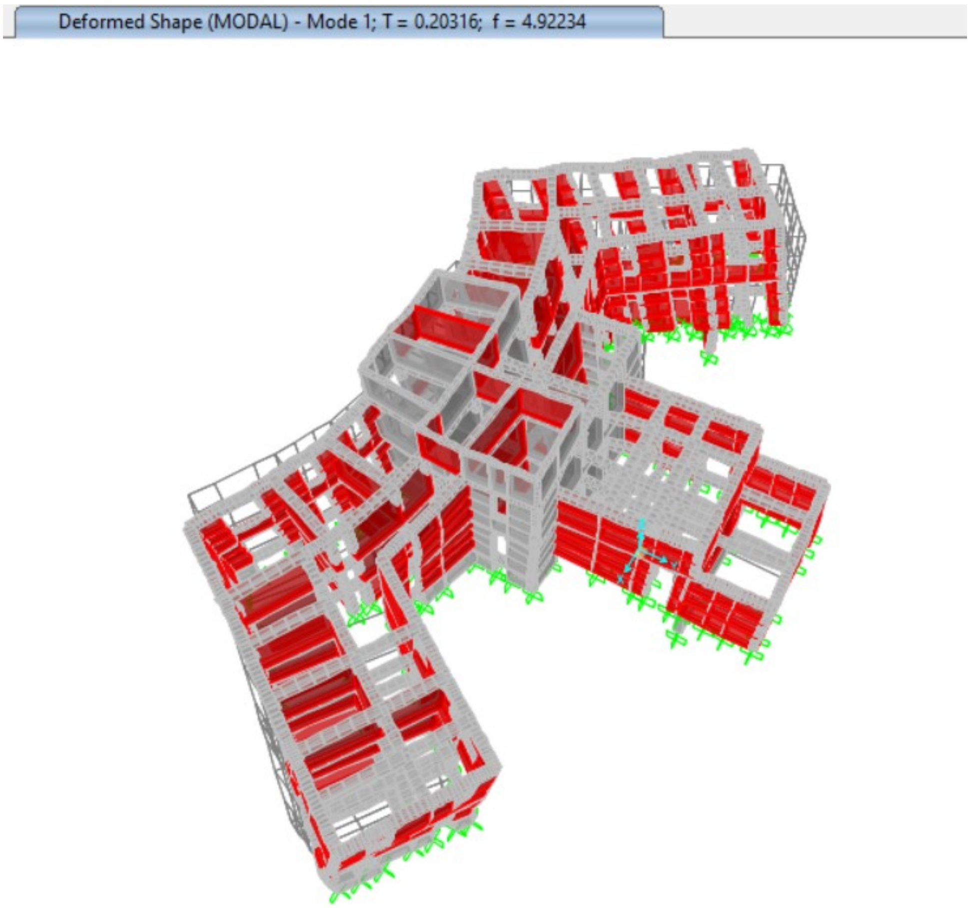

Figure 9.7: Modal Deformation Mode Rz Model V.3 Piazza XX Settembre

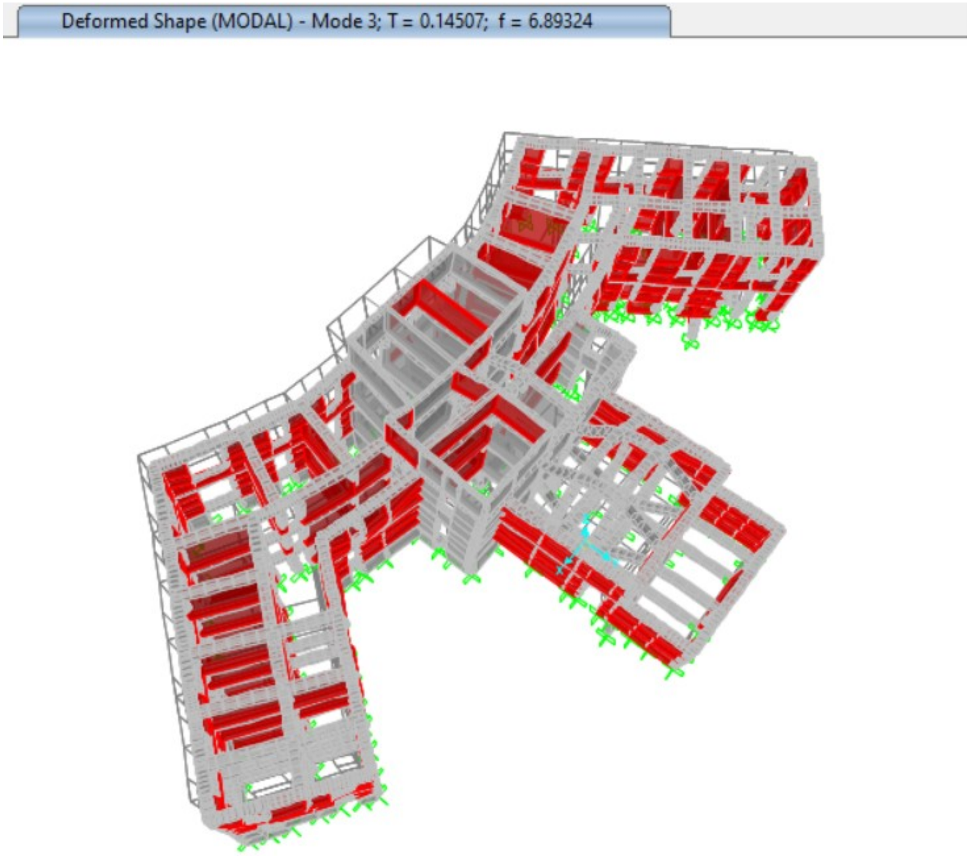

Figure 9.8: Modal Deformation Mode Ty Model V.3 Piazza XX Settembre

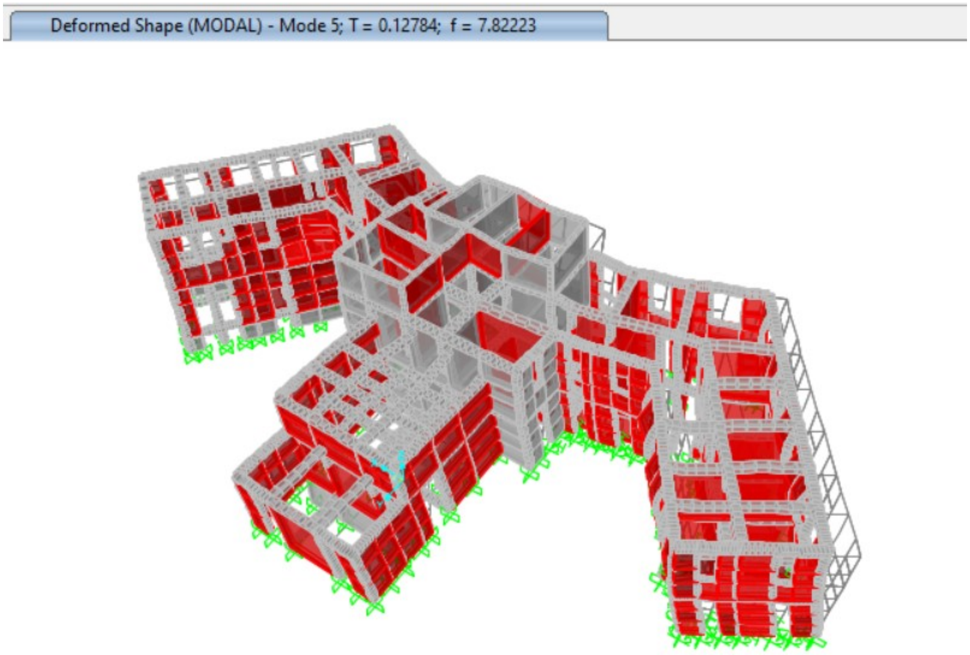

Figure 9.9: Modal Deformation Mode Tx Model V.3 Piazza XX Settembre

Building Piazza XX Settembre Step by Step Analysis						
Description	**Mode Rz**		**Mode Ty**		**Mode Tx**	
AVT retrieved Frequencies [Hz]	5.08		6.63		7.85	
Model V.0	4.083	-19.63%	5.032	-24.10%	5.818	-25.89%
Model V.1	4.497	-11.47%	5.495	-17.12%	6.250	-20.38%
Model V.2	4.733	-6.83%	5.745	-13.35%	6.412	-18.32%
Model V.3	4.922	-3.10%	6.893	3.97%	7.822	-0.35%

Table 9.9: Manual Calibration Step Model V3 - Evolution of Frequencies for Gap reduction Piazza XX Settembre

As appreciated in table 9.9 the objective was to increase the frequency of the structure with respect to Model V.2, for such purpose, the Stiffness must be increased and the mass reduced. Calibrating the model in this case required reducing the loads that will be converted into masses for the modal analysis and altering the stiffness, which as known is directly proportional to the young modulus of the materials therefore the chosen modifications to be done for Model V.3 were increased the Young Modulus of the materials. Note that the Density Mass of the masonry was also reduced due to the great uncertainty this material represented during the on-site tests.

9.2 Via Concezione

For this case of study the beginning of the analysis will be based on the results for Analysis V.0 recalling table 8.10 8.11 using those values as starting point several new models will be created trying to achieve better solutions each time until reaching a desirable difference percentage with respect to the values obtained in the AVT. (Goal- Difference less than 15% in all 3 principal modes)

9.2.1 Via Concezione Model V.1

For modal calibration Model V.1 variable parameters change is used to update the F.E model and close the gap between the experimental values and the results obtained from the solution of the eigenvalue and eigenvector problem will be reported in table 9.10:

it´s important to highlight that considering the variability related to the additional unaccounted load due to the presence of internal partitions in the floor slab of which there is no direct knowledge derived from core sampling on the floors or endoscopic test for the definition of the composition of the finishing works it was decided to affect the superimposed load calculated in equation 8.44 **reducing the load from** $6.5\frac{kN}{m^2}$ **to** $5.8\frac{kN}{m^2}$

Via Concezione		**Model:**	**Version V.1**	
Material	**Location**	**Compressive Strength [Mpa]**	**Elastic Modulus [MPa]**	**Density Mass [Kg/m3]**
Concrete	Basement	14	30000	2294.75
	Ground Floor	9.8	30000	2288.5
	First Floor	13.2	30000	2300.7
Masonry	Ground Floor	0.86	1500*	1500
	First Floor	0.86	1500*	1500

Table 9.10: Mechanical Properties Via Concezione Model V.1

Ahead will be introduced the result for the solution of the Eigenvalue and Eigenvector problem, the overall behaviour will be discussed in the closing remarks of the thesis.

Mode	**Frequency [Hz]**	**Period [s]**	**UX**	**UY**	**SumUX**	**SumUY**	**RZ**	**SumRZ**
1	3.911	0.2557	0.1044	0.0032	0.1044	0.0032	**0.6124**	0.6124
2	4.418	0.2263	0.0000	0.0000	0.1044	0.0032	0.0000	0.6124
3	5.705	0.1753	0.0000	0.0000	0.1045	0.0032	0.0000	0.6125
4	6.056	0.1651	0.0378	**0.6707**	0.1423	0.6739	0.0004	0.6129
5	6.131	0.1631	0.0003	0.0017	0.1425	0.6756	0.0001	0.6130
6	6.417	0.1558	**0.5789**	0.0364	0.7214	0.7120	0.1064	0.7194
7	6.874	0.1455	0.0081	0.0001	0.7295	0.7121	0.0008	0.7201
8	8.991	0.1112	0.0012	0.0000	0.7307	0.7121	0.0001	0.7203
9	9.104	0.1098	0.0000	0.0051	0.7307	0.7172	0.0040	0.7243
10	9.508	0.1052	0.0000	0.0022	0.7307	0.7193	0.0008	0.7251
11	9.725	0.1028	0.0001	0.0001	0.7308	0.7194	0.0003	0.7254
12	9.878	0.1012	0.0000	0.0004	0.7308	0.7198	0.0001	0.7255
13	10.054	0.0995	0.0004	0.0000	0.7312	0.7198	0.0000	0.7255
14	10.221	0.0978	0.0013	0.0000	0.7325	0.7198	0.0001	0.7256
15	10.260	0.0975	0.0002	0.0001	0.7327	0.7200	0.0000	0.7256

Table 9.11: Results Modal Via Concezione Mode V.1 Analysis: Frequency, Periods and Modal Mass Participation Ratios

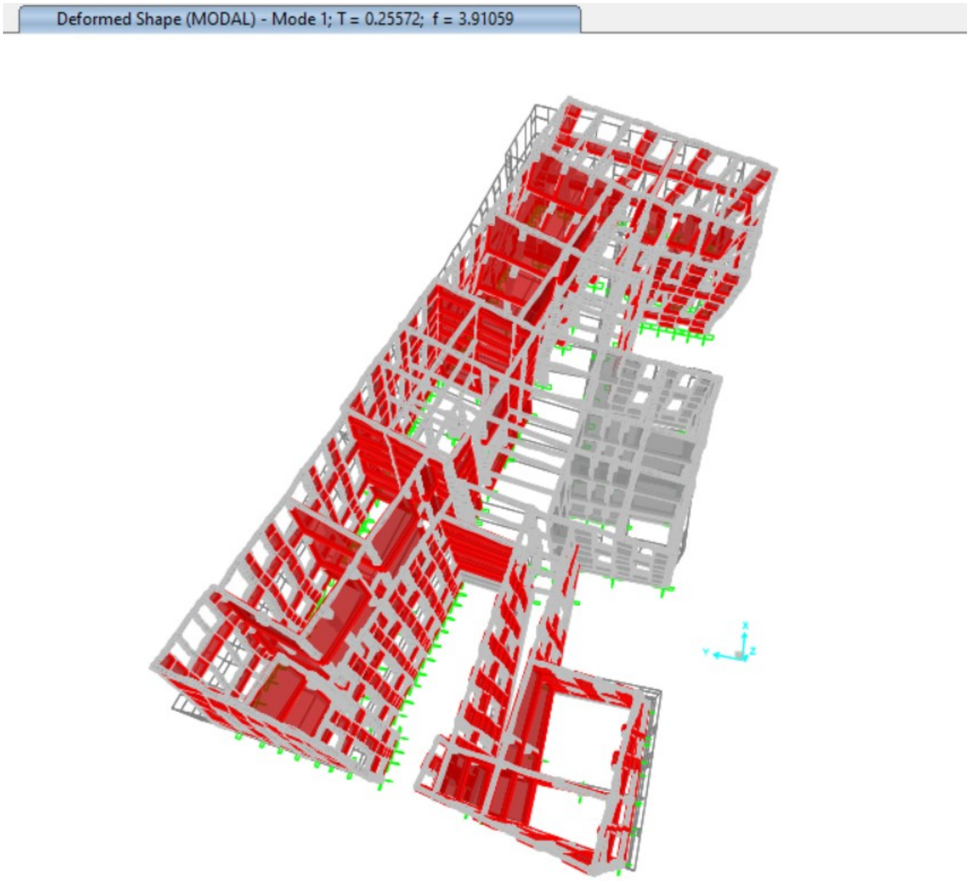

Figure 9.10: Modal Deformation Mode Rz Model V.1 Via Concezione

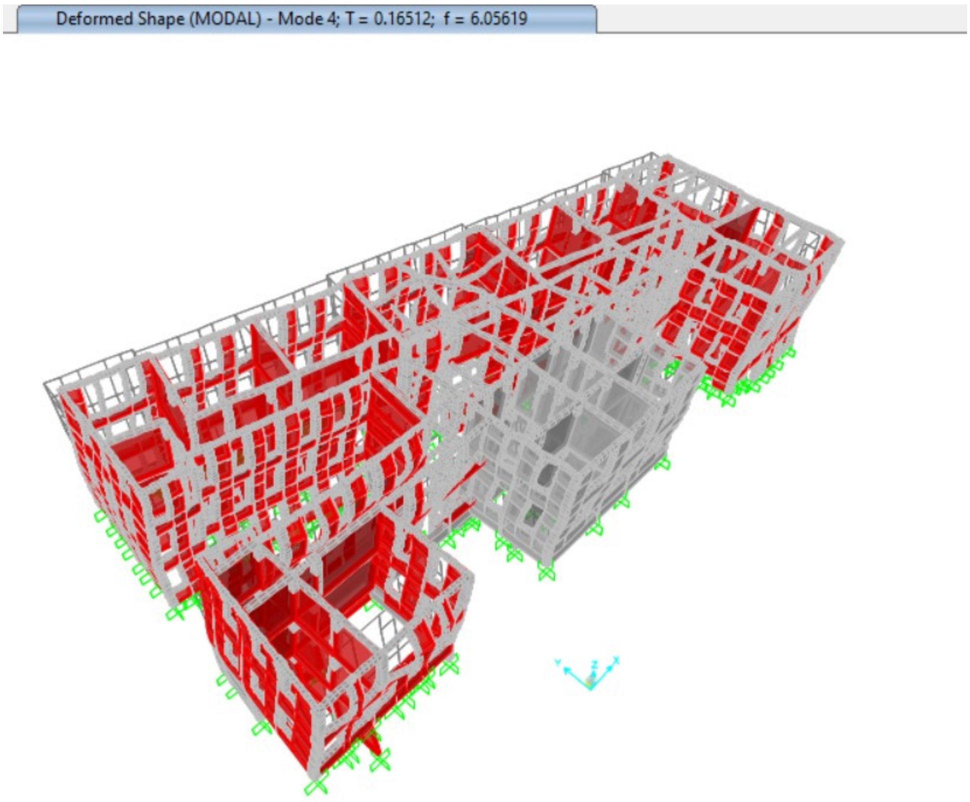

Figure 9.11: Modal Deformation Mode Ty Model V.1 Via Concezione

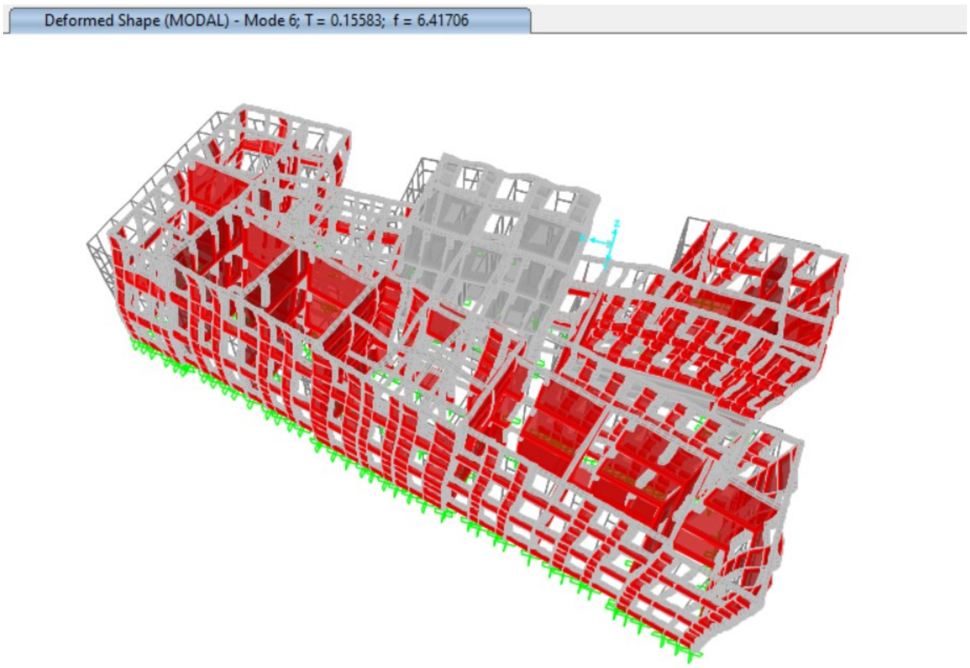

Figure 9.12: Modal Deformation Mode Tx Model V.1 Via Concezione

Building Via Concezione Step by Step Analysis						
Description	**Mode Rz**		**Mode Ty**		**Mode Tx**	
AVT retrieved Frequencies [Hz]	4.29		6.37		8.03	
Model V.0	3.671	-14.44%	5.887	-7.58%	6.264	-21.99%
Model V.1	3.911	-8.84%	6.056	-4.93%	6.417	-20.09%

Table 9.12: Manual Calibration Step Model V1 - Evolution of Frequencies for Gap reduction Via Concezione

As appreciated in table 9.12 the objective was to increase the frequency of the structure with respect to Model V.0, for such purpose the Stiffness must be increased and the mass reduced. Calibrating the model in this case required reducing the loads that will be converted into masses for the modal analysis and altering the stiffness, which as known is directly proportional to the young modulus of the materials therefore the chosen modifications to be done for Model V.1 were reducing the superimposed load and increased the Young Modulus of the materials.

9.2.2 Via Concezione Model V.2

For modal calibration Model V.2 variable parameters change is used to update the F.E model and close the gap between the experimental values and the results obtained from the solution of the eigenvalue and eigenvector problem such will be reported in table 9.13:

it´s important to highlight that considering the variability related to the additional unaccounted load due to the presence of internal partitions in the floor slab of which there is no direct knowledge derived from core sampling on the floors or endoscopic test for the definition of the composition of the finishing works it was decided to maintain the value used in Model V.1 for the superimposed load calculated in equation 8.44 **retaining in this iteration a load of** $5.8\frac{kN}{m^2}$

Via Concezione		**Model:**	**Version V.2**	
Material	**Location**	**Compressive Strength [Mpa]**	**Elastic Modulus [MPa]**	**Density Mass [Kg/m3]**
Concrete	Basement	14	31000	2294.75
	Ground Floor	9.8	31000	2288.5
	First Floor	13.2	31000	2300.7
Masonry	Ground Floor	0.86	1500*	1500
	First Floor	0.86	1500*	1500

Table 9.13: Mechanical Properties Via Concezione Model V.2

Ahead will be presented the result for the solution of the Eigenvalue and Eigenvector problem, the overall behaviour will be discussed in the closing remarks of the thesis.

Mode	**Frequency [Hz]**	**Period [s]**	**UX**	**UY**	**SumUX**	**SumUY**	**RZ**	**SumRZ**
1	4.017	0.2489	0.1044	0.0027	0.1044	0.0027	**0.6126**	0.6126
2	4.491	0.2227	0.0000	0.0000	0.1044	0.0027	0.0000	0.6126
3	5.799	0.1724	0.0000	0.0000	0.1044	0.0027	0.0000	0.6126
4	6.170	0.1621	0.0328	**0.6755**	0.1372	0.6782	0.0004	0.6130
5	6.232	0.1605	0.0002	0.0023	0.1374	0.6804	0.0001	0.6130
6	6.537	0.1530	**0.5881**	0.0315	0.7255	0.7119	0.1064	0.7194
7	7.267	0.1376	0.0040	0.0002	0.7295	0.7121	0.0003	0.7197
8	9.158	0.1092	0.0012	0.0000	0.7308	0.7121	0.0001	0.7199
9	9.392	0.1065	0.0000	0.0050	0.7308	0.7171	0.0041	0.7240
10	9.842	0.1016	0.0000	0.0020	0.7308	0.7191	0.0008	0.7247
11	9.879	0.1012	0.0001	0.0001	0.7309	0.7192	0.0003	0.7250
12	10.222	0.0978	0.0000	0.0003	0.7309	0.7195	0.0001	0.7251
13	10.244	0.0976	0.0004	0.0000	0.7313	0.7195	0.0000	0.7251
14	10.425	0.0959	0.0000	0.0005	0.7313	0.7200	0.0000	0.7251
15	10.430	0.0959	0.0009	0.0000	0.7322	0.7200	0.0005	0.7256

Table 9.14: Results Modal Via Concezione Mode V.2 Analysis: Frequency, Periods and Modal Mass Participation Ratios

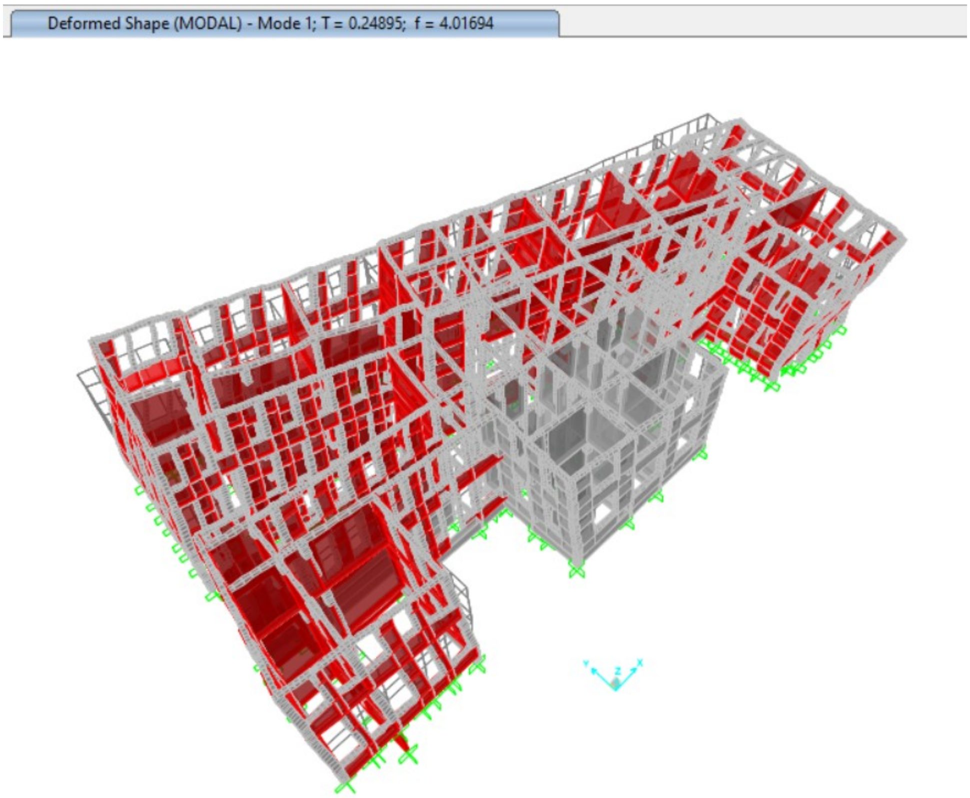

Figure 9.13: Modal Deformation Mode Rz Model V.2 Via Concezione

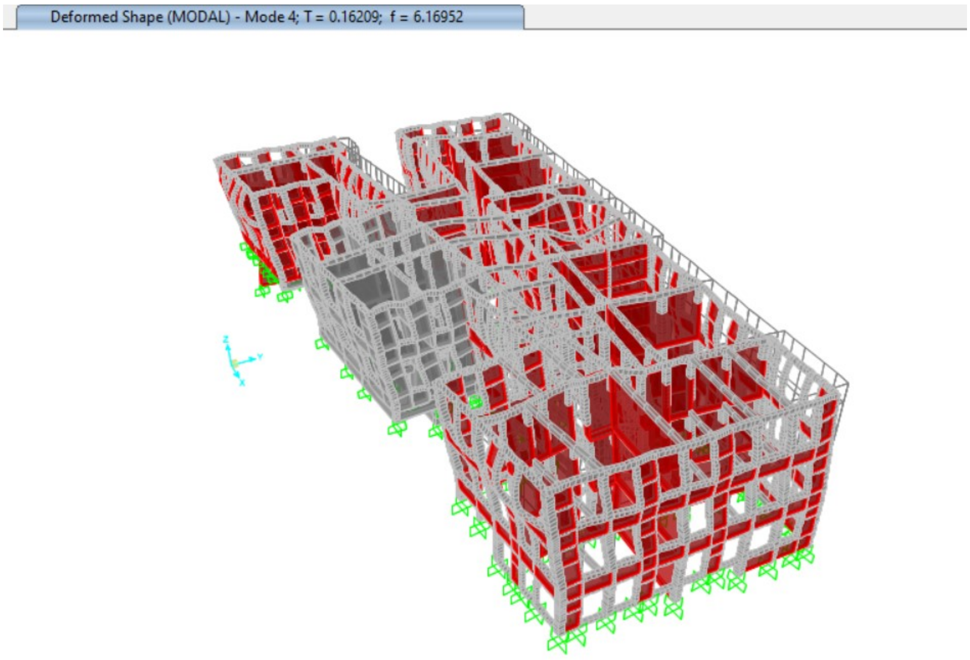

Figure 9.14: Modal Deformation Mode Ty Model V.2 Via Concezione

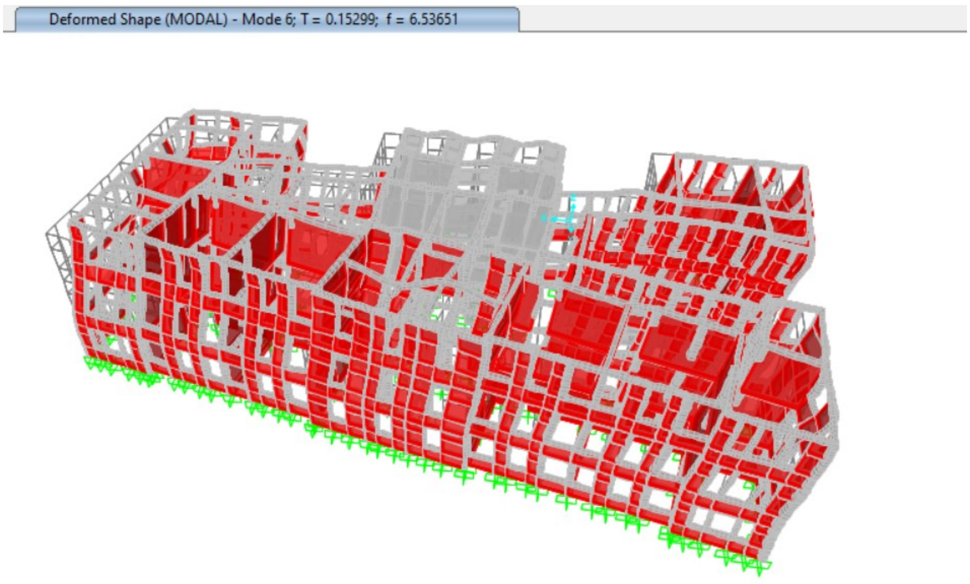

Figure 9.15: Modal Deformation Mode Tx Model V.2 Via Concezione

Building Via Concezione Step by Step Analysis						
Description	**Mode Rz**		**Mode Ty**		**Mode Tx**	
AVT retrieved Frequencies [Hz]	4.29		6.37		8.03	
Model V.0	3.671	-14.44%	5.887	-7.58%	6.264	-21.99%
Model V.1	3.911	-8.84%	6.056	-4.93%	6.417	-20.09%
Model V.2	4.017	-6.37%	6.170	-3.15%	6.537	-18.60%

Table 9.15: Manual Calibration Step Model V2 - Evolution of Frequencies for Gap reduction Via Concezione

As appreciated in table 9.15 the objective was to increase the frequency of the structure with respect to Model V.1, for such purpose the Stiffness must be increased and the mass reduced. Calibrating the model in this case required reducing the loads that will be converted into masses for the modal analysis and altering the stiffness, which as known is directly proportional to the young modulus of the materials therefore the chosen modifications are to be done for Model V.2 was to increased the Young Modulus of the materials.

9.3 Final Remarks Manual Model Calibration

In pursuit of achieving the predetermined goal of maintaining a difference percentage below 15% for the three modes, each case was independently studied obtaining interesting outcomes. Piazza XX Settembre during the third iteration, a viable solution was derived. It is imperative to acknowledge that this outcome was attained within the parameters of experimental and technical uncertainty. Primarily, the increase in masonry stiffness through the Young Modulus was implemented with the understanding that experimental data on the material was inconclusive and did not align with considerations specified in the Italian National Annex for such elements. A parallel scenario was observed for the load directly acting on the membrane floor, where the computed load, accounting for the analysis performed in equation 8.44 where solid concrete over-slab and durable finishing was considered, was found to be theoretically heavier. However, sensitivity analyses suggest that, in reality, the weight might be lesser, leading to the observed reduction.

For the outcomes concerning Via Concezione, following two rounds of manual calibration, satisfactory results were achieved for the rotational mode on the Z-axis and the Y-axis translation. However, with respect to the X-axis translation, the objective was not met due to a difference percentage of approximately 19%. Subsequently, a comprehensive comparison and in-depth analysis will be conducted, considering that the identified discrepancy might be rooted in procedures executed prior to the manual calibration of the modal parameters.

Chapter 10

Artificial Intelligence Model Calibration.

In this chapter, the automatic calibration method for the two models will be described considering the previous concepts described in as introduced in preceding chapters, the method will be particularising the choice of structural parameters considered within the optimisation process. The calibration aims to minimise the difference between the experimental frequencies measured on-site and the numerical ones obtained from the F.E models. in order to validate the dynamic behaviour of the latter.

To proceed with the identification of the structures under study, an Artificial Intelligence algorithm was used in order to dynamically vary the structural parameters of the building to reach an optimisation process now consolidated in the literature such as the Genetic Algorithm (GA). This algorithm is based entirely on stochastic processes inspired by Darwinian evolutionary law, starting from a population composed of multiple individuals. Each individual represents a solution to the problem, and then an updating process begins to switch and compare characteristics of the population in order to identify the best individuals in each generation. At the end of the process, it will converge towards a single individual, which will represent the optimal solution.

The selection of the best individuals occurs through random processes which are repeated at each iteration in the following order:

1. Random generation of an initial population at iteration 0.
2. Selection of parents using the Roulette Wheel technique.
3. Creation of children starting from the selected parents through single-point, double-point crossover operations or with combinations of the characteristics of the corresponding parents (at each iteration the optimiser will be able to choose the best operation based on the characteristics of the selected individuals and the number of variables involved).
4. Evaluation of the characteristics of the children by calculating a fitness or an index representative of the goodness of the individual (the better the individual, the more likely he will be to survive the next iteration).
5. Mutation of the characteristics of the population thanks to which new individuals with different characteristics compared to those observed so far are randomly introduced into the population. This operator intervenes within the process only when the probability of activation is exceeded (generally very low).
6. Updating the population by keeping only the individuals that exhibit the best characteristics and discarding all solutions considered inferior.
7. The population obtained in step 6) will be used as a starting solution for the next iteration, thus obtaining a cyclic process for which steps (2), (3), (4), (5) and (6) are repeated until a satisfactory fulfilment of the process interrupts the cycle.

Considering the previous main phases of the algorithm, as well as the techniques used to update the parameters, it is necessary to proceed with the overview of the mathematical formulation for the optimisation process which takes the following form:

Minimise:

$$W = f\left(x_i\right); i = 1, \ldots, n \tag{10.1}$$

Under the consideration of:

$$(x_i^{\ell} < x_i < x_i^u) \tag{10.2}$$

Where:

$$f\left(x_i\right) = \text{abs}\left(P_e - P_n\left(x_i\right)\right) \tag{10.3}$$

In equation 10.3 represents the Objective Function (OF) or same known as Target Function of the problem. Specifically, the objective function of the process is expressed in terms of the difference between the experimental target frequency, P_e, obtained through the OMA techniques adopted for the interpretation of the signals and the numerical one,P_n, obtained from the models. It can be seen how the function $P_n(x_i)$ appears to be dependent on the parameters x_i adopted for the calibration of the model. Minimising this difference means reproducing the dynamic behaviour of the models accordingly with the experimental frequencies recorded on site. In this case, as shown in the previous chapters, the recorded frequencies and the detected fundamental modes have a gap between them greater than the unity in the three interested modes (translational in X and Y and/or rotational around Z); therefore it was decided to proceed by adopting as the OF to minimise the total difference given by the sum of the differences obtained between the measured frequency and the numerically derived one for each mode of vibration to which a significant participating mass of the structure was associated. The interpretation of the signals and the evaluation of the modal parameters allowed the identification of patterns and correspondence between the experimental measurements and the models.

x_i represents the generic variable of the system (e.g., stiffness of the masonry or concrete) which varies dynamically, throughout the optimisation process, within an interval defined by a lower limit, x_i^l, and an upper limit, x_i^u

Ahead for each structure under study some of the considerations adopted will be introduced and discussed regarding the choice of optimisation parameters and the corresponding upper and lower limits of the variability interval, as well as, the definition of an adequate OF compatible with the aims of the study. Furthermore, in the following paragraph, emphasis will be placed on some assumptions adopted as a starting point for the calibration of the models on the basis of the author's experience and the information obtained from the investigation campaign.

10.1 General considerations

The success of a calibration process derives from a careful and consistent choice of the structural parameters considered as variable and the corresponding variability ranges, which contribute significantly to the achievement of a solution that faithfully but above all realistically reproduces the dynamic behaviour of the structure. For such reasons, it was preferred to proceed with a general manual calibration of the buildings in order to evaluate the effects of each structural parameter, weighing its sensibility on the dynamic behaviour of the buildings under study.

The results obtained from the interpretation of the signals using OMA techniques made it possible to identify the main frequencies for each building. Due to the structural characteristics of the buildings which have low overall heights as well as high stiffness conferred by the confined masonry elements, it was not possible to obtain the mode shapes associated with each detected frequency with equal reliability. Hence, the experimental frequencies will serve as a reference point for the model calibration of the present study.

Furthermore, the important irregularities in the layout of the elements and a limited characterisation of the walls and concrete elements deriving from the brief investigation campaign contribute to increasing the level of uncertainty on the actual mechanical behaviour of the same. Added to those existing limitations must be considered the uncertainties derived from the actual weight and composition of the horizontal surfaces, for which no inspection has been foreseen aimed at characterising the concrete (full slab) and/or any waterproofing and finishing layers placed inside the flooring of the typical slab.

Below are the assumptions adopted for each building and the reasons for such choices.

10.1.1 Piazza XX Settembre:

In the context of the structure located via Concezione, the three main frequencies identified through the analysis of experimental signals OMA - AVT are presented below:

- 1st mode of vibration - Freq=5.08 Hz
- 2nd way of vibration - Freq=6.63 Hz
- 3rd way of vibration - Freq=7.85 Hz

The three frequencies are located at a certain distance from each other with a mutual difference of approximately 1-2 Hz, below are recalled the modes computed from the eigenvalue and eigenvector analysis:

- 1st mode of vibration - Freq=4.083 Hz – mainly torsional mode
- 2nd mode of vibration - Freq=5.032 Hz – mainly X translational mode
- 3rd mode of vibration - Freq=5.818 Hz – mainly Y translational mode

Analysing the behaviour, the model exhibits a higher stiffness than that obtained from the experimental data (lower frequencies for all three modes) as well as a reduced frequency gap between the various modes.

Aside from the case of Via Concezione, from the test campaign it was not possible to obtain useful information aimed at refining the model and/or inserting structural elements that could improve the dynamic behaviour of the building, making it closer to that assumed on the basis of the experimental data. In other words, no tests, destructive or otherwise, were carried out near the walls of the stairwell.

Despite the absence of evidence that supported, for this case study, the presence of reinforced concrete walls should be considered a reasonable assumption valid for the building in Piazza XX Settembre, on the basis of the technology available at the time of the construction and the similar construction typology of the two buildings.

By assigning to the perimeter walls of the stairwell (refer to Figure 10.1), throughout their height, properties similar to those of the reinforced concrete elements. lying on the same plane, the results obtained from the modal analysis show significant improvements in reproducing the dynamic behaviour observed from the experimental measurements in terms of frequencies:

- 1st mode of vibration - Freq=5.43 Hz – mainly torsional mode
- 2nd mode of vibration - Freq=6.76 Hz – mainly translational mode along X

- 3rd mode of vibration - Freq=7.3 Hz – mainly translational mode along Y

Although the values of the fundamental frequencies of the structure are still distant from those detected, it is possible to note an improvement in terms of their distribution within the frequency range. These reflections have allowed the writer to adopt this model as a starting point for its optimised calibration.

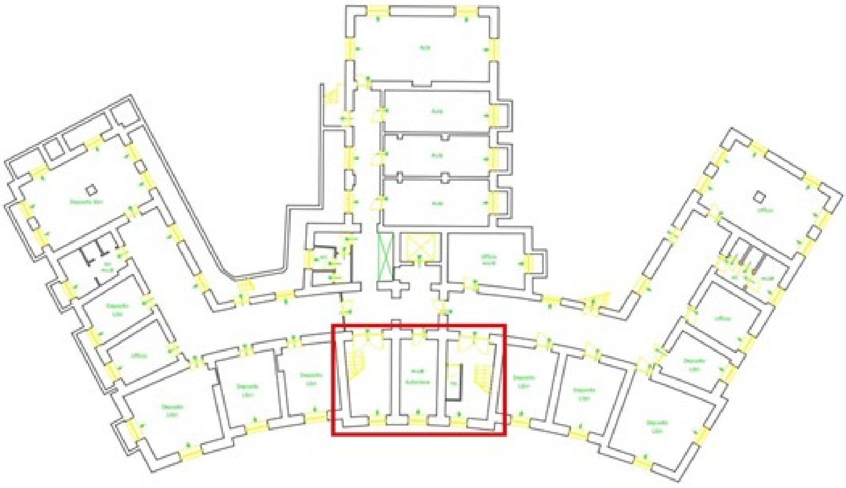

Figure 10.1: Area modelled using RC shear walls in Piazza XX Settembre

10.1.2 Via Concezione:

In the context of the structure located in via Concezione, subsequently are recalled the three main frequencies identified through the analysis of experimental signals OMA - AVT.

- 1st mode of vibration - Freq=4.29 Hz
- 2nd way of vibration - Freq=6.37 Hz
- 3rd way of vibration - Freq=8.03 Hz

The three frequencies are located at a certain distance from each other with a mutual difference of approximately 2 Hz. From the experimentally measured frequencies there is a significant discrepancy with the ones obtained numerically, which are also reported below:

- 1st mode of vibration - Freq=3.671 Hz – mainly torsional mode

- 2nd mode of vibration - Freq=5.887 Hz – mainly translational mode along Y
- 3rd mode of vibration - Freq=6.264 Hz – mainly translational mode along X

The differences lie in the values of the individual frequencies and, furthermore, the model seems not to be able to reproduce, already in this preliminary phase, a clear difference in the frequency gap is obtained with respect to the experimental data.

From this first analysis, in order to improve the identification of frequencies, was proceeded with the modelling in the presence of a stairwell entirely made of concrete rather than masonry.

From the inspection carried out by the laboratory contracted by the University of Messina (according to the technical report the identification of the survey is: IS10ID) at the wall on the basement floor overlooking the central corridor, reported in the technical report "Structural investigations at the Department of Cognitive, Psychological and Pedagogical Sciences and Cultural Studies", was possible to observe the presence of an extensive concrete area which suggests the presence of reinforced concrete partitions. along the core of the stairwell.

This assumption was extended to the perimeter wall of the stairwell for the entire height of the building (see Figure 10.2), allowing to obtain a preliminary model with a dynamic behaviour more in line with that obtained from the interpretation of the experimental signals. The mechanical characteristics of these shear walls were assumed to be equal to those adopted for the reinforced concrete elements. located on the same level.

To demonstrate what has been said, the frequency values are reported with an indication of the modal shapes obtained from this first calibration:

- 1st mode of vibration - Freq=5.07 Hz – mainly torsional mode
- 2nd mode of vibration - Freq=6.23 Hz – mainly translational mode along Y
- 3rd mode of vibration - Freq=6.73 Hz – mainly translational mode along X

Although the values of the fundamental frequencies of the structure are still distant from those measured, it is possible to note an improvement in terms of their distribution within the frequency range. The first modal shape reproduces a mainly torsional behaviour, while the flexural frequencies along Y and X are related to the second and third one.

These reflections have allowed the writer to adopt this model as a starting point for its optimised calibration.

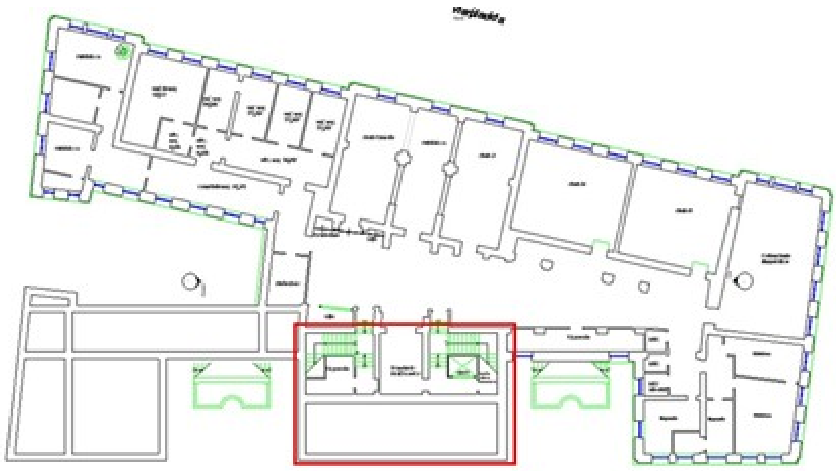

Figure 10.2: Area modelled using RC shear walls in Via Concezione

10.2 Identification of Variable Structural Parameters and definition of their variability intervals

After discussing the hypotheses assumed prior to the process of optimising the structural parameters of the model, were set the variables for each building. Given the uncertainty derived from a lack of knowledge of the mechanical properties of the materials used in the structural components and the probable heterogeneity of their distributions among the internal structural even if they were the same, a standardised assumption was performed for that matter.

As a result, 5 variables were set for each structure, considering the acceptable range in which the algorithm can assign the subjects or individuals. Below, the parameters adopted for the optimisation of the model calibration process and the respective extremes of variability will be listed in detail.

Note that for the masonry elements, it was decided to adopt the same range of variability provided by the NTC2018 standard reported in Table C8.5.I (Circular of 2019). Specifically, it was considered to adopt the threshold values of stiffness (E) and specific weight (w) relating to a type of masonry "made of solid bricks and lime mortar". Furthermore, this range takes into consideration the results obtained from the mechanical characterisation of the masonry obtained by testing with single and double flat jacks.

For the reinforced concrete elements, however, not being able to rely on values suggested by the standard, we proceeded by identifying a reasonable range of variability for the type of construction being analysed. Furthermore, this range took into account the results obtained from the mechanical characterisation of the concrete obtained through compression testing of cores taken on-site, whenever the results were compelling to the engineering criteria of the author.

10.2.1 Building in Piazza XX Settembre

The variables adopted for the optimisation of the calibration process and the related variability ranges adopted for the aforementioned case study can be summarised as follows:

1. Stiffness of the external and internal perimeter masonry expressed as the Young Modulus E with a variability range equal to:

$$800\frac{\mathrm{N}}{\mathrm{mm}^2} < E < 2000\frac{\mathrm{N}}{\mathrm{mm}^2} \tag{10.4}$$

   Given the significant difference reported by the outcome of the tests with a flat jack on the masonry on the ground floor compared to that performed on the first floor, it was preferred to report a maximum value of the masonry higher than that foreseen by the standard for the masonry type in question but lower than the maximum one detected on site.

2. Specific weight of the external and internal perimeter masonry w with a variability range equal to:

$$1500\frac{\mathrm{kg}}{\mathrm{m}^3} < w < 2200\frac{\mathrm{kg}}{\mathrm{m}^3} \tag{10.5}$$

3. Stiffness expressed as the Young Modulus $E_c m$ of all the concrete elements of the structure (vertical elements, horizontal elements and the stiffening elements placed on the facades of the buildings and/or on some internal walls). Based on the results of the investigation campaign, it was deemed appropriate to adopt a single stiffness value regardless of the level of interest as the outcome of the compression tests on the concrete cores showed similar values between elements placed at various heights of the structure. The variability range adopted is equal to:

$$26000\frac{\mathrm{N}}{\mathrm{mm}^2} < E_{\mathrm{cm}} < 35000\frac{\mathrm{N}}{\mathrm{mm}^2} \tag{10.6}$$

4. Dimensions of stiffeners (expressed in terms of equivalent area A) which corresponds to secondary framing elements made of reinforced concrete. Considered for all internal and external walls of the building with a variability range equal to:

$$225(15 \times 15)\mathrm{cm}^2 < A < 900(30 \times 30)\mathrm{cm}^2 \tag{10.7}$$

5. Variation (positive or negative increase) in the load relating to non-structural G2 permanent elements such as (weight of the flooring and additional unaccounted load due to the presence of internal partitions) of which there is no direct knowledge deriving from core sampling on the floors or endoscopic for the definition of the composition of the finishing works. The variability range adopted is equal to:

$$-10\frac{kN}{m^2} < G_2 < +10\frac{kN}{m^2} \tag{10.8}$$

10.2.2 Building in Via Concezione

The variables adopted for the optimisation of the calibration process and the related variability ranges adopted for the Via Concezione case study can be summarised as follows:

1. Stiffness of the external and internal perimeter masonry expressed as the Young Modulus E with a variability range equal to:

$$600\frac{\mathrm{N}}{\mathrm{mm}^2} < E < 1800\frac{\mathrm{N}}{\mathrm{mm}^2} \tag{10.9}$$

   Given the significant difference reported by the outcome of the tests with a flat jack on the masonry on the ground floor compared to that performed on the first floor, it was preferred to report a maximum value of the masonry higher than that foreseen by the standard for the masonry type in question but lower than the maximum one detected on site.

2. Specific weight of the external and internal perimeter masonry w with a variability range equal to:

$$1500\frac{\mathrm{kg}}{\mathrm{m}^3} < w < 2200\frac{\mathrm{kg}}{\mathrm{m}^3} \tag{10.10}$$

3. Stiffness expressed as the Young Modulus E_cm of all the concrete elements of the structure (vertical elements, horizontal elements and the stiffening elements placed on the facades of the buildings and/or on some internal walls). Based on the results of the investigation campaign, it was deemed appropriate to adopt a single stiffness value regardless of the level of interest as the outcome of the compression tests on the concrete cores showed similar values between elements placed at various heights of the structure. The variability range adopted is equal to:

$$26000\frac{\mathrm{N}}{\mathrm{mm}^2} < E_{\mathrm{cm}} < 35000\frac{\mathrm{N}}{\mathrm{mm}^2} \tag{10.11}$$

4. Dimensions of stiffeners (expressed in terms of equivalent area A) which corresponds to secondary framing elements made of reinforced concrete. Considered for all internal and external walls of the building with a variability range equal to:

$$225(15 \times 15)\text{cm}^2 < A < 900(30 \times 30)\text{cm}^2 \tag{10.12}$$

5. Variation (positive or negative increase) in the load relating to non-structural G2 permanent elements such as (weight of the flooring and additional unaccounted load due to the presence of internal partitions) of which there is no direct knowledge deriving from core sampling on the floors or endoscopic for the definition of the composition of the finishing works. The variability range adopted is equal to:

$$-10\frac{kN}{m^2} < G_2 < +10\frac{kN}{m^2} \tag{10.13}$$

10.3 A.I Optimisation Results.

The results obtained from the optimisation will be presented for each case of study, as well as, the algorithm setting criteria will be illustrated.

The outcome of the calibration was the optimal values obtained for the variables in order to minimise the difference between the experimental and numerical calculations for each building.

Also, the solution for the eigenvectors and eigenvalues problems using such optimised variables are presented below.

10.3.1 A.I Results for Piazza XX Settembre

For piazza XX Settembre the algorithm was set by adopting the following parameters:

- Number of individuals equal to 200
- Maximum number of iterations equal to 100
- Number of children generated at each iteration equal to 100
- Probability of mutation equal to 5%

Consistent with such launching parameters and the ranges expressed in the previous chapter the results are presented here:

$$E = 1950 \frac{\mathrm{N}}{\mathrm{mm}^2} \tag{10.14}$$

$$w = 1500 \frac{\mathrm{kg}}{\mathrm{m}^3} \tag{10.15}$$

$$E_c m = 30100 \frac{\mathrm{N}}{\mathrm{mm}^2} \tag{10.16}$$

$$A = 900(30x30)\mathrm{cm}^2 \tag{10.17}$$

$$G_2 = 5.7 \frac{\mathrm{kN}}{\mathrm{m}^2} \tag{10.18}$$

The calibration of the model using the optimal parameters obtained from the optimisation process led to the following fundamental frequencies:

A.I Optimised Period [s]	A.I Optimised Numerical Frequency [Hz]	Experimental Frequency [Hz]	Difference percentage [%]	Ux	Uy	Rz
0.20	4.92	5.08	-3.10%	0.0926	0.0004	0.7153
0.15	6.89	6.63	3.97%	0.0006	0.7099	0.0047
0.13	7.82	7.85	-0.37%	0.7269	0.0013	0.1030

Table 10.1: Results for the Eigenvalue and Eigenvector problem using Genetic Algorithm in Piazza XX Settembre

The table 10.1 reported the fundamental periods and their associated frequencies in the first two columns. In the third column, for each mode, the percentage difference with respect to the corresponding target frequency is assumed to be equal to those obtained experimentally. It's possible to observe how the first and second frequencies obtained from the model show a minimal percentage difference compared to those obtained experimentally. The third frequency, however, shows a higher but satisfactory difference percentage. In the remaining three columns, the modal participating masses associated with each mode were reported which confirms the presence of a predominantly torsional component associated with the first mode, a mainly translational component along X associated with the 2nd mode and a mainly translational component along Y for the 3rd mode.

10.3.2 Via Concezione

For Via Concezione the algorithm was set by adopting the following parameters:

- Number of individuals equal to 200
- Maximum number of iterations equal to 100
- Number of children generated at each iteration equal to 100
- Probability of mutation equal to 5%

Consistent with such launching parameters and the ranges expressed in the previous chapter the results are presented here:

$$E = 1650\frac{\mathrm{N}}{\mathrm{mm}^2} \tag{10.19}$$

$$w = 1500\frac{\mathrm{kg}}{\mathrm{m}^3} \tag{10.20}$$

$$E_c m = 28900\frac{\mathrm{N}}{\mathrm{mm}^2} \tag{10.21}$$

$$A = 900(30x30)\mathrm{cm}^2 \tag{10.22}$$

$$G_2 = 5.6\frac{\mathrm{kN}}{\mathrm{m}^2} \tag{10.23}$$

The calibration of the model using the optimal parameters obtained from the optimisation process led to the following fundamental frequencies:

A.I Optimised Period [s]	A.I Optimised Numerical Frequency [Hz]	Experimental Frequency [Hz]	Difference percentage [%]	Ux	Uy	Rz
0.25	4.02	4.29	-6.37%	0.10436	0.00266	0.61255
0.16	6.17	6.37	-3.15%	0.03280	0.67548	0.00038
0.15	6.54	8.03	-18.60%	0.58812	0.03146	0.10637

Table 10.2: Results for the Eigenvalue and Eigenvector problem using Genetic Algorithm in Via Concezione

As seen in table 10.2 reported the fundamental periods and their associated frequencies (first two columns. In the third column), for each mode, the difference percentage with respect to the corresponding target frequency assumed to be equal to those obtained experimentally was calculated. It is possible to observe how the first and second frequencies obtained from the model show a minimal difference percentage compared to those obtained experimentally. The third frequency, however, shows a higher but satisfactory percentage difference. In the remaining three columns, the modal participating masses associated with each mode were reported which confirm the presence of a predominantly torsional component associated with the first mode, a mainly translational component along Y associated with the 2nd mode and a mainly translational component along X 3rd mode.

Chapter 11

Conclusions and Future Applications

The study involved an interesting comparison between traditional Operational Modal Analysis (OMA) techniques, namely EFDD and SSI-cov, and the innovative i-AOMA method. This approach, integrating Machine Learning and Artificial Intelligence algorithms, signified a shift in understanding and characterising the dynamic behaviour of structures. For the two methodologies respectively applied in both cases of study is detected evident relationship for the retrieved values. Combining the methodologies provided a comprehensive and interconnected perspective on the results. The interaction between these techniques and experimental setups offered a global vision of the overall response of the structure, relating to the way in which, depending on the configuration of the setup, particular frequencies are activated. Particularly the i-AOMA has perceived a sufficient similarity with the output of the EFDD and SSI-cov (calibrated with the criteria of a committee of specialised advisors in the topic) nevertheless an intrinsic marginal error is detected particularly regarding recursive patterns in obtained modal parameters creating a limiting in further refinement by using for instance Modal Assurance Criterion (MAC). So a future application of the i-OMA method a wider assessment of the number of subjects and iterations is proposed, refining in the process the algorithm to operate within the new ranges and under this modification it may derive possibly the optimal identification of the modal vectors allowing a better modal calibration of the model under study. The formulation of virtual finite element models for two specific structures, integrating survey data and insights obtained from technical inspections, represents a compelling methodology for characterising these types of structures. The validation of material properties data, obtained from laboratory reports, is achieved by assessing its conformity with the modal results of iteration 0. This is thanks to the assessment of the level of disparity between the derived frequencies through Operational Modal Analysis (OMA) /(i-AOMA). Ultimately, these models serve as an initial validation mechanism for on-site data, facilitating a substantive comparison with experimental test results.

Regarding the modal calibration, using an Artificial Intelligence method based on Genetic Algorithms demonstrated a remarkable similarity in correspondence with experimental measurements and manual calibration, fully validating both methodologies in terms of retrieving a calibrated model. In the consecutive tables 11.1 11.2 can be fully appreciated the results for both cases of study compelling to all the main methodologies applied.

Building Piazza XX Settembre Final Results of studied Methodologies						
Description	**Mode Rz [Hz]**		**Mode [Ty]**		**Mode 3 [Tx]**	
AVT	5.08		6.63		7.85	
retrieved Frequencies [Hz]	Frequency[Hz]	Diff [%]	Frequency[Hz]	Diff [%]	Frequency[Hz]	Diff [%]
Model based in Technical Report Properties	4.08	-19.63%	5.03	-24.10%	5.82	-25.89%
Manually Calibrated Model	4.92	-3.10%	6.89	3.97%	7.82	-0.35%
A.I Optimised Model	4.92	-3.10%	6.89	3.97%	7.82	-0.37%

Table 11.1: Piazza XX Settembre Final Results of studied Methodologies

Building Via Concezione Final Results of studied Methodologies						
Description	**Mode Rz [Hz]**		**Mode [Ty]**		**Mode 3 [Tx]**	
AVT	4.29		6.37		8.03	
retrieved Frequencies [Hz]	Frequency[Hz]	Diff [%]	Frequency[Hz]	Diff [%]	Frequency[Hz]	Diff [%]
Model based in Technical Report Properties	3.67	-14.44%	5.89	-7.58%	6.26	-21.99%
Manually Calibrated Model	4.02	-6.37%	6.17	-3.15%	6.54	-18.60%
A.I Optimised Model	4.02	-6.37%	6.17	-3.15%	6.54	-18.60%

Table 11.2: Via Concezione Final Results of Studied Methodologies

Particularly, the level of alignment in the results for the A.I Optimized the model and the Manually Calibrated Model reached in the case of Piazza XX Settembre reveals a percentage of difference with respect to the values of the AVT frequencies below 4

A relevant aspect of the model identification process was the consideration of a concrete shaft located in the stairwell and in the elevator vertical conduct for both buildings. The verification of this assumption, supported by preliminary investigations, underscored the importance of accurate modelling. Attempts to model shafts as masonry in a preliminary calibration revealed the inadequacy of such an approach, emphasising the necessity of aligning model assumptions with actual structural surveys and characteristics.

In summary, this master's thesis not only advances the understanding of modal parameter analysis but also showcases the potential of integrating traditional and cutting-edge techniques, including Artificial Intelligence, to enhance the accuracy and reliability of structural assessments. The findings of this research contribute valuable insights to the field of civil engineering and provide a foundation for further exploration and refinement of structural health monitoring methodologies.

Chapter 12

Bibliography

[1] 4.5Hz Geophone Sensor. https://www.seis-tech.com/4-5hz-geophone-sensor/. Accessed: September 25, 2023.

[2] Università degli Studi di Messina - Presentazione. https://www.unime.it/ateneo/presentazione. Accessed: September 18, 2023.

[3] O. Acharya, A. Dahal, and K. C. Shrestha. Confined masonry in seismic regions: Application to a prototype building in nepal. *Structures*, 47:2281–2299, 2023.

[4] B. Barros, B. Conde, M. Cabaleiro, M. Solla, and B. Riveiro. Multi-objective optimization-based model calibration of masonry bridges. *Case Studies in Construction Materials*, 19:e02306, 2023.

[5] M. Chang and S. N. Pakzad. Optimal sensor configuration for flexible structures with multi-dimensional mode shapes. *Smart Materials and Structures*, 24(5):055012, apr 2015.

[6] K. Demirlioglu, S. Gonen, and E. Erduran. On the selection of mode shapes used in optimal sensor placement. pages 85–92, 01 2023.

[7] M. A. Erberik, C. Citiloglu, and G. Erkoseoglu. Seismic performance assessment of confined masonry construction at component and structure levels. *Bulletin of Earthquake Engineering*, 17(2):867–889, 2019.

[8] D. Foti, N. I. Giannoccaro, V. Vacca, and M. Lerna. Structural operativity

evaluation of strategic buildings through finite element (fe) models validated by operational modal analysis (oma). *Sensors*, 20(11), 2020.

[9] M. Khan and M. Ali. Optimization of concrete stiffeners for confined brick masonry structures. *Journal of Building Engineering*, 32:101689, 2020.

[10] S. Kumar, M. Abdul Akbar, and A. Thakur. Seismic analysis of a g+3 confined masonry building with aac infill using sap 2000. *Materials Today: Proceedings*, 74:718–725, 2023. 3rd International Conference on Recent Advances in Mechanical Engineering Research and Development.

[11] G. Marano, G. Monti, and G. Quaranta. Comparison of different optimum criteria for sensor placement in lattice towers. *The Structural Design of Tall and Special Buildings*, 20:1048 – 1056, 12 2011.

[12] N. Mendes and P. B. Lourenço. Sensitivity analysis of the seismic performance of existing masonry buildings. *Engineering Structures*, 80:137–146, 2014.

[13] M. Mitchell, R. Link, A. Bayraktar, A. Altunişik, B. Sevim, T. Türker, M. Akkose, and N. Coskun. Modal analysis, experimental validation, and calibration of a historical masonry minaret. *Journal of Testing and Evaluation - J TEST EVAL*, 36, 11 2008.

[14] C. C. . G. E. Murat Altug Erberik. Seismic performance assessment of confined masonry construction at component and structure levels. *Bulletin of Earthquake Engineering*, 17:867–889, 2019.

[15] V. Nicoletti, D. Arezzo, S. Carbonari, and F. Gara. Expeditious methodology for the estimation of infill masonry wall stiffness through in-situ dynamic tests. *Construction and Building Materials*, 262:120807, 2020.

[16] F. J. Pallarés, M. Betti, G. Bartoli, and L. Pallarés. Structural health monitoring (shm) and nondestructive testing (ndt) of slender masonry structures: A practical review. *Construction and Building Materials*, 297:123768, 2021.

[17] D. P. Pasca, A. Aloisio, M. M. Rosso, and S. Sotiropoulos. Pyoma and pyoma_gui: a python module and software for operational modal analysis. *SoftwareX*, 20:101216, 2022.

[18] A. Poulimenos and S. Fassois. Parametric time-domain methods for non-stationary random vibration modelling and analysis — a critical survey and comparison. *Mechanical Systems and Signal Processing*, 20(4):763–816, 2006.

[19] C. Rainieri and G. Fabbrocino. Operational modal analysis of civil engineering structures. *Springer, New York*, 142:143, 2014.

[20] S. Rajput and N. Singh. Comparative study of different infill materials in confined masonry using analytical model. *Materials Today: Proceedings*, 2023.

[21] F. Ranjbaran, M. Hosseini, and M. Soltani. Simplified formulation for modeling the nonlinear behavior of confined masonry walls in seismic analysis. *International Journal of Architectural Heritage*, 6(3):259–289, 2012.

[22] M. M. Rosso, A. Aloisio, J. Parol, G. C. Marano, and G. Quaranta. Intelligent automatic operational modal analysis. *Mechanical Systems and Signal Processing*, 201:110669, 2023.

[23] G. Saudi, P. Reynolds, M. Zaki, and H. Hodhod. Finite-element model tuning of global modes of a grandstand structure using ambient vibration testing. *Journal of Performance of Constructed Facilities*, 23(6):467–479, 2009.

[24] S.Cattari and S. Lagomarsino. Seismic assessment of mixed masonry-reinforced concrete buildings by non-linear static analyses. *Earthquakes and Structures*, 4:241–264, 2013.

[25] A. Shabani, M. Feyzabadi, and M. Kioumarsi. Model updating of a masonry tower based on operational modal analysis: The role of soil-structure interaction. *Case Studies in Construction Materials*, 16:e00957, 2022.

[26] A. Shabani and M. Kioumarsi. Optimal sensor placement techniques for modal identification of historical masonry structures. *Procedia Structural Integrity*, 42:147–154, 2022. 23 European Conference on Fracture.

[27] K. Zhou and Q.-S. Li. Modal identification of high-rise buildings under earthquake excitations via an improved subspace methodology. *Journal of Building Engineering*, 52:104373, 2022.

[28] K. Zhou, Q.-S. Li, and X.-L. Han. Modal identification of civil structures via stochastic subspace algorithm with monte carlo–based stabilization diagram. *Journal of Structural Engineering*, 148(6):04022066, 2022.

[29] K. Zhou, L.-H. Zhi, J.-F. Wang, X. Hong, K. Xu, and Z.-R. Shu. An improved stochastic subspace modal identification method considering uncertainty quantification. *Structures*, 51:1083–1094, 2023.

List of Figures

List of Tables